TECHNISCHE UNIVERSITÄT MÜNCHEN
TUM School of Engineering and Design

Improving the 2.45 GHz Microwave Processing of Fiber Reinforced Plastics

Daniel Manuel Teufl

Vollständiger Abdruck der von der TUM School of Engineering and Design der Technischen Universität München zur Erlangung des akademischen Grades eines

Doktors der Ingenieurwissenschaften

genehmigten Dissertation.

Vorsitzender:	Prof. Dr.-Ing. Manfred Hajek
Prüfer der Dissertation:	Prof. Dr.-Ing. Klaus Drechsler
	Prof. Dr.-Ing. Peter Middendorf

Die Dissertation wurde am 29.04.2021 bei der Technischen Universität München eingereicht und durch die TUM School of Engineering and Design am 18.08.2021 angenommen.

Technische Universität München
Lehrstuhl für Carbon Composites
Boltzmannstraße 15
D-85748 Garching bei München

Tel.:+ 49 (0) 89 / 289 - 15092
Fax: + 49 (0) 89 / 289 - 15097
Email: info.lcc@ed.tum.de
Web: www.asg.ed.tum.de/lcc/

Declaration

Ich erkläre hiermit ehrenwörtlich, dass ich die vorliegende Arbeit selbstständig und ohne Benutzung anderer als der angegebenen Hilfsmittel angefertigt habe; die aus fremden Quellen (einschließlich elektronischer Quellen) direkt oder indirekt übernommenen Gedanken sind ausnahmslos als solche kenntlich gemacht.

Die Arbeit wurde in gleicher oder ähnlicher Form noch keiner anderen Prüfungsbehörde vorgelegt.

.....	.....
Ort, Datum	Unterschrift

Acknowledgement

First, I want to thank Prof. Klaus Drechsler for making my work possible at the institute. Without him, I would not have had the equipment or the chance to investigate microwave processing as I did; without the founding of LCC, I probably would not even have found my way into research.

Just as important as the opportunity to do something meaningful are the people who accompanied me and helped me on my way. The results were made possible by many students, technicians, administrative staff, and colleagues. The students helped with most of the investigations and a lot of practical work before and during this study. Thank you all! I hope that I was able to help you as well in some ways as you did me. I hope that you are all well on your way to becoming engineers and scientists of yourselves! Without our technicians and testing team... not one trial would have been possible. You built up and "tamed" the equipment and are responsible for a smooth ride and many a short-dated trials during this process—Thank you! All the technical infrastructure remains in your hands, just as all the financial and bureaucratic infrastructure remains in the hands of the administration. I do not know how many orders were processed, collected and accounted, how many letters were sorted, how much office supplies ordered by our administration, how much work it was for you to organize our funds, or how often you answered my questions. I surely don't know what you do for me and all my colleagues behind the scenes. Be assured, however, of my heartfelt thanks for all you have done and continue to do, and I am very glad that you are there. I want to thank all my colleagues who are always open to discussing matters, and who freely provide me with feedback. A lot of decisions were based on your input and opinions,

Last but foremost I thank my family and friends. The way to this dissertation was long an rough. I am glad that you are all still here and nobody was lost on the way. While I didn't like it at the moment, your bugging kept me going. More than ever I know that I can always count on your help.

Abstract

In the field of composite curing, Microwave processing shows a potential of up to 50% cycle time reduction in combination with huge energy savings. However, it is not picked up by industry. A potential reason for this is a too low technology readiness level in some details of microwave processing of composites. Consequently, an effort is made to enhance two important areas of microwave processing: Process Control and Absorber Technology. The progress is validated by using a mechanical investigation of manufactured composite samples.

In this work, the investigation of process control mechanisms and manufacturing trials shows the importance of considering microwave's peculiarities. A result of this investigation shows that a better temperature homogeneity and a more stable process are realized by three methods: 1. by increasing the randomness in the microwave field through Mode-Stirrers, a constant Magnetron Change, and higher Magnetron Count; 2. by matching the available microwave power to the heated mass through a Dead-Load and a Maximum Power Level; and 3. by adapting the control parameters.

Furthermore, to advance the absorber technology for microwave processing, a manufacturing process for a variable absorber is defined and demonstrated at laboratory scale. The distinct influences of two carbon blacks and a silicon carbid on the dielectric properties of an epoxy resin are quantified. This results in a design space of an adaptable microwave absorber. This absorber system can be used in the development of microwave optimized tools, as a baseline for the validation of microwave heating process simulations, and for further research.

The progress made in microwave processing is validated using manufacturing trials. For these, samples are prepared and tested using oven and microwave at identical process conditions. A minor difference between the configurations in the development of the glass transition temperature (T_g) and the inter-laminar shear strength (ILSS) is observed. The T_g of microwave cured samples is higher at reduced cure temperatures that do not result in full cure. However, the T_g is similar and as expected at full cure. A microwave cure cycle, optimized for microwaves direct heating using constant heating rates and no dwell times, yields the best ILSS results while reducing the cycle time. In conclusion, the mechanical differences will only be of relevance if a very narrow target for the composite properties exists.

Overall, the technology readiness level in two areas of microwave processing is advanced and an improved foundation for further development is presented.

Kurzfassung

Bei der Aushärtung von Faserkunststoffverbundbauteilen ermöglicht die Mikrowellenhärtung eine Zykluszeitreduzierung von bis zu 50% verbunden mit großen Energieeinsparungen. Dennoch wird die Mikrowellenprozessierung von seiten der Industrie nicht aufgegriffen. Eine mögliche Ursache hierfür ist der geringe Technologische Reifegrad in einigen Bereichen der Mikrowellenverarbeitung von Verbundwerkstoffen. Um dies zu ändern werden in dieser Arbeit zwei wichtige Bereiche der Mikrowellenverarbeitung weiterentwickelt — die Steuerung des Prozesses und die Absorbertechnologie. Die Entwicklungen werden mit einer mechanischen Untersuchung gefertigter Faserverbundproben validiert.

Die Untersuchung der Prozessführung und die Durchführung von Herstellungsversuchen zeigen wie wichtig es ist die physikalischen Wirkmechanismen der Mikrowellenheizung zu berücksichtigen. Eine bessere Temperaturhomogenität und ein stabilerer Prozess werden durch drei Ansätze erreicht: 1. Erhöhung der zufälligen Variationen im Mikrowellenfeld mittels Modenrührern, einem konstanten Wechsel der Magnetrons und einer höheren Anzahl genutzter Magnetrons; 2. Abstimmung der verfügbaren Mikrowellenleistung an das eingebrachte Gut mittels einer Totlast und einer Leistungsbegrenzung; 3. Anpassung der Regelparameter.

Neben der Prozessführung wird in dieser Arbeit ein Herstellungsprozess für einen variablen Absorber definiert und im Labormaßstab demonstriert. Diese Weiterentwicklung der Absorbertechnologie legt den Grundstein zur Mikrowellenverarbeitung komplexer Bauteile. Als Grundlage für variable Absorber werden die Einflüsse zweier Industrieruße und eines Siliciumcarbidpulvers auf die dielektrischen Eigenschaften eines Epoxids quantifiziert. Hieraus wird der Arbeits- und Grenzbereich eines variablen Mikrowellenabsorbers abgeleitet. Das hierüber definierte Absorbersystem kann zukünftig bei der Auslegung mikrowellenoptimierter Werkzeuge eingesetzt werden und bildet eine Grundlage für die Validierung von Prozesssimulationen und weiterer Forschung.

Die erzielten Fortschritte in der Mikrowellenprozessierung werden durch Fertigungsversuche validiert. Hierzu werden Probeplatten unter identischen Prozessbedingungen und Temperaturen mittels eines klassichen Umluftofens und einer Mikrowelle hergestellt. Diese Untersuchung offenbart einen geringen Unterschied in der Entwicklung der Glasübergangstemperatur. Mikrowellengehärtete Platten erreicht

schon bei niedrigeren Temperaturen, welche nicht für die vollständige Härtung ausreichen, höhere Werte für den Glasübergang. Bei vollständiger Härtung entspricht der Glasübergang den Erwartungen. Ebenso wird eine Erhöhung der ertragbaren scheinbaren interlaminaren Schubspannung bei Nutzung eines mikrowellenoptimierten Temperaturzyklus beobachtet.

Insgesamt wird der Technologische Reifegrad in zwei Bereichen der Mikrowellenprozessierung weiterentwickelt und es werden verbesserte Grundlagen für weitere Entwicklungen gelegt.

Contents

Nomenclature

Sign	Unit	Description
b	mm	specimen's width
D_p	m	penetration depth
ε_r^*	-	complex relative permittivity
ε_r'	-	relative permittivity i.e. real part of ε_r^*
ε_r''	-	loss factor i.e. imaginary part of ε_r^*
ε_f	-	elongation of bending specimen
E_f	GPa	bending modulus
E	$^{\mathrm{V}}/_{\mathrm{m}}$	electric field
E_i	$^{\mathrm{V}}/_{\mathrm{m}}$	inner electric field
F	N	force
f	Hz	frequency
h	mm	specimen's thickness
H	$^{\mathrm{A}}/_{\mathrm{m}}$	magnetic field
λ	m	wavelength
L	mm	supporting width
L'	mm	pressure fin distance
m_{ij}	g	mass of i contained in j
φ_{ij}	-	volume-fraction of i in j
p	W	power
Q	-	Q-Factor
ϱ	$^{\mathrm{g}}/_{\mathrm{cm}^3}$	density

Sign	Unit	Description
s	mm	deformation
σ_f	MPa	bending stress
T_g	°C	glass transition temperature
T_{g-DMA}	°C	glass transition temperature measured using a DMA
$\tan(\delta)$		dissipation factor
τ_{ILSS}	MPa	inter-laminar shear strength
V	cm^3	volume
v	-	volume filling factor

Acronyms

4-pt 4-point bending

A resin

B hardener

C accelerator

CA cured absorber

CB carbon black

CFRP carbon fiber-reinforced plastic

CO2e CO2 equivalent

cov coefficient of variation

CTE coefficient of linear thermal expansion

DAC dual asymmetric centrifuge

DMA dynamic mechanical analysis

DOC degree of cure

DoE design of experiments

DSC differential scanning calorimetry

FLAME Faserverbund-Leichtbau mit Automatisierter Mikrowellenprozesstechnik hoher Energieeffizienz

FoM figure of merit

FRP fiber-reinforced plastic

FVC fiber volume content

GDP Gross Domestic Product

GFRCE glass fiber-reinforced cyanate ester

GFRE glass fiber-reinforced epoxy

GFRP glass fiber-reinforced plastic

GRP glass fiber reinforced thermosetting plastic

IPCC Intergovernmental Panel on Climate Change

ISM industrial, scientific and medical

KIT Karlsruher Institute of Technology

LB Printex® L Beads

LDS life datasheet

Load Dead-Load

MB master-batch

MChan Magnetron Change

MCoun Magnetron Count

MDSC modular differential scanning calorimetry

MLR Multiple Linear Regression

MPC model predictive control

NCF non-crimp-fabric

O_ref reference cycle

OAN oil absorption number

PEI polyetherimide

PES polyethersulfone

PID proportional integral derivative

PTFE polytetrafluorethylen

PU polyurethane

RT room temperature

RTM resin transfer molding

SD standard deviation

SD/Tm standard deviation (SD) divided by Temperature Mean

SD/Tr SD divided by Temperature Rise

SEM scanning electron microscope

SiC silicon carbid

Sin Sinus Function

Spr/Tm Temperature Spread after heat-up divided by Temperature Mean

Spr/Tr Temperature Spread after heat-up divided by Temperature Rise

Spread Temperature Spread after heat-up

Stir Mode-Stirrers

Tmean Temperature Mean

Trise Temperature Rise

TRL technology readiness level

VARI vaccuum assisted resin infusion

VHM180 *Vötsch Hephaistos 180/200*

VIT Vötsch Industrietechnik

XE2B Printex® XE 2 B

List of Figures

List of Tables

1 Introduction

1.1 Background

From 1990 to 2016 only one of the eight Intergovernmental Panel on Climate Change (IPCC) sectors achieved an incline in emissions of CO2 equivalent (CO2e). While all other sectors reduced CO2e emission, solely the transport sector showed an increase in emissions of CO2e by 25% [1].While in 1990 international aviation was only responsible for 9% of the transport sectors CO2e emissions, it is responsible for 54% of its rise. In 2017 more than 16% of the European transport emissions were due to international aviation. Even more, the amount of emissions in aviation is expected to increase further. Eurocontrol estimates a growth of 53% in European air traffic by 2040 [2]. Airbus and Boeing estimate that their service fleets will more than double[1] in the next twenty years [3], [4].

These dramatic numbers are a consequence of a more open and mobile society that developed in the last 30 years and is still growing. Consequently, while a certain increase must be accepted, all measures must be utilized to reduce the CO2e emissions with respect to environmental change. A well established cornerstone to reduce fuel consumption and thus CO2e emission is seen in the lowering of vehicle masses. Nearly independent of the transport path—street or air—, a reduction of fuel consumption and CO2 emission between 0.5% to 0.8% per 1% weight saving is estimated [5]–[7]. In the last years, an important role in the mass reduction has been taken over by lightweight materials like fiber-reinforced plastics (FRPs). The potential of FRPs was already utilized in the early 60's when glass fiber-reinforced plastic (GFRP) was used for gliders [8]. In the last tweny years, their potential came into public focus again. Well known projects are the Boeing Dreamliner, the Airbus A350 XWB, and the BMW i3 which all focus on the utilization of carbon fiber-reinforced plastic (CFRP). Apart from these flagship projects, the importance of FRPs is apparent in their market development. The market of glass fiber reinforced thermosetting plastic, for example, develops with the real Gross Domestic Product (GDP) of the European Union [9]. This correlation with the GDP shows a wide use of these materials.

[1] Airbus estimates a growth from 19,800 passenger aircrafts in 2018 (> 100 seats) to 45,300 in 2037; Boeing estimates by a growth of their overall fleet—including freighters—from 24,400 in 2017 to 49,500 in 2037

Consequently, accompanying the wide propagation of composite materials and increasing market volume, new manufacturing technologies are developed. A step that commonly takes up a big share in the production time of composite materials—provided that the load carrying fibers get embedded in a thermosetting plastic matrix—is the curing of this matrix [10]–[13]. The application of high temperatures for long times—often above 140 °C and several hours for aviation applications—is very time and energy consuming. New manufacturing technologies, therefore, often aim to reduce the cure cycle time and energy consumption. One concept to increase heat-up efficiency can be found in virtually every kitchen. Here, microwaves are used to heat food faster than can be done using hotplates or ovens. Electromagnetic waves—microwaves—penetrate the material and interact with it; this heats the materials surface and core. This enables for homogeneous in-depth heating which might be used for the cure of composite materials. Accordingly, research has been done in the field of 2.45 GHz microwave processing of composites. Starting in the 90s, the basic feasibility on a laboratory scale has been proven. In 2005 the next step was taken; a new industrial microwave system called "Hephaistos" was introduced [14]. Since then, a platform existed that enables the flexible microwave cure of composites on industrial scale. Several studies using it showed a potential of 38%–50% cycle time reduction in combination with huge energy savings [15]–[18]. However, most companies involved in publicly funded studies (compare [18], [19]) did not invest further in the use of this promising technology. Only one participant, GKN Aerospace, conducted further studies and advanced the processing of CFRP. GKN, however, worked behind closed doors and gave only very slight insights in some talks [20]–[22]. To the author's best knowledge, GKN stopped their development within 2018 due to reasons not directly related to the microwave technology.

Now, why are the promising results of 50% cycle time reduction not followed up upon? A reason for the hesitant reaction to microwave processing may be found in the companies planning horizon. 66% of the participants of the German Forel study of 2018 [23] stated that they estimate the readiness of a technology on the question if it can be used for the next product or earlier. Only 20% of the participants have a longer planning horizon for decision making. With this planning horizon and past developments in mind, the technology readiness level (TRL) (compare Fig. 1-1) of microwave processing will discussed in the next section. From this discussion, the field of action and research questions are derived.

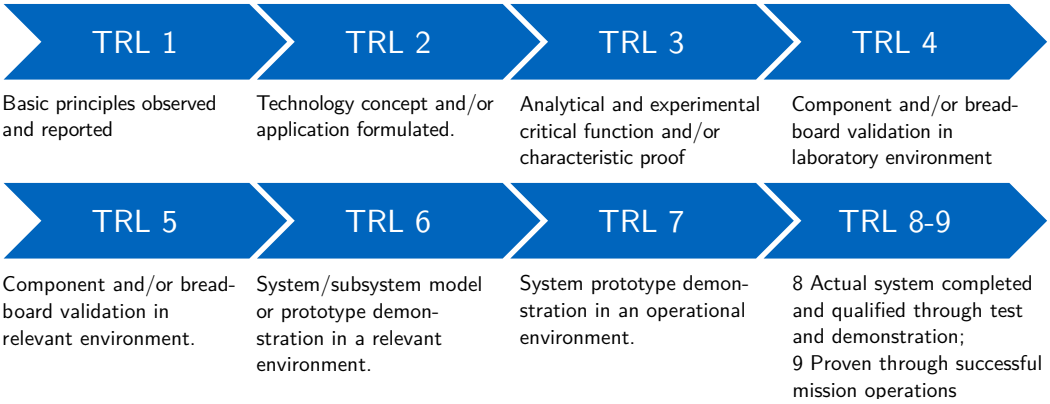

Fig. 1-1 Technology readiness level definition by the U.S. Department of Defense [24].

1.2 Technology Readiness Level Evaluation of Microwave Processing

Jamier, Irvine, and Aucher state that a simple TRL model like in Fig. 1-1 "... has various limitations. One of which is the oversight of the inherent nature of setbacks in the process of technology maturity."[25] They consequently propose a 2-dimensional TRL approach that is shortly introduced. The approach will then be used for the TRL evaluation of microwave processing from which the research questions will be derived. The basic concept of the model, which is named "*Leitat* Technology Readiness Pathway" after their founders' company, is the mapping of the TRL to several stages, compare Fig. 1-2. When developing the next stage, it

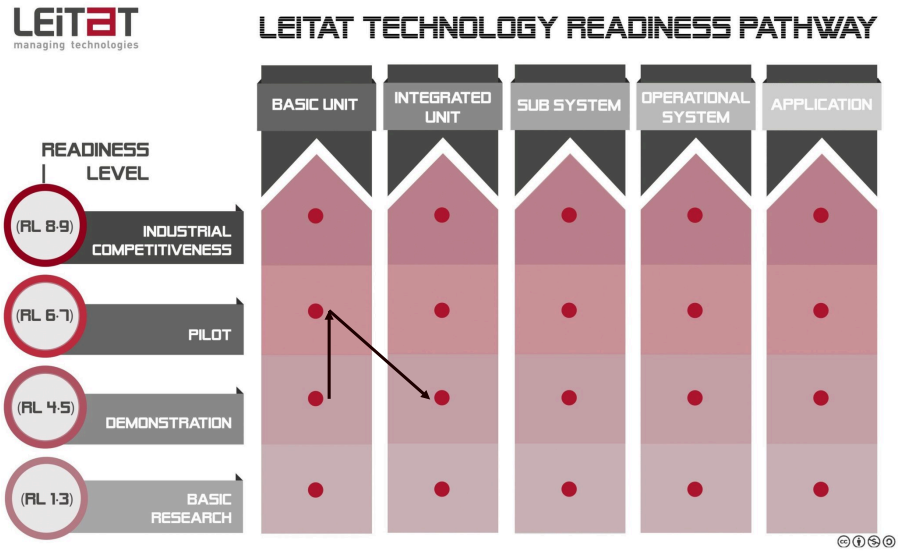

Fig. 1-2 2-dimensional Leitat model to map complex technology readiness levels.[25]

might be necessary to take a step back in the TRL. Jamier, Irvine, and Aucher give the example of up-scaling a material production after material development.

The material was validated at pilot level 6–7. The up-scaled manufacturing process, however, starts at the demonstration level TRL 4. This step back in TRL is mapped on the horizontal axis. This method is adapted and used for the following TRL evaluation[2] of microwave processing.

As with the Leitat model, different areas of microwave processing are rated separately and their TRL put next to each other. The following areas will be used for the TRL evaluation:

Microwave Cure the basic concept of microwave heating.

Industrial Equipment the development of flexible and industrial sized equipment.

Absorber Technology microwave absorbing auxiliary to control heating.

Process Control influence of process settings and environment.

Tooling Technology microwave compatible and adapted tools.

Part Manufacturing composite parts at different levels of complexity.

The first identified stage, the validation whether microwave cure of composites is feasible, has been investigated and demonstrated at laboratory level. The basic mechanism of microwave cure, therefore, is classified as TRL 4. As second stage, flexible equipment was developed for an industrial scale. Starting from first theoretical investigations, laboratory setups, and the experimental proof [26], [27] (TRL 1–3) the development went on up to the industrial "Hephaistos" equipment [14]. This system has been validated in laboratory environment over the last years at different institutes [16]–[18]. Due to no demonstration in an industry environment, the equipment is classified as TRL 4 for composite applications. The classification of the next four areas must be done on the basis of two different development branches—a public Ph.D. thesis and the developments of GKN Aerospace. Both were founded in a publicly funded project using the "Hephaistos" equipment [19]. Even so, only the first branch is publicly available and can freely be developed further. Since nevertheless both branches exist, they are both discussed to determine the TRL at the beginning of this dissertation, compare Fig. 1-3.

The first public branch lead to Fabrice Gaille's Ph.D. thesis [16]. Within the publicly funded project, absorber material's were investigated. The investigations stopped as an available material that suited the basic requirements was found. This material was then used by Gaille to manufacture flat CFRP specimens on different tooling materials. Metallic tools were identified as the only suitable option for tooling. In regard to TRL evaluation, an absorber was found and its basic us-

[2]The original approach and the adaptations made are licensed under the Creative Commons Attribution-NonCommercial-ShareAlike 4.0 International License as marked by

ability experimentally proven leading to TRL 3. Consequently, simple plates were manufactured without any geometrical variance. Both tooling technology and part manufacturing are classified as TRL 3, compare Fig. 1-3. The influence of process settings and environment was not investigated or documented by Gaille.

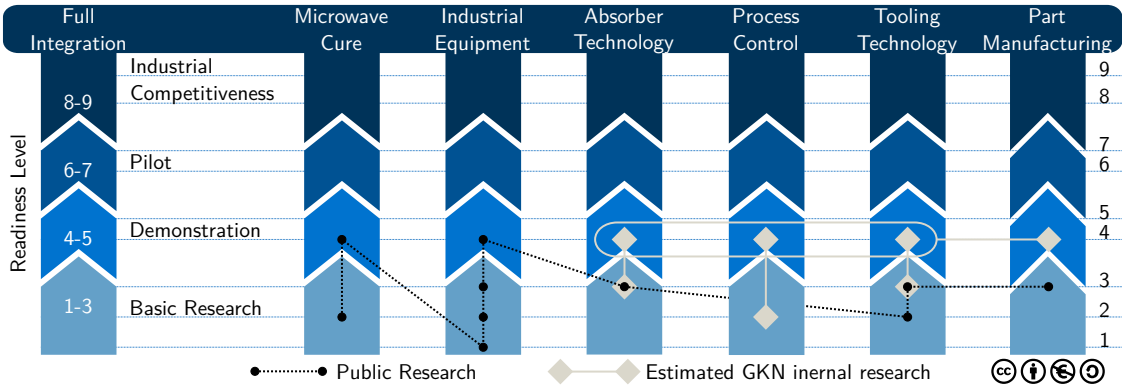

Fig. 1-3 Technology readiness level estimation of microwave sub-systems based on the Leitat Technology Readiness Pathway [25].

The second branch was followed by GKN Aerospace. Only vague information is available on the company's internal and proprietary investigations [20]–[22], [28]. The central outcome that can be assessed is the successful cure of geometrical complex CFRP parts. According to information voiced during a presentation they contain metallic inserts as well as sandwich areas [22]. The parts were manufactured using CFRP tools. Judging from the parts' complexity it is estimated that good progress was made in all three areas of absorber technology, process control, and tooling technology. Since GKN worked in a laboratory environment, they are estimated to have reached TRL 4 within all areas as depicted in Fig. 1-3.

1.3 Motivation and Definition of Research Questions

The TRL definition of section 1.2 is currently set by two technical developments that have one substantial difference. On the one hand, Gaille states that only highly thermal conductive metal tools are feasible to produce simple plates. On the other hand, GKN manufactures complex parts using CFRP tools that have a low thermal conductivity. This dissent comes from different development stages and viewpoints on absorber technology and process control. It shows, that by neglecting certain points—absorber technology and process control—, different findings may be the outcome. The research in this thesis is motivated by the resulting insight that all areas of the complex microwave processing must be taken into account. Consequently, its overall goal is to provide a new and solid

foundation for further developments and to improve the TRL if possible. This leads to the following four research questions out of three microwave sub-systems.

1. Research Question—Process Control
What is the relationship between available process control mechanisms and the processability of a material using microwaves in a practical use case?

2. Research Question—Process Control
How do certain universal process control mechanisms influence the temperature distribution in processed materials?

3. Research Question—Absorber Technology
What are the effects of different additives on the dielectric properties i.e. microwave absorption of an epoxy resin?

4. Research Question—Part Manufacturing
Does microwave processing of GFRP samples using a microwave optimized setup influence the properties of the material?

1.4 Outline of the Thesis

This thesis is structured in 5 content-related chapters (2–6) and the summary.

First, the state of the art is presented in chapter 2 . The fundamentals of microwave processing are explained before relevant literature is summed-up. The sum-up focuses on microwave equipment used in publications and on the mechanical properties of microwave processed epoxies and epoxy composites. Finally, tooling for microwave processing and absorber materials are discussed.

The third chapter presents the equipment, procedures, and materials used in this study.

Chapter 4 deals with the first two research questions in three steps. First, the Hephaistos equipment is described in detail. Adaptations to the equipment necessary to increase processability of composites are introduced. The second part of Chapter 4 describes the set-up and evaluation of an investigation to quantify the influence of these adaptations and further process control mechanisms. Last, lessons learned during the manufacturing trials of this thesis are documented to note down the progress made.

Following this, the principal idea and results of a concept study for an adaptable microwave absorber are presented in chapter 5. The study's setup is explained including the amount of additives and sample configurations used on the basis of

a statistical experiments. Subsequently, the evaluation of measurements is done starting with an investigation of errors and interpretation of the raw-data. The chapter ends with the development of an absorber model and thus answering research question 3.

Chapter 6 presents the results of a study comparing the mechanical properties of oven and microwave processed GFRP samples. Temperature controlled cure cycles and optimized processes are used to guarantee a one-to-one comparison of the heating technologies. The results of glass transition temperature (T_g), inter-laminar shear strength (ILSS), and 4-point bending (4-pt) investigations are presented and discussed to handle research question 4.

The thesis closes with an overall summary, the conclusions, and recommendations for further developments. The answers to the research questions are summarized, the development in TRL is presented, and possible further steps are addressed.

2 State of the Art

2.1 Fundamentals of Microwave Processing

2.1.1 Principal of Microwave Matter Interaction

In literature, different approaches are made to make the principle of microwave matter interaction understandable. Here, however, the needed information are presented to give the right context in an easy to understand manner. Fundamentally, the behavior of electromagnetic waves and their ways to interact with materials can be described by the Maxwell equations and the appropriate boundary conditions. For this, Roger Meredith gives a very understandable description using an electric capacity in his *Engineers' handbook of industrial microwave heating* [29] based on his work with Metaxas in their book *Industrial Microwave heating* [30]. Starting on the description of the electric and magnetic field by using a capacitor and electrical circuits, the Maxwell equations are used to lead over to the definition of electromagnetic waves. Important to know is, that microwaves are electromagnetic waves of a certain wavelength range between 1 m and 1 mm. With regards to microwaves—independent of the physics behind electromagnetic waves in general—the first things to know are

- that microwaves propagate in one direction,
- that they are defined by an exchange of electric (E) and magnetic (H) fields,
- and that the direction of propagation, the electric field, and the magnetic field are perpendicular to each other (Fig. 2-1).

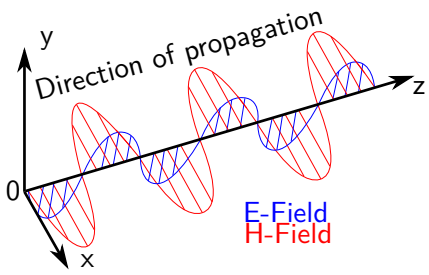

Fig. 2-1 Representation of an electromagnetic wave.

Consequently, the power flow of a electromagnetic field is in propagation direction. The energy transferred by an electromagnetic field per unit area and unit time, or its intensity, is called the energy flux density (p) having the unit $\mathrm{W/m^2}$. It is the vector cross product between the electric (E) and magnetic (H) field

$$p = E \times H. \tag{2-1}$$

If an electromagnetic wave hits a material, the microwaves interact with it. The energy of the wave is partially reflected, absorbed, or transmitted [31]. Transmission takes place if the radiation is not fully absorbed or reflected. The amount of energy absorbed by dielectric materials mainly depends on their complex relative permittivity

$$\varepsilon_r^* = \varepsilon_r' - j\varepsilon_r''. \tag{2-2}$$

The real part of the permittivity ε_r' represents the capability to store electromagnetic energy whereas the loss factor ε_r'' mainly dominates the energy dissipation. Both, $\varepsilon_r'$and ε_r'', depend not only on the microwave frequency and material temperature but also on moisture content, physical state, and composition. The permittivity and loss factor are useful to determine the possible power (p) that is dissipated per volume (Ad) in a workload by the dielectric heating equation from [29]

$$p = 2\pi f \varepsilon_0 \varepsilon_r'' E_i^2. \tag{2-3}$$

The inner electric field E_i depends on the permittivity and the orientation of the E-field vector to the surface of the dielectric. Depending on the E-field's orientation, it is in the range of $1 < E_{ext}/E_i < \varepsilon_r'$; the frequency f will in most cases be set and cannot be varied in most industrial setups. The normalized power-dissipation in a thin layer of 1 mm is visualized in Fig. 2-2 under the simplification of $E_i = E_{ext}/\varepsilon_r'$ and a 2.45 GHz setup. It can be seen, that any increase in the loss factor having constant permittivity increases power-dissipation. An increase in the permittivity having a constant E_{ext} and loss factor decreases the dissipated power.

A further item to comprehend the influence of complex relative permittivity is the penetration depth (D_p) into the material

$$D_p = \frac{\lambda_0}{2\pi\sqrt{2\varepsilon_r'}} \frac{1}{\sqrt{\left(1 + \left(\frac{\varepsilon_r''}{\varepsilon_r'}\right)^2\right)^{0.5} - 1}}, \tag{2-4}$$

where λ_0 is the wavelength of the electromagnetic wave in vacuum. This penetration

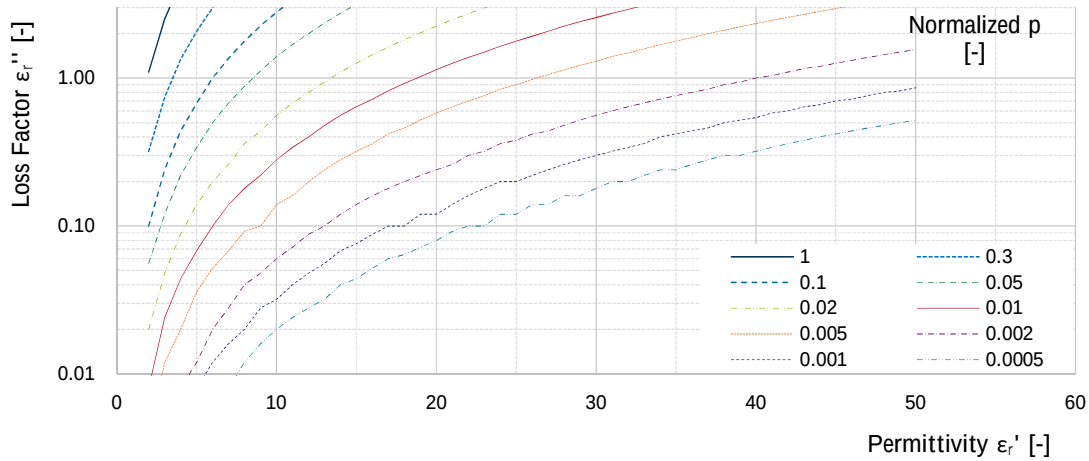

Fig. 2-2 Power dissipation over different ε_r' and loss factor ε_r'' using $E_i = E_{ext}/\varepsilon_r'$. Power-dissipation normalized for the highest value. Steps and notches are of numerical nature due to increments.

depth is defined as the depth into a material at which the power flux has fallen to e^{-1} of its surface value [29], [30]. On the one hand, D_p gives a good first impression how much energy may be transferred through a material if it is not the main material to be heated i.e. a tool or an auxiliary. Low losses and reflections occur in a media having high D_p. On the other hand, for a material that has a D_p that is in the range of the material's thickness, the variation of power dissipated throughout the material may negatively influence the in-depth heat distribution for materials that have low thermal conductivity. Fig. 2-3 shows graphs of varying penetration depths in dependence of the permittivity and loss factor. When one of the factors is held constant, a clear decrease in penetration depth can be seen for a rising loss factor while a rising permittivity slightly increases D_p.

In addition to the penetration depth the loss tangent or dissipation factor

$$\tan(\delta) = \frac{\varepsilon_r''}{\varepsilon_r'} \tag{2-5}$$

is often used to judge and compare materials in regard to their ability to convert electromagnetic energy into heat. It clarifies that $\varepsilon_r'$and $\varepsilon_r''$are both necessary and must have a certain ratio for effective heating.

What is most important to keep in mind however, is that both, the permittivity and loss factor, vary over temperature. Through this, the heat-up characteristic may change during a process and may be different for areas of an object with temperature inhomogeneities. For example, DGEBA—a epoxy component—changes its permittivity from 4 to 5.6 between 20 °C and 200 °C. In the same temperature range, its loss factor ε_r'' varies between 0.7 and 1.7 [19], compare Fig. 2-4.

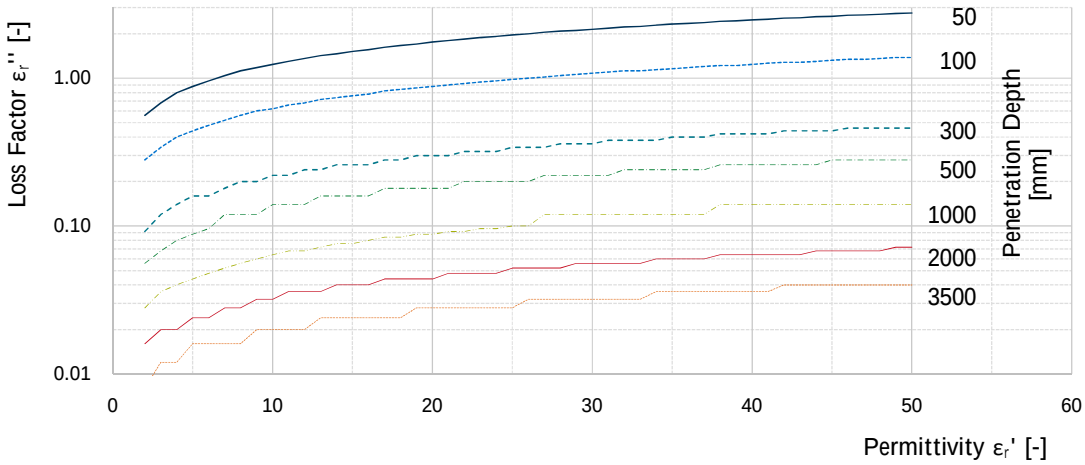

Fig. 2-3 Variation of penetration depths in dependence of permittivity ε_r' and loss factor ε_r''. Steps and notches are of numerical nature due to increments.

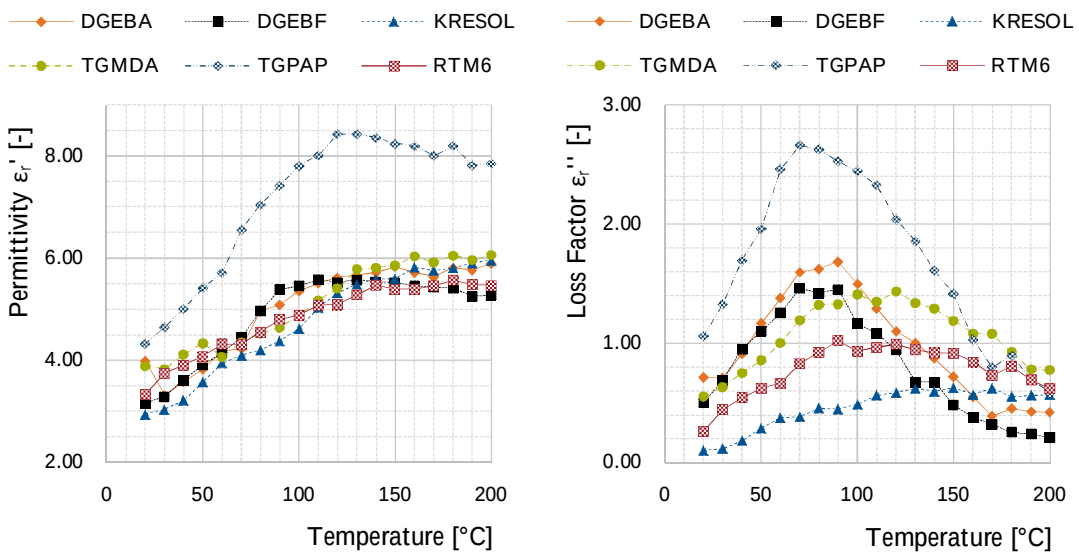

Fig. 2-4 Examples of temperature dependence of ε_r' and ε_r'' of different resins. (Data from [19])

For the reader more interested in the physical background, an extended description of the microwave matter interaction can be found in Thostensons's paper "Microwave processing: fundamentals and applications" [31] and Mathias Meyer's PhD thesis "Herstellung von Kohlenstofffaserverstärken Kunststoffbauteilen mit Hilfe von Mikrowellen" [15]. In these works, the microwave interaction and heating based on the molecule build-up and with reference to the relexation times are described. Similar in-depth knowledge is given in Meredith's "Engineer's Handbook of Industrial Microwave Heating" [29] and in Metaxas's "Foundations of Electroheat".

2.1.2 Methods of Microwave Generation and Transmission

Microwaves are generated by vacuum electronic tubes, mostly in form of klystrons, traveling wave tubes, or magnetrons. In this work, as well as in domestic microwaves, a magnetron is used to generate the electromagnetic waves. A magnetron is a vacuum tube with a simple build-up and mode of operation. The outer border of the magnetron is an anode formed as a circular cavity resonator. In the resonator's center an electron emitting hot cathode is placed; a magnetic field is aligned axial through the cavity, see Fig. 2-5. When a high DC-voltage is applied to anode and cathode of the magnetron, electrons that flow from cathode to anode are deflected by the magnetic field due to the Lorentz force; the electrons spiral outwards. By passing the resonant cavities, the electrons induce an electromagnetic high-frequency field. The geometry of the resonant cavities—and thus the magnetron geometry—defines the frequency of the electromagnetic field. Through an output coupling loop this alternating electric field is emitted.

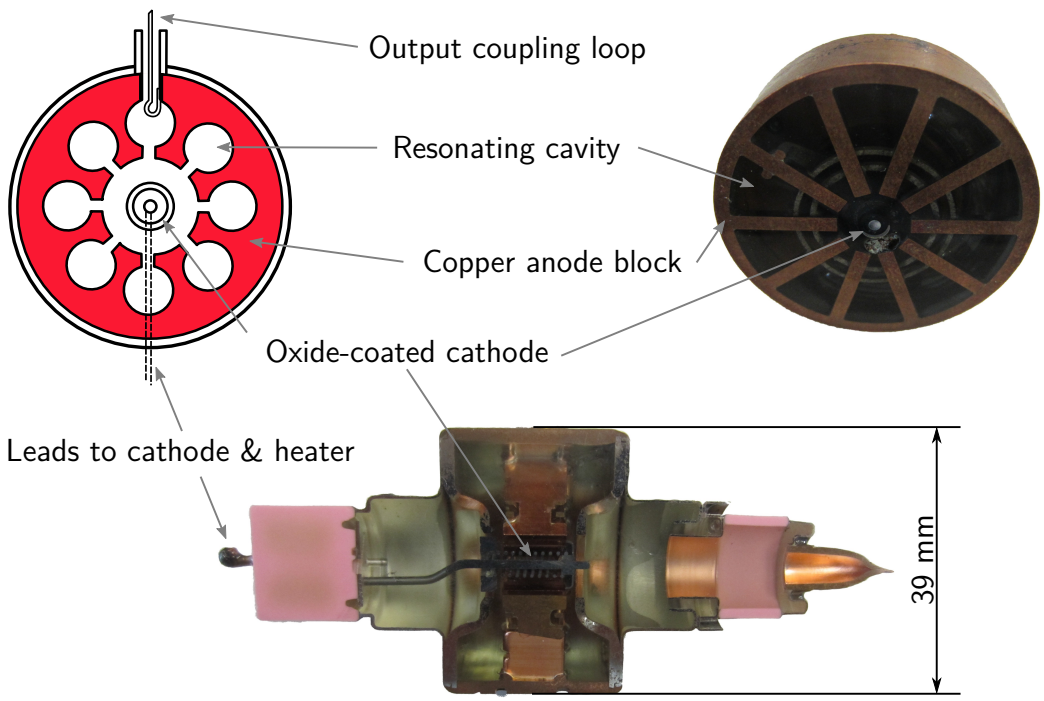

Fig. 2-5 Magnetron of a domestic microwave and function principal (Without magnets, heat sink, and other attachments). (Schematic by Ian Dunster [32][1]; photographs provided by Volker Nuß, KIT)

[1]Original figures made available under Creative Commons Share alike 3.0 and 2.0at. Composition by Daniel Teufl under CC Attribution-ShareAlike 4.0 International License (`https://creativecommons.org/licenses/by-sa/4.0/`)

The frequency of the emitted electromagnetic waves is a consequence of the magnetron's geometry. Thus, the frequency and the magnetron size are connected; higher frequencies result in smaller magnetrons. This, in combination with the standardized ISM bands[2] of 915 MHz, 2.45 GHz, and 5.8 GHz, leads to a wide spread use of 2.45 GHz magnetrons in domestic microwave applicators. With a tube diameter of about 4 cm these 2.45 GHz magnetrons

- can be cooled easily compared to smaller 5.8 GHz magnetrons.
- can be build into relatively small equipment compared to bigger 915 MHz magnetrons.
- have comparatively low manufacturing costs.

The first two factors and the good suitability of 2.45 GHz microwaves for heating dishes lead to the wide spread use of magnetrons in domestic microwaves. Through this, they are widely available at low cost. They must, however, be hand-picked to meet industrial requirements[3]. Apart from other restrictions, industrial microwave can be a comparably low cost equipment.

2.1.3 Microwave Applicator Design Principals

A lot of information regarding an optimized microwave applicator design can be found in Roger Meredith's "Engineers Handbook of Industrial Microwave Heating"[29]. The figure of merit (FoM), for example, can be seen as abstract number that describes the quality i.e. homogeneity of a microwave applicator. It is higher if more modes have a resonant frequency within a specified bandwidth of the applicator. These modes are influenced by several factors like the applicators size, geometry, the workload processed, and metallic hardware inside the applicator. A further ratio describing the number of possible modes i.e. resulting homogeneity is the Q-factor. The Q-factor takes the workload into account. An approximation of the Q-Factor given by Metaxas and Meredith [30] for a spherical load is

$$Q = \frac{\varepsilon_r'}{\varepsilon_r''}\left(1 + \frac{(\varepsilon_r' + 2)^2}{9\varepsilon_r'}\left(\frac{1-v}{v}\right)\right) \tag{2-6}$$

where v is the volume filling factor $\frac{\text{load-volume}}{\text{cavity-volume}}$. The calculation of the FoM or the Q-Factor are not feasible for huge, complex applicators using several sources and complex loads like used in this study. However, an analytical approach of Guido Link and Vasileios Ramopoulos to quantify the system efficiency and its correlations to applicator size, microwave coupling as well as dielectric properties and

[2]industrial, scientific and medical radio bands
[3]According to a remark of Stefan Betz, *Vötsch Industrietechnik*, November 2018

size of materials to be processed is recommended [33] at this place. The following implications—derived and simplified by the given works—are relevant for basic microwave processing. They can be seen as important for a homogeneous electric field with wide spread modes, good temperature distribution, and an efficient process:

1. a mismatch between applicator and workload size should be avoided
   workload-size $\not\ll$ applicator
2. a mismatch between the applicator loss and workload loss—as might be described by their Q—should be avoided
   workload loss $\not< $ applicator loss
3. metallic hardware has a significant influence on the electric field distribution

These three rules are strong simplifications for the ease of understanding. However, they do interact and do not include all circumstances. For example, a small workload with high losses might be processed in a huge applicator. Likewise, high applicator losses compared to the workload loss primarily lower the efficiency but the process might, nevertheless, be suitable.

2.2 Microwave Facilities used in Composite Research

In the published research since 1990 different microwave facilities have been used. To discuss the relevance of these, three categories are introduced:

domestic and modified domestic microwaves Equipment that is originally designed for domestic applications i.e. food.

custom laboratory build-ups and laboratory equipment Equipment that is build-up of components for scientific purposes or has a limited size that enables mostly laboratory use.

industrial sized equipment Equipment that has the size and theoretical capabilities for industrial manufacturing of composite parts of at least $500 \times 500 \times 500\,\mathrm{mm}^3$.

The following sections introduce these three categories and present the according literature.

2.2.1 Domestic Microwaves

In domestic microwaves the electromagnetic waves are generated by one magnetron and fed into the multimode chamber. Due to the simple setup, three drawbacks occur. First, the chamber is designed for cooking. Consequently, there is only a

small size variation between different models. Due to the small size only a limited amount of modes is possible; a distinct field pattern exists. This is confirmed by statements of Wallace, Attwod and Day [34] and Tanrattanakul and Jaroendee [35]. To overcome this first drawback, many domestic microwaves are equipped with a revolving turntable that moves the load through the pattern. This mechanic namely was used by Boey and Lee [36] and by Nightingale and Day [37], [38]. The second disadvantage of domestic microwaves is their power output control. In general, the power output is controlled using a pulsed operation: for example, to reduce the microwave power from 1000 W to 500 Watt the on-time of the magnetron is halved. This behavior is explicitly documented and reported by Nightingale and Day [37], [38] and by Tanrattanakul and Jaroendee [35]. This pulsed operation, however, only reduces the absolute energy over a longer process. The power level and thus electromagnetic field strength during the on time is constant and very high. In Nightingales and Days publication of 2002 they report "A vaccuum bag arrangement could not be used for the full microwave curing process because the presence of the carbon fibres caused a spark as soon as the power was switched on". The occurrence of the described arcs are a result of a voltage breakdown that is a result of high local field strengths—as consequence of the high power level. Using pulsed operation, this effect occurs independent from the applied power as the temporary field is always at its maximum level. Tanrattanakul remarks on the last problem using domestic microwaves. As he writes: "In this work, the applied power was based on physical performance and mechanical properties of cured samples. No air bubbles and no burning were criteria for good performance specimens."[35], [39] This shows, that, since the power can only be set—but not controlled—the process must be defined indirectly. The material is heated at a set level for a set time and the result is investigated. Through this, the process can hardly be compared to regular, temperature controlled, curing processes. Noteworthy is a novel approach by Wallace, Attwood, Day, and Frank to restrict the power output and thus behavior of domestic microwaves in 2006 [34]. By introducing a capacitor between transformer and magnetron they reduced the power output of the magnetron. They restricted the temporary field in its maximum level. They than used an additional and well known—but not commonly documented—trick to reduce the power input into the sample: they introduced a 1% sodium chloride solution in water into the microwave. This solution absorbs some energy and again reduces the energy input into the sample. The quality and simultaneously the field strength of the system is reduced. While this reduces negative effects like potential arcing, the system's overall efficiency is reduced.

2.2.2 Custom Laboratory Build-Ups and Laboratory Equipment

The custom laboratory build-ups are less similar in their appearance and behavior than domestic microwaves. Consequently, they will be discussed separately. First, comparably to the previously described domestic microwaves—and thus sharing all their drawbacks—, a $200\times200\times200\,\mathrm{mm}^3$ chamber that has one 500 W magnetron in pulsed operation is used by Boey and Lee [40], by Boey and Yue [41], and by Yue and Looi[42] between 1990 and 1995. For the second equipment, no size or power is given by Bai, Djafari, Andréani, and François in [43]. It can be assumed that Bai et al. used the same setup as depicted in another study of Bai and Djafari published also in 1995 [44]. In the latter study, a specimen size of up to $250\times36\times3\,\mathrm{mm}^3$ is given for microwave samples. Due to the higher width of 180 mm for thermally cured samples and the depicted experimental device, it is possible that the samples were cured in a waveguide applicator. Whether the depicted device has less or more drawbacks than domestic microwaves cannot be said. The applicator's behavior is not discusses by the authors. Third, a multi mode stainless steel cavity with a dimension of $300\times298\times202$ mm was used by Boey, Yap, and Chia [45] and by Boey and Yap [46] to cure pure resins. Connected to the steel cavity, a 2.45 GHz magnetron powered by a variable power D.C. generated up to 1.26 kW. Through this variable power D.C. a constant and lower electric field can be generated. This negates one major drawback of domestic microwaves. However, no temperature control was implemented and the process only rated by the downstream sample measurements.

An interesting custom setup using a rotary device is used to manufacture samples of $260\times80\times3\,\mathrm{mm}^3$ in a PTFE mold in two further studies. It is used by Rao R., Rao S., and Sridhara [47] and by Mooteri, Sridhara, Rao S., Prakash, and Rao R. [48] in their 2006 publications. They describe the equipment as "custom-designed, multi-mode, microwave cure equipment with suitable positioning of multiple magnetrons" and give a maximum power of 2.4 kW. The used power supply, however, is not mentioned. Rao's description of two processes—one continuous and one pulsed—allows for two interpretations. On the one hand, switching power supplies could be used; they enable to control the microwave power output without pulsing. This would allow for a continuous process in a wide range. On the other hand, if three or more magnetrons are built-in, the continuous process could have been done using only one or two magnetrons. Summarizing, Rao's and Mooteri's equipment sets itself apart from the other custom build-ups by three points: sophisticated rotary device, multiple magnetrons, and a possible power control using switching power supplies.

A likewise unique equipment is described in two other publications; a microwave heating equipment using a network analyzer and frequencies of 4–8 GHz. This setup

was used by Yusoff for his thesis published in 2004 [49] and Papargyris, Day, Nesbite, and Bakavos for a paper published in 2008 [50]. With help of a traveling wave tube amplifier, up to 250 W output power were fed into a multi mode microwave applicator in form of a brass cavity. A PTFE mold inside the brass cavity was used by Yusoff, a mold out of a machinable "Macor" ceramic was used by Papargyris. The samples of $300/200 \times 200 \times 3\,\mathrm{mm}^3$ were cured with help of a simple closed loop temperature control. Furthermore, the frequency applied was adapted to the load through the network analyzer. Both, the closed loop control and the adaption of the frequency can be seen as beneficial for the temperature control and homogeneity. However, the described setup can hardly be used for industrial purposes for three reasons. First, a single network analyzer alone costs above ten thousand Euro. Second, not all frequencies used are part of the industrial, scientific and medical (ISM) radio bands. Last, the available power of a network analyzer in combination with an amplifier is not enough for big parts and high temperatures.

An interesting study published in 2020 by Guan et al. presents a microwave system that is introduced into an autoclave[51]. The equipment is used to manufacture $20 \times 20\,\mathrm{cm}^2$ carbon fiber-reinforced plastic (CFRP) samples using 0–4000 W. A single channel optical fiber fluorescence temperature measurement system in combination with a closed loop control is used for process control. According to the authors "Microwaves were introduced into four longitudinally distributed microwave transmission channels [...] through the slot antenna [...], and a uniform electric field was formed in the microwave cavity." However, no information with respect to the temperature homogeneity inside the test samples is given.

The four last laboratory microwaves, compare Fig. 2-6, might even be used for industrial production. They have temperature controllers and magnetron configurations adequate to design industrial microwave cure processes. However, all four have a limited size. The equipment used by Thostensons and Chou [52] has a volume of $0.5\,\mathrm{m}^3$ and a power of 0–6 kW that "can be varied continuously"; whether this is achieved by pulsing or variable power supplies is not specified. An equipment of similar size was used by Meyer [15] and Danilov [53] in their theses. While both do not give the equipment's size, Danilov state's he used a microwave by Fricke & Malla. A Fricke & Malla equipment—that equals a schematic given by Meyer—is depicted on the research institute's website [54]. Consequently, the depicted microwave most certainly was used by Meyer and Danilov. It is estimated to have a volume of about $0.512\,\mathrm{m}^3$ ($3 \times 0.8\,\mathrm{m}$), compare Fig. 2-6 (3). According to Meyer's thesis the equipment contains a pyrometer and a fiber optical sensor for temperature measurements. The microwaves are generated by at least tow mag-

[4]Figure from Nanjing Sanle Group Co., `http://www.sanlemicrowave.com/Files/20140317102118_8964.jpg`, visited 01. August 2018

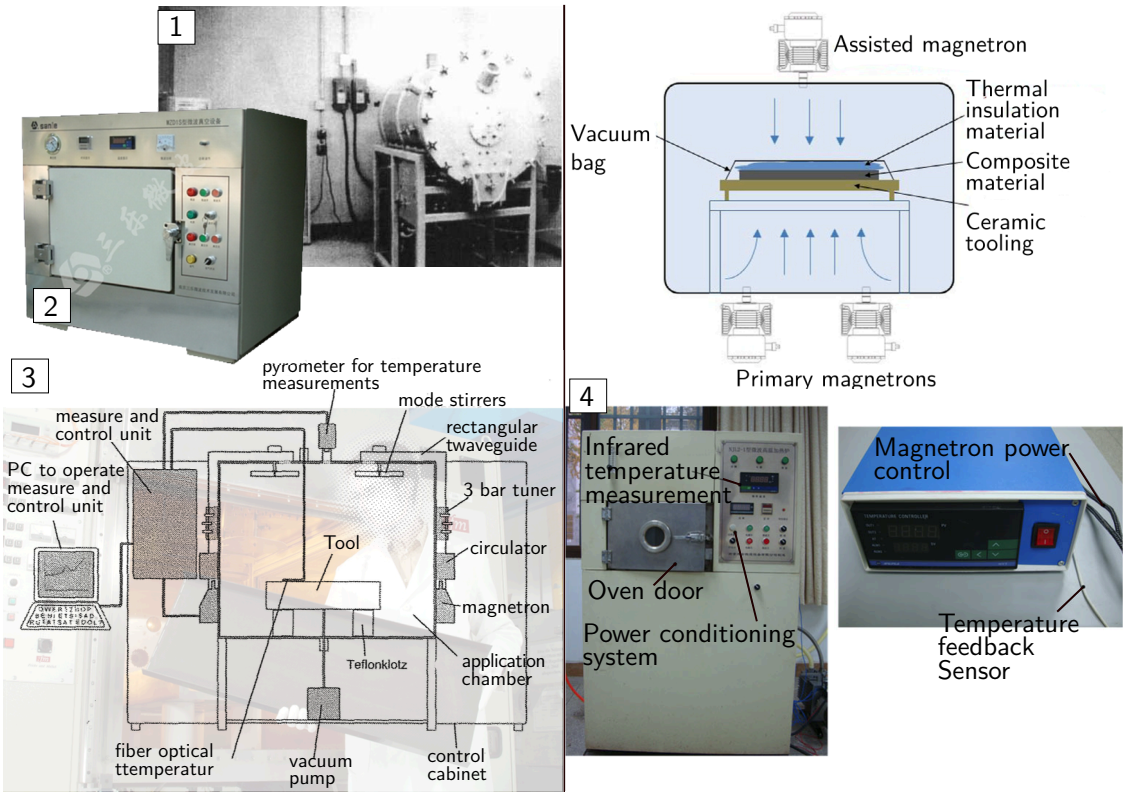

Fig. 2-6 Laboratory microwaves used in different studies. **(1)** by Thostenson and Chou in 2001 [52]; **(2)**[4]by Xu et al. in 2016 [55]–[57]; **(3)** by Meyer in his thesis 2007 [15] with underlay of [54] (and potentially Danilov in 2013 [53]); **(4)** by Li N. et al. in 2014 [58], [59].

netrons with circulators and 3 bar tuners. Two mode stirrers and a measure and control unit guarantee a homogeneous field and temperature distribution. The third "microwave oven" used by Li N., Li Y., Hang, and Gao [58] and by Li Y., Li N., and Gao [59] to manufacture $10\times10\,\mathrm{cm}^2$ samples has a power of 0–2.4 kW. The microwaves are generated by three magnetrons with variable power output. Last, a WZD1S-03 industrial microwave oven by Nanjing Sanle Microwave Technology (1 kW, variable power) is used in three studies. One by Xu, Wang Xi., Wei, and Du [57], another by Xu, Wang Xi., Cai, Wang Xu, Wei, and Du [56], and the last by Xu, Wang Xi., Liu, Zhang, Li Z., and Du [55]. Like the prior equipment used by Li, it has a very small size of $360\times360\times270\,\mathrm{mm}^3$ comparable to domestic equipment.

2.2.3 Industrial Sized Equipment

There are reports of four different industrial sized microwave types designed for the manufacturing of composite materials between 2007 and 2020, see Fig. 2-7.

The first industrial equipment—a microwave autoclave—is mentioned by Meyer in his thesis [15] and was patented by Binder, Graeber, and him [60]. Since 2016 the

patent is lapsed. Meyer describes an autoclave with a diameter of 2 m and 24 microwave sources that are distributed equally around the equipment's circumference. It is stated that pretrials using a microwave segment (orig. "Mikrowellensegment") in an autoclave were done and no influence by the autoclave's pressure was seen. The microwave autoclave is further mentioned by Stroehlein et al. in 2007 [61]; by Herbeck, Podkorytov, and Stroehlein in 2008 [62]; and by Wiedman in 2009 [63]. Herbeck et al. specify the microwave autoclave with a diameter of 1.6 m, a length of 4 m, a conventional heating power of 231 kW, and 96 W microwave power. Most certainly, this represents four of the modules described by Meyer. In all publications, only references—but no data—to composites tested after cure with the microwave autoclave are given.

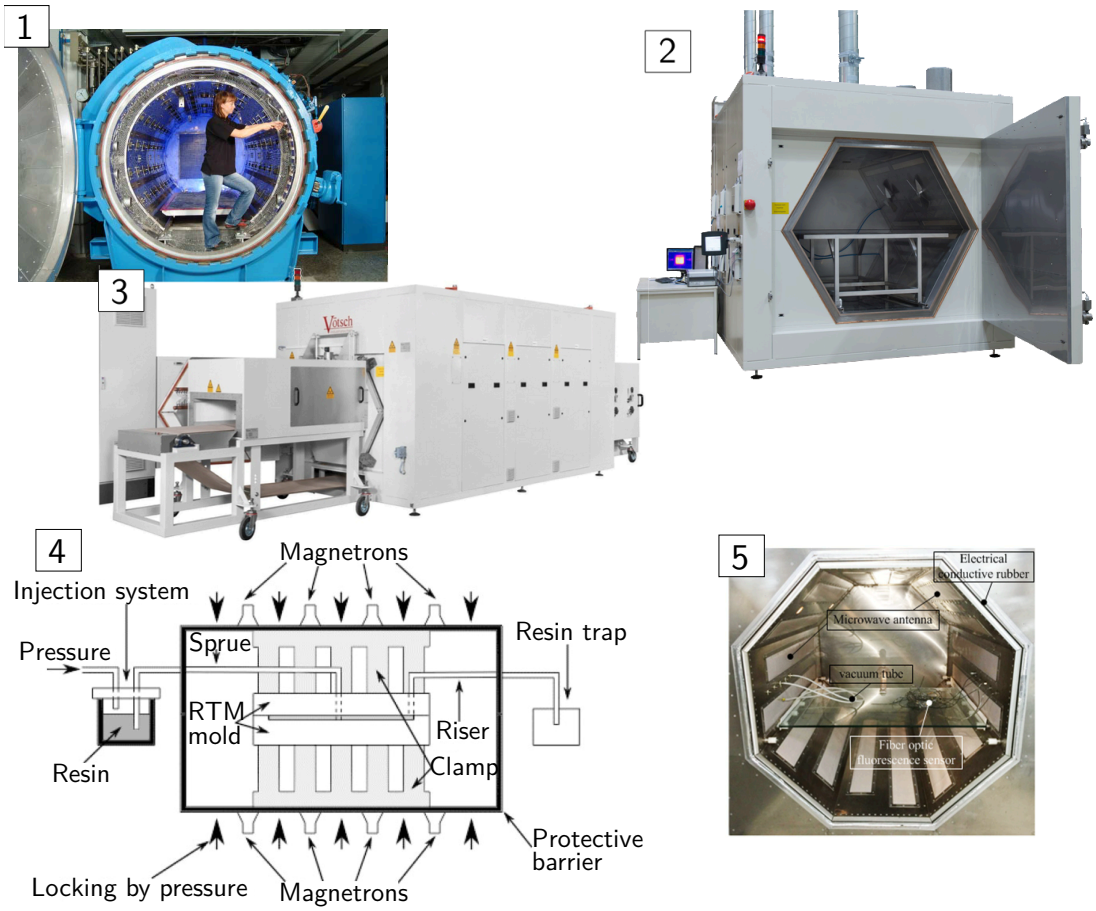

Fig. 2-7 Industrial sized microwaves used in publications. **(1)** microwave autoclave with 1.6 m diameter and 4 m depth[62]. **(2)** *Hephaistos* with 1.8 m diameter and 2 m depth. **(3)** hybrid *Hephaistos* with 1 m diameter, 3 m depth, and conveyer belt [18]. **(4)** Microwave press from Maenz [64]. **(5)** octahedron microwave designed by Li Nanya and follow researchers [65].

Up to 2014, since no data was published using the microwave autoclave, only investigations using different applicators from the *Hephaistos* system produced by Vötsch Industrietechnik (VIT) were published ([16]–[19], [21], [22], [66]–[74]). Apart from

Fabrice Gaille's and Kwak's Ph.D theses in 2012 and 2016 [16], [17] and a publication by Kwak, Robinson, Bismarck, and Wise [72], all of these publications were in form of conference presentations, project reports, and non-reviewed conference papers. The specialty of the *Hephaistos* microwaves is their hexagonal shape. This patented polygonal shape [75] increases the field homogeneity according to their developers [27], [76]. VIT currently produces this modular microwave system in two hexagonal sizes with 1 m and 1.8 m outer diameter. In depth, the microwave system consists of 1 m modules; each of this is equipped with up to 12 magnetrons. A hybrid microwave systems where the microwave chamber is build-up as a convection oven and equipped with 18×2 kW magnetrons using switching power supplies was build at the end of 2014 [18]. This hybrid system additionally was designed with exchangeable front/back openings for rotary or conveyer belt feed through systems, compare Fig. 2-7 middle left. Other *Hephaistos* systems with one module (12×0.85 kW) of 1 m diameter and two–three modules (24–36×0.85 kW) with 1.8 m diameter were used in the publications cited above. The principle of the modular polygonal microwave system is patented by the Karlsruher Institute of Technology (KIT) [75]. *Vötsch Industrietechnik* builds the equipment under license. It must be noted, that the *Hephaistos* system is still constantly improved by KIT and VIT. For example, in 2016 Yiming Sun (KIT) published his Ph.D. thesis "Adaptive and Intelligent Temperature Control of Microwave Heating Systems with Multiple Sources" that investigates predictive, neural network, and reinforcement learning control systems for the *Hephaistos* system. The investigated systems activate specific magnetrons for long periods with the aim to establish a more homogeneous temperature distribution. VIT has currently implemented one of these control systems into their internal testing equipment.

The next-to-last industrial microwave is a press system equipped with 30×0.85 kW magnetrons described by Maenz, Mühlstädt, Jandt, and Bossert [64] in 2015. The microwave chamber has a size of 1400×700×650 mm^3 with 15 magnetrons in each top and bottom. While "Each magnetron can be controlled independently", no special power supply is mentioned; a pulsed power control can be assumed. The microwave press system uses chalk filled PE clamps to transfer the force to the mold. The mold used, as stated by the author, is made from Ebalta ebaboard LX that degrades above 90 °C. Consequently, the setup in the presented study strongly limits the applications.

The last big microwave equipment is an octahedron microwave manufactured by a Chinese research team. The design follows KIT's patent used to build the *Hephaistos* system. The octahedron microwave is described in several papers by Li N., Li, Y. Hao, and Gao [65], by Zhou, Li Y., Li N., Hao, and Liu C. [77], and by Li N., Li Y., Jelonnek, Link, and Gao [78]. It has an absolute power of 0–20 kW

distributed over sixteen antennas. While no size of the octagon is given, an outer diameter slightly above 1 m can be estimated from Fig. 2-7 under the assumption that a visible antenna covers have a width of about 15 cm.

2.3 Properties of Microwave Processed Epoxies and Epoxy Composites

2.3.1 Glass Transition Temperature

The first resin property investigated after microwave cure was the glass transition temperature (T_g). The T_g varies with a polymer's chain length and structure; it gives an indication for the resin's degree of cure. It is, therefore, a good indicator for the influence of a process change on the cure of a resin or composite.

In 1990 Boey and Lee published results on the T_g after microwave cure in a letter [36]. They compared microwave cured samples of epoxy with an amine hardener to conventionally cured samples via the dynamic mechanical analysis (DMA). For two low microwave power settings, a T_g comparable and higher to the conventional T_g is reached; for the highest power settings a slightly lower T_g is reached. For a possible explanation Boey an Lee state "at this rating a sufficiently high temperature had been reached that gelation was achieved very quickly, and the gelled material in its rubbery state was thermally degraded to some extent before glass transition occurred." In 2001 Boey an Yap investigated the effect of three different amine curing agents 4,4´-diaminodiphenyl-sulfone (DDS), 4,4´-diaminodi- phenylmethane (DDM) and meta-phenylene diamine (mPDA) on the glass transition temperature [46]. For DDM and mPDA oven and microwave cure result in similar glass transition temperatures. For DDS the result was significantly lower. Boey and Yap attribute this to "the sluggish reaction of DDS with epoxy and hence the entrapment of the functional group in the crosslink network." In 2006, Wallace et al. published another work on a pure epoxy resin's T_g with an amine hardener [34]. The microwave cured samples show a T_g that is slightly above that of the thermal cured samples at the same degree of cure. In the investigated case, the difference in T_g is found in a more dominant epoxy amine reaction for microwave-cured samples; the network structure differs.

The T_g of glass fiber-reinforced plastic (GFRP) samples with amine curing epoxy system were investigated in two works in 2006: One by Mooteri et. al [48], the other by Rao R., Rao S., and Sridhara [47]. For both works the same microwave equipment containing a rotary mold is used. The temperature is logged during the process and the power profile defined by the composite temperature. Consequently, while

the power inputs of microwave processes are defined manually, they are designed to meet temperature profiles that can be seen as reasonable for the investigated resin systems. For this setup, Mooteri et al. get similiar T_gs for microwave and conventional cured samples; Rao et al.'s microwave samples have a slightly increased T_g. However, the highest temperature reached by Rao's microwave cure is ≈6 °C above the conventional cure temperature. A study published in 2017 by Colangelo, Russo, Cioffi, and Fraternali investigating the microwave cure of an amine hardening epoxy for civil applications, demonstrates that there is no significant difference in T_g as well [79].

CFRP samples using the same resin system as used by Rao et al. (*Araldite LY5052* with *Aradur HY5052*) were manufactured by Papargyris et. al using thermal and microwave resin transfer molding (RTM) [50]. The temperature controlled process resulted in no significant difference between the measured T_gs of microwave and conventional cured samples. However, a difference in the behavior at lower temperatures (-80 to -40 °C) is observed. This difference is attributed to an alteration in the cross-linking path. Unidirectional carbon prepreg samples manufactured using a Hephaistos system by Kwak et al. in 2011 yielded a T_g according to the manufacturer's datasheet[72]. In his thesis, Gaille compares CFRP samples with RTM6®, a pre-mixed epoxy amine resin system, cured in an oven with samples cured in a Hephaistos system [16]. The characterization using modular differential scanning calorimetry (MDSC) showed a lower curing percentage and, consequently, lower T_g for microwave cured samples. However, Gaille used higher heating rates for all microwave trials and shorter curing times for 2 out of 3 microwave processes. For the slightly lower T_g of the microwave cure cycle using the same cure time Gaille argues that the air in "the thermal oven stays warm after the process [...] at the cure temperature (180 °C). It implies that the resin continues to reticulate, [...]". The argument is valid and gives—especially in combination with the lower curing percentage—a reasonable explanation for the slight T_g difference. In a paper published in 2020 Guan et al. investigate CFRP prepreg samples cured at high pressures in an autoclave using a microwave insert [51]. For cure, they applied different temperature profiles with variations in heating rate, curing temperature, and holding time using the microwave. The differential scanning calorimetry (DSC) results of the different cure profiles are presented in form of the epoxy's degree of cure (DOC). Guat et al.'s only interested is in whether the DOC is above 95 %; this is achieved by all samples. In more detail, they measure a DOC of 98.86 % with a variance of 0.29 %. No direct comparison to a conventionally cured composite is made.

An epoxy system with a methylene hardener was investigated by Nightingale in her PhD thesis [37]. A comparison of conventional and microwave cured samples via

DMA showed similar T_g. Tanrattanakul and SaeTiaw, in 2005, published their work on the microwave influence on 8 anhydride cured epoxy resin systems [39]. In detail, one epoxy resin cured using two different anhydride hardeners and different accelerators was investigated—8 combinations in total. Furthermore, different amounts of accelerator combined with different curing times in oven and microwave are tested. While the oven temperature is set to 150 °C, the applied microwave power "was based on the physical performance of the cured samples. No air bubbles and no burning were criteria for good specimens." Consequently, the T_g values of oven and microwave cured samples are similar for some but not all configurations. The study yields no clear results. As Tanrattanakul and SaeTiaw state at one point in their paper, when remarking on the mechanical properties, "It is essential to design the optimal curing conditions for each resin system to obtain the optimal properties." With this and the definition of the microwave cure cycle above in mind, the varying results will not be discussed further; no clear reasoning for possible effects can be found using the database at hand and the used process.

2.3.2 Interface and Shear Behavior

Agrawal and Drzal published an paper on single fiber pull-out trials using glass, aramid, and carbon fibers embedded in a epoxy matrix and cured using oven and microwave [80]. The interfacial shear strength of glass- and aramid-epoxy specimens was found to be 15% lower for microwave cured samples compared to oven cured samples. The shear strength of carbon fiber specimens, on the other hand, was 70% higher. In their trials with carbon fibers, Agrawal and Drzal saw a extensive heating near the filament. First, they observed thermal matrix degradation under microwave curing when using the same power as for glass or aramid samples. From this on, they conducted a test setup to estimate the interface temperature of carbon fiber and epoxy matrix; an increased interphase temperature was estimated. The faster curing reaction in the interphase region, compared to the bulk matrix, was seen as dominant factor for the increased carbon fiber pull-out strength. In a letter in 1991, Boey and Yue investigated the shear strength between "single silica E-glass panel(s)" using an epoxy interlayer [41]. They showed that after a much smaller curing time—less than 20 min in the microwave compared to 12 h thermal curing—a higher maximum strength could be reached. Bai and Djafari cured unidirectional E-glass/epoxy composites with a microwave and investigated it using transverse tensile and 4-point short beam tests inside a scanning electron microscope (SEM) in 1995 [44]. Taking the presence of voids, the fiber volume content (FVC), and the matrix strength into account, the interface's strength is calculated by the transverse tensile test results. Without consideration of the opening angle

of the debonded interface, the thermally cured samples have a 3% higher interface strength that is not seen as significant by the authors. With consideration of the opening angle, that is 65° for microwave cured and 90° for thermal cured samples, the microwave cured samples' interface strength is higher. Like with the initial results for transverse tensile tests, the interface strength calculated directly from the short beam bending tests is comparable. Nevertheless, Bai and Djafari support the thesis that the microwave samples' interface is stronger due to the "mechanism of rupture". In detail, they support this with the occurrence of microcracks inside the matrix of microwave cured samples during both tests; these microcracks did not occur in conventionally cured samples. Yue and Looi compared the interfacial properties of glass fiber/epoxy composites cured with oven and microwave using two custom methods: compression double lap shear tests and single fiber pull-out tests [42]. While the compression lap shear tests resulted in approximately double the average shear strength for microwave specimens compared to conventionally cured specimens, the pull-out tests delivered different results. In the pull-out tests the interfacial strength of thermaly cured samples is two times the strength of microwave cured samples. Yue and Looi ascribe these opposing results to a higher interfacial friction stress and matrix shrinkage pressure in thermally cured samples. They conclude, that the fiber pull-out tests should be used for characterization of the interfacial properties and that "thermal processing leads to composites with higher [interfacial] strength compared to microwave processing." A study from Rao R., Rao S., and Sridhara in 2006 shows higher inter-laminar shear strength (ILSS) properties for microwave cured GFRP samples compared to oven cured samples [47]. However, in both configurations—using a room temperature curing system and a high temperature curing system—the T_g of microwave cured samples is higher due to an elevated cure temperature, compare section 2.3.1 above. Additionaly, the conventionally cured samples of configuration one were held at room temperature while the microwave cured samples were heated after infiltration. Hereby, the viscosity of the resin system is most certainly decreased. Consequently, the wetting behavior of microwave manufactured samples changes compared to conventionally cured ones.

Nightingale and Day did ILSS investigations in 2002 on 8 layer unidirectional CFRP samples cured in an autoclave and 16 layer 0°/90° samples cured in a microwave[38]. The two tested resin systems were formulated with a PEI toughening agent. While the study is very interesting, the main weakness of it is the failure to compare identical lay-ups between autoclave and microwave processing. Thus, no clear interpretation of the microwave's influence is possible. Likewise, no comparison between heating technologies was made by Guan et al. in their 2020's paper [51]. CFRP samples with 10 layers were manufactured inside an autoclave using a microwave

insert for heating. ILSS tests were then used to capture the influence of variations in heating rate, curing temperature, and holding time. Im summary the results are that: a high heating rate of 8 °C compared to 4 an 6 °C decreases the ILSS properties; the curing temperature does not change the ILSS properties; a longer holding time (30, 60, or 90 min) increases the ILSS properties. With respect to the analysis of the curing temperature's influence, however, it must be said that the temperature was only measured using one optical temperature sensor. No information on the temperature distribution is given. Papargyris et al. did a direct comparison of ILSS values using identical lay-ups in 2008 [50]. Here, the ILSS properties of microwave cured samples is 9% higher compared to conventionally cured ones. In the interpretation of the results Papagyris gives three possible explanations for the increased shear strength: a lowering in the resin viscosity due to higher heating rates in microwave cure, the greater amount of resin between the fiber layers due to the slightly higher thickness of microwave cured samples, and the sligthly lower void content (0.6% to 1.7%) of microwave samples.

Meyer describes a comparison of tension tests of bidirectional CFRP laminates in 0°and 45°direction in his PhD thesis from 2007 [15]. The laminates were manufactured using an infusion process and the RTM6® matrix, a multimode microwave chamber, and a very well designed manufacturing process. Samples cured using a microwave and three temperature profiles are compared to a reference oven process. The reference microwave process was adapted to take a longer through heating time of the oven process into account. The second microwave process had a reduced dwell time at 180 °C: from 90 min to 60 min. The last microwave process used an increased heating rate to reach cure temperature: from 1 °C/min to 3 °C/min. After compensation for a varying FVC, the mechanical properties of microwave and oven cured specimens are comparable. This is confirmed by an additional microwave reference trial reproducing the oven's higher FVC. However, a different failure mechanism is observed for oven and microwave cured specimens. This difference is ascribed to a pre-existing material damage of the fibers in combination with a lower FVC for all microwave specimens. In his PhD thesis from 2012 Gaille investigated the ILSS properties and the fiber matrix interface of CFRP having a RTM6® matrix [16]. This material combination is similar to that of Meyer's investigation. Taking the standard deviation into account, no difference in ILSS values was seen between thermally cured samples (90 min@180 °C) and microwave cured samples (60–90 min@180 °C). Provided that both oven and microwave samples were cured using a comparable heating ramp, investigations of the fiber matrix interface of compression tested samples using SEM showed no difference. In comparison, microwave samples cured with a higher heating ramp of 5 °C/min compared to 1 °C/min showed a more brittle failure that Gaille attributed to a strong fiber-matrix adhesion. Overall, the results of both Gaille's and Meyer's investigation align.

Kwak, Robinson, Bismarck and Wise did a very extensive investigation on the behavior of microwave cured CFRP in 2015 [74]. They tested unidirectional and ±45° samples with 2.4 mm thickness. The first were tested with tension in both directions and compression in 90°. The latter were tested for in-plane shear strength. The oven cured samples yielded 11% higher values for the 90° tension test and 9% higher values for the shear strength. Kwak et al. give no explanation for the "little variation in in-plane shear strength" but mention two possible reasons for the reduced tensile strength. First, the FVC of microwave samples is lower; this could be attributed to a reduced compaction due to the vacuum setup. Second, the microwave samples have a higher void content. This is ascribed to a higher microwave heating rate that reduces the time to remove air (10 °C/min compared to 2 °C/min). In contrast to 90° tension and shear, the compression strength of microwave cured samples was increased by up to 35%. The increased compression strength in fiber direction is attributed to a higher degree of cure next to the fibers. A concentrated microwave heating near the fibers as reported in other studies [77], [80] can increase the degree of cure near them and result in a more brittle but stronger interface. This thesis is supported by SEM investigations that show more matrix remaining on the carbon fibers cured using microwave after 90° tension trials.

In 2016, Zhou, Li, Hao, and Liu developed and applied a novel characterization method for the fiber matrix interface: a improved fiber bundle pull-out test, see Fig. 2-8. The test is designed to overcome problems with arcing by exposed car-

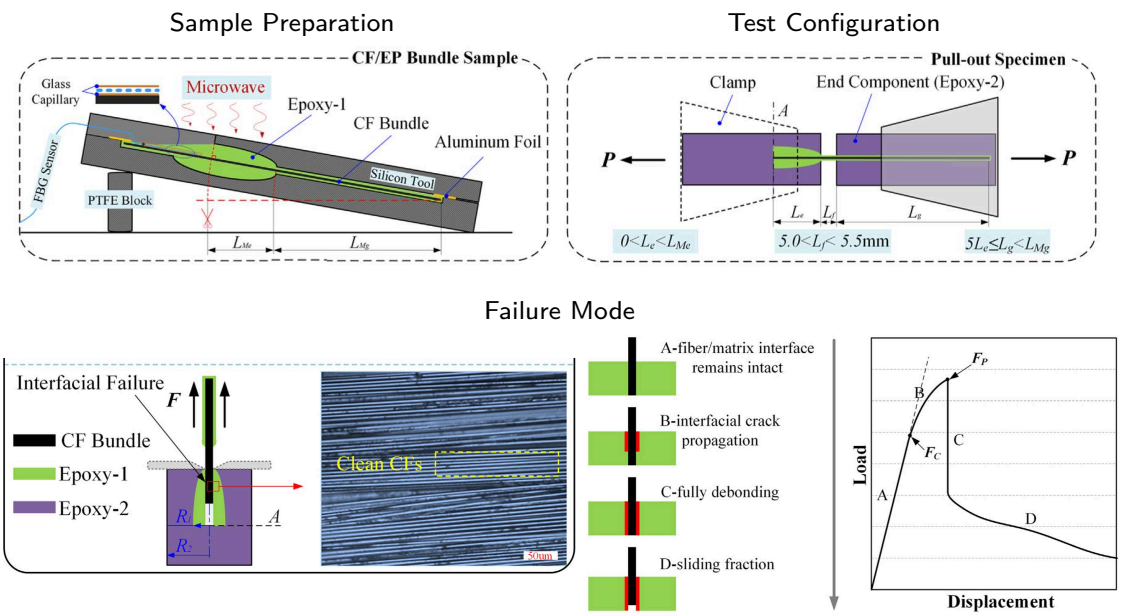

Fig. 2-8 Novel fiber bundle pull-out test designed and used by Zhou et al. [77].

bon fibers occurring with conventional pull-out tests and microwave curing. The novel method was used to reproduce some prior single fiber pull-out studies us-

ing different material systems. The test designed by Jing et al. has a very good agreement with the prior results. Likewise, ILSS tests and the fiber bundle pull-out test results did behave in the same way for those material systems. Subsequent, pull-out tests of conventionally and microwave cured carbon fiber pull-out samples were done. The comparison showed a strong interfacial shear strength improvement for microwave processed carbon samples of >50 MPa compared to 36 MPa. Further investigations to characterize the interface of E-glass samples showed no such improvement. Through this, and investigations of the carbon-epoxy interface's spectrum, the authors conclude that a selective heating in proximity to the carbon fibers—no chemical mechanism—is responsible for the enhanced fiber matrix interface for the carbon fiber tests.

2.3.3 3- and 4-Point Bending Tests

Zhou, Shi, Mei, Yuan and Fu give a very short insight into the bending strength of a pure epoxy resin (E44) cured using a maleic anhydride[81]. As expected, the bending strength varies in dependence of the amount of curing agent. Noteworthy, a higher bending strength is measured for microwave processed samples.

The investigation of Boey and Lee in 1990 showed similar bending strength for oven and microwave cured GFRP specimens [40]. Depending on the power-level of the microwave, the strength varied slightly. For the highest power-level and increased process time, the flexural properties decreased. Tanrattanakul and Jaroendee investigated the tensile and flexural properties of GFRP [35]. The setup of the study is nearly identical to the one published by Tanrattanakul and SaeTiaw in 2005. Foremost, like in the prior study, "the applied power was based on physical performance and mechanical properties of cured samples. No air bubbles and no burning were criteria for good performance specimens." Consequently, as described in more detail in section 2.3.1, the results variate strongly and will not be discussed in detail. In addition to the T_g, Mooteri et al. investigated the flexural properties of an amine hardened GFRP in their 2006 study [48]. The flexural strength of the microwave cured samples is 4% below that of oven cured samples. However, the conditions during cure varied drastically for both configurations. Microwave samples were cured in a closed teflon mold with a direct heat input after infiltration and without vacuum. In contrast, the thermally cured samples were cured for 24 h at room temperature under vacuum and post-cured afterwards. Both, the missing compaction during the curing process for microwave specimens and the lower thermal stresses during room temperature cure of conventional samples, influence the laminate in favor of the thermal cure. With these circumstances in mind, the 4% difference in flexural strength can be neglected. Maenz, Mühlstädt, Jandt, and

Bossert in 2015 [64] determined the 3-point bending properties of GFRP cured with a microwave and post-cured in an oven[64]. There was no difference in bending properties for completely thermally cured and microwave pre-cured samples.

Nightingale and Day investigated the flexural properties of CFRP with 15w% polyetherimide (PEI) as toughening agent inside of two matrices. Since the autoclave trials were done with unidirectional samples and the microwave postcured trials with 90°/0° samples no comparison is possible. In Papagyris's, Day's, Nesbitt's and Bakavos's 2008 comparison of the bending properties of microwave and conventionally cured RTM specimens, a difference in thickness is most presumably the biggest influencing factor [50]. The microwave specimens in the investigation are thicker than the conventionally cured ones and thus have a lower FVC of 27% compared to 33%. After normalizing the FVC of microwave cured samples to 33%, the flexural modulus and strength of samples produced with different cure mechanisms is comparable.

2.4 Tooling for Microwave Processing of Fiber Reinforced Plastics

In the production of fiber-reinforced plastics (FRPs) a tool is necessary to give the final part its shape. The form and material of the tool strongly depend on the application. For example, prototyping tools are often out of polyurethane (PU) foam whereas tools for high volume production are often out of high strength steel or irnvar—a very expensive iron– nickel alloy that has a very low coefficient of linear thermal expansion (CTE) below $1.2{\cdot}10^{-6}$ 1/K. For small to intermediate production numbers, composite tools are used on a regular basis; they have the benefit of a similar CTE. Of course, the material price and manufacturing costs for tools differ strongly with the material.

The questions is, which tooling-materials can be used for microwave processing of FRPs? This will be answered in three steps. First, a classification for materials according to their microwave interaction is introduced. Second, the different material classes are utilized in conceptual tools. Last, these concepts will be compared to tools used in literature.

2.4.1 Classification of Materials in Respect to their Penetration Depth

For the classification of tools, materials are categorized into four categories according to their penetration depth: opaque, virtually opaque, virtually transparent, and transparent. These categories and the according D_p were defined by the author. The categories give an indication for a material's behavior and thus potential usability. In this way, the classification is the basis for further thought experiments and developments. A prior version of the categories and tool concepts been presented and published by the author at the SAMPE EUROPE Conference 2014 [82].

First, opaque materials like metals or other conductive materials completely reflect the microwave radiation. In principal, a very slight heat-up occurs through eddy currents at the surface. However, this heat-up is not relevant and more of theoretical nature. Due to the total reflection of microwaves, these materials can be used as shielding. Second, virtually opaque materials are defined by a penetration depth below 30 cm; the low penetration depth can be due to high reflective losses (CFRP), absorption losses (carbon black (CB), silicon carbid (SiC)), or—as in most cases—a combination of both. Heat-up mostly takes place due to dielectric losses, compare 2.1.1. It must always be kept in mind, that reflection dominated materials heat-up less than absorption dominated materials. They cannot, however,

be distinguished by D_p alone. The third material category, virtually transparent, is defined by 30 cm< D_p ≤200 cm; the power dissipation varies strongly over the combination of ε_r', ε_r'', the materials thickness, and other materials present. If a strong absorber like a virtually opaque material is heated simultaneously, the virtually transparent material may barely heat-up in comparison. The last category of transparent materials has a penetration depth above 200 cm. Close to no power is dissipated in these materials and no relevant heat-up occurs. However, special attention has to be paid when working with transparent materials and when they do heat-up due to heat transfer effects. The dielectric properties and losses of some materials changes abruptly at certain temperatures; they may suddenly get virtually transparent or even opaque. After this, a rapid and unexpected heating of the formerly transparent material can quickly become disastrous. The definitions introduced are listed in Tab. 2-1.

Tab. 2-1 Definition of material categories according to the penetration depth.

	Category	Penetration Depth	Material Examples[5]
I	Opaque	$D_p \leq 0.1\,\text{mm}$	Metals, conducting materials
II	Virtually Opaque	$0.1\,\text{mm} < D_p \leq 30\,\text{cm}$	CFRPs, SiC, absorber filled plastics
III	Virtually Transparent	$30\,\text{cm} < D_p \leq 200\,\text{cm}$	GFRPs, PA, PVC@120 °C, some ceramics
IV	Transparent	$200\,\text{cm} < D_p$	PTFE, PVC@25 °C, PE, PC, AL_2O_3

2.4.2 Conceptual Tools with Respect to Material Categories

In the following section, opaque, virtually transparent, and transparent materials will be used for conceptual closed tools. In all of these concepts, the application of virtually opaque material with strong absorption properties is discussed as a heating element. The restriction of closed tools is chosen as the more restrictive case. Also, the consequences of the introduced thought experiments on closed tools can more easily be transfer to half mold tools than it would be possible in the other direction.

[5] A variety of literature values of dielectric material properties and their penetration depth is given in appendix A.1, page 145.

Tools out of Opaque Base Material

At first, opaque materials i.e. metals as one extreme are considered as tooling material. Due to the low D_p<0.1 mm the energy input in these tools is minimal and they do not heat-up in a 2.45 GHz electromagnetic field. For this, without another material as partner they are unsuitable for closed tools and of only limited suitability for half sided tools. In the first case they do not heat up. In the second case they still act as heat sinks. In combination with a virtually opaque high loss material, however, the reflective character of opaque materials can be utilized. Especially since metal tools are already widely available and used on a daily basis. As is depicted in Fig. 2-9, the part is completely shielded by the closed tool; there can be no interaction between processed material and the microwave radiation. Furthermore, most electric conductive and thereby opaque materials have a com-

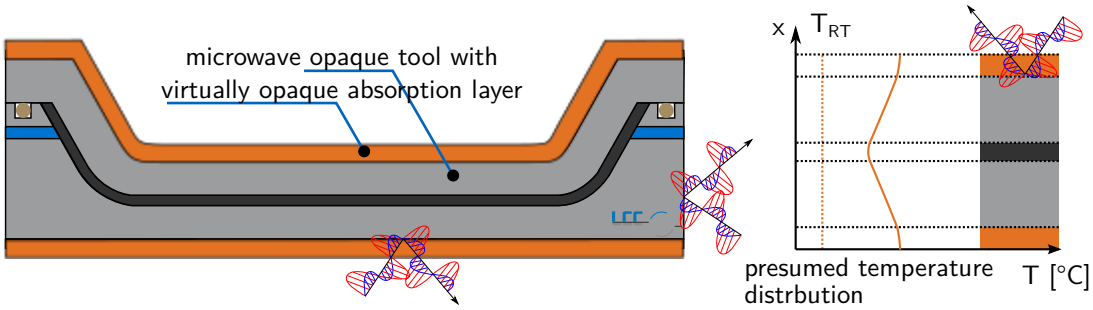

Fig. 2-9 Exemplary opaque tool with virtually opaque absorption layers for heating.

parably high thermal conductivity. Local variations in the thickness or complexity of part or tool can be overcome by heat conduction during a process. This way, any part may be processed independent of its complexity. Likewise, the independence of local heat introduction should enable the use of several tools almost independent from each other. Opaque materials, nevertheless, always must be heated and prevent the energy efficient utilization of the microwave technology.

Tools out of Transparent Base Material

Second, transparent materials as the other extreme are discussed. Examples of these materials are Peek, PTFE, PE, and some ceramics. They all are characterized by a D_p that exceeds 200 cm. As a consequence of the high D_p, a tool out of these materials does not heat up under microwave radiation, compare Fig. 2-10 top. The electromagnetic waves pass through the transparent material and only heat up the part. On the one hand, this direct heat input into the part is energy-efficient and desirable. On the other hand, edge regions may heat up disproportionately due to the irradiation from more than one side. Likewise, certain materials like CFRP or metals can interact with the electric field in an uncontrolled manner. If the transparent material has a high thermal conductivity, transparent tools will, like opaque tools, act as a heat sink. If the materials thermal conductivity is very low,

the tools may work as an insulator. To counter the first problem, a combination with a virtually opaque or virtually transparent material is introduced. A heating layer out of these materials is introduced inside the tool, compare Fig. 2-10 bottom. As with pure transparent material, the microwaves penetrate the outer tooling area. But, rather than heating only the part, the boundary layer is heated as well. Adaptions to these boundary layers in absorption properties or geometry can counter some problems of completely transparent tools. By the application itself, the tool does not act as a heat sink any more. A weaker absorber can be used in the edge regions to react to compensate the irradiation from all sided. Consequently, a uniform part temperature could be accomplished with only minor loss in efficiency while the bulk of the tools material stays at a lower temperature.

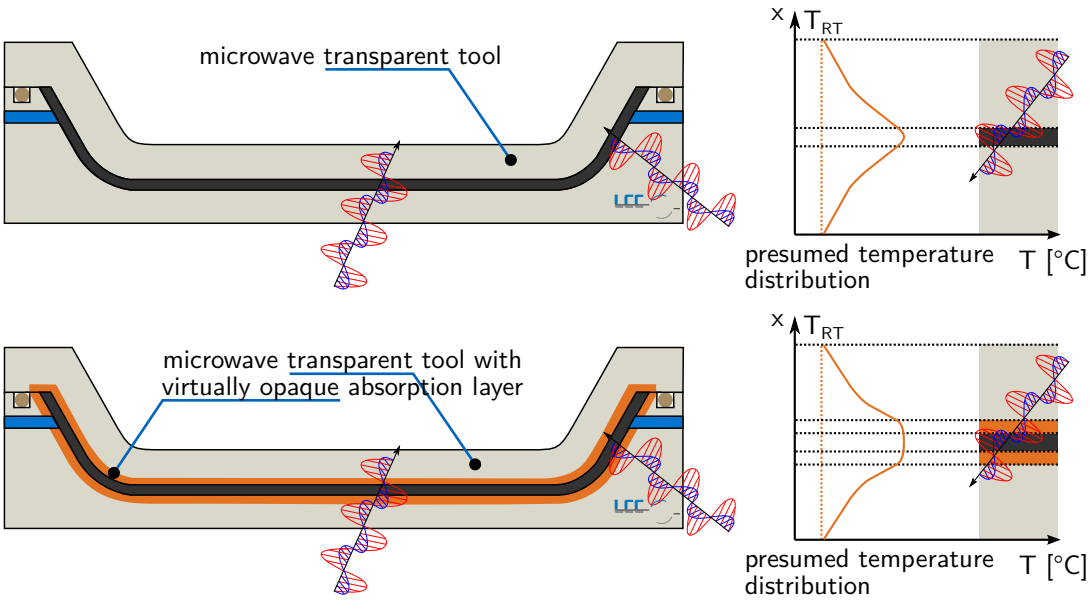

Fig. 2-10 Exemplary transparent tools with and without virtually opaque absorption layers for heating.

Unfortunately for all concepts using unconventional transparent tooling materials, the materials are very expensive (ceramics), hard to manufacture (ceramics, PTFE), and sometimes very soft (PTFE, PEEK). Also, the application of a resistible boundary layer to these materials is currently not state of the art and needs further research in itself.

Tools out of Virtually Transparent Base Material

Last, tools out of virtually transparent materials are regarded. They have a penetration depth of 30–200 cm and do consequently heat-up to some degree under microwave irradiation. GFRP is the most prominent material example in this category since, like metal, it is already used as tooling material.

In the design of a virtually transparent tool the properties of all introduced materi-

als are important. Foremost, the tooling material, part material, and overall design have to be compatible to each other. To have a defined task sharing—the tool gives the form, the part is cured—the tool should absorb less energy than the part. One the one hand, energy absorption by the tooling material must be reduced. Therefore, the tool's D_p must be considerably higher than its wall thickness. On the other hand, energy absorption by the part must be maximized. Therefore, the processed part's D_p must have the same dimension as its thickness and the D_p should be considerably smaller than that of the tool. If the parts D_p is additionally a result of absorption and not of reflection, the bulk of microwave energy is transmitted to the part.

While the part heats up, the tool will stay comparatively cold. With this approach, a homogeneous temperature distribution can be reached for geometrical simple parts. However, if the part's wall thickness has high variations or different materials are processed simultaneously, for example when metallic inserts are used, the temperature will be inhomogeneous. Metallic inserts act as heat sink and thick part areas will absorb less or more energy—depending on the penetration depth, heat transfer effects, and part geometry. In these cases, an additional absorption layer can be adapted locally to support the heat-up of the part and reduce temperature inhomogeneity, Fig. 2-11. Such an additional absorption layer may also be beneficial if the penetration depth of the parts material is significantly lower than its wall thickness. The layer will, like in the example above for fully transparent tools using an absorption layer, counteract the heat flow from part to tool.

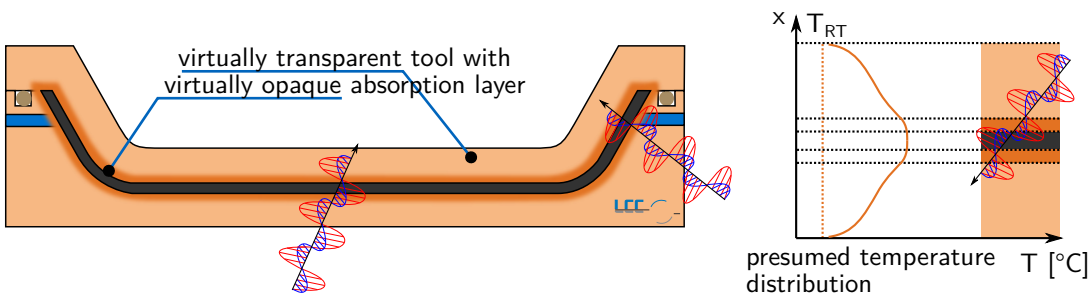

Fig. 2-11 Exemplary virtually transparent tool using a virtually opaque absorption layer for heating.

2.4.3 Tools Used for Microwave Processing in Literature

The following section presents tools used in literature. The focus will be kept on publications working with laboratory or industrial equipment, compare sections 2.2.2 and 2.2.3.

Opaque Tools

One sided metallic tools have been used in some studies using industrial microwaves. A presentation of aluminum tools for microwave processing of CFRP is given by Meyer in his Ph.D.Thesis in 2007 [15]. Meyer uses one sided U-shaped aluminum tools to activate the binder of carbon fiber stacks and cure specimens. Furthermore, a aluminum mold with a borosilicate glass topping is used to manufacture pure resin plates. In his thesis, Meyer recommends tooling concepts that only use metallic surfaces at the edge and microwave transparent material at the bottom. This is proposed to shield the edge area of carbon composites, prevent arcing, and improve microwave usability.

An investigation comparing aluminum, invar, and CFRP tools has been discussed in the context of conferences [71], [73] and was published in Gaille's Ph.D.Thesis [16]. All three tool variants were used with an additional virtual opaque absorber. This absorber was placed below the metal tool and on top of the vacuum set-up. The absorber is called "Kraiburg foil" according to its manufacturer. It has a D_p of 0.59 cm[16]. Gaille describes it as silicone filled with "Several additives, which absorb microwaves and which improve the thermal conductivity ...". In his study of different tools using the Hephaistos technology, only the aluminum tool yields a satisfactory and homogeneous temperature distribution. This is ascribed to the high thermal conductivity of aluminum missing in the invar and CFRP tools. Consequently, Gaille sees high temperature conductivity metals as only feasible tooling material for microwave processing. Three arguments are presented why manufacturing of suitable samples using other materials like invar and CFRP is not possible: the inhomogeneity of the microwave field, the differences in thermal convection at the middle and border of the part, and the need to compensate for complex geometries of parts.

Another publication by Kwak et al. [74] and Kwak's Ph.D.Thesis [17] likewise use a one sided aluminum mold of 400×400 mm for the manufacturing of 2.4 mm and 4.8 mm unidirectional CFRP laminates. In contrast to Gaille, Kwak ultimately argues to remove the aluminum as microwave reflecting material from the process. He proposes to use a microwave transparent mold material instead. His arguments are that the aluminum does block microwaves and acts as a heat sink. Its removal would consequently increase process efficiency.

A special case of tool, a steel mandrel for the cure of filament wound CFRP parts, was presented by Betz at a microwave symposium of the Vötsch Industrietechnik company [69] and published in a German project report [18]. In comparison to the other tools, epoxy soaked carbon rovings completely wrap the steel mandrel. The mandrel is thereby shielded itself from the microwave field and only dictates the inner geometry of the filament wound CFRP part. However, an influence of the steel mandrel that acts as heat sink is observed in the temperature measurements. Nevertheless, a reduction of process time is reported.

Transparent Tools

The commonly used transparent microwave tooling materials are unfilled plastics, mainly polytetrafluorethylen (PTFE), and ceramics. PTFE is used in a variety of studies [35], [38], [39], [47]–[49], [57]. It has a penetration depth of ≈90 m [29] and does consequently not heat-up due to irradiation in normal microwave applications. It has, however, a very high CTE of 122 $^{10^{-6}}/\kappa$ and very poor mechanical properties. Due to its poor mechanical properties and high price, PTFE is not suitable as a tooling material for industrial applications. It could neither guarantee contour accuracy nor be used for a relevant amount of parts. Ebalta ebaboard LX was used by Maenz et al. [64] as mold material. It is in all probability transparent but no data is available. However, Maenz et al. state that "Temperatures higher than 90°C induce the degradation of the mould.". Consequently, Ebalta can only be used for an initial cure of most resin systems.

A recent study by Nuhiji et. al [83] investigated five tooling materials with regard to the cure of CFRP. Of these five materials two are transparent. Two parts and thus tool geometries were investigated; a simple plate of $300 \times 300\,\mathrm{mm}^2$ and a potential "industrial" part of $1500 \times 600\,\mathrm{mm}^2$. The industrial part has a complex geometry with a concave, a flat, and a convex area. A test bed was used to investigate the plate samples and a *Vötsch Hephaistos 180/200* (VHM180) to investigate the complex samples. The transparent materials were a high temperature tooling board called Trelleborg TC460 and an Ultem™ thermoplastic. According to the manufactures homepages, the TC460 is a low-density syntactic epoxy and Ultem™ is a PEI. While Ultem™ is able to withstand the process temperatures up to 190 °C, it experienced a rapid rise in temperature during the test bed trials. According to the authors "the materials unusual and uncontrollable behavior at approximately 90 °C and 160 °C [...] as well as it's hydroscopic nature made it unsuitable for industrial trials." A complex tool from TC460 was investigated inside the VHM180. However, it was damaged during the process. The authors think that inclusions of titania particles and an epoxy adhesive used to manufacture the tool resulted in a local heat-up and consequent thermal runaway. Pictures of the damaged tool show a overheating of the epoxy adhesive with brown discoloration. In summary, like Nuhiji et. al state, "the TC460 tool cannot be considered as a feasible high temperature material for microwaving composites."

Taking a look at studies using ceramics, most were using simple flat tools in form of (glass-)ceramics [52], [55], [56], [58], [65], [77], [78]. In a German research project, tubes out of different ceramic materials were tested as tool for microwave pultrusion. While all tubes broke at some point, aluminum oxide tubes out of *Frialit F99,7hf* could be used the longest for the pultrusion of 150 m CFRP. Simple plates and the tubes are both standard products. More complex tools, however, cannot

easily be produced or they are very expensive. One way to do so is to use a machinable ceramic like *Macor* that was used by Papargyris et al. [50]. While individual geometries can be milled out of a block of this ceramic, the maximum slab size is $300 \times 300 \times 50\,\mathrm{mm}$ [6].

A novel approach to manufacture ceramic tools for microwave processing was presented at the previously mentioned microwave symposium by Kazilas [66] and in the final report of the MU-TOOL project by Moret [68]. A process mixture of the freeze and slip casting technology was used to manufacture ceramic tools with and without and additional microwave absorbing layer. A negative and positive form were manufactured so that the part could be pressed and heated from both sides. However, no infusion into the part was realized—no closed cavity existed. While the thermal gradient inside the ceramic during its use still lessens the tools durability, this is a first step in the direction of microwave process optimized tools.

Virtually Transparent and Opaque Tools

The last category focuses on GFRP and CFRP tools. GFRP, more precise glass fiber-reinforced epoxy (GFRE), as virtually transparent tooling material is mentioned by Gaille in his thesis [16] and in Nuhiji et. al's investigation [83]. On the one hand, a carbon filament burned the tool of Gaille at its first use. Nuhiji's was likewise extensively damaged at its first microwave trial: "The damage was initiated from a combination of factors including suspected stray carbon fibres, EM field concentration and void content." On the other hand, GFRE was successfully used in the author's study to manufacture samples at 120 °C. The GFRE tools of the author, however, likewise showed local burns due to entrapped carbon fibers at higher process temperatures. It is believed, that this shortcoming could be evaded by producing the GFRE tools in an completely carbon fiber-free environment and enhancing them. If an additional absorber is applied to the tool, the field strength necessary for heating can be reduced. Consequently, the carbon fiber filaments would be less critical as described later in section 4.3.1 on page 82.

Glass fiber-reinforced cyanate ester (GFRCE) is the fourth of five materials investigated by Nuhiji et. al [83]. Test bed trials yielded promising results with a comparatively low temperature spread between the chosen measurement points. During the industrial trials, the cure cycle was finished; the CFRP part was successfully cured. However, the temperature spread was relatively high. This spread resulted in a degree of cure difference over the part of 23%. Furthermore, both of the used GFRCE tools were damaged during the investigation. In the test bed trial, the edges of the manufactured CFRP panel experienced localized heating. This resulted in a damage evident by a discoloring. In the industrial trial, the tool

[6] `https://www.schroederglas.com/macor.php`, visited 21.10.2018

got damaged in two areas that overheated during the process; the CFRP demonstrator was damaged in one of these areas. The overheating is evident from thermal images recorded during the CFRP cure. In summary, GFRCE tools can in principle be used for CFRP manufacturing but further investigation and optimization would be necessary.

Better results were reached by Nuhiji et al. with their fifth and last tooling material CFRP [83]. Their test bed trials yielded only a slightly higher temperature spread of 10 °C for CFRP compared to 7 °C for GFRCE. The industrial scale part was successfully manufactured and the tool was not damaged. The degree of cure variance over the part was still 11%. Likewise, the comparison of different tooling materials by Gaille resulted in a bad temperature homogeneity for CFRP tools. However, in the light of other studies and investigations, both results must be put into perspective. On the one hand, a Hephaistos system without any documented adaptions was used by Gaille and without visible adaptions by Nuhiji et al. As is shown by the author, a huge improvement in temperature homogeneity can be reached with minor changes. On the other hand, Thomas Herkner presented results in which parts were manufactured according to aviation standards [21], [22] that include a very narrow allowed spread in temperature. As the investigations of Thomas Herkner followed the project Gailles studies were made in, it can be assumed that Herkners tools utilized the Kraiburg absorber. In comparison, Gaille and Nuhiji et al. used a CFRP tool without additional absorber. In summary, CFRP is currently the most suited tooling material for the cure of CFRP parts. However, an optimized process as well as the use and development of absorber materials for this tools is necessary.

2.5 Absorber Materials Used and Investigated

As was seen in the section above, absorber materials can be utilized for different tooling applications. They are necessary addition for a homogenous heating of complex geometries. Consequently, a closer look is taken at absorbers used in composite manufacturing.

2.5.1 Absorbers Used in Literature

Overall, the use of absorbers for heating in composite manufacturing is not well documented. To the author's best knowledge, first trials were made in the collaborative project proceeding this work. Shortly before the proceeding project, the first Hephaistos equipment was build. During the project trials were made to manufacture absorber foils using carbon filaments as fillers. The results of the trials

are very briefly described in the final project report, but no break through was made[19]. Insufficient distribution of fillers that lead to a inhomogeneous temperature response was the main problem. The trials to develop a absorber material were stopped, as a material made by Kraiburg, hence named “Kraiburg foil”, was discovered. The Kraiburg foil is a highly filled silicone material [16], [19]. It has the mixture number SFL8925/26[7] at Kraiburg Gummiwerke. The material has a very good homogeneity and high microwave absorption. This material was measured and is given with a relative permittivity $\varepsilon_r^* = 66.2$ and a penetration depth of 5.9 mm[16], [19] According to the introduced categories above, Kraiburg foil is a virtually opaque material.

Results of plates manufactured using this Kraiburg foil were published by Fabrice Gaille in [16], [71]. Robert A. Witik, Gaille, Teuscher, Ringwald, Michaud, Månson furthermore published a “economic and environmental assessment of alternative production methods for composite aircraft” where they took the setup used by Gaille into account [84]. However, in the literature at hand, the Kraiburg foil is used but is not discussed.

A patent describing composite manufacturing in a microwave applicator using the help of a “microwave-sensitive material” was registered in 2009 by Giovanni Antonio and Thomas Herkner [20], compare Fig. 2-12. Thomas Herkner, consequently, gave two presentations [21], [22] where results obtained using microwave processing were presented. In the latter of the talks, the use of ”heater packs” is mentioned. However, no specifics are given. As mentioned above, through Herkner’s involvement in the joint research project in which the Kraiburg foil was first used, it is assumed, that the Kraiburg foil—or some variant of it—was used as the mentioned heater pack.

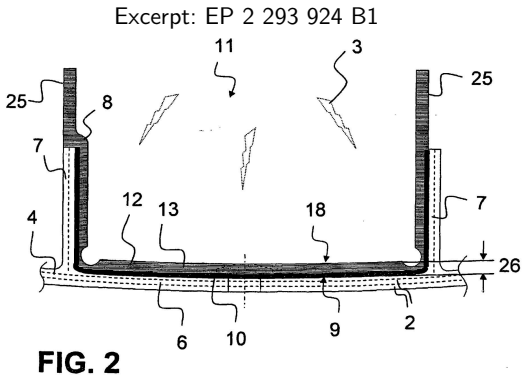

On or more layers (2) of fiber-reinforced composite material (4) that is irradiated with microwaves (3). The part consists of a base surface (6) and one or more elevations (7).

The molding tool (8) has a contact surfaces (9) and an outer surface (18). It has a supporting area (25) and thickness (26). At least one of the contact surfaces is formed with microwave-sensitive material (10) . The tool has also at least a region (12) outside the contact surface that is formed with microwave-transparend material (13).

Fig. 2-12 Excerpt from EP 2 303 553 B1 [20] of a manufacturing method for composite parts utilizing a microwave absorber. The summary text is a representation of the patent by this thesis’s author.

[7]Direct information over the phone

The manufacturing process of ceramic tools introduced above uses ferrite as absorber. In one tool, a ferrite containing layer was applied to the surface of the tool in form of a glaze. In a second geometrically more complex tool, the ferrite was distributed over the bulk of the ceramic. For the latter material, the dielectric properties were measured to be $\varepsilon_r' = 6.03$ and $\varepsilon_r'' = 0.42$ at ≈44 °C[68]. This gives a penetration depth of 11.4 cm .

2.5.2 Variable Absorber from Scratch

This short investigation into absorbers for microwave processing of composites shows that only two absorbers have previously been used. An adaption to a specific tool or special requirement variations is not possible. The Kraiburg foil cannot be changed in its properties and its composition is unknown. The ferrite absorber does only work within the reported tooling process. Consequently, first trials to manufacture epoxy-based absorbers containing CB and SiC additives were made during the Faserverbund-Leichtbau mit Automatisierter Mikrowellenprozesstechnik hoher Energieeffizienz (FLAME) project by the author [18]. The first results of a variable absorber presented below were published at [85] and in the final report of FLAME [18]. Since a follow-up investigation is done in this thesis, only the basics are presented at this point.

With the addition of the conductive CB filler Printex® XE 2 B (XE2B) and SiC particles of two sizes (FE600 and FE1200), the dielectric properties of a epoxy resin were changed and controlled in a wide area, compare Tab. 2-2. However, when looking at the D_p a big gap can be seen between mixtures of pure SiC and those containing CB. The D_p changes drastically when the CB is added and only slight variations seem possible. Consequently, a way must be found to further adjust the absorption properties. Before the material could be used as fully variable absorber its composition has to be expanded.

Tab. 2-2 Dielectric measurement values of initial absorber study with standard deviation (SD) sorted for D_p.

Configuration	ε_r'[-]	**SD**	ε_r''[-]	**SD**	D_p [cm]
EP	2.93	0.004	0.042	0.001	80.29
5 V% SiC-Mix	3.58	0.015	0.157	0.004	23.44
5 V% SiC1200	3.75	0.022	0.206	0.004	18.32
2 V% XE2B + 5 V% SiC600	10.17	0.252	3.390	0.106	1.86
2 V% XE2B + 5 V% SiC-Mix	11.00	0.230	3.752	0.087	1.75
2 V% XE2B	8.93	0.068	3.448	0.072	1.72
2 V% XE2B + 5 V% SiC1200	12.29	0.369	5.666	0.288	1.24
5 V% XE2B	27.55	0.564	11.414	0.398	0.91

Furthermore, microsections show big CB agglomerates with the used manufacturing process, compare Fig. 2-13. The manufacturing process, therefore, has to be adapted further to break up these agglomerates and guarantee reproducible samples and properties.

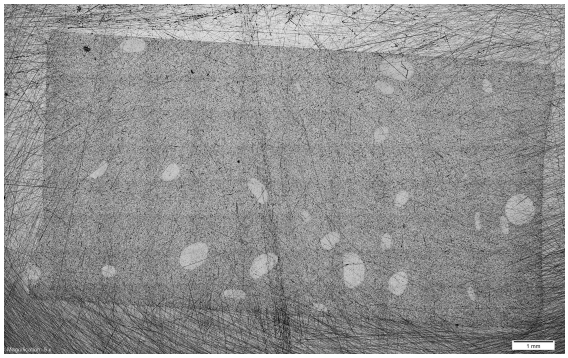

Fig. 2-13 Microsection of early absorber sample containing 2 V% XE2B shows bad CB distribution and agglomerates as big bright spots.

3 Equipment, Procedures, and Materials

3.1 Materials Used in this Thesis

3.1.1 Resin Systems Used in this Study

Biresin® CR 141, an anhydride epoxy resin from *Sika*® (Stuttgart, BW, Germany), is used as matrix material. It is used as matrix for the absorber material, manufactured glass fiber-reinforced plastic (GFRP) samples, and for GFRP-tools that are used for 120 °C microwave trials. The basic resin properties can be found in Tab. 3-1. This anhydride system was chosen because, according to experts from *Sika*®, it has a lower toxicity and tolerates high heating rates much better than an amine system.

Tab. 3-1 Properties of Biresin CR141 according to its datasheet (Appendix A.5, page 164).

Mixture		Neat Resin Specimen*	
Potlife, 100 g (RT)	>24 h	**Tensile strength**	78 MPa
Mixed viscosity, 25 °C	600 mPa.s	**Tensile E-Modulus**	3200 MPa
Mixed viscosity, 50 °C**	100 mPa.s	**Elongation at break**	3.3%
		Impact resistance	18 kJ/m^2
		T_g (ISO 11357)	139°C

* approx. values after 3 h/80 °C + 3 h / 120 °C + 3 h / 140 °C
**acc. to viscosity curve provided by Sika

3.1.2 Fiber Material Used in this Study

The fiber material used in this study is a standard E-Glass non-crimp-fabric (NCF) by *Saertex* (Saerbeck, NW, Germany). The 0° NCF (U-E-PB-606g/m^2-1200mm) has a total areal weight of 606 g/m^2 with 520 g/m^2 E-Glass in 0° on top, 54 g/m^2

E-Glass in 90°, 15 g/m^2 epoxy binder on the bottom side, and 17 g/m^2 polyethersulfone (PES) stitching (compare Appendix A.2, Tab. A-3). The applied epoxy binder on both materials is *Hexion Inc.* (Columbus, Ohio, US) Epikote™Resin 05390. At time of the study, the binder was known as *Momentive Specialty Chemicals Inc.* (Columbus, Ohio, US) Epikote Resin 05390.

3.1.3 Tooling Material Used in this Study

For the manufacturing of GFRP samples, two different types of tools were used. For most trials, glass-ceramic plates Nextrema® 724-8 by *Schott* (Mainz, RP, Germany) with a thickness of 4 mm are used. By trial it was determined that these glass-ceramics have low microwave losses; they are virtually transparent. Additionally, their low coefficient of linear thermal expansion (CTE) of α =-0.4–0.9 $^{10^{-6}}/_{\mathrm{K}}$ between 20–300 °C allows for a high temperature delta inside the glass-ceramic without failure, compare A.5, 166.

Additionally GFRP tools were used. The 120 °C-trials evaluated in this study were manufactured on tools build of CR 141 and the NCF given above. Several more plates were manufactured on identical tools with an Airtech Toolfusion 3 matrix that has a T_g up to 218 °C.

3.1.4 Additives Used for Absorber Development

Two different carbon blacks (CBs) and black silicon carbid (SiC) are used for the development and manufacturing of absorbers. The CBs strongly interact with microwaves. As a consequence, the resin-CB mixtures have a much higher dielectric properties than the pure resin. The SiC has a high thermal conductivity and may be used for fine tuning the dielectric properties.

Both CBs are products supplied by *Orion Engineered Carbons*. The first CB used is Printex® XE 2 B (XE2B); this carbon black has a very high structure and surface-area. Through this structure and surface area, conducting networks form if only small amounts of the CB are distributed evenly in a matrix. Therefore, XE2B blended in epoxy drastically increases the epoxy's electrical conductivity[86]. A measurand for this structure is the oil absorption number (OAN). XE2B has an OAN of 420 $^{\mathrm{ml}}/_{100\,\mathrm{g}}$, compare A.5 page 170. In comparison, the second carbon black used—Printex® L Beads (LB)—has an OAN of only 117 $^{\mathrm{ml}}/_{100\,\mathrm{g}}$, see A.5 page 171. While it has a lower structure than XE2B, it is still described as a high structured carbon black [86] with a strong influence on the electrical conductivity of a CB-epoxy blend.

The used SiC is *silicon carbide bw plus (black)* supplied by *Piewplow & Brandt GmbH*. It has a FEPA F 1200 grain size. This equals a mean grain size of 3 μm, compare A.5 page 172.

3.2 Equipment and Procedures Used to Manufacture Plates and Samples for Mechanical Testing

In the following section the process to manufacture GFRP samples is described. The overall process can be divided in the following three steps that are further divided in Fig. 3-1.

1. Build-up of a glass fiber preform.
2. Infiltration of the preform with the epoxy resin.
3. Cure of the laminate in oven or microwave.

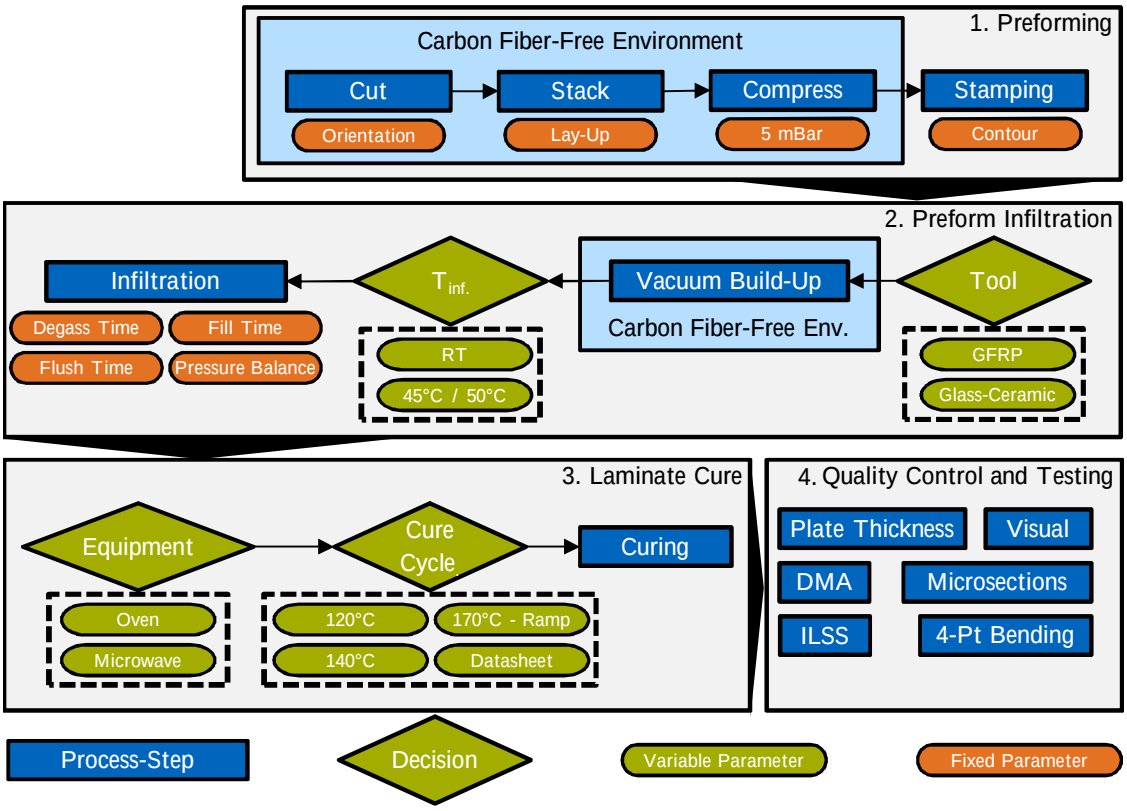

Fig. 3-1 Scheme of the manufacturing process of GFRP plates.

The first 2 process steps fundamentally influence the quality of the manufactured plates. The first step defines the fiber orientation and thus the mechanical properties. The second step ensures a void-free laminate. Therefore, special care is taken

to use well tested processes. This ensures constant conditions that allow for a solid comparison of the third step's influence. In this third step, the wet laminate is introduced into the oven or microwave. The oven or microwave applies defined temperature cycle to cure the resin. The resulting GFRP-plates are cut into specimens. These are used for quality control and testing of mechanical GFRP-properties.

3.2.1 Definition of Preforming Process

A binder-based preforming process was introduced, investigated, and optimized before specimen production. At the end of this optimization, a three step preforming process ensured constant conditions. First, layers are cut to $340 \times 520\,\mathrm{mm}^2$, stacked using a lay-up of [(+/−45°),(0°/90°), (−/+45°),90°,(+/−45°),(90°/0°),(−/+45°)], and sealed in a vacuum bag. After stacking, the set-up is heated under vacuum ($< 5\,\mathrm{mBar}$) to 140 °C for binder activation. This temperature is kept constant for 45 min to guarantee a low temperature gradient in the laminate—full heat through—before cooling. Last, the stabilized preform is stamped to $300 \times 480\,\mathrm{mm}^2$ with rounded corners ($r = 40\,\mathrm{mm}$) using a stamping iron. The rounded corners were chosen for compatibility reasons with other processes used at the workshop and to reduce possible edge effects of 90°corners.

During the subsequent microwave processing, local electric conductive contaminations, such as carbon fiber filaments, attract the microwave field and result in a much higher electrical field around the impurity; this leads to increased local heat development. Since the heat conduction in the laminate is comparably slow, the heat development results in local over-heating, which in turn damages the set-up. Therefore, a separate area in the chair's workshop is used for stacking and vacuum build-up to avoid contamination with carbon fibers, see Fig. 3-2. A similar effect—excessive heat-up of carbon fibers—is present when processing carbon fiber-reinforced plastic (CFRP) and was described by Kwak, Robinson, Bismarck, and Wise [72]. With CFRP, the edges are the problematic area. Therefore, the edges are commonly shielded using aluminum tape, compare [15], [19], [69], [77], [87], [88]. Kwak et al., however, used epoxy resin for shielding.

Fig. 3-2 Carbon fiber-free einvironment used for preforming of GFRP test plates and tools.

As mentioned, the described preforming process is a result of optimization. This took place after microsections of early manufacturing trials showed substantial voids. Early adaptions included variation in temperature, time and pressure during infiltration. However, only the manufacturing of a sample without binder showed no voids. Consequently, the preforming process and the used binder material were investigated by Louis Mahlau [89] in a supervised term project. The investigated binders were PA1541A (Co-Polyamide web by *Spunfab (Cuyahoga Falls, OH, US)*), EPIKOTE™ Resin 05311 (Epoxy powder by *Momentive Specialty Chemicals Inc. (Columbus, Ohio, US)* at the time of the study; by April 2018 distributed by *Hexion*), and the original binder material ABE003 (Co-Polyester web by *AB-Tec* (Iserlohn, NW, Germany)). The preforming process was carried out using different compaction pressures (1, 15, and 100 bar) and heating technologies (oven, press). The preforming temperature was tested and fixed before Mahlau's study. The compaction pressure did not appear to influence the porosity. The binder material was found to be the main factor influencing the porosity. As a consequence, glass fiber materials with 15 g/m² predeposited epoxy binder EPIKOTE™ Resin 05390 (Hexion former *Momentive*) were used for the studies at hand. The EPIKOTE™Resin 05390 was chosen as a replacement for EPIKOTE™ Resin 05311, since the investigated binder 05311 was not available; Saertex recommended 05390 as a successor.

3.2.2 Definition of Infiltration Process

The vaccuum assisted resin infusion (VARI) process is used for preform infiltration. The build-up for the process is depicted in Fig. 3-3.

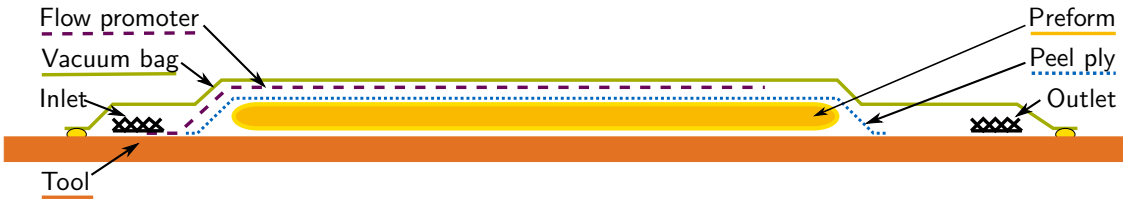

Fig. 3-3 Infiltration set-up used. The vacuum applied to the outlet sucks in the resin that is kept at ambient pressure. The resin flows from the inlet through the flow promoter into the dry preform.

Due to the resin's high viscosity of 600 mPas at room temperature (RT), initial trials were carried out at an elevated infiltration temperature of 45 °C. For microwave specimens, however, the set-up has to be transferred to the microwave equipment before the curing cycle starts. Since connecting the temperature sensors takes some time, the microwave specimens cool down between infiltration and curing. Consequently, the infiltration process was changed to RT for all configurations to maintain stable process conditions. The cycle with a maximum of 120 °C (O_120)

and the reference cycle (O_ref) have been manufactured and tested using45 °C as infiltration temperature. Consequently, the O_ref samples at RT were repeated to assess the infiltration temperature's influence. Both processes were as follows:

RT-Process: The resin was mixed and degassed for 10–15 min. The inlet was opened until the plate is completely filled (≈10–20 min), after which the plate was flushed for 10 to 15 min. Subsequently, a pressure balance at 400 mBar (absolute) is set at the outlet and the inlet/resinpot. This equalization pressure was held for 5 to 10 min. The vacuum connection was closed, the infiltrated plates were disconnected from the vacuum equipment and transferred into the oven or microwave. Here, the temperature sensors were attached and connected to the oven or microwave. For microwave processes, the vacuum connection and monitoring is reconnected to enable the detection of leakage. Consequently, the cure cycle is started.

45 °C-Processs: The resin was mixed, heated to a temperature of 45 °C in a convection oven to reduce the resin viscosity, degassed for 10 to 15 min in a vacuum oven, and kept at this temperature for infiltration. During this time, the tool and preform was pre-heated for one hour at 50 °C. It was kept at this temperature during infiltration. The inlet was opened and after the plate was completely filled, which took about 5 to 10 min, the resin valve was kept open for another 5 min for flushing. Subsequently, a pressure balance at 400 mBar (absolute) was set at the outlet and the vacuum oven that contains the resin. This equalization pressure was held for 5 to 10 min before the infiltration was finished, the inlet and outlet were closed, and the cure cycle was started.

3.2.3 Definition of Cure Cycles

The curing process has a substantial influence on the properties of epoxy resins and thereby the investigated composite materials. On the one hand, the chemical reaction that is triggered during the curing process is an exothermic one. Thus, when the resin or composite is heated too fast over a certain point, the exothermic reaction results in a thermal runaway and the material overheats. To prevent this, a dwell time at 85 °C is always maintained. On the other hand, if the maximum cure temperature is way below the resin system's target T_g of 139 °C, the material does not cure completely. Consequently, the mechanical properties are not fully developed. To observe this possible influence of varying curing conditions on the mechanical properties, three different temperature profiles using maximum temperatures of 120 °C, 140 °C and 170 °C are used for cure.

The same curing cycles will be used in oven and microwave curing; however, two slight adaptions are made in microwave processing due to differences between elec-

tromagnetic and convection heating. First, in microwave curing, the heat is generated directly in the material while there is a through heating time in convection oven curing. During oven curing, it takes approximately 15 min until the part reaches the oven's temperature. Consequently, the dwell time is reduced by these 15 min for microwave processes. By this, for processes that have three dwell times, microwave processes save up to 45 min of cycle time. Secondly, the microwave controller only takes the hottest temperature sensor into account. The average temperature in microwave processing, however, is slightly lower in all observed cases. As a result, the control temperature for microwave processes during the dwell time is increased by 2.5 °C.

With these adaptions, three different temperature cycles are compared; a fourth temperature cycle is used for reference in the oven only, see Tab. 3-2 and Fig. 3-4.

Tab. 3-2 Different cure cycles with start and infiltration temperatures used in this study. 5 °C/min heating and cooling ramps are used between temperatures if not given otherwise.

Start	**RT**	**50 °C**	**85 °C [min]**	**120 °C [min]**	**140 °C [min]**	**170 °C [min]**	**Cycletime [min]**
O_120	No	Yes	75	60	-	-	170
MW_120	Yes	No	60	45	-	-	141
O_140	Yes	No	75	75	45	-	238
MW_140	Yes	No	60	60	30	-	194
O_dyn	Yes	No	70 °C to 110 °C with 1 °C/min			35	122
MW_dyn	Yes	No	70 °C to 100 °C with 1 °C/min			20	99
O_ref	Yes	Yes	195	195	195	-	628

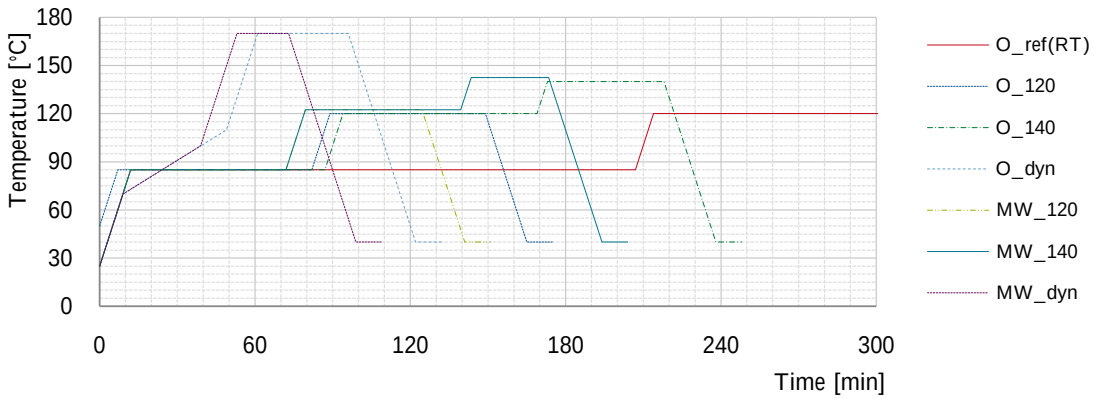

Fig. 3-4 Different cure cycles used. Microwave cycles have a dwell time that is reduced by 15 min and a dwell temperature that is increased by 2.5 °C. O_ref is not drawn completely due to its length.

The reference cycle (O_ref) is the cure cycle used to obtain the mechanical and thermal properties of the resin stated in the datasheet. It is 3 h at 80 °C, 120 °C, and 140 °C. Due to its length of over 10 h it is only investigated in the oven. The first comparing temperature cycle (O_120 / MW_120) ends after a shortened 120 °C dwell time, resulting in an incompletely cured resin. This is done to enhance possible effects of microwave curing that occur before full cure. The second cure cycle (O_140 / MW_140) has a longer 120 °C phase and adds a short 140 °C cure phase. Through the 140 °C addition, the degree of cure shall be pushed near to its maximum value. The last comparing cycle (O_dyn / MW_dyn) is carried out with the intention of microwave optimization; a steady temperature rise up to 170 °C is used to potentially utilize the in-depth heating of microwaves. To take the exothermic reaction into account, a very slow heating rate of 1°C/min starting at 70 °C is applied. This slow heating rate is maintained up to 100 °C in the microwave and, taking the through heating time into account, up to 110 °C in the oven.

3.3 Equipment and Procedures Used to Manufacture Absorber Samples

In the following section the equipment and process to manufacture absorber samples is described. The process can be divided in three steps that are further divided in Fig. 3-5.

1. Production of a master-batch (MB). Homogeneously distribute the carbon black (CB) and break up agglomerates in one component of the resin.
2. Mixing of absorber by adding further resin components and additional particles.
3. Further manufacturing of absorber to samples or absorber layers.

The first 2 process-steps define the absorber properties. A MB with a fixed CB-content is produced and used for the absorber production. The production of this intermediate MB has three benefits. Foremost, the production process of the MB can be defined and repeated with constant conditions; the process conditions do not change with the absorber's CB content. Secondly, the higher CB-content increases the viscosity of the mixture. This, in term, increases the shear-forces during the process. Increased shear forces—up to a level—are beneficial for the break-up of agglomerates. Last, several different absorber mixtures can be done using one MB.

The resulting absorber mixture can than be further processed to samples for characterization or to absorption layers. The production of absorption layers was investigated by Nora Weiner [90] and is not discussed in this work.

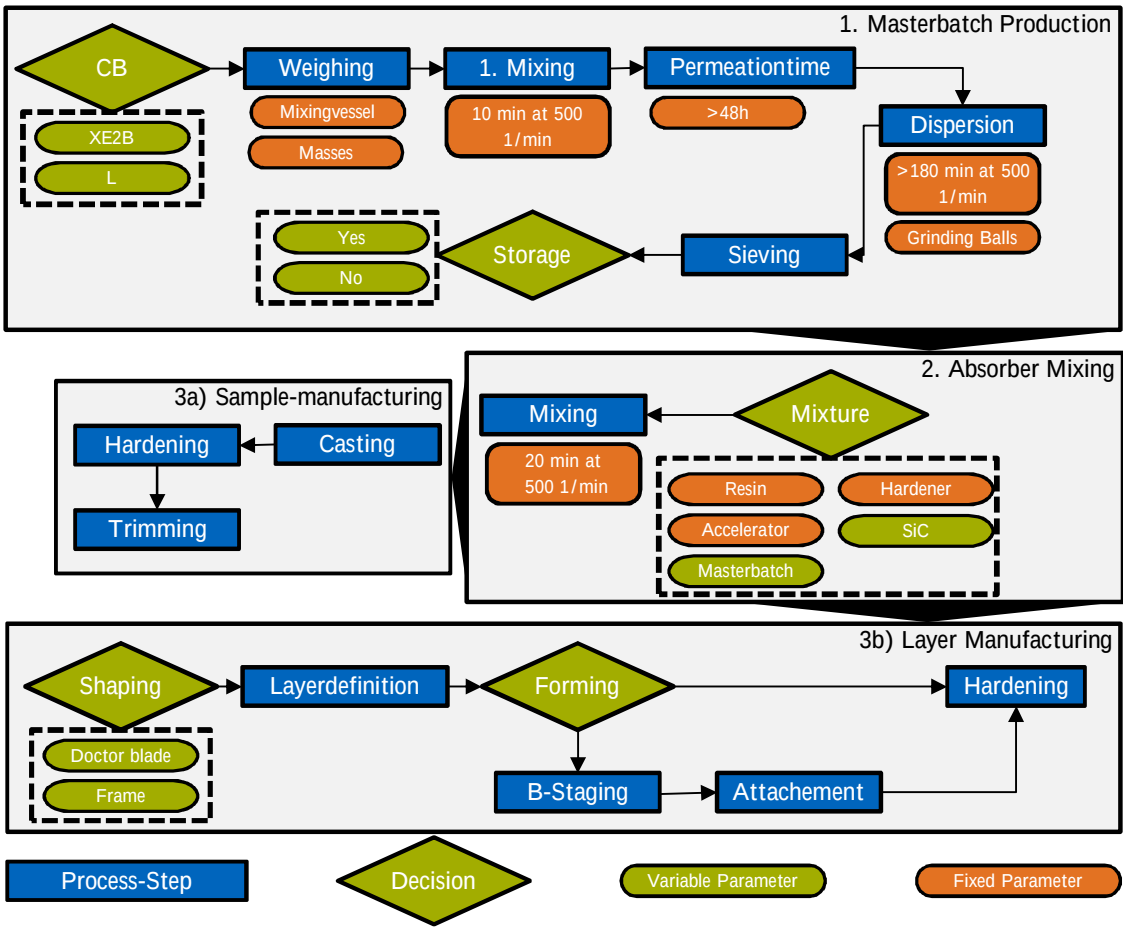

Fig. 3-5 Scheme of the manufacturing process of absorber materials in form of specimens or layers.

3.3.1 Calculation of Component Masses for Masterbatch and Absorber Composition

For both, the master-batch and the cured absorber (CA) the CB content and silicon carbid content are defined per volume. Thus, to calculate the needed masses during mixing, the density of MB and CA are calculated first. From this on, the masses needed are determined using the corresponding volume fraction (φ) and density (ϱ) of each ingredient.

The MB's density ϱ_{MB} is calculated by

$$\varrho_{MB} = \varphi_{CB_{MB}} \varrho_{CB} + \left(1 - \varphi_{CB_{MB}}\right) \varrho_A \tag{3-1}$$

where $\varphi_{CB_{MB}}$ is the volume-fraction of the carbon black in the master-batch and ϱ the density of the CB ($1.8\,{}^{\mathrm{g}}/_{\mathrm{cm}^3}$) respectively A-component of the resin system ($1.16\,{}^{\mathrm{g}}/_{\mathrm{cm}^3}$). For the manufacturing of the MB the needed masses (m) are now

calculated by

$$m_{CB_{MB}} = \varphi_{CB_{MB}} \frac{m_{MB}}{\varrho_{MB}} \varrho_{CB} \tag{3-2}$$

and

$$m_{A_{MB}} = (1 - \varphi_{CB_{MB}}) \frac{m_{MB}}{\varrho_{MB}} \varrho_A. \tag{3-3}$$

For further calculations, the shrinkage during the resin's cure has to be taken into account. To get a defined CB-content (φ_{CB}) in the solid resin, the right amount of carbon black has to be added via the master-batch. Therefore, the calculations for the cured absorber are more complex. First, the density of the cured absorber (ϱ_{CA}) is calculated taking the addition of the second additive, SiC, into account:

$$\varrho_{CA} = \varphi_{CB_{CA}} \cdot \varrho_{CB} + \varphi_{SiC_{CA}} \cdot \varrho_{SiC} + (1 - \varphi_{CB_{CA}} - \varphi_{SiC_{CA}}) \cdot \varrho_{rsol}. \tag{3-4}$$

The density of the solid resin ϱ_{rsol}=1.2 g/cm³ is given in the datasheet. Ongoing from the cured absorber's density, the volume (V) of the target mass can be calculated by $V_{CA} = \frac{m_{CA}}{\varrho_{CA}}$. The masses of the SiC can now be calculated directly via its volume fraction

$$m_{SiC} = \varphi_{SiC_{CA}} \cdot V_{CA} \cdot \varrho_{SiC}. \tag{3-5}$$

While this gives directly the SiC-mass that is added to the mixture, the CB-mass has to be added by the master-batch. With the needed CB-volume

$$V_{CB_{CA}} = \varphi_{CB_{CA}} \cdot V_{CA} \tag{3-6}$$

the needed MB-mass is determined by

$$m_{MB_{CA}} = \frac{\frac{(1-\varphi_{CB_{MB}})}{\varphi_{CB_{MB}}} V_{CB_{CA}}}{\varrho_A} + \frac{V_{CB_{CA}}}{\varrho_{CB}}. \tag{3-7}$$

Here, the first summand of the equation equals the resin mass added using the MB. Since the ratio of mixture of the resin is given in mass-percentage (100:90:2; A:B:C), the mixed resin mass is given by $1.92 \cdot A$. Consequently, the A component that has to be added is given by

$$m_{A_{CA}} = \frac{m_{CA} - (m_{CB_{CA}} + m_{SiC_{CA}} + 1.92 m_{A_{MB}})}{1.92} \tag{3-8}$$

The mass of hardener (B) and accelerator (C) is given when the first term of equa-

tion 3-7 and $m_{A_{CA}}$ are added and multiplied by the corresponding mass-fraction of 0.9 or 0.02

$$\begin{pmatrix} m_B \\ m_C \end{pmatrix} = \left(\frac{\frac{(1-\varphi_{CB_{MB}})}{\varphi_{CB_{MB}}} V_{CB_{CA}}}{\varrho_A} + m_{A_{CA}} \right) \cdot \begin{pmatrix} 0.9 \\ 0.02 \end{pmatrix} \quad . \tag{3-9}$$

3.3.2 Production of Masterbatches by the Homogenization of Absorber Particles by Means of Speedmixer

The production of each master-batch is done according to and documented in a life datasheet (LDS) (see Appendix A.2). The 5-step process was defined by the author in general and further investigated and refined by Lena Ametsbichler in a term project [91].

1. Mixture of Masterbatch

As first step, 150 g MB-mixture, consisting of resin (A) and CB, is homogenized for 10 min at 500 $^1/_{\text{min}}$ in a 250 ml tin container using a dual asymmetric centrifuge (DAC) *Speedmixer^{TM} DAC 3000 HP* by Hauschild.

2. Permeation Time

After the initial mixing, the MB is stored for at least 48 h. During this time the rough CB is saturated and wetted by the resin. In Ametsbichler's work a positive influence on the agglomerate size after dispersion was seen due to this permeation time.

3. Dispersion

The dispersion is again done in the DAC for at least 180 min at 500 $^1/_{\text{m}}$. To increase the introduced shear forces 60 g of 1 mm ceramic grinding balls (A.5, 173) are added for this step. The addition of the grinding balls to break up agglomerates in the DAC was proposed by Mr. Rockstein from the CB manufacturere *Orion Engineered Carbons*. During the mixing, the grinding balls roll over each other and thereby break up agglomerates between them.

While Ametsbichler proposed a mass of grinding balls proportional to the mixed MB, the amount of grinding balls was kept constant while the absolute MB mass was increased in this study. It is assumed that the distribution and thus effect of the balls in the vessel during mixing is not changed by the addition of more material. With this assumption, the agglomerates can be broken up nevertheless through the conservatively chosen mixing time of 180 min. This was confirmed by the same analysis methods Ametsbichler used.

4. Quality Control using a Grindometer

After the dispersion by the DAC the MB is checked for agglomerates using a 25 µm grindometer, see Fig. 3-6. For the test, two drops of the mixture are put on the upper, deep end of the grindometer's channels. These drops are then spread using a scraper in a smooth, slowe stroke through the channels; the material is investigated for scratch marks at a flat angle immediately after the distribution. A visible scratch mark indicates the the size of possible leftover agglomerates, compare middle Fig. 3-6. This process is repeated for three times and documented in the LDS. If several of the measurements indicate agglomerates above 7.5 µm at least 30 min of dispersion time in the DAC are added; an additional quality control is done afterwards.

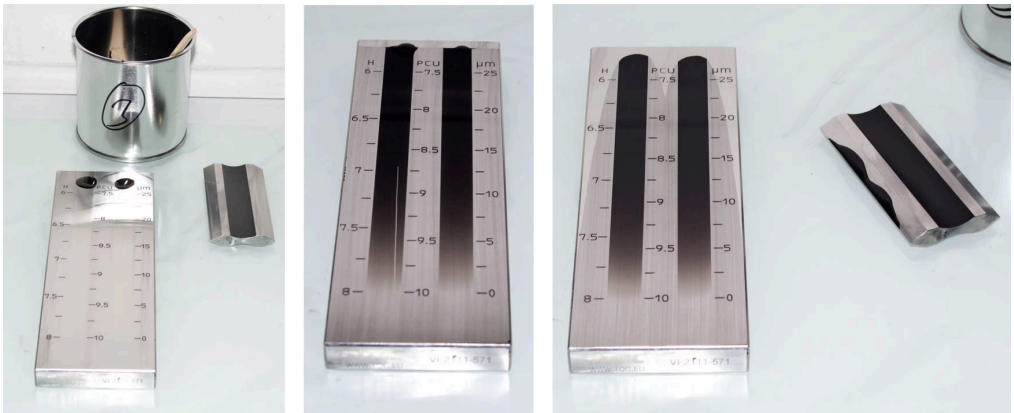

Fig. 3-6 Quality control of MB using a grindometer. From left to right: Application of sample; test with 12.5 µm agglomerates; test without agglomerates.

5. Sieving

Last, when the MB has a sufficient quality, the MB is pressed through a metallic sieve having a small mesh. This retrieves the grinding balls and the pure MB can be used for further sample processing.

3.3.3 Manufacturing of Test-Specimens for Dielectric Testing by Means of Casting and Grinding

Ongoing from the MB, the absorber mixture is prepared using the following four steps:

1. Addition of further additives (SiC) if needed.
2. Addition of A, hardener (B), and accelerator (C).
3. Mixing in DAC for 20 min at 500 $^{1}/_{\text{min}}$.
4. Quality control using the grindometer if no SiC or other abrasive is used.

The use of a MB in the production of a absorber mixture ensures that a constant quality is reached throughout all samples in regard to the particle distribution and size. Thus, the absorber properties are independent from variations in particle distribution. The geometry of the samples, while not influencing the physical properties, does have a strong influence on the measurements. As will be described in the following section 3.4.2, a deviation from the calibrated sample size has a huge influence on the measured dielectric properties. Therefore, the three manufacturing steps for the test specimens are specifically designed to result in samples of precise size.

1. Casting

First, the samples are cast in aluminum forms with a diameter of 7.8 mm and a height of 15 mm, compare Fig. 3-7. To ensure a good quality in size and surface, the diameter of the aluminum forms was defined using a reamer.

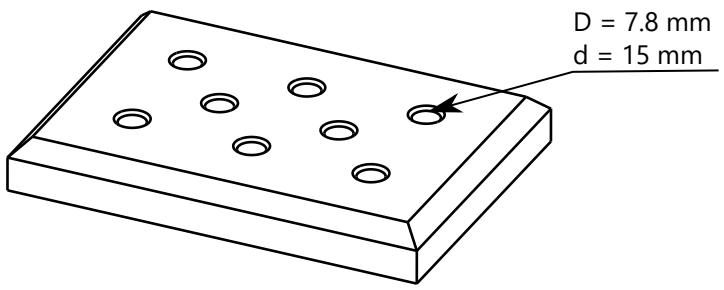

Fig. 3-7 Castingform with 15 mm depth to define the 7.8 mm diameter of the dielectric specimens.

2. Cure and Demold

The samples are cured using the standard temperature cycle of the resin according to the datasheet, compare appendix A.5, and heating ramps of 1 $^{\circ}\mathrm{C}/\mathrm{min}$. After cool-down, the samples are removed from the form. Two of the 8 cast samples are prepared for microsections. A fringe on the remaining samples is clipped so that simple cylinders remain.

3. Lengthening

Last, the samples are trimmed to the target length of 10±0.05 mm. For this, an adapter for a Struers TegraPol-21 polishing machine equipped with a Struers TegraForce-5 sample holder was constructed, see Fig. 3-8. With this adapter, up to four samples are put in a fixture and are sanded down using a FE 320 sandpaper in two steps. In the first step, a short stamp is used to smoothen the topside of each sample. In the second step, a longer stamp is used that produces 10.0±0.2 mm long specimens.

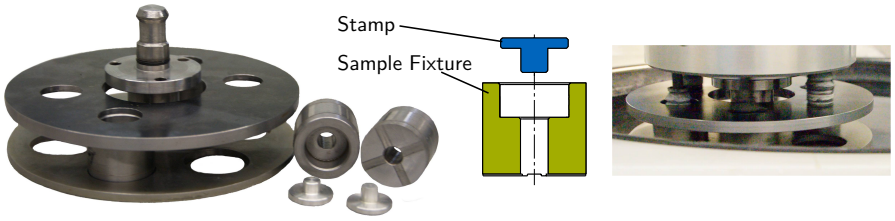

Fig. 3-8 Grinding fixture for shortening the dielectric samples to their 10 mm length.

3.4 Test Procedure for Absorber Samples – Cavity Perturbation Technique

3.4.1 Measurement Principle

There is a variety of measurement techniques to determine the dielectric properties of materials. Depending on the estimated material properties, the relevant frequency, and the appearance (liquid/solid, large/small) of the material, different techniques can or must be used. In this study, a custom build measurement set-up designed by Vasileios Ramopoulos of the Karlsruher Institute of Technology (KIT) is used. In the following the measurement principle is outlined. The system itself, and a second system used for calibration, is described in more detail by Ramopoulos et. al. in [92] respectively Soldatov et al. in [93].

The set-up consists of a cylindric chamber where the 2.5 GHz microwaves are coupled at one side and decoupled at the opposite site, compare Fig. 3-9. Due to the

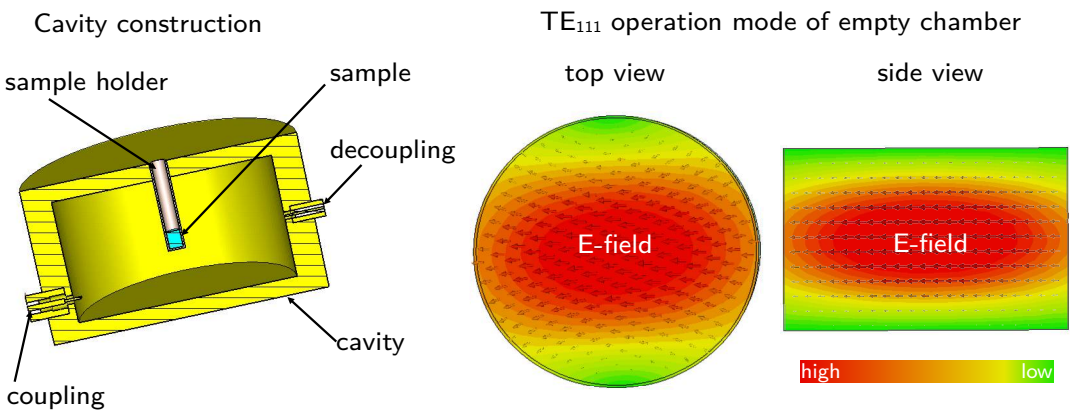

Fig. 3-9 Cavity design and field pattern of cavity perturbation measurement set-up (figure adapted from [94]).

chamber design, only one mode (TE_{111}) is possible and the field pattern of the chamber can be predicted numerically. The geometry of the chamber results in a distinct resonant frequency (f_{ref}) and quality factor (Q_{ref}). Those factors are measured continuously. When a sample is introduced, both the resonant frequency

and the quality factor are shifted resulting in a f_s and Q_s. This shift can be used to determine the dielectric properties using the cavity perturbation theory

$$\varepsilon_r' = \frac{1}{A}\frac{(f_{ref} - f_s)}{f_{ref}}\frac{V_C}{V_s} + 1 \tag{3-10}$$

$$\varepsilon_r'' = \frac{1}{B}\left(\frac{1}{Q_s} - \frac{1}{Q_{ref}}\right)\frac{V_C}{V_s} \tag{3-11}$$

where V_C is the volume of the chamber, V_s is the volume of the sample, and A and B are calibration factors. They are determined using a numerical simulation. However, both calibration factors depend on the dielectric properties ε_r' and ε_r'' of the sample. Consequently, under the assumption of a defined chamber geometry, specimen geometry, and position of the specimen, the resulting f_s and Q_s are calculated for a range of dielectric properties. The sample's dielectric properties can then be determined by matching the calculated and measured frequency and quality factor shift.

3.4.2 Systematic Errors

The following three systematic errors are known, were observed, and—if possible—are considered during measurements and evaluation.

Calibration Error

The first systematic error is made by the calibration. Since the calibration assumes a perfect formed chamber and a defined sample position and size, it does not fit perfectly with reality. However, all samples are measured using the same calibration. As a result, the samples can be compared to each other without problem.

Assembly Error

Likewise, the calibration assumes a perfect contact between the chamber and its lid. In reality, the contact between lid and chamber changes the quality factor. This was observed during the studies as a sample fell inside the resonator. After opening the chamber to remove the sample, the measured values dropped by ≈15-20%. The repeated opening, cleaning, and closing of the chamber increased the measured values by ≈10% above the initial measurements. Consequently, all measurements were repeated using the cleaned chamber; all prior measurements were discarded. As with the calibration error, all measurements were done using one constant set-up and can be compared.

Sample Positioning

The error made by the positioning of the sample has a systematic component. On the one hand, the in-depth positioning inside the chamber influences the results. By arranging the sample holder according to its position in the model, this error is

minimized. On the other hand, an influence of the radial orientation of the sample holder on the measurements can be seen when rotating it; there is no perfect perpendicularity between sample holder and the horizontal axis of the chamber. To take this into account, the sample holder and cavity were marked and all samples measured using the same orientation of the holder.

3.4.3 Random Errors

Sample Geometry and Size

As stated by Ramopoulos in [92], the measurement error by a tolerance of ± 0.2 mm in sample length and of ± 0.1 mm in sample diameter is up to $\pm 3.7\%$ for the permittivity ε_r' and up to $\pm 15\%$ for the loss factor ε_r''. To minimize this known statistical error, the production process was defined as described in section 3.3 above. Since the error through both deviations from the model, length and diameter, changes linearly with the deviation, compare equation 3-10 and 3-11, reducing both tolerances has a big influence. Overall, 85% of the manufactured specimens are between 10 ± 0.05 mm in length.

Handling of Samples and Measurement Procedure

To minimize systematic errors, every sample is handled in a identical way during all measurements. Nevertheless, random errors occur—they are a part of every measurement. Apart from the always slightly varying sample position this variance comes from changes in the measurement device itself like minimal changes in currents or part temperature. To ascertain this random error, a sample is measured for thirty times in between other samples. Every measurement is done according to the same procedure as a regular measurement. In other words, 5 measurements are done in close succession between sample series. The sample is replaced after every single measurement.

This random error investigation shows no drift inside each measurement block or over time, compare Fig. 3-10. Relative to their mean value, the overall variance is below $\pm 0.5\%$ for the permittivity ε_r' and below $\pm 3\%$ for the loss factor ε_r'' at the measured point.

3.5 Procedures and Equipment Used for Quality Control and Testing

3.5.1 Preparation of Samples for Quality Control and Testing

After manufacturing and before cutting, the thickness of every plate is measured at 12 distinct points as a first quality control. After this the reference cuts and

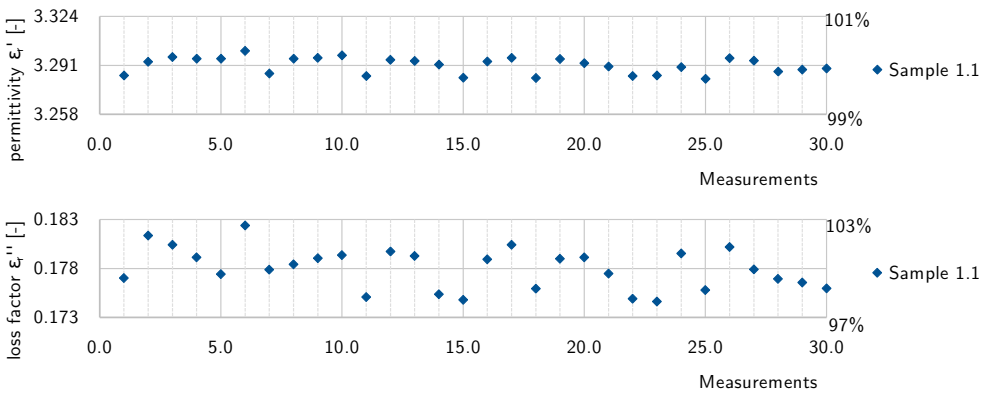

Fig. 3-10 Random error of ε_r' and ε_r'' measurements.

coupons are marked, compare Fig. 3-11. A buss saw of type "Tiger 1505A" by *Metallquattro OHG* equipped with a water cooled diamond blade was used for the reference cuts. From the sample coupons, all specimens were wet-cut using a buss saw "DV 25" by *Batisti Meccanica GmbH* equipped with a diamond blade and high precision sliding table. The positions of 4-point bending (4-pt), inter-laminar shear strength (ILSS), dynamic mechanical analysis (DMA), and microsection samples is shown in Fig. 3-11. The test procedures will be described in the following sections.

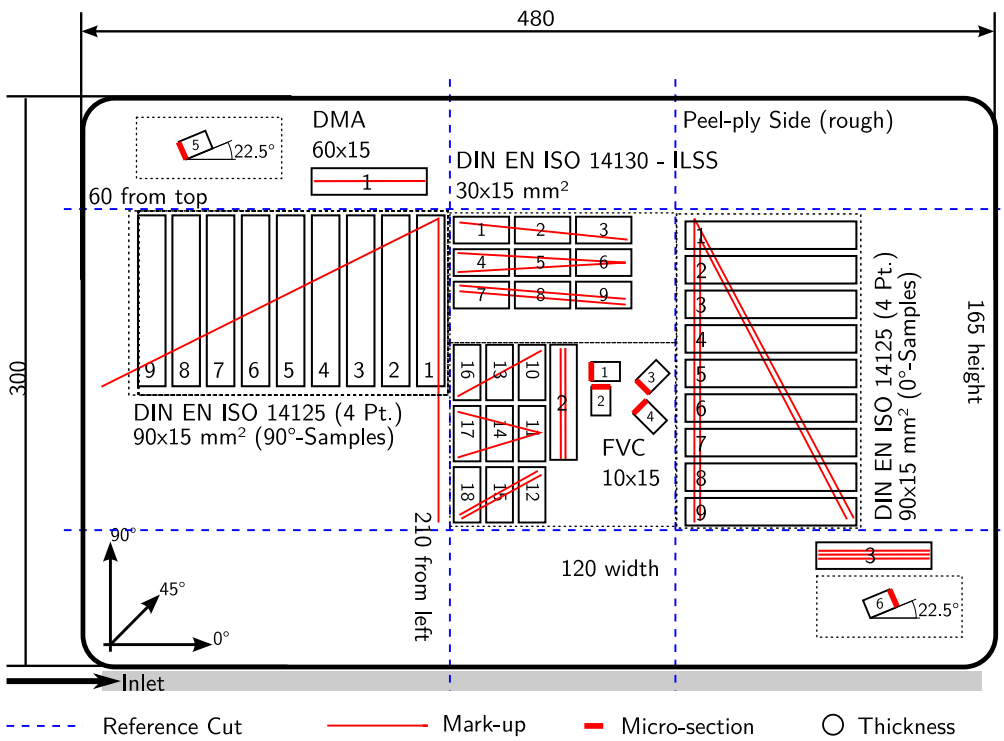

Fig. 3-11 Cut-out plan of sample with positions of quality control and mechanical test specimens. (Measurements in mm).

3.5.2 Dynamic Mechanical Analysis for Glass Transition Temperature Observation

A basic criterion to compare the degree of cure of an epoxy resin system is the glass transition temperature (T_g). The T_g can be measured by different phenomena such as the change in specific heat, the mechanical characteristics, or the optical properties. Since the different measurement methods base on different physical principals, the values vary and can not be compared directly. Due to the ease of its measurement, the mechanical definition of the glass transition temperature is used in this work. It is measured using the dynamic mechanical analysis (DMA) via a *Q800 DMA* by *Texas Instruments*. The test configuration is a double cantilever set-up, see Fig. 3-12. The DMA is used to apply a cyclic bending load on the specimen; the peak of the resulting $tan\,(\delta) = \frac{E''}{E'}$ during a temperature rise defines the T_g. To

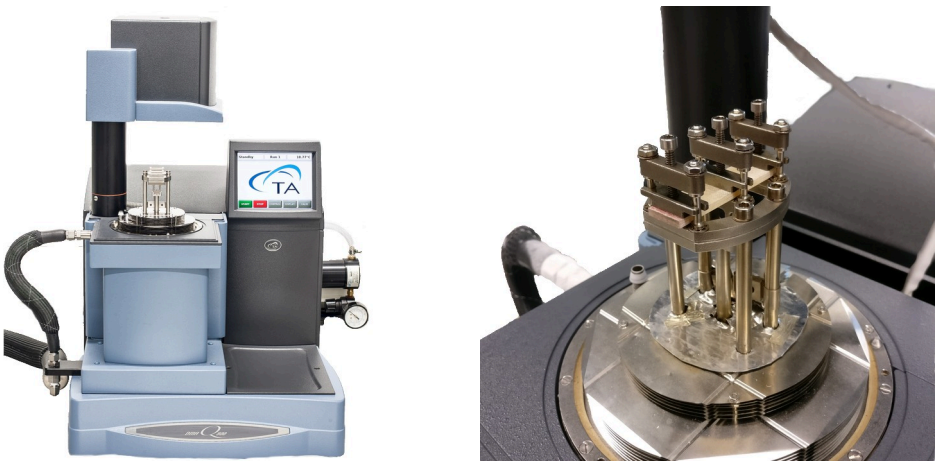

Fig. 3-12 *Q800 DMA* of Texas Instruments and double-cantilever bending rig with specimen (by Oberrauch [95], reworked by Author).

measure the T_g, samples of 60 to 15 mm^2 are used. They are tested using a support span of 50 mm. The amplitude for the trials is set to 20 μm and the frequency to 1 Hz. Both parameters were determined beforehand with pretrials to ensure linear behavior of the material during the measurements. For each measurement the sample is put into the set-up, the chamber is closed, and the procedure started. Now, the DMA heats chamber and sample to 70 °C. After a a soak time of 10 min, it heats the sample using 2 °C/min to 170 °C under the cyclic loading. The measurement parameters, the output of a measurement, and an evaluation are depicted in Fig. 3-13.

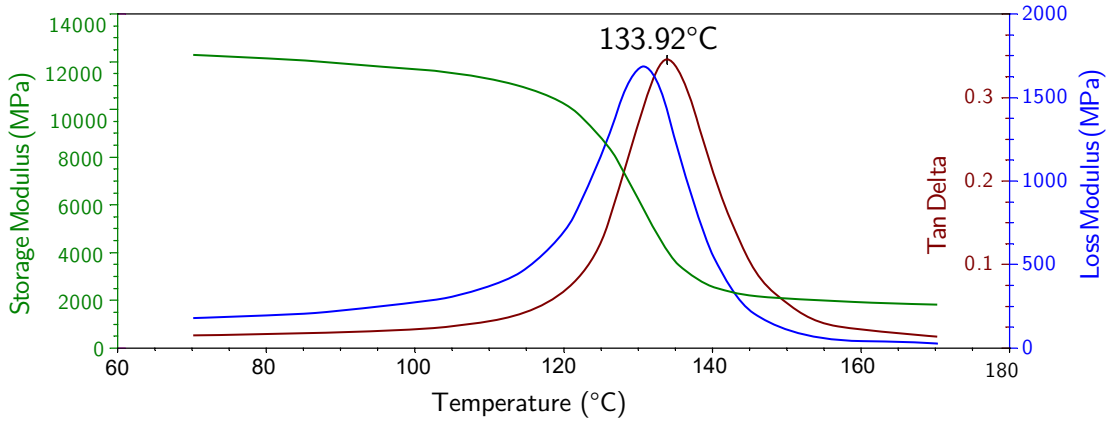

Fig. 3-13 Recording of DMA measurement with evaluation of the T_{g-DMA} at the peak of tan(δ). Heat up to 70 °C and soak time are not recorded by the DMA.

3.5.3 Inter Laminar Shear Strength Tests for Mechanical Investigation

The inter-laminar shear strength (ILSS) tests are based on DIN EN 14130 [96]. For the tests, a universal testing machine Hegewald and Peschke electromechanical drive using a 10 kN class 1 load cell is used. The test speed is set to 1 mm/min. The radii of the test rick follow the standard; the supports have 2 mm radii, the pressure fin has a radius of 5 mm. A supporting width of 17 mm (5 times the nominal sample thickness plus 2 mm) is used for all tests; the samples break due to shear. First, a caliper is used to measure the width and thickness out to two digits of each specimen at three points. The mean values of these measurements are used for calculating the apparent shear strength after the test. Samples where one of the measured thickness values deviates more than ±0.2 mm of the series mean thickness were tested but excluded afterward. A maximum of 9 and a minimum of 6 valid samples of 30 to 15 mm^2 are tested for every plate in each 0° (A) and 90° (B) direction. For testing, each sample is placed on the test rig with peel ply side pointing in pressure fin direction as seen in Fig. 3-14. The test is initiated and recording starts when a load of 5 N is reached to ensure specimen contact. For the evaluation, the apparent shear strength

$$\tau_{ILSS} = \frac{3}{4} \cdot \frac{F}{b \cdot h} \tag{3-12}$$

is calculated, where F is the force at failure, b is the width, and h the thickness of the specimen. All samples that underwent a specific cure temperature profile are averaged and the according 95% confidence intervals are calculated.

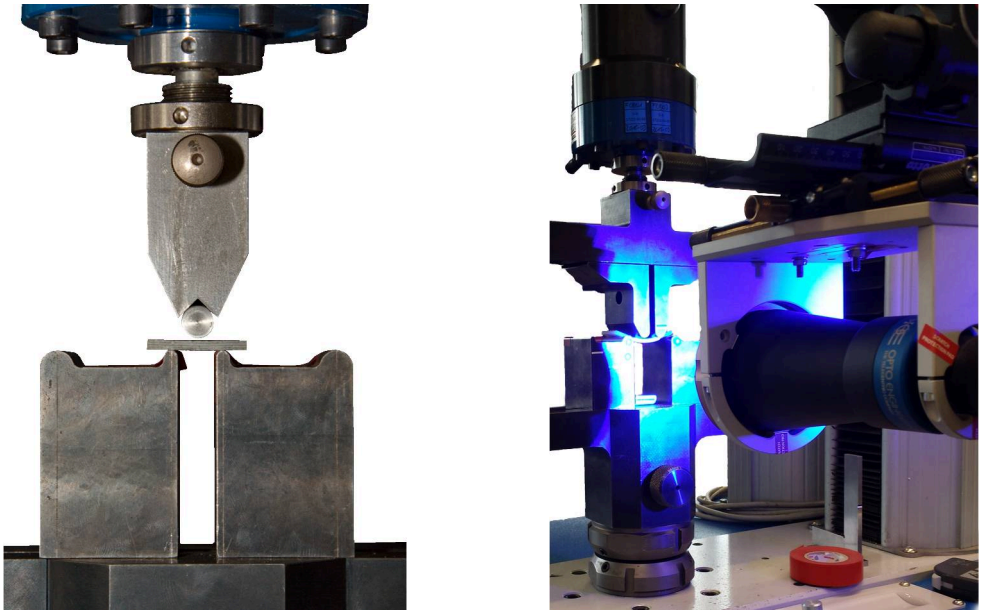

Fig. 3-14 Left: Frontal view of ILSS test set-up.
Right: Side view of illuminated 4-pt test set-up with video extensiometer.

3.5.4 4Pt-Bending Tests for Mechanical Investigation

The 4-point bending (4-pt) tests are based on DIN EN 14125 [97]. For the tests, a universal testing machine Hegewald and Peschke electromechanical drive using a 10 kN class 1 load cell is used. The test speed is set to 2 mm/min. The radii of the test rick follow the standard; the supports and pressure fins have 2 mm radii. The supporting width L is adjusted to be in the range of ±1% of

$$L = 22.5 \cdot h_{\text{series}} \ , \tag{3-13}$$

where h_{series} is the mean thickness of the sample series. Likewise, the distance between the pressure fins L' is adjusted to be in the range of ±1% of

$$L' = \frac{L_{\text{measured}}}{3} \ . \tag{3-14}$$

The samples deformation in the center is measured using an optical video extensiometer. The video extensiometer measures the absolute movement between the samples top or bottom edge and a fixed point at the support fixture. For this, the side of each specimen is highlighted using a white touch-up pen. A caliper is used to measure the width and thickness out to two digits of each specimen at three points before the test. The mean values of the measurements are used for following evaluations. Samples were one of the measured thickness values deviates more than ±2% of the samples mean thickness or the width deviates more than ±3% of the samples mean width are tested but excluded afterwards. A maximum of 9 and a

minimum of 6 samples of 90 to 15 mm^2 are tested for every plate in 0° (A) direction. Each sample is placed on the test rig with peel ply side pointing in pressure fin direction. Recording starts when an initial load of 5 N is reached. For the evaluation, the bending stress σ_f, the (relative) elongation ε_f, and the flexural modulus E_f are calculated according to DIN EN 14125 [97]. The equations for large deformations

$$\sigma_f = \frac{FL}{bh^2}\left\{1 + 8.78\left(\frac{s}{L}\right)^2 - 7.04\left(\frac{sh}{L^2}\right)\right\}, \tag{3-15}$$

$$\varepsilon_f = \frac{h}{L}\left\{4.70\frac{s}{L} - 14.39\left(\frac{s}{L}\right)^3 + 27.70\left(\frac{s}{L}\right)^5\right\}, \text{ and} \tag{3-16}$$

$$E_f = 500(\sigma''_f - \sigma'_f) \tag{3-17}$$

are used, where s is the current deformation of the specimen, σ''_f is the bending stress at $\varepsilon''_f = 0.0025$, and σ'_f is the bending stress at $\varepsilon'_f = 0.0005$ given by equation 3-16 above. All samples that underwent a specific cure temperature-profile are averaged and the according 95% confidence interval is calculated.

3.5.5 Microsections for Laminate and Absorber Quality Control

During preparation of the GFRP samples, 6 specimens were cut out under different angles and at varying positions, see Fig. 3-11 above. These specimens were embedded in an epoxy matrix and microsections prepared. The inspections of the samples revealed one lay-up error in a sample plate. Apart from that, some stray voids on singular microsections, compare Fig. 3-15, were found. However, due to the very local and thus random character of the investigation, no correlation between the microsections and the mechanical properties was evident.

Fig. 3-15 GFRP microsection showing exemplary voids.

For dielectric measurements 8 samples were cast of each configuration. Two of these samples were embedded and microsections prepared. The microsections done for all compositions showed good absorber quality and no abnormalities. Compilations of all microsections were done for inspection and documentation, compare Fig. 3-16.

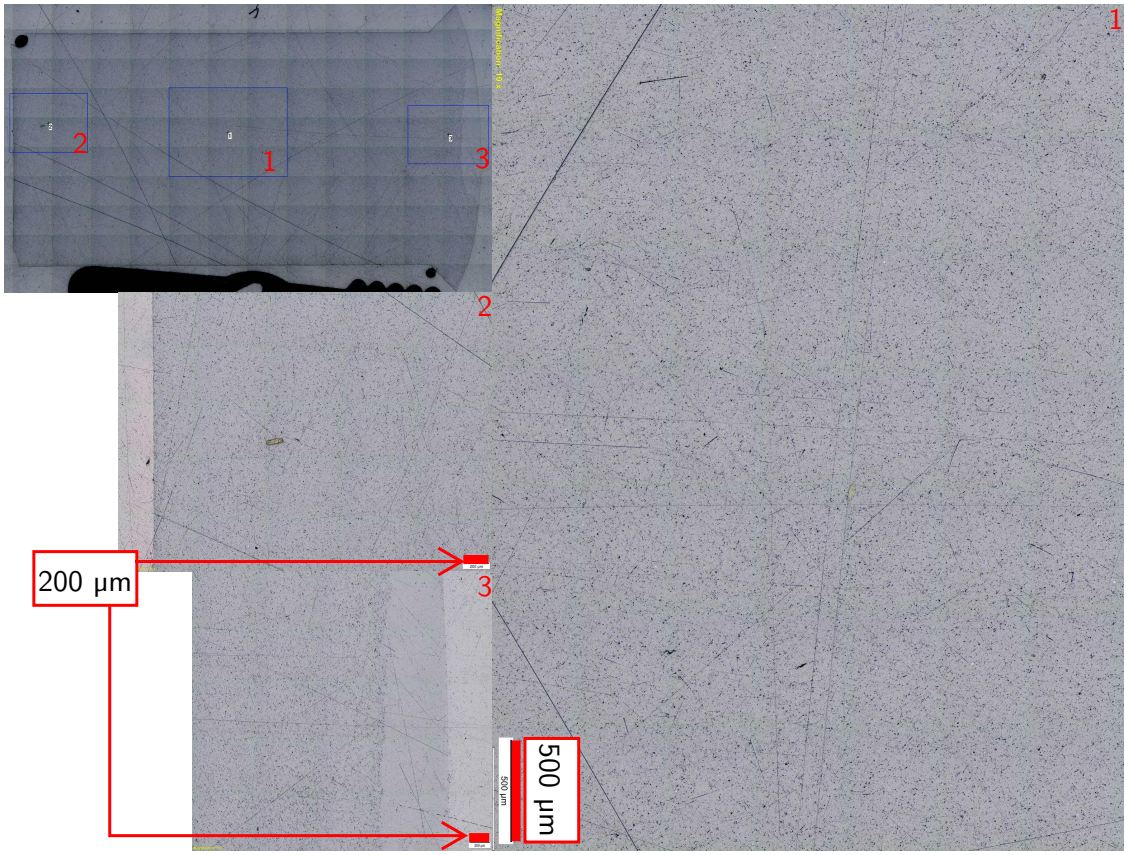

Fig. 3-16 Exemplary compilation of absorber microsection photos with 0.5 V% carbon black Printex® L Beads and 1.5 V% silicon carbid.

4 Microwave Applicator, Adaptions, and Lessons Learned during Manufacturing

4.1 Microwave Applicator Hephaistos CA 180/200

The microwave utilized in this study is a *Vötsch Hephaistos 180/200* (VHM180) microwave applicator, see Fig. 4-1. It has a hexagonal shape with an outer diameter of 1.8 m and a depth of 2 m. The hexagonal shape increases the field homogeneity according to [27], [76]. In depth the applicator consists of two modules of which each is equipped with 12 1 kW magnetrons. These magnetrons emit their power into slit rectangular waveguide antennas that irradiate the process chamber. The magnetrons can be activated individually or in any combination. This provides a nominal power output of 1 to 24 kw. In addition, the nominal power output of the overall magnetron combination can be limited in a range of 10 to 100%. This is arranged by a pulsed operation of the magnetrons. The magnetrons are only active for the given fraction of a 2 s interval, the interval being a hard-coded value in the *Vötsch* Controller. The real maximum power output of a single magnetron normally lies slightly below its nominal value. Due to additional losses inside the waveguide antenna used to couple the microwaves into the process chamber, the real power per magnetron is approximately 0.85 kW. This maximum value has been measured using a calorimetric measurement setup using a flowing water load provided by Karlsruher Institute of Technology (KIT)[98].

The absolute power output of the equipment, however, has no practical relevance for the manufacturing trials; the power level is controlled by the part temperature over a proportional integral derivative (PID)-control algorithm of the *Vötsch* controller. The PID-control parameters are important to reach a stable process. Experience from the KIT and LCC show, that a more homogeneous temperature distribution is reached if the power output variations i.e. control oscillations are minimized. For this reason, the PID-parameters are adapted before and during the plate production. Likewise, the amount of magnetrons is restricted, a constant wa-

Fig. 4-1 *Vötsch Hephaistos 180/200* located at the Chair of Carbon Composites with its capabilities and additions. The hexagon has a diameter ov 1.8 m and a depth of 2 m.

ter load introduced, the magnetrons constantly changed during the process, and mode stirrers added to reach a stable process with homogeneous temperature distribution. A systematic study of this influencing factors is given in the following section.

4.2 Influence of Modifications and Control Parameters on Temperature Homogeneity

4.2.1 General Design of Temperature Homogeneity Study

Initial trials to cure glass fiber-reinforced plastic (GFRP) using a *Vötsch* microwave located at the KIT showed a good temperature homogeneity. However, during the initial operations of LCC's VHM180 and throughout the first manufacturing trials, this could not be reproduced. While both systems have the same size and magnetron configuration, KIT's equipment is controlled by a custom made LabView program. Through comparison of these two microwave systems and discussions with Guido Link KIT, Volker Nuß from KIT, and Stefan Betz (Vötsch Industrietechnik) several factors were identified that might influence the temperature homogeneity and thus process stability. These changes were introduced on the fly and simultaneously for specimen manufacturing. While this improved the process stability and temperature homogeneity, the factors' influences could not be attributed. Consequently, a study was set up to investigate the influence of different parameters to simplify or further improve the process.

4.2.2 Setup and Realization of Homogeneity Study

The setup for this study is designed to exclude possible influencing factors that are not part of the investigation. For this, a test piece of blackened 3 mm nitrile/styrene-butadiene rubber (NBR/SBR) is placed on a virtually microwave transparent carrier material of 10 mm POM-C. The setup is suspended on two crossed clothesline ropes out of polyester. This configurations is than repeatedly heated for 5 min followed by a cool-down phase of at least 70 min. A video is recorded of every heat-up using a Flir A325sc, a 90° wide angle optic, and a 1 Hz recording frequency. To furthermore guarantee stable conditions over different parameter-sets, the test piece is pressed on the support using a vacuum bag setup, the main switch of the microwave stays on, and the build-up is not touched between trials. The setup can be seen in Fig. 4-2. The short heat-up time results in a low temperature rise and

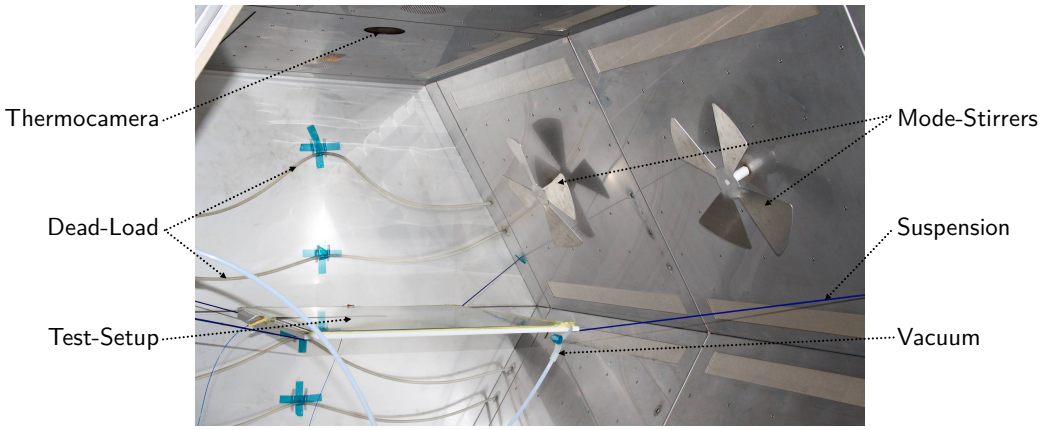

Fig. 4-2 Test setup used for homogeneity study inside the VHM180.

reproducible conditions. In combination with the pressure of the vacuum setup a constant heat flow is assumed. Through the POM-C plate and clothesline ropes a possible influence of the support is eliminated. The onetime set up guarantees that all thermal camera videos can be evaluated in an identical area.

Modde is used to set-up a design of experiments (DoE) study using the following 5 test parameters that are summarized in Tab. 4-1.

Mode-Stirrers (Stir)

The Mode-Stirrers are slowly turning reflective fans out of aluminum. Per module 1 Mode-Stirrer with a diameter of 40 cm is installed. The mode-stirrers are a qualitative factor that is either **Off** or **On**.

Dead-Load (Load)

The Dead-Load is introduced in the equipment in form of a flowing water load. The Dead-Load's amount of water inside the microwave mainly defines the absorbed power. This amount of water is defined by the PA-tube (inner diameter 8 mm) that is lead through the equipment. To further compensate the temperature dependent

absorption properties, the water flow is kept constant by a marking on the faucet. For trials without Dead-Load the tubes are emptied using a compressed air pistol. Load is a qualitative factor set to either **No** or **Yes**.

Sinus Function (Sin)

The Sinus Function is a parameter that is set in the *Vötsch* Controller. It can be turned on or off and its period can be defined from 60 s upwards. When active, the %-power-level of the magnetrons is superposed by a sine; a set 50%-power-level would change continuously over the set period. The %-power-level is defined as a quantitative factor using the three levels **0 s**, **60 s**, and **120 s**.

Magnetron Count (MCoun)

The number of active magnetrons per module defines the minimum and maximum power level. While up to 12 magnetrons per module are possible, the resulting power of 2.4 kW (10%) to 24 kW (100%) would overheat the setup. Depending on the Magnetron Count the %-power level is adapted to get a constant power of nominal 1 kW per module. The Magnetron Count is defined as a quantitative factor using the three levels **1**, **3**, and **5** magnetrons; the %-power level is set to 100%, 33.3%, and 20% accordingly.

Magnetron Change (MChan)

Magnetron Change describes the intervall at that magnetrons are changed periodically. This is only possible when only a subset of magnetrons is active; for the current investigation, this is always the case. By changing the magnetron selection, more radiation sources from different directions are used over the process. The Magnetron Change is programmed manually by actively changing a magnetron mask. The magnetron change is defined as a multilevel factor using the time values **0 s**, **10 s**, and **30 s**.

Tab. 4-1 Test parameters used in homogeneity study, their type of implementation in Modde, and their levels.

Factor	Short	Type	Low (0)	Mid (0.5)	High (1)
Mode-Stirrers	Stir	Qualitative	No	-	Yes
Dead-Load	Load	Qualitative	Off	-	On
Sinus Function	Sin	Quantitative	0	60	120
Magnetron Count	MCoun	Quantitative	1	3	5
Magnetron Change	MChan	Multilevel	0	10	30

For the realization of the designed study, the parameters Sinus Function, Magnetron Count, and Magnetron Change are transferred into Simpati programs, compare Fig. 4-3. The other two factors are defined manually before every trial. The Mode-

Stirrers are turned on and of via a remote control. The faucet supplying the Dead-Load's water is set to a defined position if required; the tubes are emptied using a compressed air pistol before trials without Load. When the Dead-Load and Mode-Stirrers are adjusted, the trial is started in three steps. Simpati's logging of the VHM180's states is activated, the Simpati program is started, and the thermal camera recording is triggered. After the Simpati program is finished, the logging and recording are stopped. The next run is started after the cool-down phase of at least 70 min.

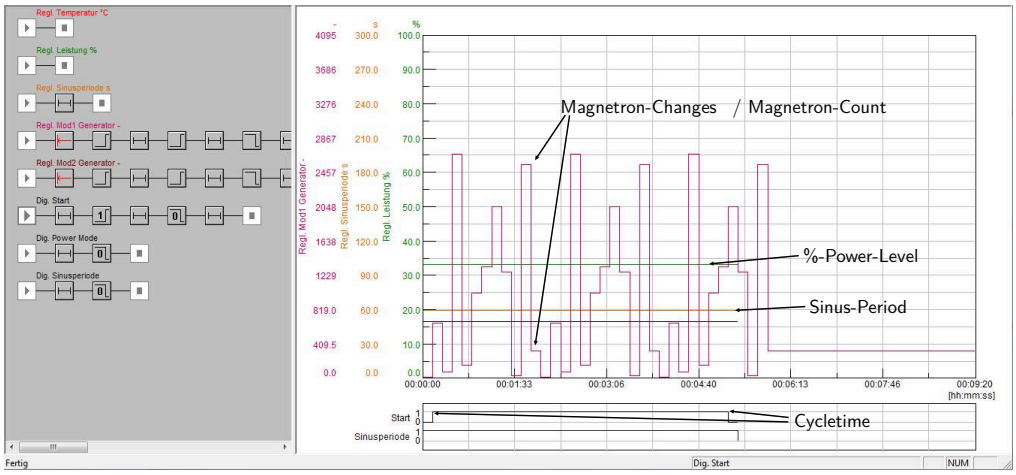

Fig. 4-3 Simpati interface with a programmed test cycle and the according configurations.

4.2.3 Responses used to Evaluate the Homogeneity Study

As responses, the recordings of the thermal camera are analyzed using the camera software FLIR ResearchIR Max. Since the setup is not touched between trials, a fixed area is defined for evaluation and used in every recording, compare Fig. 4-4. By those means, a fixed area and a fixed evaluation toolkit are defined. To furthermore guarantee comparable evaluation times, the first frame of the recording and the frame showing the highest temperature in the absorber area are evaluated. From the frames of those set points, the following three types of responses are inspected.

Temperature Responses

Two different Temperature responses are determined; the Temperature Mean (Tmean) and the Temperature Rise (Trise). Tmean or Tm is the average temperature of the absorber given by the thermal camera after irradiation. For three reasons the temperature has a slight offset to the real value: the correct emissivity is unknown, the wide angle optic distorts the picture, and a mesh is in front of the camera optic to shield it from microwaves. However, since these factors are the same between trial, Tmean can be used for comparison. The second temperature

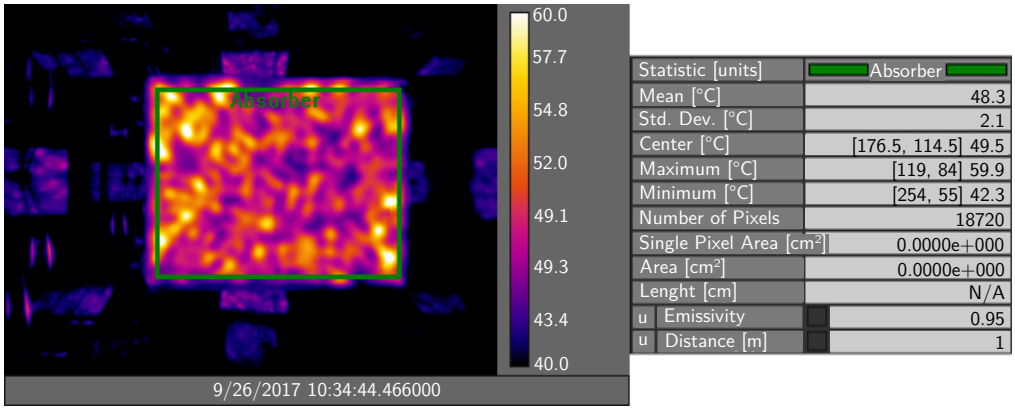

Fig. 4-4 Exemplary thermal camera image showing the region of interest used for all evaluations and evaluation statistics. A fixed scale between 40 °C and 60 °C is used for all exported figures.

response is Trise or Tr. It is defined as Tmean after irradiation minus Tmean of the first frame.

Standard Deviation and Relative Standard Deviations

The standard deviation (SD) of the absorber area is calculated from all 18,720 pixels of the absorber's thermal image after heat-up. It gives a direct indication of the temperature homogeneity. Since the size of SD may be influenced by the absolute size of the values, two additional relative responses will be investigated; the SD will be divided by Tmean (SD/Tm) and Trise (SD/Tr). The first, $\frac{\mathrm{SD}}{\mathrm{Tm}}$, is the coefficient of variation (cov) of the Temperature Mean. The second, $\frac{\mathrm{SD}}{\mathrm{Tr}}$, could be seen as the cov of the Temperature Rise.

Spread and Relative Spread

The Temperature Spread after heat-up (Spread) is the delta between the coldest and hottest pixel of the absorber area's 18,720 pixels. In combination with the SD's evaluation it may give an indication for factors that result in extreme local temperatures. As with SD, the relative Spread in relation to the Temperature Mean (Spr/Tm) i.e. $\frac{(T_{Max} - TMin)}{T_{Mean}}$ and in relation to the Temperature Rise (Spr/Tr) are investigated.

The thermal-images used for evaluation and the the according statistics can be found in A.3.

4.2.4 Methodology used During Evaluation of Homogeneity Study

During the statistical evaluation the results are fitted with Multiple Linear Regression (MLR); so, MLR is used to find a connection between factors and responses i.e. to build a model. Modde is used as a toolset for this statistical fitting and

evaluation of the study. The extensive Modde manual was used as guideline for interpretation[99], [100].

In the following, the plausibility of the data is checked using the factors Tmean and SD. Furthermore, the basic methodology during evaluation is described using the examples of these models. The following 6 steps are described in detail for the two responses and are checked for every model evaluation. After the inspection of each model, the results will be correlated with the trials' absolute results and their significance for real applications will be assessed.

1. Measurements Error and Total Variation

To check for errors in the measurements and get an indication of the reproducibility of the setup, the response variation of replicates is compared to the overall variation. While the replicate-variation is comparably big for Tmean, the reproducibility looks good for SD, compare Fig. 4-5. In numerical values, the ratio between the replicates delta and maximum delta is calculated. For Tmean this gives a rate of 14%, for SD a rate of 1%. Since the data of SD is clustered in the lower area, an additional numerical ratio is calculated; the ratio between replicates' delta and the upper and lower quartile. This neglects the extreme values and gives a ratio of 4.3% that is still very good. Overall, the ratio between error and variation is acceptable. The graphs for all responses can be found in A-4.

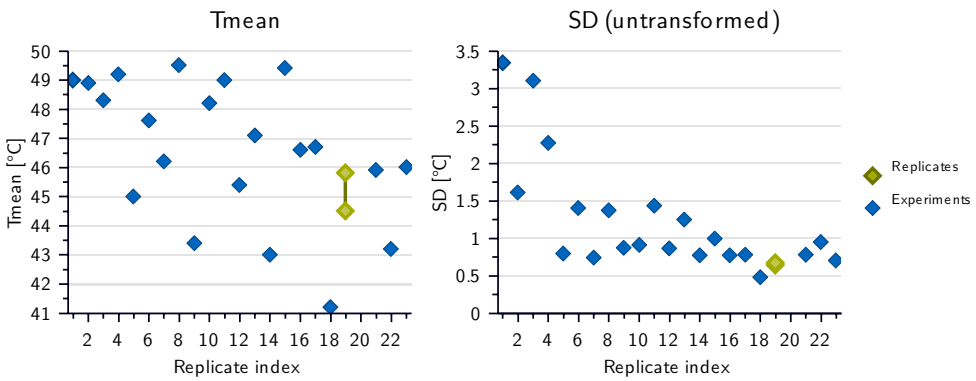

Fig. 4-5 Reproducibility graphs of exemplarily evaluated models of Tmean and SD.

2. Normal Distribution Check of Data and Transformation

In general, data can be seen as normal distributed if the distribution is bell-shaped. If this is not the case, transformation of the data can be beneficial for the model quality. For the trial at hand, the Tmean is normal distributed. SD initialy leans to the left. After a logarithmic transformation using $10log(y)$—as Modde recommends—a close to normal distribution is achieved, compare Fig. 4-6 SD_0 to SD˜. The transformation is marked by an attached "˜". Apart from SD, a logarithmic transformation furthermore leads to a normal distribution of the responses

SD/Tm, Spread, Spr/Tm, and Spr/Tr. The SD/Tr leans to the left even after a transformation; it is transferred anyway since it increases the model quality and it will be compared to the other SD-models. All histograms can be found in Fig. A-5.

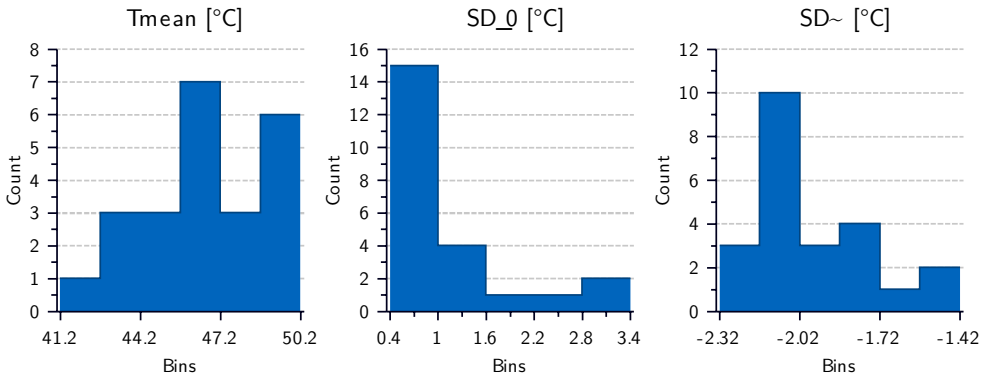

Fig. 4-6 Histograms of exemplarily evaluated models of Tmean and SD. The histogram for SD is given before (SD_0) and after (SD˜) transformation.

3. Investigation of Model Factors and Adaption

Next, the model's factors are investigated for significance. In the investigation a factor is seen as significant when the 95% confidence interval does not cross $y = 0$. During the initial observation, all interaction of the three "magnetron factors" Sin, MChan, and MCoun and the square terms of MChan and MCoun are evaluated, compare Fig. 4-7. To adapt and improve the model, all insignificant interactions and insignificant square terms are excluded. The resulting models are discussed below and can be found as a compilation in Fig. A-7.

4. Model Quality Check

The model quality is described by four parameters. Each of this would be 1 for a perfectly fitted model. The first parameter, the model fit R2, represents the quality of fit in the investigated range; it should be at least 0.5. Both, the mean temperature model's R2 and SD model's R2 are close to 0.9, compare Fig. 4-8. This indicates a very good agreement between models and measured values. R2, however, overestimates the models extrapolation quality. The second parameter, Q2, is an indication for this prediction quality. It generally underrates the models total quality. It should be at least 0.25 for a good model. Both Q2 are above this critical threshold. The model validity—as third factor—indicates statistical problems in the model if it is below 0.25; this is not the case. Last, the reproducibility, as investigated before, is good. At this point, SD can be marked as the more promising parameter. The quality of all further responses' models are discussed below and can be found as a compilation in A-6.

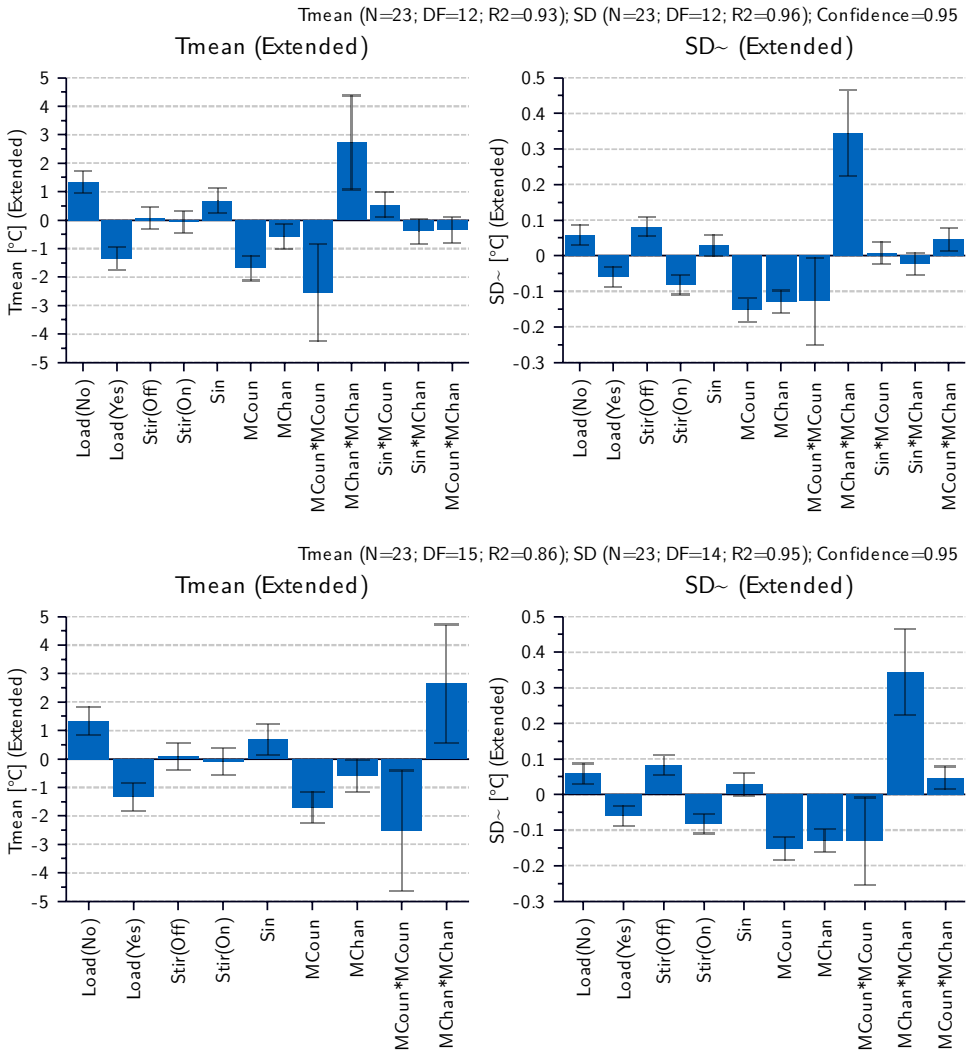

Fig. 4-7 Coefficient plots of exemplarily evaluated models of Tmean and SD before and after exclusion of insignificant interaction and square-terms with 95% confidence intervals.

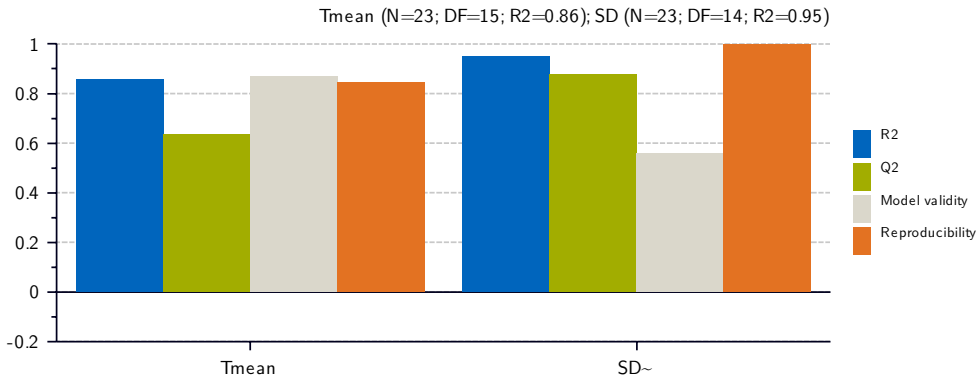

Fig. 4-8 Summary of fit of exemplarily evaluated models of Tmean and SD after insignificant interaction terms and square terms are excluded from the models show good quality of fit.

5. Check of Residuals for Normal-Distribution and Outliers

The investigated residuals represent the difference between trials and ideal model. The normal probability distribution of these residuals is checked for normal distribution and outliers. A normal distribution can be affirmed if deleted studentized residuals are close to a line. Probable outliers would show a high deviation of ±4 SD. In the investigation at hand, the residuals are normal distributed, compare Fig. 4-9 below and A-8. The check of the normal distribution of Trise showed an outlier, trial N5. A re-investigation of the logs showed that the cycle was not programmed correctly—5 magnetrons instead of 3 were active for one of the modules. The run was excluded from all investigations and is not part of any evaluation in this thesis.

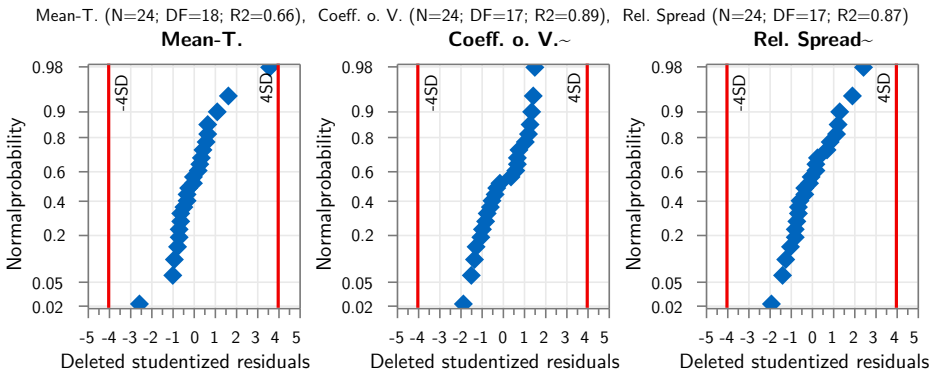

Fig. 4-9 Normal probability distributions of exemplarily evaluated models of Tmean and SD after exclusion of insignificant interaction and square terms are normal distributed.

6. Check of Residuals for an Influence of Run Order

Last, a possible influence of the test or run order is checked. For this, the deleted-studentized-residuals are plotted over the run order. When the test order has no influence on the results, the residuals are randomly distributed. This is the case for the study at hand, compare Fig. 4-10 and Fig. A-9 in the appendix.

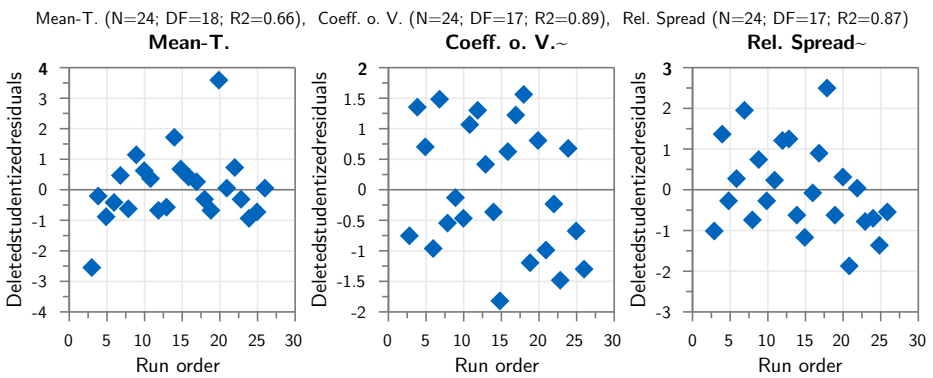

Fig. 4-10 Deleted-studentized-residuals over the run order of exemplarily evaluated models of Tmean and SD show that the test order has no influence.

4.2.5 Evaluation of Homogeneity Study for Three Main Response Types

Since previous section shows that the data is plausible and no oddities occurred, the main models are sound and results can be interpreted. In the following, the response types and their models will be presented. As in the previous section, the measurement error, normal distribution, and model quality will be stated. Afterwards the model terms will be discussed.

Temperature Responses

The measurement error relative to the total variation is better for Temperature Rise (5.4%) than for Temperature Mean (13.8%). Like the data of Tmean, the data of Trise is normal distributed without transformation (Appendix A.3, Fig. A-5). While the model for Tmean is good, the model for Trise is excellent with a R2 and Q2 above 0.9, compare (Fig. 4-11). The significant model factors are similiar for both models and can be divided in four. First, the Dead-Load and Magnetron Count have a distinct influence on the temperature responses. Secondly, the Magnetron Change and Sinus Function have a minor influence that is barely significant for the mean Temperature. Furthermore, a quadratic influence of both the Magnetron Change and number can be seen; this indicates that the correlation between these factors and the temperature responses is non-linear. Last, the amount of active magnetrons in combination with an active Sinus Function interact and, in combination, have a positive influence on Trise, compare Fig. 4-11.

The difference in model quality can be ascribed to the test setup and a variable start temperature. The start temperature is not controlled. It, therefore, varies between 33.9–37.4 °C in the extremes and between 35.2–36.5 °C for the quartiles. In contrast, the temperature rise is constant and linear over each test. It lies in a range of 7.2–13.7 °C. While the Temperature Rise is high enough to overshadow the random variance in start temperature, the start temperature increases the variation of the Temperature Mean after heat-up. Since the models' terms are identical, only the Trise model will be used for the interpretation of the terms.

The influence of the first factor, Dead-Load, on Trise is to be expected. The same microwave power is applied but the constant Dead-Load absorbs energy that is lost for heating the actual load. The second factor, Mode-Stirrers, do only influence the wavepattern. Consequently, no influence on Trise is the expected behavior. In contrast, the influence of the third factor, the Sinus Function (Sin) is not obvious. If the Sin increases and decreases the %-power level in the same way, no influence should be seen. The magnetrons are turned on and of only a fraction of a 2 s

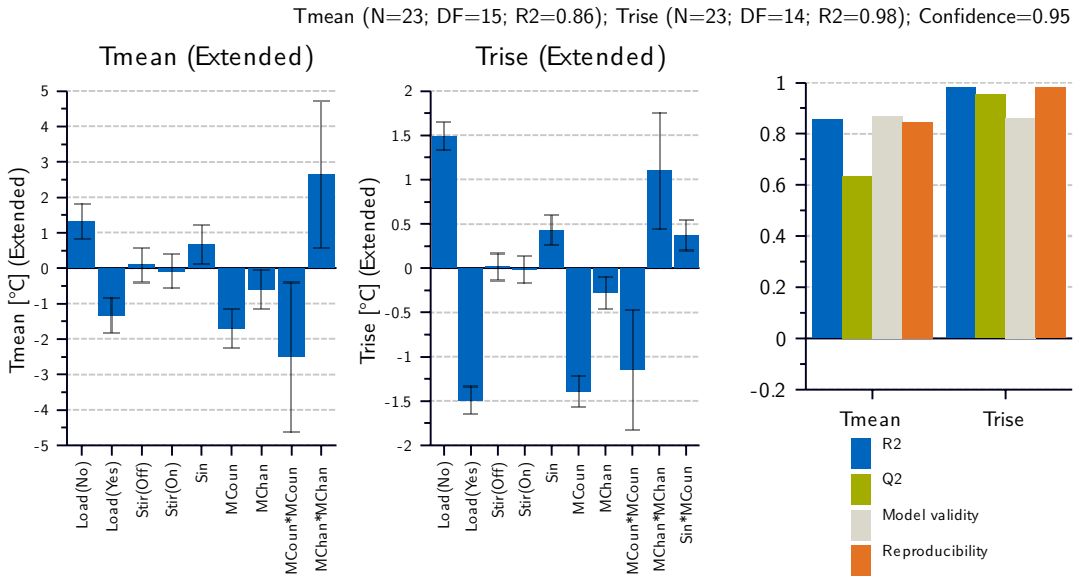

Fig. 4-11 Coefficients with 95% confidence intervals and model quality plots of Temperature Responses.

interval for a Magnetron Count of 3 and 5. The consequent higher on-time could result in a higher efficiency due to warm-up effects. However, without knowing the exact mechanism applied by the Simpati Controller, only assumptions can be made. With the observed influence of Sin on the magnetron's power output, the interaction detected between Sin and MCoun can be explained. For the low MCoun configuration, 1 magnetron, the %-power level is set to 100%. Consequently, the Sin cannot influence the power output. No influence for 1 magnetron paired with a positive influence for 3 or 5 magnetrons results in the visible "interaction" between these two factors.

The influence of the Magnetron Count and their quadratic term is, likewise, to be found in the on-off mechanism by which the power output is controlled. The magnetrons have a short start-up time and thus do not deliver 33% or 20% power when turned on this fraction of a 2 s interval. Since this effect does not occur using 1 magnetron, and is more prominent for 5 than for 3 magnetrons, a quadratic interaction is detected, see Fig. 4-12. A similiar start-up effect occurs when changing the magnetrons in a short interval for MChan. A slight decrease in Trise is seen when changing the magnetrons every 10 s. The effect lessons when increasing the time between magnetron changes to 30 s, compare Fig. 4-12. Due to the low effect strength, an interaction MCoun*MChan cannot be seen. Consequently, it cannot completely be excluded that this effect is only due to the switching of 1 magnetron configuration, where normally no change occurs.

Apart from the influence the Sinus Function has on the energy input in the setup,

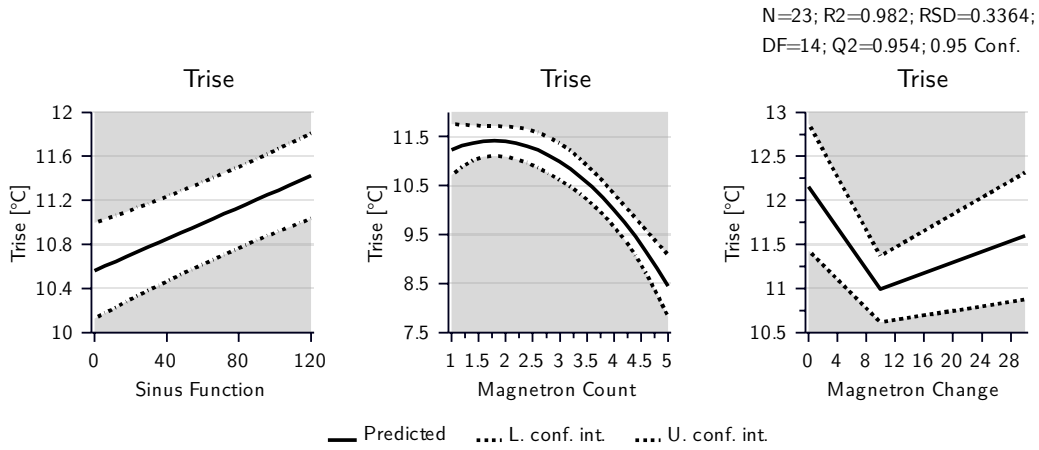

Fig. 4-12 Influence of Sin, MCoun, and MChan on the temperature-rise with 95% confidence interfalls.

no unexpected effects occurred. Overall, the difference in the temperature responses is of minor interest for practical applications; processes will either be temperature controlled or defined using absolute power levels. The observed difference would only slightly lessen the energy efficiency of a process.

Standard Deviation

The variation of repetitions relative to the total variation—the reproducibility—is best for SD with 1%; both, the division by Tmean and Trise increase the ratio between repetition and total variation to to 3.7% respectively 3.3%. The same can be seen in the model quality; while SD has a R2 of 0.95, SD divided by Temperature Mean (SD/Tm) and SD divided by Temperature Rise (SD/Tr) have a lower R2, compare Fig. 4-13. While Q2 is behaves in the same manner, the model validity is higher for SD's derivates. Since the model validity is above 0.5 for all models and mainly dominated by the reproducibility, this can be neglected. The comparison of the models factors show consistent significant factors for SD and SD/Tm. However, for SD divided by Temperature Rise (SD/Tr), the positive influence of the Dead-Load vanishes, compare Fig. 4-14. Activated Mode-Stirrers, a higher Magnetron Count, and the Magnetron Change influence the standard deviation and the derived responses to a lower level. The sinus has no significant influence. A quadratic effect for MChan can be seen, indicating a non-linear behavior. Likewise, an interaction between Magnetron Count and Magnetron Change has only just a significant influence on SD.

Although they differ slightly, all three models have a good quality. When looking at the results of Tmean and Trise above, putting SD in relation to Tmean is not seen as

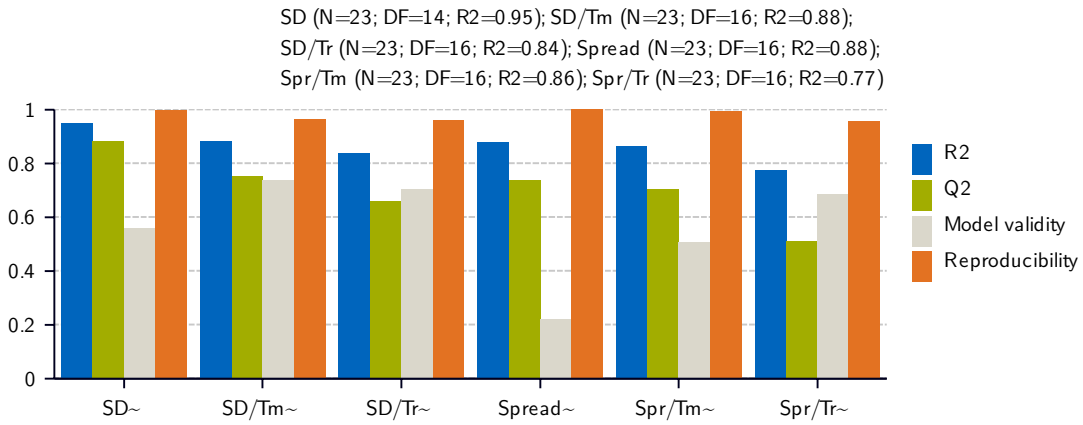

Fig. 4-13 Model quality for SD and Temperature Spread models of homogeneity study.

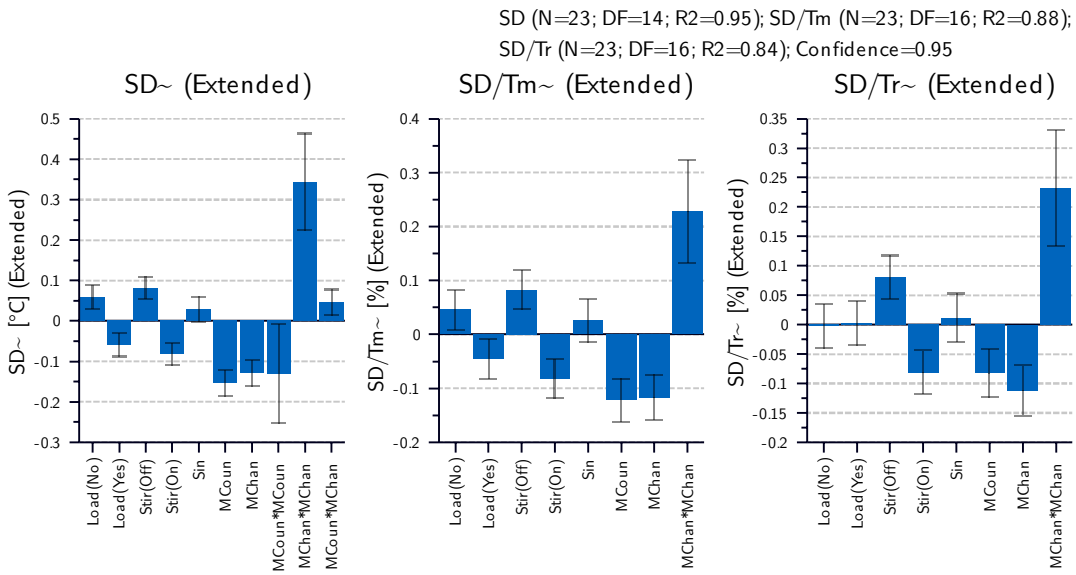

Fig. 4-14 Coefficients of SD-response with 95% confidence intervals.

productive; the random influence of the start temperature on Temperature Mean mainly adds noise. The canceling effect of the normalization using Temperature Rise, however, changes the model fundamentally. Consequently, only the models for SD and SD/Tr will be discussed further. In SD's model, the Dead-Load has a positive i.e. reducing effect that is not present after a division by Trise. Trise, in turn, is affected strongly by the Load. Out of this, it can be deduced that the influence of the Dead-Load on SD in the test setup comes primarily through the Dead-Load's influence on Trise; a lower Temperature Rise due to the Dead-Load results in a proportionally lower SD. There is, however, no influence of the Dead-Load in a temperature controlled process. It is found that the size of SD, therefore, is directly proportional to the temperature delta during heat up. Consequently,

SD/Tr is more promising to predict the influence on the standard deviation in a process.

For SD/Tr the significance of Mode-Stirrers, Magnetron Count, and Magnetron Change is similar. However, the influence of MChan is higher as the combination of the other two factors, compare Fig. 4-15. When SD/Tr is multiplied with the average temperature rise of all trials Tr_{mean}=10.6 °C, the summarized benefit for the recalculated SD* is 1.3 °C. Overall, the sum of the three significant factors' influence on SD* can reduce the maximum recalculated SD* (N3) by 43% where no variation is taken into account, compare Tab. 4-2.

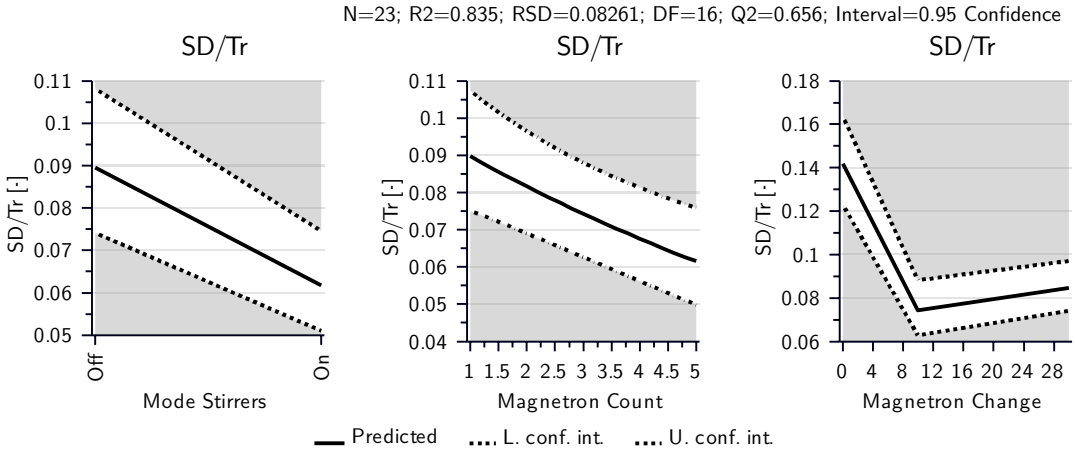

Fig. 4-15 Effect of Mode-Stirrers, Magnetron Count, and Magnetron Change on SD/Tr.

Tab. 4-2 Numerical influence of the factor levels' on SD/Tr according to Fig. 4-15 and recalculation of SD* via multiplication of Tr_{mean}.

	Factor Levels and Influences			**Measured Values**		
	Stir	**MCoun**	**MChan**	**Min**	**Mean**	**Max**
Levels	Off—On	1–5	0–10	N21	-	N3
Delta	-0.028	-0.028	-0.068	0.07	0.11	0.28
SD* Change	-0.30	-0.30	-0.72	0.74	1.16	2.96

SD* = SD/Tr·Tr_{mean}
N3: Load = Yes; Stir = Off; Sin = 120; MCoun = 1; MChan = 0 (Spread = 26.3 °C)
N21: Load = Yes; Stir = On; Sin = 60; MCoun = 3; MChan = 10 (Spread = 7.2 °C)

Temperature Spread

The temperature spread has a very low variance in the repetitive trials; the ratio between spread and error is, therefore, very small. The ratio is <1% for the Spread, 1.6% for Temperature Spread after heat-up divided by Temperature Mean (Spr/Tm), and 4.2% for Temperature Spread after heat-up divided by Temperature Rise (Spr/Tr). This very small error results in a bad model validity; the model's error is significantly larger than the pure error from the reproducibility. By this connection, the model validity increases for the derived responses Spr/Tm and Spr/Tr since both have a higher data error i.e. a lower reproducibility. The R2 of the main Spread model is still close to 0.9 and its derivative's R2s are above 0.75; the models are still adequate, compare Fig. 4-13 above.

The significant factors influencing the spread mostly correspond with the factors influencing SD, compare Fig. 4-16 and above. While the Spread's coefficient's deflections are similar to SD's deflections, their confidence intervals are much bigger. One difference is the significant influence of the Sin on the Spread that is not significant for SD. This can be ascribed to the higher sensitivity of the Spread to extreme values. Due to the similarities between Spread and SD, the interpretation is reduced to the relevant differences.

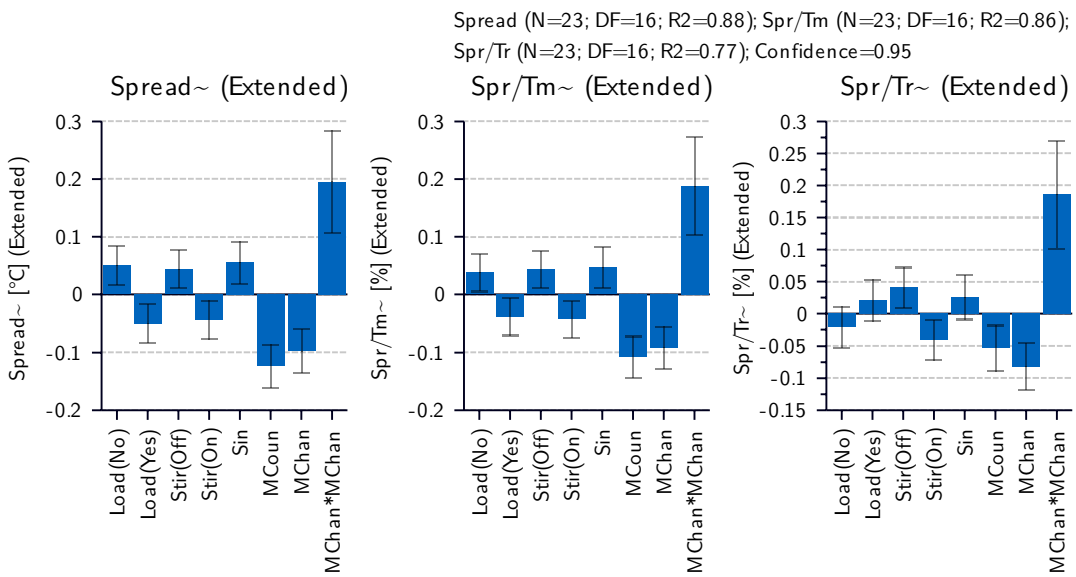

Fig. 4-16 Coefficients of Temperature Spread responses with 95% confidence intervals.

The investigation of the effects of significant model terms shows more difference between Spread's and SD's model. While for SD, the Magnetron Change is the clearly dominant factor, it is less dominant for the Temperature Spread after heat-up; a possible improvement of -5.6 °C of the Spread by MChan is followed by a

only slightly smaller possible improvement of -4.4 °C by MCoun. The Mode-Stirrers only have a minor benefit of -1.5 °C. In contrast, the Sinus Function has an equally sized negative effect of 1.9 °C, compare Fig. 4-17 and Tab. 4-3. In combination, Stir, MCoun, and MChan can—most theoretically—reduce the spread by 11.48 °C or 43% when set in ratio to the maximum spread of 26.3 °C. This actually equals the benefit-percentage of the three factors on SD.

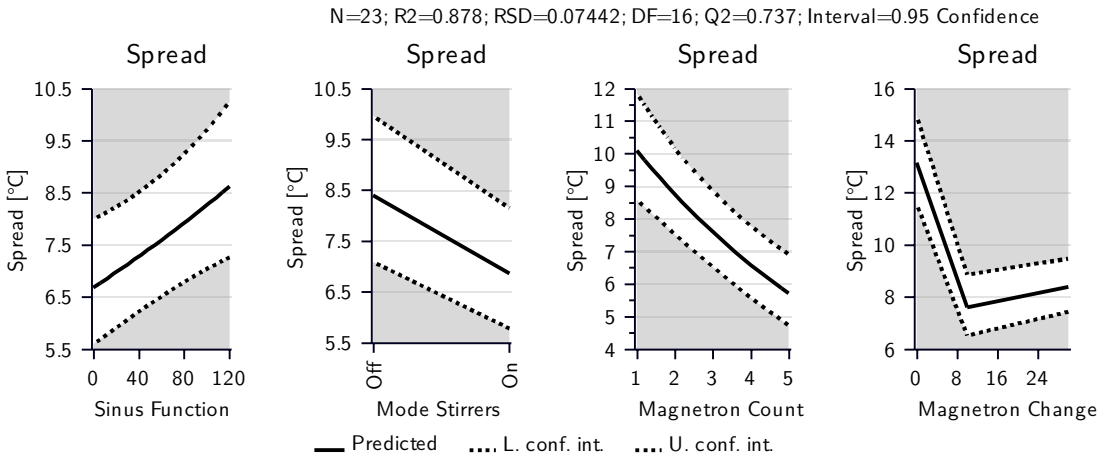

Fig. 4-17 Effect of significant factors on the Spread.

Tab. 4-3 Numerical influence of the factor levels' on Spread according to Fig. 4-17.

	Factor Levels and Influences				Measured Values		
	Sin	**Stir**	**MCoun**	**MChan**	**Min**	**Mean**	**Max**
Levels	0–120	Off–On	1–5	0–10	N20	-	N3
Spread Change	1.94	-1.54	-4.38	-5.56	5.1	10.32	26.3

N20: Load = Yes; Stir = On; Sin = 0; MCoun = 5; MChan = 30
N3: Load = Yes; Stir = Off; Sin = 120; MCoun = 1; MChan = 0

4.2.6 Summary of Homogeneity Study

A test setup was defined to investigate the influence of 5 parameters: Mode-Stirrers (On/Off), Dead-Load(No/Yes), Sinus Function (0/60/120 s), Magnetron Count (1/3/5), and Magnetron Change (0/10/30 s). The design of the test excluded other influencing factors. With this setup and the software Modde 10.1 a design of experiment was conducted and evaluated with regard to three response types acquired using a thermal camera: temperature development, standard deviation, and temperature spread. The resulting models for these responses were tested for their quality and relevance with respect to their error, normal distribution,

significant factors, model quality, and systematic errors. All models are good and fit to be evaluated. For the first response, the temperature development, it was shown that the Dead-Load and number of magnetrons i.e. using a lower %-power level has the highest influence on the temperature rise and therefor on the energy efficiency. The second response type, standard deviation (SD), can be optimized using a regular change of magnetrons, the use of mode stirrers, and by using more magnetrons. The Magnetron Change has a stronger effect on SD (reduction by -0.72 °C) than Mode-Stirrers and Magnetron Count in combination (-0.3/-0.3 °C). The last response type, Temperature Spread after heat-up, is influenced similar as the SD but shows an additional dependence on Sin. The sinus function increases the Spread slightly. Magnetron Count and Magnetron Change have a comparable positive influence on the Temperature Spread (reduction by -4.4/-5.6 °C), Mode-Stirrers a much smaller positive effect (-1.5 °C) that is in the magnitude of Sinus Function's negative effect (1.9 °C). It is shown that the changes to the equipment and the control strategy have an overall positive effect on the temperature homogeneity of a single test specimen. That each adaption has a positive influence that is relevant for practical applications can be seen in the section 4.3.2 below. In future work, the interaction of several test specimens inside the applicator should be investigated.

4.3 Lessons Learned During Manufacturing of Microwave Specimens and Other Trials

4.3.1 Lessons Learned in Regard to Preforming of Microwave Specimens

As described in section 3.2.1, a carbon fiber free environment is necessary to manufacture GFRP samples on a transparent tool using no additional absorbers. However, the environment used in this study was not enough to achieve this. After process optimizations, samples up to 120 °C were manufactured without problems. Since at higher temperatures more power is needed, burnings occurred that were traced back by their appearance to entrapped carbon fibers. Internal investigations in a not completely finished student thesis showed, that the heat introduced into a filament strongly depends on filament length and the microwave power level. The power level at that a carbon fiber impurity burns depends on the filament length. Consequently, the higher the power level the higher the chance that a carbon fiber impurity has critical lengths, heats up, and locally burns the matrix. After this, the burned matrix is a good absorber and heats up further; the process must be

stopped to prevent a fire. A factor additionally influencing this carbon fiber burnout is the ongoing cure of the GFRP. On the one hand, more energy input is needed to reach higher temperatures due to heat transfer effects. On the other hand, the dielectric properties of the matrix change and the energy conversion inside the material is reduced. Thus, to maintain a constant heating rate or temperature, the microwave power is increased by the controller. The higher the microwave power, the more energy is transferred to a filament; shorter filaments that are entrapped get critical, overheat, and burn the set-up. This is especially problematic for the set-up at hand where nearly no energy is transferred directly to the tool. If the tool itself did absorb some energy and therefore heat up under irradiation, the energy input needed in the GFRP would be reduced. For future applications, completely transparent tools should be avoided when working with pure GFRP in a carbon fiber-reinforced plastic (CFRP) environment.

4.3.2 Lessons Learned in Regard to the Microwave Curing Process

In general, the exothermic reaction of a resin, the change of its dielectric properties during cure, and the influence of the manufacturing set-up (tooling material, plate thickness etc.) is highly specific for every process. Through this, it is impossible to get universal rules out of the one investigated set-up. Thus, no specific investigation was carried out in this regard, but rather, the process was adapted step by step and according to lessons learned. The following, therefore, can only give a slight insight.

Adapting control parameters, in combination with the methods described in the homogeneity study above, was most beneficial for reaching a stable process needed for specimen manufacturing, as can be seen in Figure 4-18. With regard to the PID control parameters, only the integral and differential factors have been increased and adapted. It is believed that this mainly had to be done due to the high response time of the used temperature sensors. While the energy input and, therefore, temperature gradient changes instantly with the power level, the temperature sensors lack behind in their true value. A higher differential factor reacts stronger to the gradient of the temperature measurements—which occurs earlier if not instantly—and counteracts the delayed value change and overshoot. The higher integral value likewise helps to make the system react slower. However, while the higher integral value makes the system more stable at temperature steps below 120 °C, it results in a behavior that is too slow at higher temperatures. Heat radiation and transfer results in faster cooling or slower heating, see Fig. 4-18 bottom 120 °C–140 °C. As a possible solution for this problem, Promaglaf®-HTI 1100 insulation plates by Pro-

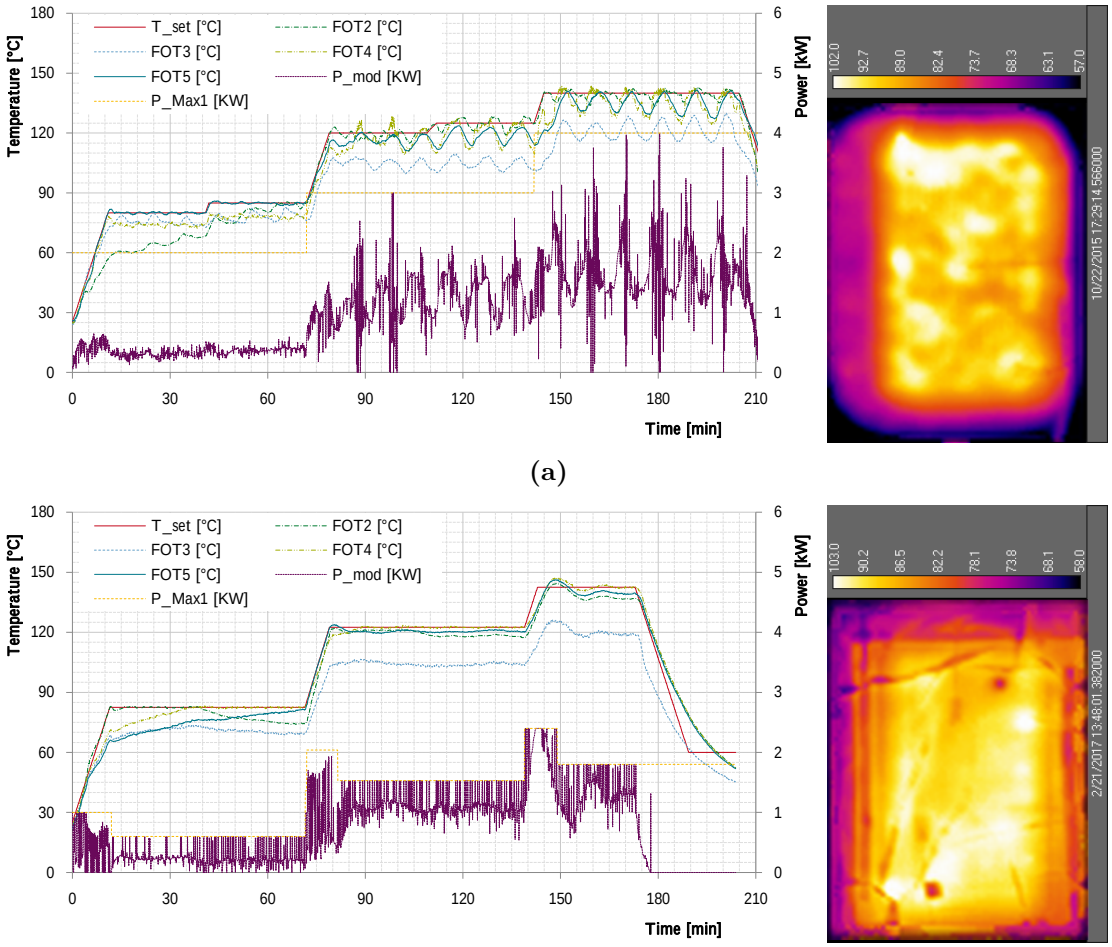

Fig. 4-18 Microwave temperature and power log with thermal images at approximately 165 min. (**a**) Early stage of process using a water load but without mode stirrers or adapted control parameters. Strong control oscillations occur and temperature homogeneity is poor; (**b**) Adapted process using a water load, mode stirrers and adapted control parameters. Control oscillations are minimizend and temperature homogeneity is increased.

mat (Ratingen, NW, Germany) (Apendix A.5, page 169) were used surrounding the set-up in form of a box. While this decreased the necessary microwave power and enhanced temperature homogeneity, it also obscured the set-up from thermal imaging. The practice was canceled after a smoldering fire—probably due to a carbon fiber contamination—was detected only after serious smoke development.

Apart from the equipment's integrated PID control parameters, at least four factors are essential for stable microwave processing the GFRP-plates as was confirmed by the latter study above. First and foremost, the number of magnetrons is limited according to the needed heating power. While this contradicts a need to use as many sources as possible to generate a chaotic field, it restricts the magnetrons simultaneously active. With this, the field intensity is capped and carbon-fiber burn-out is less likely. Second, to be able to use more than one magnetron per module also the

power needed is very low, a constant water flow through an 8 mm tube in the back of the microwave is maintained; the %-power level to reach the target temperature is shifted to higher values. Without this, the PID controller reaches a lower limit of 10% since the curing of the GFRP plate only needs a few hundred Watt. Third, to homogenize the field through more "chaos", the active 2, 3, or 4 magnetrons per module are changed every 10 s, compare study above. Finally, the mode stirrers i.e. slowly turning reflective fans were added to reach an assumable, constantly changing electromagnetic field. As a result of these four changes and the adaption of the control parameters, the power input and temperature distribution over the plate gets more homogeneous and constant as was shown in Fig. 4-18 and validated in the homogeneity study above.

4.3.3 Lessons Learned in Regard to the Tooling Material

It can be assumed that the two tooling material used have no relevant influence on the process or the test results. It was observed that there is a difference in the heat-up characteristic of GFRP and glass-ceramic tools; the GFRP heats up slightly while the glass-ceramic stays cold. Consequently, the temperature gradient between the manufactured plate's edge and the tool is lower for the GFRP tools. However, this only changes the temperature distribution approximately 3 cm around the edge. An influence on the test specimen's properties by this can be ruled out due to their position, compare Fig. 3-11. Furthermore, no indication for an influence of the tooling material on the manufacturing was observed. No influence on the mechanical properties was seen during the evaluation.

4.3.4 Lessons Learned in Regard to Energy Consumption of the Used Hephaistos System

The core benefit of microwave heating is its direct in-depth heating. This direct heating can be beneficial for the energy consumption in two ways: the cycle time can be reduced and only the part is heated. However, the microwave equipment's energy consumption plays a major role in the possible energy efficiency. The *Vötsch Hephaistos 180/200* used was assessed to this regard in a supervised thesis by Buck [98]. For the assessment, Buck used a custom-build calorimetric measurement setup provided by KIT and a three phase energy logger (Fluke 1730). The calorimeter is used to measure the microwave power output, the energy logger to measure the equipment's active, reactive, and apparent power. In more detail, the calorimetric setup consists of up to three spirals of 1 m in diameter. The spirals were introduced into the microwave and connected to a constant water flow, compare Fig. 4-19. The water flow and temperature rise during irradiation is measured and both values are

used to calculate the microwave energy absorbed by the water. The energy logger was connected to the VHM180's trunk line in the control cabinet. To evaluate the

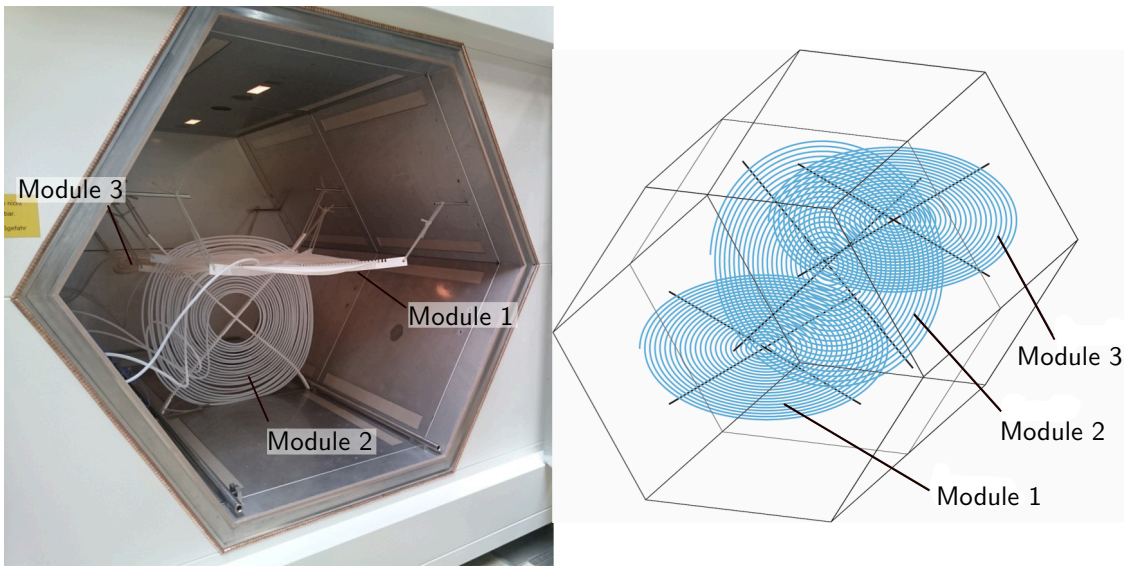

Fig. 4-19 Calorimetric measurement setup inside the VHM180.

equipment's efficiency, the active power measured by Buck is put in relation to the corresponding calorimetric microwave power in different scenarios:

Idle Equipment The idle equipment with closed door.

Power control via active magnetrons A constant microwave power is set by activating several to all magnetrons. For example 12 of 24 active magnetrons equal 50 % power.

Power control via pulsed magnetrons A constant microwave power is set by activating several to all magnetrons at defined power levels. For example 12 of 24 magnetrons at a 50 % power level equal 25 % power.

The idle equipment requests 2.5 kW to 3.5 kW depending on whether the ventilation (up to 0.6 kW), lights (0.2 kW), and magnetrons (0.2 kW) are activated. During heating operation, the equipment's efficiency[1] lies between 40 % and 70 %. The pure microwave efficiency[2] lies between 51 % and 80 %, compare Tab. 4-4. What can be seen here is that magnetrons that are constantly active have a higher power consumption compared to magnetrons that are running at lower power levels by pulsed power control; pulsed magnetrons have a higher efficiency in the VHM180.

With respect to the absolute power output, the constantly active magnetrons deliver a slightly higher heating power compared to the pulsed magnetrons. This effect

[1] conversion rate from the active power transferred from the power line to heating power

[2] conversion rate from electric input power to heating power through adjustment of active power by equipment's idle power consumption

is more dominant when less magnetrons are active,compare Tab. 4-4. This relationship may partly be explained by a very short start-up time of the magnetrons in pulsed operation. When looking at the heating power per magnetron in constant operation, the heating power is lower for more active magnetrons. A possible explanation for this is an interaction between magnetrons caused by slightly different eigenfrequencies.Overall, the average heating power of a magnetron is 0.87 kW.

Tab. 4-4 Power efficiency for power control via number of active magnetrons or pulsed magnetrons.

Set Power [%]	**25**		**50**		**75**		**100**
Active Magnetrons	6	24	12	24	18	24	24
Active Power [kW]	13.6	9.8	23.1	16.0	31.4	22.2	37.9
Heating Power [kW]	5.5	5.1	10.8	10.1	15.6	15.5	20.3
— **per Magnetron** [kW]	0.92	0.85	0.9	0.84	0.87	0.86	0.85
Equipment Efficiency [%]	40	52	47	63	50	70	54
Microwave Efficiency* [%]	51	73	53	77	55	80	58

*Active power adjusted by approximate power consumption of idle equipment

With this data, the following section takes a look at a curing process used in this thesis. For this, it is important to bear in mind that the equipment is an all-round equipment for scientific purpose. Here are two examples where this influences the observations: first, the maximum power output and size is far greater than needed for the application at hand; second, since the later installation of switching power supplies was planned early on, each magnetron is actively cooled by a separate fan opposed to a central cooling in regular equipment. An equipment designed for a certain load would have a lower idle power consumption and thereby higher efficiency for the MW_140 cure process of a single plate we will look at. During the MW_140 trials (compare Fig. 4-18b), the power output is controlled using 2, 3, or 4 pulsed magnetrons per module that are changed every 10 s, compare section 4.3.2 above. Overall, 0.5 kW nominal microwave power, 1 kW per Magnetron, are used during the 85 °C phase, 2.2 kW during the 120 °C phase, and 2.8 kW during the 140 °C phase. The actual heating power according to the measurements—into a water load—would be 0.85 kW per magnetron or 85 % of the given values. If 4 kW of equipment power consumption is used on top of the heating power, this gives us a rough and optimistic estimation of the equipment's efficiency for this one particular application between 10–40 %. This example shows that an adequate equipment is needed if efficiency and power consumption must be optimized. At the end, this could mean the difference between 10 % and 70 % energy efficiency.

5 Concept Study for an Adaptable Microwave Absorber

5.1 Principal Idea and Aim of Absorber Study

Composite parts, in general, are seldom simple. The fiber material and layer by layer manufacturing enables for optimized design. A good design—that is one that meets the applications requirements while using the composite's benefits—will most certainly save mass or increase functionality in comparison to a metal part. As a result, such parts will have varying thickness, local sandwich areas, or will even be build-up by a material mix. In conventional processes, even the most complex part can be heated up evenly with a sufficient temperature homogeneity. By reducing the heat-up rates and introducing long dwell times only small temperature gradients occur—the part always adapts the tools or environments temperature. In contrast, the direct interaction of microwaves with different and varying part areas will—without further measures—lead to a inhomogeneous temperature distribution. For example, think of a part with varying thickness. The heat up by the microwave interaction results in a in-depth volumetric heating. Simultaneous, the heat flow cools the part over its surface. Consequently, a thinner part area of the same temperature emits the same amount of energy than a thicker area. However, it absorbs less energy over its smaller "local" volume. The temperature of the two areas, thin and thick, will diverge

The principal idea behind a microwave absorbers is to react to this circumstance. The addition of an absorber can compensate for local variations. The lack of energy input in thinner part areas can be compensated by an additional absorber. However, this addition has to be adapted depending on the local requirements of a part. There even can be more than one change in thickness, additional material changes, or geometric conditions—like corners—that influence heat-up. All of these variations will need specific absorber properties or geometric variations.

For this reason, this study aims to provide an adaptable absorber system that can be applied in different scenarios. It will be usable for numeric and experimental investigations of new tooling concepts in future studies. Building upon a prior investigation described in section 2.5.2 on page 40, the production process was

optimized as described in section 3.3 on page 50. With this optimized process, an investigation is conducted to define the adaptable microwave absorber system. The investigation and its results are described in the following sections. In combination with the manufacturing process for absorbers, this investigation provides the data basis for further studies.

5.2 Setup and Realization of Absorber-Study

As is known from the early absorber study, the carbon black (CB) Printex® XE 2 B (XE2B) drastically increases the dielectric properties. Hence, XE2B and a second carbon black Printex® L Beads (LB) are investigated. As a third additive, a silicon carbid (SiC) with a F 1200 grain is used for potential fine tuning of the dielectric properties.

During optimization of the master-batch (MB) production LB was used as carbon black and MBs with 4% CB were manufactured and processed. This MBs allow for a maximum CB content of 2.19 V% inside the cured epoxy resin. However, the MB production of a 4 V% MB using the established process and XE2B is not possible. The influence of XE2B on the MB's viscosity is very high due its surface area; XE2B agglomerates are not broken up completely during mixing and the resulting paste cannot be sieved properly. Consequently, XE2B MBs with 2.5 V% and LB MBs with 4 V% were produced. This MBs were used to produce dielectric specimens with a defined CB-content. The specimen configurations were defined according to design of experiments methods for later evaluation using the software Modde. For every of the following concentrations, 8 dielectric specimens were produced and at least 5 specimens were measured. Samples only containing carbon black are investigated with 0.5 V% and 1.25 V%. One sample series using a mixture of both CBs, each 0.625 V%, is produced. For LB additional 2 V% samples are manufactured and measured. Under the aspect of fine-tuning, the SiC content is varied between 0 V% and 1.5 V% plus one sample series at 8 V% for each CB. An overview of the produced configurations is shown in Tab. 5-1. The detailed list of all sample configurations are shown in Appendix A.4, Tab. A-5.

Tab. 5-1 Matrix overview of manufactured absorber sample series.

SiC	**0 V% CB**	**0.5 V% CB**	**1.25 V% CB**	**2 V% CB**
0 V%	Sika CR141	LB / XE2B	LB / XE2B / Both	LB
0.75 V%	-	-	(3×LB) / XE2B	-
1.5 V%	-	(2×LB) / XE2B	LB / XE2B	LB
8 V%	-	LB / XE2B	-	-

5.3 Evaluation of Absorber-Studies' Dielectric Measurements

The evaluation of the absorber study, manufactured according to section 3.3 and measured according to section 3.4, is done in 4 parts. First, possible errors and variations in the measurements are investigated by taking a look at the raw-data. Second, a first interpretation of the measurements is done. Third, Modde is used to generate and check models for the four responses permittivity (ε_r'), loss factor (ε_r''), dissipation factor ($\tan(\delta)$), and density (ϱ). For this, the three additive are seen as factors, compare Tab. 5-2. Last, the models for ε_r' and ε_r'' are used to define the design space of the adaptable microwave absorber.

Tab. 5-2 Test parameters and their levels used for absorber-study evaluation.

Factor	Short	Type	Low	Mid	High
Printex L Beads	LB	Quantitative	0 V%	1.25 V%	2.0 V%
Printex XE2B	XE2	Quantitative	0 V%	0.5 V%	1.25 V%
SiC	SiC	Quantitative	0 V%	0.75 V%	1.5 V%

3 Additional Points:

0.625 V% of each LR6 and XE2 0.5 V% XE2 + 8 V% SiC 0.5 V% LR6 + 8 V% SiC

5.3.1 Investigation of Errors and Variations at Hand of the Raw-Data

Variations Inside each Sample Series

To compare the sample variance of each series the coefficient of variation (cov) is used; it is given by the relation between standard deviation (SD) and each series's mean measurement value. The average $\text{cov}_{\varepsilon_r'}$ and $\text{cov}_{\varepsilon_r''}$ of all LB series are lower than that of XE2B series, compare Tab. 5-3. The average error of the LB samples is in the range of the determined random error of the measurement device. This random error of 0.5% for ε_r' and 3% for ε_r'' was measured at comparably low $\varepsilon_r' = 3.3$ and $\varepsilon_r'' = 0.18$. XE2B samples have ε_r' in the range of 4.5–7.5 and ε_r'' in the range of 1.2–4.0. The larger variation inside the XE2B series can most certainly be attributed to a higher random error at the much higher dielectric properties. The cov of all measurement series can be found in appendix A.4, Tab. A-5.

As a consequence of the random error, possible variation in each sample series cannot be determined.

Tab. 5-3 Average and maximum coefficient of variation of all sample series sorted by CB.

	$\mathbf{COV}_{\varepsilon'_r-avg}$	$\mathbf{COV}_{\varepsilon'_r-max}$	$\mathbf{COV}_{\varepsilon''_r-avg}$	$\mathbf{COV}_{\varepsilon''_r-max}$
LB	0.4%	0.6%	1.1%	1.9%
XE2B	1.2%	2.3%	3.0%	4.3%

Variations Between Production Batches

During specimen manufacturing, up to four sample series containing 6 or more samples are mixed with one specific master-batch simultaneously. Two sample configurations were repeated with different MB at different times. The MBs 003, 004 and 005 were used to manufacture samples with 1.25% LB and 0.75% SiC—hereafter configuration (A). The MBs 004 and 005 were used to manufacture samples with 0.5% LB and 1.5% SiC—hereafter configuration (B). These sample configurations (A) and (B) are used to look into variations between production batches i.e. MBs. First, the mean of each configuration's measurement values $\varepsilon_{r-i-\text{avg}}$ is calculated—i.e. all measurements of MBs 003, 004 *and* 005. Second, the relative deviation of each sample series' mean of the configuration ε_{r-i}—i.e. MBs 003, 004 *or* 005—to this mean is determined. The resulting relative deviation $\Delta\varepsilon_{\text{rel}}$ is described by

$$\Delta\varepsilon_{r-\text{rel}} = |\frac{\varepsilon_{r-i-\text{avg}} - \varepsilon_{r-i}}{\varepsilon_{r-i-\text{avg}}}|, \tag{5-1}$$

where ε_{r-i} isthe mean ε'_r or ε''_r of a series and $\varepsilon_{i-\text{avg}}$ the equivalent average of the according configuration—i.e. several series. With this metric, configuration (A) has a variation of up to 2.5% in ε'_r and up to 15.5% in ε''_r, see Tab. 5-4. The variation in (B) is 0.1% for ε'_r and 3.3% for ε''_r. The variation in (B) is in the range of measurement errors. Configuration (A) will be discussed further due to the high variation.

Tab. 5-4 Comparison and relative error of repeated sample series' dielectric properties.

	1.25LB+0.75SiC (A)				**0.5LB+1.5SiC (B)**			
MB	ε'_{r-i}	$\Delta\varepsilon'_{r-\text{rel}}$	ε''_{r-i}	$\Delta\varepsilon''_{r-\text{rel}}$	ε'_{r-i}	$\Delta\varepsilon'_{r-\text{rel}}$	ε''_{r-i}	$\Delta\varepsilon''_{r-\text{rel}}$
003	3.95	2.5%	0.509	15.5%	-		-	
004	3.77	2.1%	0.395	10.4%	3.51	0.1%	0.239	1.6%
005	3.83	0.4%	0.418	5.2%	3.51	0.1%	0.247	1.6%
Average	3.85	1.7%	0.44	10.4%	3.51	0.1%	0.24	1.6%

The geometry is a huge influence factor in the measurements at hand, see section 3.4. Consequently, the length, mass, and density of the different batches is checked first. The samples based on MB 004 have a smaller length and mass than the other two of (A), compare Tab. 5-5. This explains the lowest dielectric properties of the series 004; the sample size has a direct influence.

Tab. 5-5 Average length, mass and density of repeated sample series with SD.

Config.	MB	L [mm]	SD [mm]	m [mg]	SD [mg]	ρ [g/cm³]	SD [g/cm³]
(A)	**003**	10.00	0.028	581.6	1.88	1.23	0.0014
	004	9.88	0.047	572.1	3.01	1.23	0.0029
	005	10.01	0.034	580.4	2.63	1.23	0.0017
(B)	**004**	10.02	0.019	584.97	1.11	1.24	0.0020
	005	10.03	0.019	586.15	1.10	1.24	0.0031

However, the samples of batch 003 and 005 are equal in their length, mass and density. They differ nonetheless. There is no recorded difference in the production of the MBs 003 and 005 that could explain the difference. One oddity is found in MB 005. It showed agglomerates of up to 15 µm during its grindometer control. As a consequence, it was mixed again for 50 min and the agglomerates were broken up. The prolonged mixing time of 005 could have lead to a better homogenization. However, this would have lead to higher dielectric properties. This correlation can be seen when taking a look at the very badly mixed samples with 2% XE2B of the pre-study, see section 2.5.2, and the samples with 1.25% XE2B of the current study.. The former had a ε_r' of 8.93 and a ε_r'' of 3.45, the latter a ε_r' of 7.36 and ε_r'' of 4.05. A better homogenization will thus, most certainly, yield higher dielectric properties. The longer mixing of MB 005 does not explain the difference. Likewise, the microsections did not show any difference between the samples. Currently there is no explanation to be found in the records for the high spread between different batches. In further studies this differences must be taken into account or investigated. Foremost, it should be estimated whether such a seemingly random difference would have a relevant influence in a tooling application.

Summarizing, the samples from MB 004 show lower dielectric properties due to their length. An explanation for the high dielectric properties of 003's measurements were not found. However, with the knowledge that 004's error is geometrical, the overall variation is presumably below the calculated 15.5%. As will be seen in the next sections, the data can be used to determine a clear influence of the additives and get a model for the adaptive absorber.

5.3.2 Investigation of Additives Influence at Hand of the Raw-Data

For a first visual evaluation of the additives influence, the loss factor (ε_r'') is plotted against the permittivity (ε_r'). All LB samples will be investigated first, see Fig. 5-1. At a first glance, a linear behavior can be seen. A linear regression of all samples that only contain LB confirms this with a coefficient of determination R^2 close to 1. The slope of the regression $m = 0.49$ shows that the LB's influence on ε_r' is two times its influence on ε_r''. Next, we are taking a look at the samples with added SiC. When comparing these series to the regression line it can be seen, that compared to LB the SiC has a higher influence on ε_r' than on ε_r''.

For the samples with 1.25 V% LB, that showed a big difference between their properties, this influence is only visible when looking at MB 004 and 005 separately. Remarkably, the influence of added SiC seems to be independent from the contained LB. Samples that were added 1.5 V% SiC at 0.5 V%, 1.25 V%, and 2 V% LB all show a similar offset to the pure LB-samples, compare Fig. 5-1.

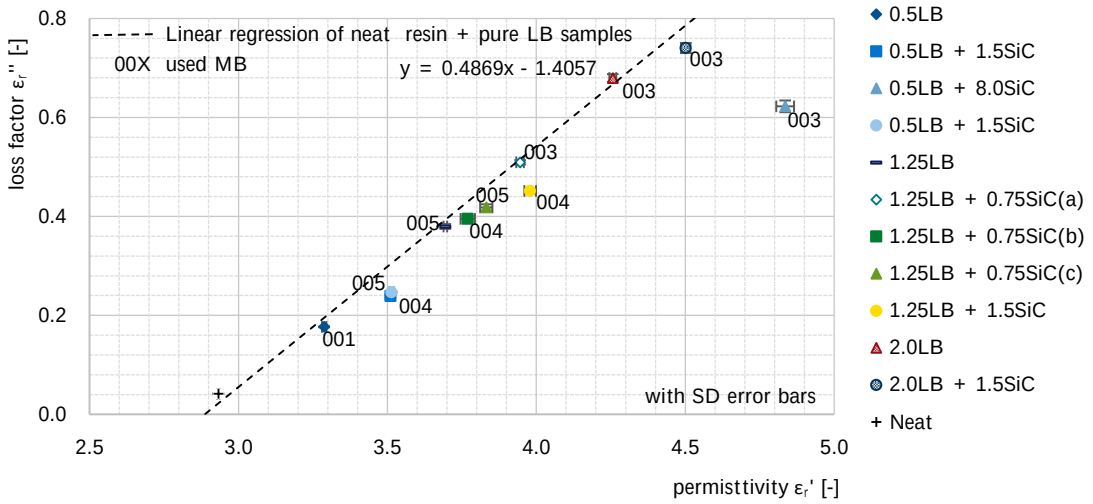

Fig. 5-1 Dielectric measurements of all LB samples with SD error bars of each series and used master-batch.

After this first look at the LB samples, the XE2B samples will be evaluated in the same manner. For the visual inspection, the already discussed LB and all XE2B samples are drawn in Fig. 5-2. This is feasible due to the high influence of XE2B on the dielectric properties. The smallest used amount of XE2B—0.5 V%—push both ε_r' and ε_r'' stronger than 2 V% of LB. For comparison, a linear regression of the XE2B sample is done. It is important to bear in mind, however, that the linear regression of XE2B samples can only be done using the neat resin and two XE2B data points. A non linear influence would go undetected. Nevertheless, with a slope

of $m = 0.91$, it is safe to say that XE2B has a higher influence on the loss factor than LB.

The comparison of samples containing only XE2B, to those that contain additional SiC, gives inconsistent results. The influence of 1.5 V% and 8 V% SiC added to 0.5 V% XE2B looks similar to the LB results; the SiC influences ε_r' stronger than ε_r'' compared to both carbon blacks. These samples are all of MB 001. In contrast, the addition of 1.5 V% of SiC to the 1.25 V% XE2B mixture of the same batch results in a lower loss factor and higher permittivity. The 1.25 V% XE2B sample containing 0.75 V% from another MB has again significantly lower values for both properties. Since it was already observed for LB samples, the big drop-off is most probably caused by variations in the MBs. Due to this high deviation at the upper range of the investigation, the 1.25 V% XE2B/0.75 V% SiC samples from MB 001 are excluded from the following DOE analysis. The probable uncertainty in the other XE2B samples is kept in mind.

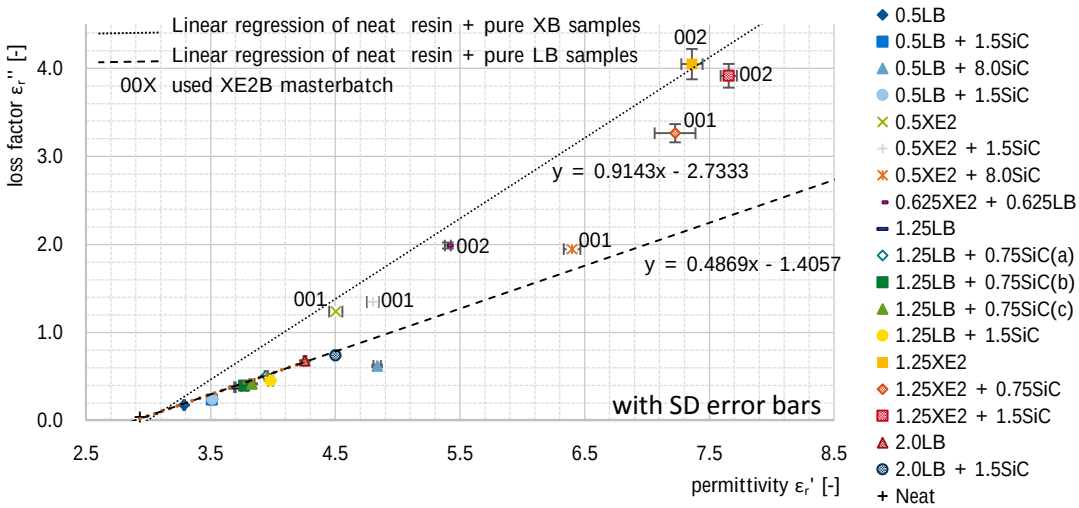

Fig. 5-2 All dielectric measurements of the absorber study with SD error bars of each series and XE2B master-batch.

5.3.3 Control of DoE Study Results using Modde

The three main responses for the design of experiments (DoE) evaluation are the permittivity (ε_r'), the loss factor (ε_r''), and the dissipation factor ($\tan(\delta)$). The density (ϱ) is evaluated in the same manner for comparison. Similar to as described in section 4.2.4 the Multiple Linear Regression (MLR) is used to fit the model responses. In the following, the models are checked in six steps using the same methodology as for the evaluation of the homogeneity study in section 4.2.4 page 70. In every step, the model adaptations and results are give for all responses: ε_r',

ε_r'', $\tan(\delta)$, and ϱ. After the models are checked and evaluated, the models and their relevance will be discussed.

1. Measurement Error and Total Variation

For the DoE-evaluation, the measurement error is determined by looking at the replicates. The variation of replicates must be small in relationship to the total variation to be able to evaluate the data. The measurement error is very low compared to the total variation for all responses. The relation between replicate variation and absolute variation is 3.7% for the permittivity, 2.9% for the loss factor, 4.5% for the $\tan(\delta)$, and 1.7% for the density. This very small spread in the replicates can be seen in Fig. 5-3. A very good model can be expected.

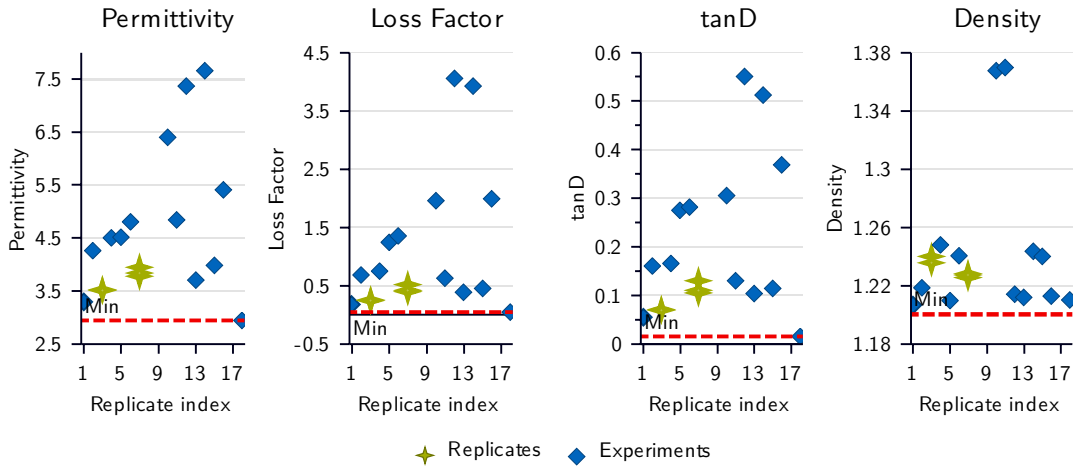

Fig. 5-3 Trials with replicates of absorber study to check the total variation against replicate spread.

2. Normal Distribution Check

The normal distribution check shows whether the investigation meets the statistical expectation of a symmetrical distribution around the mean. From this viewpoint, the normal distribution of all four responses is skewed i.e. leaning to the left, see Fig. 5-4. If the distribution is not skewed, a better model is expected. However, the skewness of the distributions is founded in the high amount of samples with low range properties, compare Fig. 5-2; the skewness can be expected. Additionally to the expected behavior, only the transformation of permittivity has a positive influence on model quality. Consequently, none of the responses are transformed.

3. Investigation of Model Factors

The model factors influence can be seen in the coefficient plots. A factor is significant if its 95% confidence interval is fully positive or negative. All factors of the model are significant, compare Fig. 5-5. This coincides with the results of the investigation of additive influence above. Additionally, to the linear factors, the

quadratic term of XE2B has a significant influence. Fig. 5-5 shows the scaled and centered coefficients. This means, it shows the influence of 1 V%LB, 0.0625 V% XE2B and 0.75 V% SiC. The effect of each factor will be discussed in more detail later on.

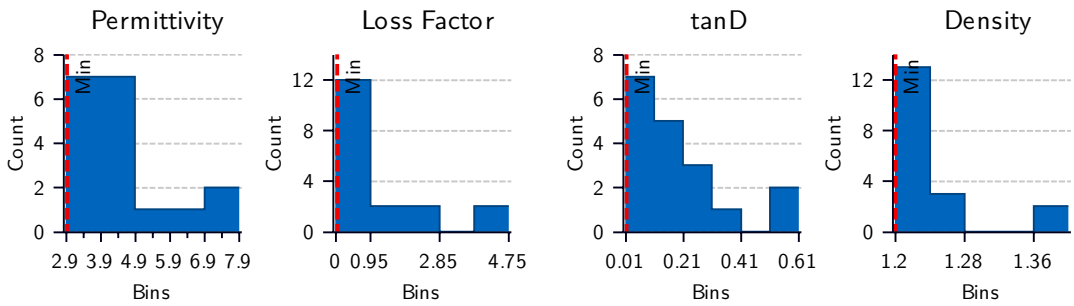

Fig. 5-4 Histograms of evaluated and adapted models of absorber study.

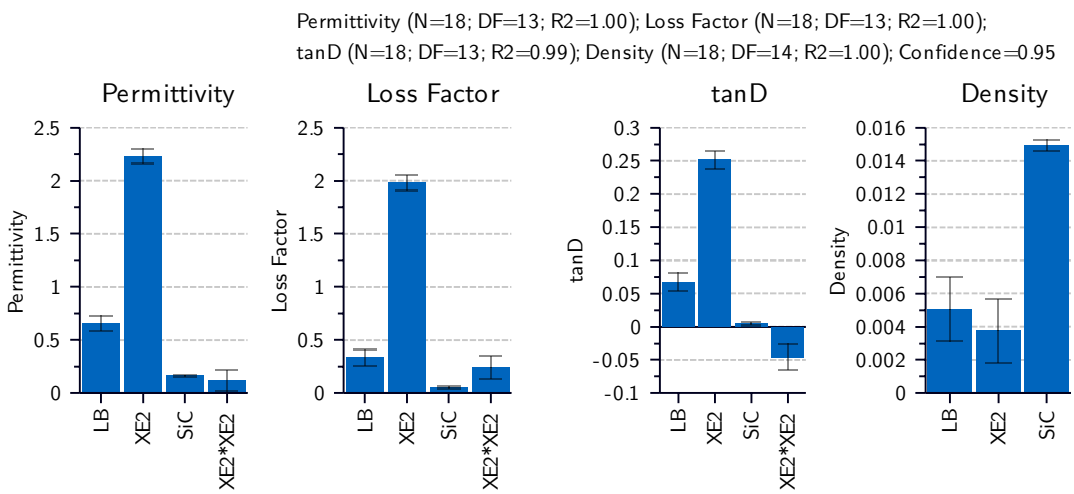

Fig. 5-5 Coefficient plots of evaluated and adapted models of absorber study.

4. Model Quality Check

The model quality is described by four factors that would each be 1 for a perfectly fitted model. All models are excellent as can be seen in Fig. 5-6. The R2 values, that explain how well the models fit the data, are close to 1 for all four factors. The Q2 values, that give an indication for the models' capabilities to predict new data, are similar good. The same is true for the third factor, reproducibility. The third factor—model validity—is above 0.25 for all factors. Therefore, no statistical problems are present.

5. Check of Residuals for Normal Distribution and Outliers

The normal probability distribution is used to detect outliers. For all four responses,

the deleted studentized residuals are normal distributed, compare Fig. 5-7. While some values have high studentized standard deviations, for example experiment number 10 for the permittivity and number 15 and 13 for the loss factor, no sample meets the outlier criteria of 4 SD. Consequently, no experiments or samples are excluded of the study at this point.

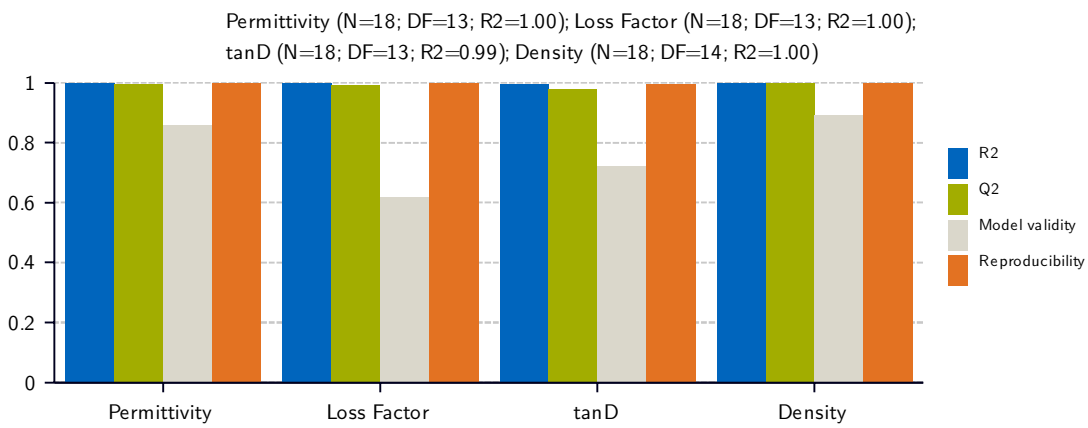

Fig. 5-6 Summary of fit of absorber study after adaptations.

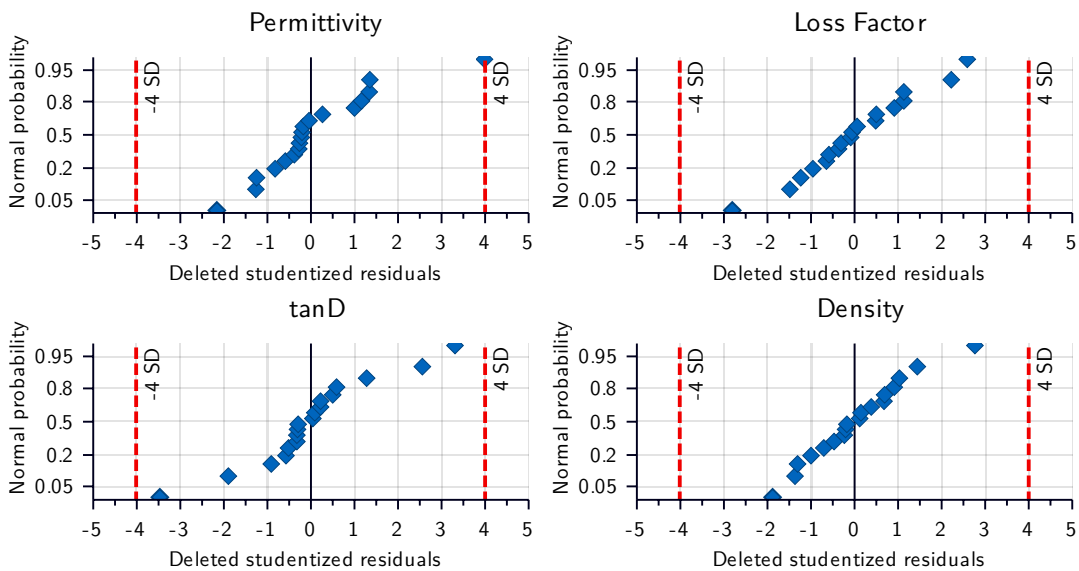

Fig. 5-7 Normal probability distribution of absorber studie's residuals of the adapted models.

6. Check of Residuals for an Influence of Run Order

Last, the deleted studentized residuals are checked for an influence of the run order i.e. measurement order. Residuals that constantly rise or fall would indicate some influence of the run order. In the study at hand, the residuals do not follow any order and are normal distributed around 0. No correlation between measurement

order and residuals exists, as can be seen in Fig. 5-8. This confirms the investigation conducted in section 3.4.3, page 58.

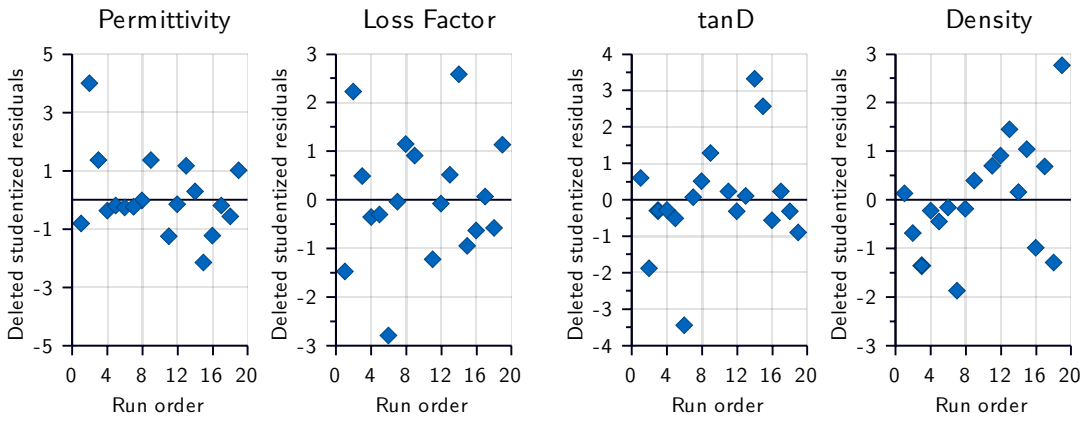

Fig. 5-8 Residuals over run order of absorber study.

5.3.4 Evaluation of DoE Study

As was shown in the section beforehand, the model at has a very good quality and may be evaluated. The evaluation will be done in 3 steps. First, the influence of the different additives will be illustrated. Second, the model terms and fit will be presented. Last, a graphical representation of the design space and the model's boundaries will be presented.

Additive Influence

The influence of the additives that was described during the raw-data evaluation is confirmed by the DoE evaluation. Namely:

- LB influences ε_r' twice as much as ε_r''.
- XE2B initially influences ε_r' 1.3 times as much as ε_r''.
- SiC influences ε_r' three times as much as ε_r''.

Special attention has to be paid to XE2B. Due to the quadratic influence of the CB, the factor shrinks with higher XE2B volume percentage. The described influences are illustrated in the prediction plots in Fig. 5-9. It shows the development of each factor while all others are kept at zero. The prediction intervals plotted around the responses represent the range in that the next observation i.e. absorber mixture will fall with a confidence of 95%.

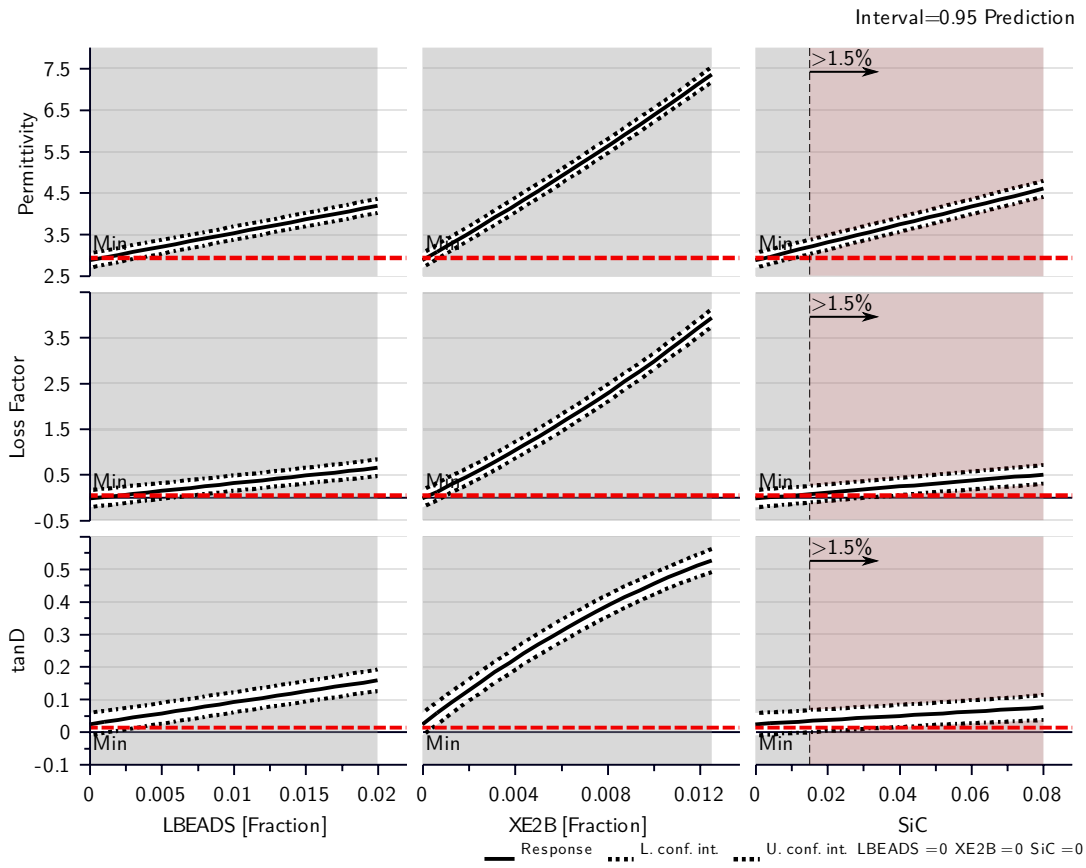

Fig. 5-9 Prediction plots of DoE study. Each graph with all other additives set to 0 to predict the raw influence. The minimum values are defined by the measurement values of the pure resin.

Model Terms and Fit

Modde fits the model to minimize the overall error. It does not, however, allow to set a fixed point. Consequently, the constant model terms that should yield the properties of the pure resin are off. With 2.88 for the permittivity and -0.025 for the loss factor, the constant model terms of the dielectric properties in Tab. 5-6 are below the resin's properties (2.93 / 0.042). This is also visible in the prediction graphs in Fig. 5-9 that cut the minimum values i.e. resin properties. The model factors may, nevertheless, be used to estimate mixture properties i.e. responses—ε_r', ε_r'' or $\tan(\delta)$ in the models boundaries.

With the factors from Tab. 5-6, the responses can be calculated by

$$\text{Response} = LB\varphi_{LB} + SiC\varphi_{SiC} + XE2B\varphi_{XE2B} + XE2{*}XE2\varphi_{XE2B}^2 + C.$$

with the model factors LB, $XE2B$, SiC, $XE2{*}XE2$, the model's constant C, and the chosen volume fractions φ_i.

Tab. 5-6 Factors of the fitted absorber model.

	LB	XE2B	SiC	XE2*XE2	Constant
ε'_r	65.6353	320.205	21.5535	2992.37	2.87601
ε''_r	33.5747	238.942	6.60342	6223.72	-0.024730
$\tan(\delta)$	6.7302	54.6651	0.642545	-1160.04	0.024013

Graphical Representation and Model Boundaries

The possible design space of the adaptable microwave absorber is defined by the introduced model factors and the model boundaries i.e. extreme values. The boundaries will be discusses after the introduction of the design space.

In general the design space of a single mixture containing two additives may be defined by four vectors that draw a parallelogram. Starting from the data-point of pure resin, resin with CB as tip is added to draw the first vector. From that point forward, SiC is added and its influence results in the second vector's tip. Going on from here, subtracting the additives in reverse order, first CB than SiC, draws the third and fourth vector—only resin and SiC and again the pure resin as tips. In vector notation, tip-minus-tail, this gives:

$$\begin{pmatrix} \varepsilon'_{r\mathrm{CB}} - \varepsilon'_{r\mathrm{R}} \\ \varepsilon''_{r\mathrm{CB}} - \varepsilon''_{r\mathrm{R}} \end{pmatrix}, \begin{pmatrix} \varepsilon'_{r\mathrm{CB+SiC}} - \varepsilon'_{r\mathrm{CB}} \\ \varepsilon''_{r\mathrm{CB+SiC}} - \varepsilon''_{r\mathrm{CB}} \end{pmatrix}, \begin{pmatrix} \varepsilon'_{r\mathrm{SiC}} - \varepsilon'_{r\mathrm{CB+SiC}} \\ \varepsilon''_{r\mathrm{SiC}} - \varepsilon''_{r\mathrm{CB+SiC}} \end{pmatrix}, \text{ and } \begin{pmatrix} \varepsilon'_{r\mathrm{R}} - \varepsilon'_{r\mathrm{SiC}} \\ \varepsilon'_{r\mathrm{R}} - \varepsilon''_{r\mathrm{SiC}} \end{pmatrix}.$$

The design spaces created in this manner are drawn in Fig. 5-10. Since the design space of XE2B is much bigger than the space defined by LB samples, only 0.5 V% XE2B and 2 V% LB are plotted. Only the minimum of XE2B is investigated to mirror the uncertainties observed at higher XE2B concentrations.

To discuss the model boundaries, two inaccuracies of the graphical representation are presented before discussing the design spaces' boundaries and usability. First, the simple visualization in form of a parallelogram out of linear vectors leads to a small deviation for the design space of XE2B. The linear vectors neglect XE2B's quadratic influence. However, this divergence is minimal in the drawn lower area with only 0.5% XE2B. In respect to the aim of the illustration—to give a first impression of the design space—this is negligible. Second is an important inaccuracy that occurs in the orientation of the first and fourth vector. The starting point of the first and end point of the fourth vector are defined using the pure resin's dielectric properties. By this, these vectors have another slope than the ones defined purely by the model. The pure resin of the model, 0% additives, has a offset as described above. Consequently, both vectors have a lower gradient than their upper and opposite counter and distort the parallelogram. This shift is very obvious in

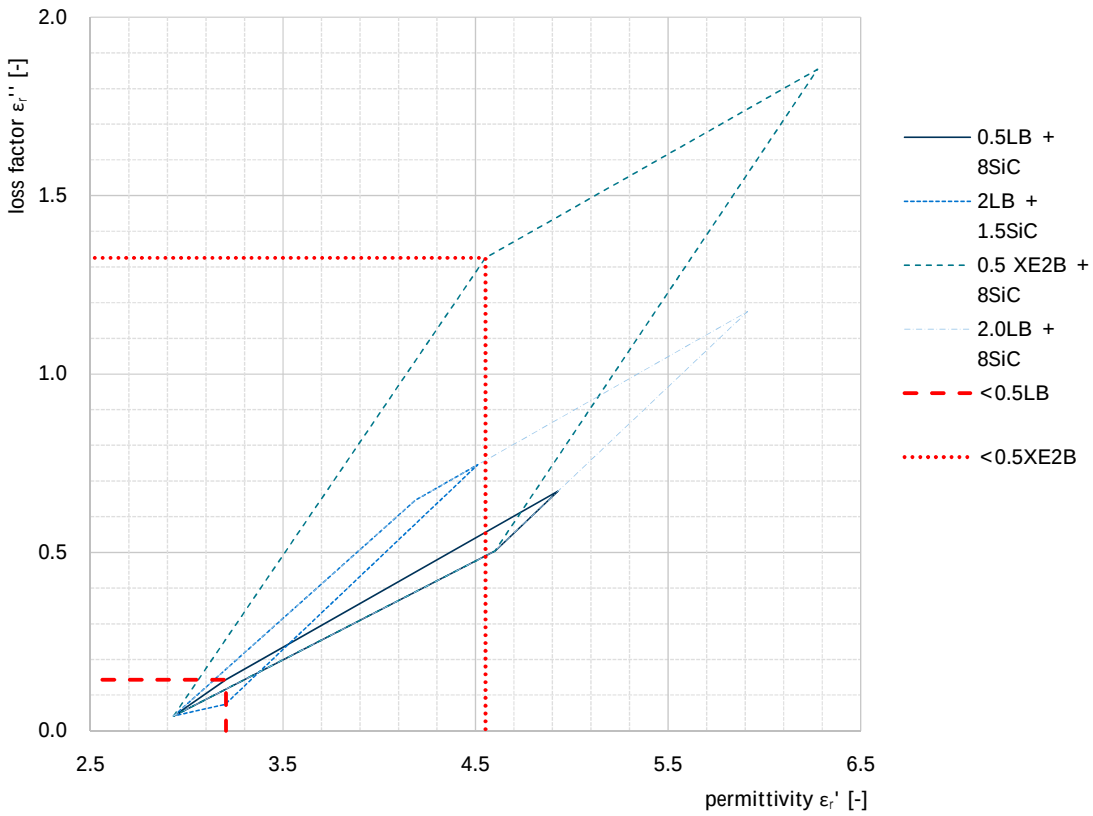

Fig. 5-10 Design spaces of adaptable microwave absorber with mark-up of dead-zone below 0.5 V% LB.

the lower are of the 2% LB configuration with 1.5%SiC. The result is a nearly horizontal orientation of the vector $\begin{pmatrix} \varepsilon'_{r\mathrm{R}} - \varepsilon'_{r\mathrm{SiC}} \\ \varepsilon'_{r\mathrm{R}} - \varepsilon''_{r\mathrm{SiC}} \end{pmatrix}$, compare Fig. 5-10.

This inaccuracies make it obvious that the drawn design space may not be used for a reliable prediction in its bottom area. It cannot be said whether a set point may be reached using any mixture below 0.5 V% LB. A similar uncertainty is present for pure XE2B mixtures. However, given the possibility to combine the carbon blacks and the much higher influence of XE2B, only the are below 0.5 V% LB is seen as dead-zone. In addition to this lower dead-zone, the upper and lower limit of the utilized design space's should be avoided due to the models uncertainty. When the boundaries are respected and not used to their extend, a variable absorber chosen out of this region is manufacturable and can be used for design purposes.

For further work using the presented model, it should be taken into consideration that it uses all measured data to predict possible dielectric properties. This makes it possible to define the design space with adequate precision. However, before manufacturing certain specimens, it is recommended to re-evaluate the data in the

necessary range or take a closer look at local model quality. For example, if only the dielectric property range below 2 V% SiC is used, the XE2B samples may be excluded from the evaluation to improve the prediction quality.

5.4 Summary of Absorber-Study

A process to manufacture adaptable absorbers using epoxy resins was established, section 3.3, page 50. With this, an investigation to test the absorber's capabilities was set up and conducted, section 5.2, page 90. Two carbon blacks (CBs), Printex® L Beads (LB) and Printex® XE 2 B (XE2B), were used to raise the dielectric properties. The addition of a silicon carbid (SiC) was investigated for fine tuning. The whole process from sample manufacturing to measurement of the specimens was thoroughly investigated and standardized in the process. The adaptable absorber was characterized with help of DoE and a model defined, section 5.3.3, page 95. Last, the model was used to visualize the design space, Fig. 5-10 page 102. The model of the adaptable absorber system—with now known dielectric properties over a wide range—can now be used for future investigations and further studies. For example, it can be utilized to design a microwave tool using the appropriate process and heat-up simulations prior to manufacturing the tool and validating the simulation.

6 Investigation of the Mechanical Properties of Glass Fiber Reinforced Plastics

In this chapter the question whether microwave processing under comparable conditions influences the material properties will be investigated. This is done in 5 steps. First, a look is taken at the influence of the infiltration temperature. Second, the glass transition temperature (T_g) development for different cure cycles is investigated. In the third and fourth part the inter-laminar shear strength (ILSS) and 4-point bending (4-pt) properties are checked. Last, the results and their meaning will be discussed in a short summary.

Part of this investigation of mechanical properties has been previously published by the author [70].

6.1 Influence of the Infiltration Temperature on the Material Properties

During the investigation the resin was infiltrated at two different temperatures. First trials were done using an infiltration temperature of 45 °C. The hot infiltration, however, results in a disruption of the microwave processing and an unwanted cool down. To that effect, later samples were infiltrated at room temperature (RT). Whether this change in processing has a relevant influence on the properties will be determined in this section. To assess the influence of start and infiltration temperature on the ILSS properties, independent sample, double sided t-tests are conducted using a significance level $\alpha = 0.05$. The t-test's results are stated in the form (t(degrees of freedom) = t-value, p = p-value, d = Cohen's d). The result is significant when the p-value is smaller than the significance level α. Cohen's d gives an indication of the effect strength of a statistically significant difference. A value above 1 is seen as indication of a large effect in this thesis.

Influence of Infiltration Temperature on T_g

A significant difference is seen for the T_g of RT infiltrate samples (134.59 °C, SD=0.19) and 45 °C infiltrated samples (133.82 °C, SD=0.27) as is evident by the p-value being smaller than the significance level α: ($t(5)$=5.37, p=0.003, d=2.99), see also Tab. 6-1. While the difference in glass transition temperature measured using a DMA (T_{g-DMA}) between RT and 45 °C infiltrated reference plates is significant and Cohen's d is very high, the actual difference is only 0.77 °C. The mismatch is below common variations in T_{g-DMA} measurements. It could be due to some constant variation on the different DMA test dates that lay 4 months apart. The high value of Cohen's d d is a result of the very low standard deviation (SD) of the sample series compared to the difference between means.

Tab. 6-1 Values and test statistics of independent sample, double sided t-tests of reference plates manufactured using different infiltration temperatures.

Propertie		O_ref-RT Mean	O_ref-RT SD	O_ref-45 Mean	O_ref-45 SD	t-tests
T_g	[°C]	134.6	0.19	133.8	0.27	$t(5) = 5.37$, $p = 0.003$, $d = 2.99$
τ_{ILSS-A}	[MPa]	42.2	1.53	41.4	1.44	$t(31) = 1.6$, $p = 0.12$
τ_{ILSS-B}	[MPa]	46.9	2.1	45.6	1.67	$t(31) = 2.16$, $p = 0.039$, $d = 0.22$
σ_f	[MPa]	460	17.62	469	21.99	$t(23) = 1.2$, $p = 0.056$
E_f	[Gpa]	16.1	0.35	16.4	0.53	$t(23) = 1.89$, $p = 0.068$
ε_f	[%]	4.3	0.15	4.3	0.18	$t(23) = 0.2$, $p = 0.84$

Influence of Infiltration Temperature on τ_{ILSS}

No significant difference can be seen for the apparent shear strength in 0°-direction. However, a significant difference can be seen for the apparent shear strength τ_{ILSS} of RT infiltrate samples ($\tau_{ILSS-B-RT}$ = 46.88, SD=2.1) and 45 °C infiltrated samples ($\tau_{ILSS-B-45}$ = 45.59, SD=1.67) in 90°-direction ($t(31)$=2.16, p=0.039, d=0.22). The difference of 1.29 MPa between the τ_{ILSS-B} is way smaller than each SD. This can likewise be seen in the small effect strength of $d = 0.22$, compare Tab. 6-1 Due to the only very small significant difference in one direction, both reference cycles will be seen as one for the following comparison.

For two singular RT samples τ_{ILSS} deviated more than two standard deviations downward from their plates mean value (Sample RG-t3-22-IS-A-05 (τ_{ILSS-A} = 36.4 MPa) and Sample RG-t3-20-IS-B-11 (τ_{ILSS-B} = 42.0 MPa). As this singular behavior of two specimens is most certainly due to laminate defects, these specimens were classified as outliers and excluded from the above and following evaluations.

Influence of Infiltration Temperature on bending properties

There is no significant difference between the bending strength σ_f, the bending modulus E_f, and the maximum elongation during 4-point bending ε_f, compare Tab. 6-1. Both reference cycles will be seen as one for the following comparison.

6.2 Development of Glass Transition Temperature for Different Cure Cycles and Heating Methods

All of the following values are presented in Fig. 6-1 and listed in Tab. 6-2 below. The reference cure cycles done according to the resin's datasheet yield a T_g of 134.6 °C and 133.8 °C. As expected, the T_g of the O_120 cycle at 129.4 °C (SD=0.57) is the lowest of all. The O_120 has a T_g that is 4.4 °C below the reference's T_g. The T_g of the O_140 is at 131.44 °C (SD=0.52) slightly higher than O_120's followed by the dynamic 170 °C cycle's T_g of 132.87 °C (SD=0.75). The MW_120 cure cycle, however, yields a T_g of 134.1 °C (SD=0.43) that lies between the two reference configurations. The glass transition temperatures of MW_140 and MW_dyn lie slightly below with 133.5 °C (SD=1.22) and 132.2 °C (SD=$n.g.$). In summary, all three oven cycles result in a average T_g that is below that of the reference cycle. The microwave specimens all have a higher T_g than their oven counterpart. The 120 °C microwave cycle even results in a T_g similar to that of reference cycle (O_ref).

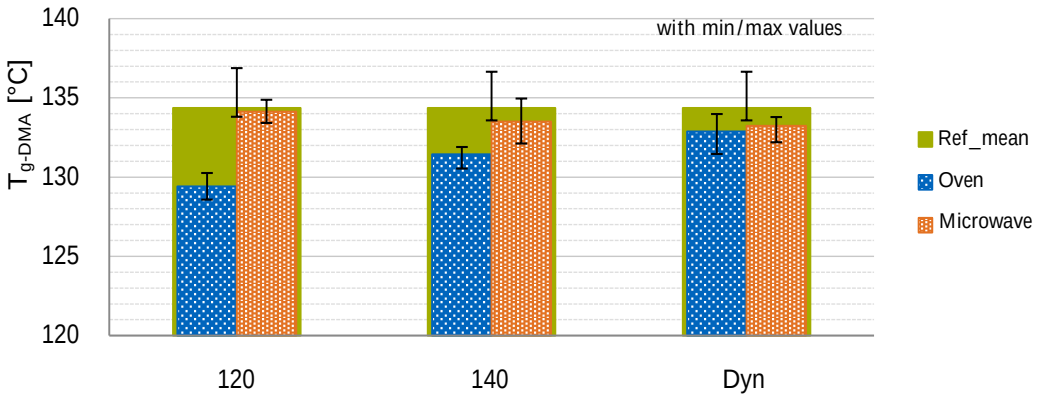

Fig. 6-1 T_g comparison of different cure cycles and methods. Since only three measurements for MW_dyn exist, the Min-Max values are given as error bars instead of SD for all configurations.

One possible explanation for the resin's behavior at 120 °C microwave cure can be found in studies investigating the influence of microwave curing on the reaction path of epoxy resins. This phenomenon was investigated in greater depth by Marand, Baker and Graybeal in 1992 [101], by Wei, Hawley and Demeuse in 1995 [102],

Tab. 6-2 T_{g-DMA} values of all temperature cycles and their statistics.

		O_120	O_140	O_dyn	O_ref	MW_120	MW_140	MW_dyn
Mean	(°C)	129.4	131.4	132.9	134.4	134.1	133.5	133.2
min	(°C)	128.6	130.5	131.5	133.6	133.4	132.1	132.2
max	(°C)	130.3	131.9	134	136.7	134.9	135	133.8
Count	(-)	8	6	9	14	12	5	3
SD	(°C)	0.57	0.52	0.75	0.98	0.43	1.22	n.g.
95%-conf	(°C)	0.47	0.55	0.58	0.56	0.27	1.52	2.23

and by Wallace, Attwood, Day, and Heatley in 2005 [34]. These studies show that microwave curing may change the rate of cross-linking due to a change in reaction path. For example, "the epoxy amine reaction is more dominant in the microwave-cured samples than the other possible curing reactions including the epoxy-hydroxyl reaction" while curing PR500 by 3 M [34]. It can be assumed that similar effects occur during the curing of the present anhydride system. One study conducted by Tanrattanakul and Sae Tiaw in 2005 [39] for an anhydride system is ignored since the present set-up is temperature controlled and the investigated was not. In the investigation, "the applied [microwave] power was based on the physical performance of the cured samples. No air bubbles and no burning were criteria for good specimens". The criteria bubbles and burning would only be met at very high temperatures in the resin. Thus, it can be assumed that the microwave curing in Tanrattanakul and Sae Tiaw's study still took place at much higher temperatures than the compared oven curing. This would most probably result in higher—or at least different—T_g values independent of other influencing factors. Apart from these, the author knows off no in-depth studies that compare the reaction paths of anhydride systems undergoing microwave and conventional cure. However, a further indication of the change in reaction path is that the visual appearance differs between O_ref and MW_120 cured samples. The used resin system turns a brown to reddish tone for all cure cycles exceeding 140 °C; the MW_120 and other 120 °C-cured plates have a cloudy, white appearance. This change in color is best shown in early microwave-cured samples with a high temperature variance, compare Fig. 6-2.

To sum up, the T_g of the oven specimens develops as expected while the microwave specimens show the reference cycles T_g after only 30 min cure at 120 °C. This can be confirmed by a double sided, independent sample t-test between MW_120 and the combined O_refs ($t(18)=0.82$, $p=0.42$) and is most likely to to a change in reaction path.

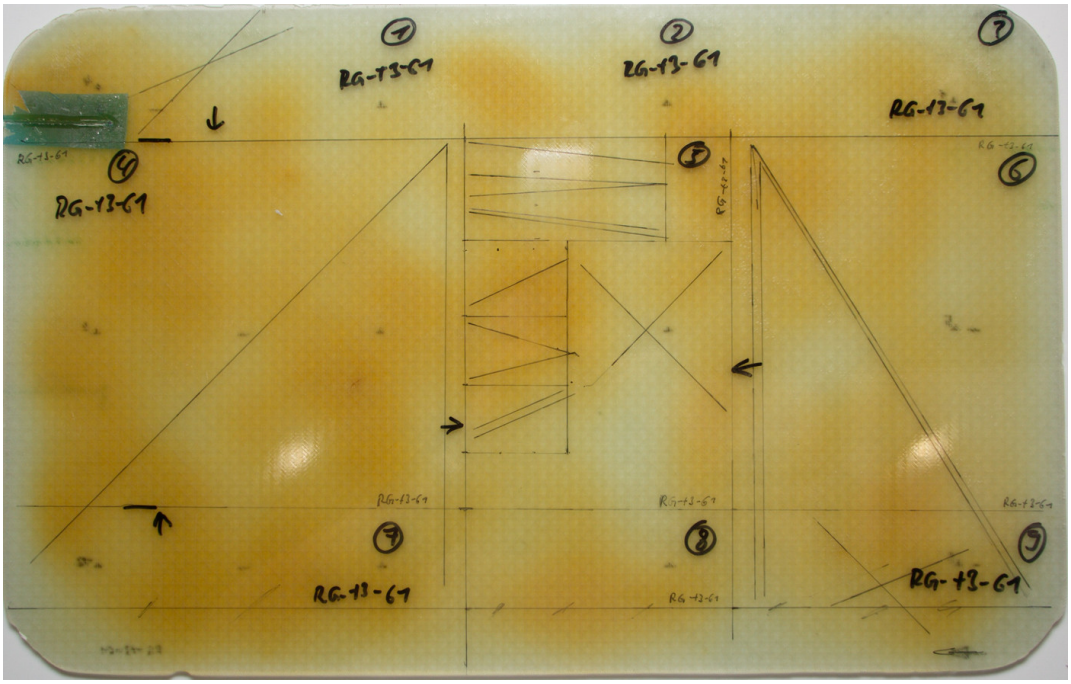

Fig. 6-2 Sample plate manufactured in a microwave process with bad temperature homogeneity during cure results in different colored areas. The temperature records of the trial are shown in Fig. 4-18 on page 84.

6.3 Inter-Laminar Shear Strength

For each process configuration, at least 2 plates were tested for their inter-laminar shear strength. Of each plate, up to 9 specimens in 0° and 90°-direction were tested. The minimum number of samples was tested for the 120 °C oven cycle for which only two plates could be used. In addition to a simple comparison of the results, double sided, independent sample t-tests using a significance level of 5% ($\alpha = 0.05$) are conducted between the results. The t-tests determine whether the difference is statistically significant before interpretation. The t-test's results are stated in the form (t(degrees of freedom) = t-value, p = p-value, d = Cohen's d). The result is significant when the p-value is smaller than the significance level α. Cohen's d gives an indication of the effect strength of a statistically significant difference. A value above 1 is seen as indication of a large effect in this thesis.

6.3.1 Modes of Failure

When taking a look at the failure load it is seen that τ_{ILSS} in the 90° direction is about 10% higher than in 0° direction. An explanation for this is found in the lay-up and resulting mode of failure. The 0° samples show a failure mode where the crack is central around the symmetry layer four. The initial point of failure for 0° specimens occur in the center area where the shear stress is highest, see Fig. 6-3. The 90° samples—with parallel orientation to the innermost symmetry layer four—fail away from the inner area. They fail in the region of layer three or five since the shear failure is constrained by the co-aligned fibers in the symmetry layer. Consequently, the calculated shear strength is higher, since it assumes a crack in the innermost layer. Independent from this difference, all samples show shear-induced failure and are evaluated according to the standard ad described in section 3.5.3.

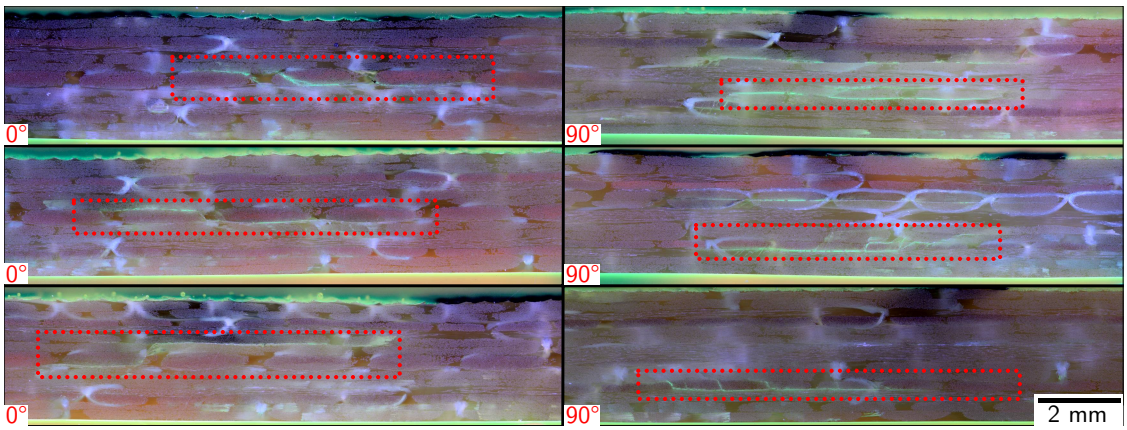

Fig. 6-3 Microsections of failed ILSS specimens in both directions with marked-up crack areas.

6.3.2 Behavior of Oven ILSS Specimen

In 0°-direction no significant difference exists in apparent shear strength of O_120, O_140, and O_ref cured samples. In contrast, the strength of O_dyn cured samples is significantly higher than all of the former three configurations as can be seen in Tab. 6-3. In 90°-direction, the O_140 cured samples have the lowest strength. Their τ_{ILSS-B} is even significantly lower than that of O_120 cured samples. Overall, the O_120 samples show a high apparent shear strength. Their shear strength is similar to that of O_ref or O_dyn cured samples; there is no significant difference. As with the 0° specimens, the highest apparent shear strength in 90°-direction is achieved by the O_dyn cured samples. The O_dyn cured strength is significantly higher than that of O_ref cured samples.

Tab. 6-3 ILSS results, test statistics and independent sample, double sided t-tests of oven cured plates.

0°	τ_{ILSS-A} [MPa]	**Count** [-]	**SD** [MPa]	**95% conf.** [MPa]	**T-Test** row to row above
O_dyn	42.8	20	1.68	0.78	
O_120	40.8	14	1.95	1.13	$t(25) = 3.11$, $p = 0.005$, $d = 1.11$
O_140	40.7	18	2.00	1.00	$t(28) = 0.08$, $p = 0.937$
O_dyn	42.8	20	1.68	0.78	$t(33) = 3.4$, $p = 0.002$, $d = 1.12$
O_ref	41.6	41	1.70	0.54	$t(38) = 2.64$, $p = 0.012$, $d = 0.72$
O_140	40.7	18	2.00	1.00	$t(28) = 1.55$, $p = 0.131$
90°	τ_{ILSS-B} [MPa]	**Count** [-]	**SD** [MPa]	**95% conf.** [MPa]	**T-Test** row to row above
O_120	47.1	17	2.51	1.29	
O_140	44.4	16	2.08	1.11	$t(31) = 3.32$, $p = 0.002$, $d = 1.15$
O_dyn	47.3	26	1.27	0.51	$t(22) = 4.88$, $p < 0.001$, $d = 1.74$
O_ref	46.1	43	1.95	0.60	$t(67) = 2.88$, $p = 0.005$, $d = 0.65$
O_140	44.4	16	2.08	1.11	$t(25) = 2.83$, $p = 0.009$, $d = 0.85$

Summarizing, the 120 °C-cycle achieves similar apparent shear strength than the reference cycle. The 140 °C-cycle in B direction shows a drop in apparent shear strength while the dynamic oven cycle beats the properties of the reference cycle in both directions by ≈1.2 MPa, compare Tab. 6-3.

6.3.3 Behavior of Microwave ILSS Specimen

In 0°-direction no difference exist in the apparent shear strength of MW_120 and MW_140 cured samples. Both configurations, however, show a significantly lower

shear strength compared to O_ref. While the strength of MW_dyn cured samples is significantly higher compared to that of MW_140 cured samples, there is no significant difference between MW_dyn's and O_ref's results, see Tab. 6-4. In 90°-direction no significant differences exists between O_ref's and MW_120's or MW_140's ILSS results. However, MW_140's τ_{ILSS-B} is significantly higher than that of MW_120. The samples cured using MW_dyn have the highest apparent shear strength of all tested specimens. Their shear strength is significantly higher than that of O_ref or the other microwave cured samples.

Summarizing, the ILSS properties of microwave processed samples are all comparatively high, see Tab. 6-4. Only in 0°-direction are the MW_120 and MW_140 cured samples significantly weaker than the O_ref samples.

Tab. 6-4 ILSS results, test statistics and independent sample, double sided t-tests of microwave cured plates.

0°	τ_{ILSS-A} [MPa]	**Count** [-]	**SD** [MPa]	**95% conf.** [MPa]	**T-Test** row to row above
MW_120	39.2	26	1.56	0.63	
MW_140	40.0	27	2.37	0.94	$t(45) = 1.45$, $p = 0.153$
MW_dyn	42.2	19	1.86	0.90	$t(43) = 3.49$, $p = 0.001$, $d = 1$
O_ref	41.6	41	1.70	0.54	$t(32) = 1.22$, $p = 0.231$
90°	τ_{ILSS-B} [MPa]	**Count** [-]	**SD** [MPa]	**95% conf.** [MPa]	**T-Test** row to row above
MW_120	45.5	20	1.57	0.73	
MW_140	46.7	25	2.18	0.90	$t(43) = 2.05$, $p = 0.046$, $d = 0.59$
MW_dyn	49.5	18	1.48	0.73	$t(41) = 5.01$, $p < 0.001$, $d = 1.45$
O_ref	46.1	43	1.95	0.60	$t(42) = 7.3$, $p < 0.001$, $d = 1.83$

6.3.4 Comparison between Oven and Microwave ILSS Specimens

For the 120 °C samples, the microwave samples in both directions have a lower shear strength than the oven specimens. Both orientations show a significant difference with a delta of 1.6 MPa between their means. For the 140 °C and the dynamic 170 °C temperature cycles, the 0° tests show no significant difference between oven and microwave samples. In contrast, the 90°tests of these cure cycles show a clear and significant difference. The MW samples have an apparent shear strength τ_{ILSS-B} that is ≈2.2 MPa higher than that of the oven specimens', see Table 6-5.

Tab. 6-5 Comparison of ILSS results, test statistics and independent sample, double sided t-tests of oven and microwave cured plates.

0°	τ_{ILSS-A} [MPa]	**Count** [-]	**SD** [MPa]	**95% conf.** [MPa]	**T-Test** row to row above
O_120	40.8	14	1.95	1.13	
MW_120	39.2	26	1.56	0.63	$t(22) = 2.6$, $p = 0.016$, $d = 0.92$
O_140	40.7	18	2.00	1.00	
MW_140	40.0	27	2.37	0.94	$t(40) = 1.1$, $p = 0.279$
O_dyn	42.8	20	1.68	0.78	
MW_dyn	42.2	19	1.86	0.90	$t(36) = 1.05$, $p = 0.3$

90°	τ_{ILSS-B} [MPa]	**Count** [-]	**SD** [MPa]	**95% conf.** [MPa]	**T-Test** row to row above
O_120	47.1	17.0	2.51	1.29	
MW_120	45.5	20.0	1.57	0.73	$t(26) = 2.22$, $p = 0.035$, $d = 0.76$
O_140	44.4	16.0	2.08	1.11	
MW_140	46.7	25.0	2.18	0.90	$t(33) = 3.32$, $p = 0.002$, $d = 1.05$
O_dyn	47.3	26.0	1.27	0.51	
MW_dyn	49.5	18.0	1.48	0.73	$t(33) = 5.2$, $p < 0.001$, $d = 1.64$

6.4 4Pt-Bending Properties

For all but two process configuration, at least 2 plates, each with up to 9 specimens in 0°-direction were tested. For the dynamic microwave cycle MW_dyn only one plate could be used for 4-pt tests. The other available plate was locally burned and only ILSS specimens were be prepared and tested. Thus, the minimum of 5 valid samples were tested for MW_dyn. One plate of the O_120 configuration was excluded for the 4-point bending investigation due to its thickness. A second O_120 plate was excluded due to a lay-up error. Consequently, only 7 valid samples were tested for the O_120 configuration. For all other configurations more than one plate and at least 11 specimens per temperature cycle are evaluated in the following sections.

In addition to a simple comparison of the results, double sided, independent sample t-tests using a significance level of 5% ($\alpha = 0.05$) are conducted between the results. The t-tests determine whether the difference is statistically significant before interpretation. The t-test's results are stated in the form (t(degrees of freedom) = t-value, p = p-value, d = Cohen's d). The result is—with a certainty of 95%—statistically significant and not random when the p-value is smaller than the significance level α. Cohen's d gives an indication of the effect strength of a statistically significant difference. A value above 1 is seen as indication of a large effect in this thesis.

6.4.1 Mode of Failure

All samples fail on the lower side due to tension strains, compare (Fig. 6-4).

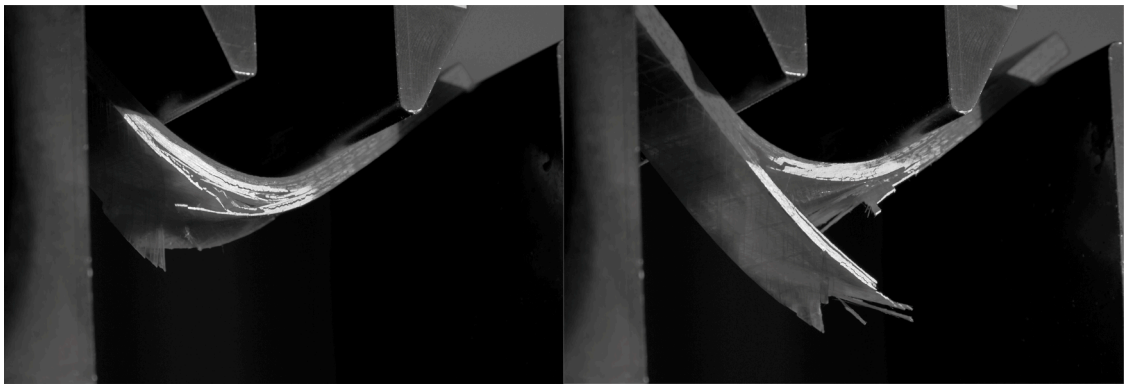

Fig. 6-4 Exemplary failure mode of two bending specimens.

6.4.2 Behavior of Oven 4Pt-Bending Specimens

Bending Strength σ_f

No significant difference in bending strength can be seen for any combination of oven cured configurations.

Modulus E_f

The samples produced using the O_ref have a significantly lower bending modulus compared to the samples produced using O_120 and O_dyn, compare Tab. 6-6. No other significant difference are present.

Elongation ε_f

No significant difference in bending elongation can be seen for any combination of oven cured configurations.

Tab. 6-6 4-pt results, test statistics and independent sample, double sided t-tests of oven cured plates.

0°	σ_f [MPa]	Count [-]	SD [MPa]	95% Conf. [MPa]	T-Test row to row above
O_120	460.1	7	9.48	8.76	
O_140	468.3	11	20.69	13.90	$t(15) = 1.15$, $p = 0.27$
O_dyn	469.3	23	13.41	5.80	$t(14) = 0.14$, $p = 0.887$
O_ref	468.8	35	21.99	7.55	$t(56) = 0.12$, $p = 0.906$
0°	**E_f [GPa]**	**Count [-]**	**SD [GPa]**	**95% Conf. [GPa]**	**T-Test row to row above**
O_120	17	7	0.33	0.31	
O_140	16.58	11	0.58	0.39	$t(16) = 1.96$, $p = 0.068$
O_dyn	16.69	23	0.46	0.2	$t(16) = 0.54$, $p = 0.594$
O_ref	16.31	36	0.48	0.16	$t(49) = 2.98$, $p = 0.004$, $d = 0.79$
O_120	17	7	0.33	0.31	$t(12) = 4.58$, $p = 0.001$, $d = 1.48$
0°	**ε_f [%]**	**Count [-]**	**SD [%]**	**95% Conf. [%]**	**T-Test row to row above**
O_120	4.22	7	0.1	0.09	
O_140	4.23	11	0.14	0.09	$t(16) = 0.29$, $p = 0.778$
O_dyn	4.27	23	0.16	0.07	$t(23) = 0.69$, $p = 0.497$
O_ref	4.31	35	0.17	0.06	$t(48) = 0.79$, $p = 0.436$

6.4.3 Behavior of Microwave 4Pt-Bending Specimens

Bending Strength σ_f

The samples produced using MW_120 have a significantly higher bending strength compared to the samples cured using MW_140 and MW_dyn. Furthermore, the bending strength of MW_dyn is significantly lower than that of O_ref, compare Tab. 6-7.

Modulus E_f

The samples cured using MW_120 have the highest bending modulus of all configurations investigated. The difference in modulus is significant compared to MW_140 cured samples and compared to the reference samples, compare Tab. 6-7.

Elongation ε_f

The MW_120 samples have a significantly lower elongation than the MW_140 samples, see Tab. 6-7. No other combination of microwave cured samples shows a significant difference in ε_f to each other or the reference cycle.

Tab. 6-7 4-pt results, test statistics and independent sample, double sided t-tests of microwave cured plates.

0°	σ_f [MPa]	Count [-]	SD [MPa]	95% Conf. [MPa]	T-Test row to row above
MW_120	479.0	17	15.56	8.00	
MW_140	457.9	11	26.95	18.1	$t(14) = 2.36$, $p = 0.033$, $d = 1.02$
MW_dyn	454.6	5	10.90	13.54	$t(14) = 0.43$, $p = 0.676$
O_ref	468.8	35	21.99	7.55	$t(10) = 2.3$, $p = 0.044$, $d = 0.67$
0°	E_f [GPa]	Count [-]	SD [GPa]	95% Conf. [GPa]	T-Test row to row above
MW_120	17.21	17	0.83	0.43	
MW_140	16.27	11	0.73	0.49	$t(24) = 3.15$, $p = 0.004$, $d = 1.18$
MW_dyn	16.96	5	0.96	1.19	$t(6) = 1.43$, $p = 0.203$
O_ref	16.31	36	0.48	0.16	$t(4) = 1.48$, $p = 0.213$
MW_120	17.21	17	0.83	0.43	$t(21) = 4.13$, $p < 0.001$, $d = 1.46$
0°	ε_f [%]	Count [-]	SD [%]	95% Conf. [%]	T-Test row to row above
MW_120	4.24	17	0.11	0.05	
MW_140	4.33	11	0.1	0.07	$t(22) = 2.2$, $p = 0.039$, $d = 0.84$
MW_dyn	4.14	5	0.2	0.25	$t(5) = 2.18$, $p = 0.081$
O_ref	4.31	35	0.17	0.06	$t(5) = 1.69$, $p = 0.151$

6.4.4 Comparison between Oven and Microwave 4Pt-Bending Specimens

Bending Strength σ_f

The oven cured 120 °C have a significantly lower bending strength than microwave cured samples. Opposed to that, the dynamically cured oven samples have a significant higher bending strength than their microwave counterparts, compare Tab. 6-8.

Modulus E_f

No significant difference in bending modulus E_f can be seen when comparing oven and microwave cured samples, compare Tab. 6-8.

Elongation ε_f

No significant difference in bending elongation ε_f can be seen when comparing oven and microwave cured samples, compare Tab. 6-8.

Tab. 6-8 Comparison of 4-pt results, test statistics and independent sample, double sided t-tests of oven and microwave cured plates.

0°	σ_f [MPa]	Count [-]	SD [MPa]	95% Conf. [MPa]	T-Test row to row above
O_120	460.1	7	9.48	8.76	
MW_120	479.0	17	15.56	8.00	$t(18) = 3.64$, $p = 0.002$, $d = 1.33$
O_140	468.3	11	20.69	13.90	
MW_140	457.9	11	26.95	18.1	$t(19) = 1.02$, $p = 0.319$
O_dyn	469.3	23	13.41	5.80	
MW_dyn	454.6	5	10.90	13.54	$t(7) = 2.61$, $p = 0.035$, $d = 1.12$

0°	E_f [GPa]	Count [-]	SD [GPa]	95% Conf. [GPa]	T-Test row to row above
O_120	17	7	0.33	0.31	
MW_120	17.21	17	0.83	0.43	$t(22) = 0.88$, $p = 0.39$
O_140	16.58	11	0.58	0.39	
MW_140	16.27	11	0.73	0.49	$t(19) = 1.1$, $p = 0.287$
O_dyn	16.69	23	0.46	0.2	
MW_dyn	16.96	5	0.96	1.19	$t(4) = 0.62$, $p = 0.571$

0°	ε_f [%]	Count [-]	SD [%]	95% Conf. [%]	T-Test row to row above
O_120	4.22	7	0.1	0.09	
MW_120	4.24	17	0.11	0.05	$t(12) = 0.6$, $p = 0.559$
O_140	4.23	11	0.14	0.09	
MW_140	4.33	11	0.1	0.07	$t(18) = 1.88$, $p = 0.077$
O_dyn	4.27	23	0.16	0.07	
MW_dyn	4.14	5	0.2	0.25	$t(5) = 1.3$, $p = 0.249$

6.5 Discussion of the Mechanical Properties of Glass Fiber Reinforced Plastics

6.5.1 ILSS Properties

The apparent inter-laminar shear strength (ILSS) of 120 °C cured microwave specimens is lower than that of oven-cured samples; all other configurations, however, yield similar or better results for microwave curing. This is especially visible for the 90° samples. The results of configurations cured using a dynamic-cure cycle—using only ramps and lacking any dwell time—consistently beat the reference cycle. The dynamic microwave-cured samples beat the reference cycle in 90°-orientation by 3.4 MPa or 7%, compare Fig. 6-5. This higher failure load parallel to the mid-plane—where the crack occurs in outer layers—can be due to lower process induced strains. This indicates a better in-depth temperature homogeneity as a result from the in-depth microwave heating.

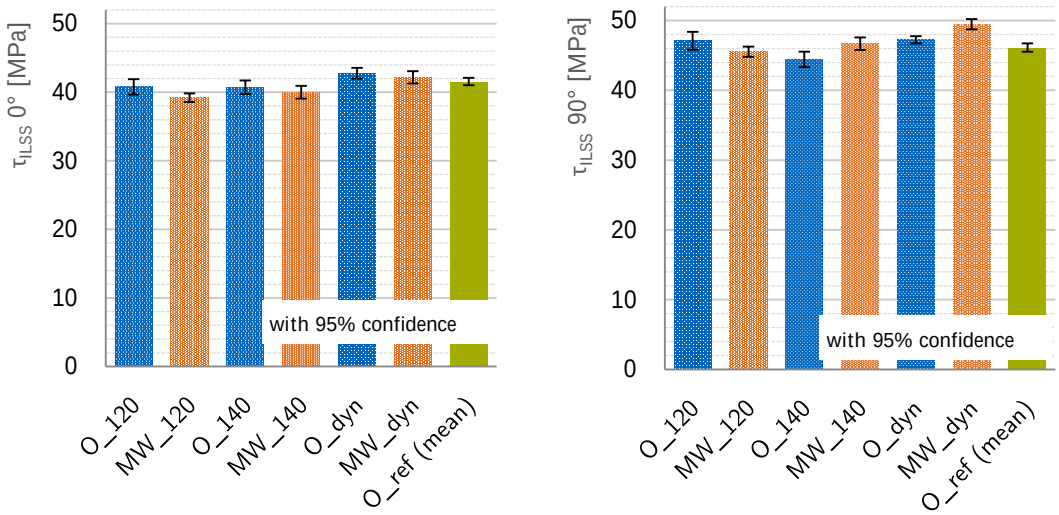

Fig. 6-5 τ_{ILSS} in 0° to the left and 90° to the right with 95% confidence interval.

6.5.2 4Pt-Bending Properties

In 4-point bending (4-pt), the 120 °C cured samples are characterized by an increased flexural modulus. However, only the difference of the MW_120 cured configuration is significant. Within this sample population, one of the three plates has a 10% higher bending modulus than the average of the other two. Since the dominant factor for the flexural modulus is the fiber orientation, the modulus increase is

most probably a result of a deviation in fiber orientation in this plate. The MW_120 specimens, additionally, show the highest overall bending strength. This cannot be ascribed to the single plate with higher bending modulus; the investigated plate is well inside the average of the others. The increased bending strength at 120 °C must be ascribed to the incomplete cure of the resin. With the additional aspect of the generally low differences between all 4-pt-tests, this deviation is well inside the expected behavior. In contrast to the 120 °C-samples, the MW_dyn samples show the lowest bending strength with a significant difference to the reference cycle (O_ref) and O_dyn. A possible reason for the bad performance of MW_dyn samples can be found in their high thickness; the used samples have a average thickness of 3.26 mm. Other plates that were tested having a similar thickness above 3.25 mm have, likewise, a low bending strength compared to their population. This includes 6 out of 11 MW_140 and 5 out of 35 O_ref samples. For example, the average bending strength of the six MW_140 specimens above 3.25 mm is 440.1 MPa ($SD = 12.71$) compared to 479 MPa ($SD = 23.74$) for the five specimens below 3.07 mm. A similar if less extreme tendency can be seen for the reference cycle. The five samples above 3.25 mm have a bending strength of 454.2 MPa ($SD = 11.84$) compared to 481.2 MPa ($SD = 22.71$) of the eleven specimens below 3.07 mm and compared to 468.8 MPa ($SD = 21.99$) of the population's 35 specimens. This examples and variations through thickness show, that the bending strength of the MW_dyn configuration is well inside the expected limits set by the other configurations. If anything, the average bending strength of 454.6 MPa ($SD = 10.9$) is comparably high with regard to the mean thickness of the tested five specimens 3.26 mm.

6.5.3 Summary of Mechanical Investigation

The question, whether microwave curing produces the same laminate quality as conventional curing, can be approved. The development of glass transition temperature (T_g) made clear that, while microwave curing produces laminate having similar mechanical properties, the path to the final product is different. This potential change in the cure-reaction will vary depending on the resin system's chemistry. It might even be, that some resin systems may extract further advantages—or disadvantages—from microwave curing. The ILSS investigation showed, that microwave curing may increase matrix dominated properties. This effect most probably comes from the in-depth heating of microwaves and will variate strongly depending on the thickness and geometry of a part. However, this is the case for every curing process due to the imminent internal stresses of any heating process. The 4Pt-bending investigation did not yield any significant differences and confirms the research hypothesis.

7 Overall Summary, Conclusions, and Recommendations

7.1 Starting Point, Research Questions, and Findings

Former and current studies point out that microwave processing promises up to 50% cure cycle time reduction [15]–[18], [51]. Nevertheless, research in microwave processing was not consequently followed up by the industry. A possible reason for this is that the overall technology readiness level (TRL) of microwave processing does not allow the integration in the next product line. The next product line is in turn the planning horizon of 66% of the industry [23]. As a result of this, the TRL of microwave processing needs to be advanced so that it can be used for near-term applications. The overall TRL development of microwave processing, however, depends on advancements in many areas. Some of these areas were neglected in the past. In this thesis, therefore, a new and more solid foundation for further developments was set. The approach chosen was to investigate singular technology areas and conduct steps to further their TRL. Four research questions were formulated that can now be answered.

What is the relationship between available process control mechanisms and the processability of a material using microwaves in a practical use case?

Wrong process parameters prevent a controlled and homogeneous heating. The right process control mechanisms are essential for microwave processability.

This first research question is answered with the lessons learned of manufacturing trials. The manufacturing of specimens required adaptations to the equipment and optimization of the microwave control parameters. Apart from an optimized preforming process, the implementation of the following measures resulted in a stable manufacturing process:

- Homogenization of the electric field through adding mode-stirrers, changing the used magnetrons constantly, and using a high number of active magnetrons.

- Addition of a Dead-Load to increase the needed energy, stabilize the microwave controller, and reduce field exaltation.
- Optimization of the microwave controller by adapting its proportional integral derivative (PID) parameters and introducing a maximum power level. The first to reduce control oscillations and the latter to reduce field exaltation.

All of these measures were identified as results of trials and in discussions with Guido Link and Volker Nuss of the Karlsruher Institute of Technology (KIT) and Stefan Betz of Vötsch Industrietechnik (VIT).

How do certain universal process control mechanisms influence the temperature distribution in processed materials?

The addition of Mode-Stirrers, a constant Magnetron Change, and a higher Magnetron Count increase temperature homogeneity. The Magnetron Change has a slightly stronger influence than the other two factors combined.

To answer this second research question, some of the changes implemented in the glass fiber-reinforced plastic (GFRP) manufacturing process mentioned above were investigated to quantify the effect strength of the process control mechanisms. The selected factors investigated were the use of Mode-Stirrers (Stir), the equipment's controller's Sinus Function (Sin), a constant Magnetron Change (MChan), the Magnetron Count (MCoun), and a Dead-Load (Load). The investigation showed that the Sinus Function and Dead-Load do not significantly influence the temperature distribution as determined by the standard deviation (SD) of the thermal image. The Dead-Load, however, increases the power needed for heating. The other three factors have a positive i.e. reducing influence on the SD. For an absolute recalculated standard deviation-range (SD^*) in the trials of 0.74–2.96 °C, the Magnetron Change has a slightly stronger effect (-0.72 °C) than Mode-Stirrers and Magnetron Count in combination (-0.3/-0.3 °C).

What are the effects of different additives on the dielectric properties i.e. microwave absorption of an epoxy resin?

The tested additives have a distinct and substantial influence on the dielectric properties.

- Printex® L Beads increases ε_r' twice as much as ε_r''.
- Printex® XE 2 B initially increases ε_r' 1.3 times as much as ε_r''.
- Silicon carbid increases ε_r' three times as much as ε_r''.

For this third research question, the effect of three additives on the dielectric properties of an epoxy resin were investigated. An absorber manufacturing process that ensures a homogeneous distribution of additives was established and used to manufacture specimens. These specimens were used to investigate two carbon blacks (CBs) and a silicon carbid (SiC) for their influence on the dielectric properties permittivity (ε_r') and loss factor (ε_r''). The first CB, Printex® L Beads (LB), has a high structure. The second CB, Printex® XE 2 B (XE2B), has a very high and open structure. The used black SiC has a FEPA F 1200 grain size; this equals a size around 3 µm. The influence of up to 2 V% of LB, up to 1.25 V% of XE2B, and up to 8 V% of SiC were investigated. The study shows that a wide range of dielectric properties can be achieved using the defined absorber manufacturing method and additives. Furthermore, each additive has a distinct influence on the dielectric properties ε_r' and ε_r''. The distinct influence of each additive helps to customize an absorber. In short:

- LB increases ε_r' twice as much as ε_r''.
- XE2B initially increases ε_r' 1.3 times as much as ε_r''.
- SiC increases ε_r' three times as much as ε_r''.

These factors were visible in a simple evaluation of the absorber measurements as well as in a DOE evaluation of the data. The latter evaluation showed that XE2B has a quadratic influence on the parameters; the factor of 1.3 decreases using a higher filling. The measurement data defines a design space for an adaptable microwave absorber that can be used for future investigations.

Does microwave processing of GFRP samples using a microwave optimized setup influence the properties of the material?

In the trials at hand, the development of the glass transition temperature in microwave curing runs ahead of the cure temperature. Microwave processing must have an influence on the reaction path of the anydride epoxy system. An increase of the inter-laminar shear strength is observed in comparison to oven cured samples for certain configurations. A dedicated microwave cure cycle using constant heating rates yields the best results. The 4-point bending investigation shows no significant differences.

To answer this last research questions, samples were manufactured using a conventional oven and a stable microwave process. The study was designed to exclude all factors except the used heating technologies' influences. Three different temperature profiles and the data sheets cure cycle were used to work out possible differences. With the epoxy system's glass transition temperature (T_g) of 139 °C

in mind, maximum temperatures of 120 °C, 140 °C and 170 °C were used for cure. Furthermore, the 170 °C cure cycle is optimized for microwave cure. It uses only constant temperature rises without dwell times. The same temperature profiles—with two slight adaptations to mind microwave's peculiarities—were used in oven and microwave cure. With regard to the GFRP properties, the development of T_g in microwave curing runs ahead of the cure temperature; the T_g of the oven specimens develops as expected. The microwave specimens show the reference cycle's T_g of 135 °C after only 30 min cure at 120 °C. The apparent inter-laminar shear strength (ILSS) of 120 °C cured microwave specimens is lower than that of oven-cured samples; however, all other configurations show similar or better results for microwave curing. The dynamic microwave-cured samples beat the reference cycle in 90°-orientation by 3.4 MPa or 7%. This higher failure load may be due to lower process induced strains as indicated by the failure behavior. It suggests a better temperature homogeneity over the thickness as a result from the in-depth microwave heating. The 4-point bending (4-pt) investigation yields no significant differences. The answer to the last research question is that a neglectable difference exists between oven and microwave cured specimens. In most applications, microwave cure—at least of GFRP—is seen as equal or better than conventional oven cure.

7.2 Conclusions

In the present thesis the necessary development steps for microwave processing were evaluated and re-estimated. Through the initial analysis of prior research, the evaluation of the state of the art, and first hand trials it became clear that there are influencing factors which were not adequately addressed or published in the past. This insight led to three investigations. The first investigation of the process control mechanisms and the second investigation of a variable absorber system were targeted to specifically further the technology readiness level of microwave processing. In contrast, the third investigation did not aim to further the technology readiness level of microwave processing. This study on the mechanical properties of GFRP was done to re-evaluate manufacturing capabilities and prior research. Below is an account on the TRL improvements through this thesis followed by improvements made in public research. The state of technology is likewise visualized in Fig. 7-1 using the TRL definition and the Leitat model described in the introduction.

The first investigation of the process control mechanisms and manufacturing trials showed the importance of minding microwave's peculiarities. By increasing the randomness in the microwave field (Mode-Stirrers, Magnetron Change, Magnetron

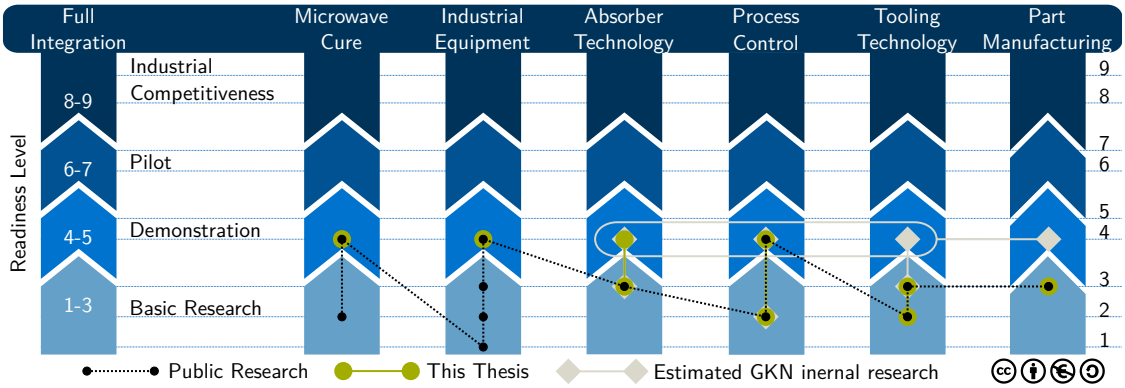

Fig. 7-1 Technology readiness level of microwave sub-systems based on the Leitat Technology Readiness Pathway [25] at the end of this thesis.

Count), matching the available microwave power to the processed part (Dead-Load, Maximum Power Level), and through adaptation of the PID-parameters a better temperature homogeneity and more stable process is realized. The process control is advanced to TRL 4 by this thesis and other work. One other work that includes a promising approach to increases temperature homogeneity is Yiming Sun's Ph.D. thesis on "Adaptive and Intelligent Temperature Control of Microwave Heating Systems with Multiple Sources"[103]. Sun investigates predictive, neural network, and reinforcement learning control systems for the *Hephaistos* system. Similiar approaches were published by Zhou et al. in 2018 in form of a "multi-pattern compensation method" [104] and Li, Li, Zhou, and Zhao in 2019 in form of a "deep learning" approach [105]. In comparison to the methods at hand, however, Sun's, Zhou et al.'s and Li et al.'s control systems are more complex. Overall, the process control in public research is classified as TRL 4. The second investigation developed and characterized a variable microwave absorber. This was done in order to be able to build tooling for the manufacturing of complex composite parts. The manufacturing process of the variable absorber was defined and demonstrated at a laboratory scale. Dielectric measurements were used to define a design space. The variable absorber technology was validated in a laboratory environment and is thus classified as TRL 4. No other investigations on an absorber for microwave processing of composites were published. Related with this advance are the TRLs of tooling technology and part manufacturing that were both confirmed by the third investigation. The manufacturing using completely microwave transparent tools with low thermal conductivity and without an additional absorber was accomplished for GFRP specimens. This aligns with the results of GKN Aerospace [21], [22] where carbon fiber-reinforced plastic (CFRP) tools were used that likewise have bad thermal conductivity. In comparison to GKN's investigations, the process was publicly developed further and an important step was undertaken to prepare for future progress in these areas. The use of simple tools and manufacturing of

GFRP plate specimens affirms the existing TRLs of 3 for tooling technology and part manufacturing.

In their entirety, the results of this thesis show the importance of an holistic approach to warrant the success of microwave processing. This approach in mind, conceptional restrictions that were stated in past research were not supported by the manufacturing trials and the homogeneity study done in this thesis. The homogeneity study's insights can be used in all future process developments. Likewise, insights gained from the study on microwave absorbers will be of assistance to further researchers and industry in the development of microwave optimized tools. In combination, the findings of this thesis set a new foundation for future developments in research and industry.

7.3 Further Research Areas, Development Areas, and Perspectives

Considerably more work will need to be done before microwave curing can widely and easily be used. The following section presents possible future research and developments in three parts. First the next steps that might be investigated in general research are proposed. Second, some industrial applications that are currently seen as feasible are presented. Last, novel concepts made possible through microwave heating as well as long term developments are given.

General Research

With respect to the current state and to broaden the applicability of microwave processing, the next investigations—in the authors opinion—should handle tooling technology. The most important step is the integration of a variable absorber into basic tooling concepts. This way, complex microwave heating scenarios can be tackled. A first step in the integration should be a heat-up simulation of metallic or GFRP tools that utilize an absorber. For example, the absorber system defined in this thesis. Singular challenges like a plate having varying thickness, having a curvature, or being made out of two materials can be used to deepen the understanding. The insights can then be used for the simulation and manufacturing of complex geometries. This cautious two step approach assures the basic understanding necessary for more complex investigations. A second research topic is the simultaneous manufacturing of multiple samples. Through the direct microwave interaction, the temperature profiles of multiple samples could differ. This should be addressed using a suitable process control strategy. In this regard, GKN proposed a power controlled process for simultaneous cure of two or more samples [22]. Another approach is the use of a predictive, a neural network, or a reinforcement

learning control system as investigated by Yiming Sun in his thesis in 2016 [103]. Yiming's system activates specific magnetrons for longer periods with the aim of establishing a more homogeneous temperature distribution. VIT is currently working on the implementation of one of these control systems into their commercial equipment. In recent time, similar approaches were published by Zhou et al. in 2018 [104] and Li, Li, Zhou, and Zhao in 2019 [105]. However, on the shop floor level and applied to three dimensional parts, the complexity of all the proposed methods could be a drawback. An approach on tooling for CFRP that can be followed was presented by Yingguang Li, Nanya Li, Jing Zhou, and Qiang Cheng [88] in 2019. Li et al. improved the microwave processability of CFRP using an additional tool modification in form of applied metal strips. These metal strips influence the microwave field distribution and increase the heat introduction into a CFRP's depth. Independent of new tooling technologies or novel control methods, manufacturing trials on more parts in parallel should be started soon. These trials can be used to identify challenges, compare the existing control strategies, and work out the industrialization process head-on.

Industrial Applications

The integration and optimization of current research results is key with regard to timely industrial application. For the Hephaistos system three developments are identified. First, an automation for the random change of magnetrons and use of as many magnetrons as possible during processing can be implemented through software updates in the current equipment. Second, Mode-Stirrers can be implemented by default in future microwaves and older equipment can be upgraded manually. Last, on mid to long term, the adaptive model predictive control (MPC) method described in Yiming Sun's thesis can be implemented for industrial applications.

Concerning microwave processing, two possible industrial near term goals can be followed. First, a follow-up on the microwave cure of thick filament wound composite parts looks very promising. Very good results have been achieved within the first research project [18], [69]. Since filament wound parts have a rotational symmetry and are rotated during the process, the influence of the complex microwave system is drastically reduced. Further optimizations like microwave optimized tools and flexible microwave compatible mounts would put the finishing touches on this process. Second, absorber dominated preforming is seen as near term goal. First feasibility trials for microwave binder activation using a flat GFRP tool, a 3 mm GFRP preform, and the Kraiburg microwave absorber showed very promising results: heat-up rates of $>20\,^{\circ\mathrm{C}}/_{\mathrm{min}}$ and an acceptable temperature homogeneity were reached within only two trials. Since the requirements on the temperature spread during preforming are less strict than for the curing process, simple absorber based tools can be realizable with small development effort. Through combination of such

absorber based tools and a conveyor belt equipped microwave [18], a high volume preforming process can most certainly be established.

Microwave Visions

Apart from these foreseeable developments in microwave processing, long term visions must focus on the consequent utilization of the direct microwave material interaction. This—more than anything else—contributes to one of the core benefits of microwave-heating: its high energy efficiency. As was seen in section 4.3.4 the overall efficiency in a microwave heating process can vary strongly. The range of physical conversion efficiency stretches from below 10% to more than 70% for a generic application. This possible ratio between the electric energy used and the heat generated inside a part is huge. However, the very high efficiency possible is currently limited by very basic hurdles like the processing of several parts in parallel that require adequate tools. Setting the energy efficiency aside, the long term vision of direct microwave material interaction has substantial practical uses and potentials. To name only two examples, the direct interaction has no set temperature limit and different materials show different heat-up characteristics. Microwave heating could consequently be used for very high temperature applications (>400 °C). Through the same principle, two matrix systems having different cure temperatures could be combined in one part and cured according to their needs using complex tools.

At the end, flexible microwave heating of composites must be seen as challenging emerging technology with huge potentials to be tapped in many directions.

Bibliography

[1] European Environment Agency. (2017). Trends and projections in Europe 2017: 2. Progress of the European Union towards its greenhouse gas emissions targets. European Environment Agency, Ed., [Online]. Available: https://www.eea.europa.eu/ds_resolveuid/c5040baff39745dfa834767388f9ed58 (visited on 10/23/2018) (cit. on p. 1).

[2] Eurocontrol. (2018). European Aviation in 2040: Challenges of Growth. Eurocontrol, Ed., [Online]. Available: https://www.eurocontrol.int/sites/default/files/content/documents/official-documents/reports/challenges-of-growth-2018.pdf (visited on 10/23/2018) (cit. on p. 1).

[3] Airbus. (2018). Global Market Forecast 2018-2037: Global Networks, Global Citizens. AIRBUS S.A.S., Ed., [Online]. Available: https://www.airbus.com/content/dam/corporate-topics/publications/media-day/GMF-2018-2037.pdf (visited on 10/23/2018) (cit. on p. 1).

[4] Boeing. (2018). Commercial Market Outlook 2018-2037. Boeing, Ed., [Online]. Available: https://www.boeing.com/resources/boeingdotcom/commercial/market/commercial-market-outlook/assets/downloads/2018-cmo-09-11.pdf (visited on 10/23/2018) (cit. on p. 1).

[5] A. Casadei and R. Broda, *Impact of Vehicle Weight Reduction on Fuel Economy for Various Vehicle Architectures: Research Report Conducted by Ricardo Inc. for The Aluminum Association, Project FB769 RD.07/71602.2*, Ricardo Inc., Ed., 2008 (cit. on p. 1).

[6] N. P. Lutsey, *Review of technical literature and trends related to automobile mass-reduction technology*, UC Davis: Institute of Transportation Studies, Davis, May 1, 2010. [Online]. Available: https://escholarship.org/uc/item/9t04t94w (cit. on p. 1).

[7] D. I. A. Poll, "On the application of light weight materials to improve aircraft fuel burn – reduce weight or improve aerodynamic efficiency?" *The Aeronautical Journal (1968)*, vol. 118, no. 1206, pp. 903–934, 2014 (cit. on p. 1).

[8] Glasfaser-Flugzeug-Service GmbH. (2008). History der Firma Glasflügel Segelflugzeugbau GmbH, [Online]. Available: http://www.streifly.de/glasfluegel-d.htm (visited on 10/24/2018) (cit. on p. 1).

[9] V. Mathes, "The composites industry: Plenty of opportunities in heterogeneous market," *Reinforced Plastics*, vol. 62, no. 1, pp. 44–51, 2018 (cit. on pp. 1, 141).

[10] L. Nele, A. Caggiano, and R. Teti, "Autoclave Cycle Optimization for High Performance Composite Parts Manufacturing," *Procedia CIRP*, vol. 57, pp. 241–246, 2016 (cit. on p. 2).

[11] A. Hemmen, "Direktbestromung von Kohlenstofffasern zur Minimierung von Zykluszeit und Energieaufwand bei der Herstellung von Karbonbauteilen," Dissertation, Universität Augsburg, Augsburg, 2016 (cit. on p. 2).

[12] A. Dong, Y. Zhao, X. Zhao, and Q. Yu, "Cure Cycle Optimization of Rapidly Cured Out-Of-Autoclave Composites," *Materials*, vol. 11, no. 3, 2018 (cit. on p. 2).

[13] D. Grauer and S. Perner, "Fast-curing epoxy prepreg system for automated processes with short cycle times," *JEC Composites Magazine*, vol. 2019, no. 131, pp. 38–40, 2019 (cit. on p. 2).

[14] L. Feher, K. Drechsler, J. Filsinger, and F. Karl, "Development of the modular 2.45 GHz HEPHAISTOS-CA2 Microwave Processing System for Automated Composite Fabrication," in *SAMPE EUROPE International Conference Paris*, 2005, pp. 328–338 (cit. on pp. 2, 4).

[15] Matthias Meyer, "Herstellung von kohlenstofffaserverstärkten Kunststoffbauteilen mit Hilfe von Mikrowellen," Dissertation, Technische Universität Carolo-Wilhelmina zu Braunschweig, Köln, 2007 (cit. on pp. 2, 12, 18, 19, 26, 35, 46, 121).

[16] F. Gaille, "Manufacturing process development for composite materials using microwave technology," Dissertation, Universität Stuttgart, Stuttgart, 2012 (cit. on pp. 2, 4, 20, 21, 23, 26, 35, 37, 39, 121).

[17] M. Kwak, "Microwave Curing of Carbon-Epoxy Composites: Process Development and Material Evaluation," PhD thesis, Imperial College London, London, 2016 (cit. on pp. 2, 4, 20, 21, 35, 121).

[18] G. Link, T. Kayser, F. Köster, R. Weiß, S. Betz, R. Wiesehöfer, T. Sames, N. Boulkertous, D. Teufl, S. Zaremba, F. Heidbrink, M. Maus, R. Ghomeshi, S. Küppers, and M. Milwich, *Faserverbund-Leichtbau mit Automatisierter Mikrowellenprozesstechnik hoher Energieeffizienz (FLAME): Schlussbericht*

des BMBF-Verbundprojektes (KIT Scientific Reports ; 7701), ser. KIT scientific reports. Karlsruhe: KIT Scientific Publishing, 2015, vol. 7701, ISBN: 9783731503965 (cit. on pp. 2, 4, 20, 21, 35, 40, 121, 127, 128).

[19] G. Link, *Innovative, modulare Mikrowellentechnologie zur Herstellung von Faserverbundstrukturen: Schlussbericht für das BMBF-Verbundprojekt*, Technische Informationsbibliothek u. Universitätsbibliothek, Ed., Eggenstein-Leopoldshafen, 2011 (cit. on pp. 2, 4, 11, 12, 20, 39, 46, 146, 148).

[20] Thomas Mathias Herkner, "METHOD AND MOLD FOR THE PRODUCTION OF PARTS FROM FIBER-REINFORCED COMPOSITE MATERIAL BY MEANS OF MICROWAVES," EP 2 293 924 B1, 2011 (cit. on pp. 2, 5, 39).

[21] Thomas Herkner, *Microwave curing of composites: The 25th annual international SICOMP conference*, Pitea Sweden, Jun. 3, 2014 (cit. on pp. 2, 5, 20, 38, 39, 125).

[22] ——, *News from the Aviation Industry: Presentation, 3rd Microwave Symposium*, Karlsruhe, Oct. 14, 2015 (cit. on pp. 2, 5, 20, 38, 39, 125, 126).

[23] M. Gude, K. Demnitz, M. Müller, M. Stegelmann, G. Meschut, M. Gerkens, J. Göddecke, D. Han, M. F. Zäh, A. Hofer, A. Schönmann, S. Schreiber, H. Lieberwirth, T. Krampitz, A. Tekkaya, M. Hahn, and S. Gies, *FOREL-Studie 2018: Ressourceneffizienter Leichtbau für die Mobilität (Wandel-Prognose-Transfer)*. Dresden: Plattform FOREL, 2018, ISBN: 978-3-86780-559-9 (cit. on pp. 2, 121).

[24] Department of Defense, Ed. (2011). Technology Readiness Assessment (TRA) Guidance, [Online]. Available: www.acq.osd.mil/ecp/DOCS/DoDGuidance/TRA2011.pdf (visited on 11/05/2018) (cit. on p. 3).

[25] V. Jamier, B. Irvine, and C. Aucher. (2018). Demystifying TRLs for Complex Technologies. Leitat Managing Technologies, Ed., [Online]. Available: https://projects.leitat.org/demystifying-trls-for-complex-technologies/ (visited on 10/24/2018) (cit. on pp. 3, 5, 125).

[26] L. E. Feher and M. Thumm, "Industrial higher frequency microwave processing of composite materials," in *Advances in Microwave and Radio Frequency Processing: Report from the 8th International Conference on Microwave and High Frequency Heating held in Bayreuth, Germany, September 3–7, 2001*, M. Willert-Porada, Ed., Springer, 2001, pp. 681–686, ISBN: 3-540-43252-3. [Online]. Available: http://www.springerlink.com/content/l8813k622w031260/ (cit. on p. 4).

[27] L. Feher and M. Thumm, "Microwave Innovation for Industrial Composite Fabrication—The HEPHAISTOS Technology," *IEEE TRANSACTIONS ON PLASMA SCIENCE*, vol. 32, no. 1, pp. 73–79, 2004 (cit. on pp. 4, 21, 65).

[28] Giovanni Antonio Marengo and Thomas Mathias Herkner, "MANUFACTURING METHOD FOR COMPONENTS MADE OF FIBER-REINFORCED COMPOSITE MATERIALS USING MICROWAVES," EP 2 303 553 B1, 2012 (cit. on p. 5).

[29] R. J. Meredith, *Engineers' handbook of industrial microwave heating*, ser. IEE power series. London: Institution of Electrical Engineers, 1998, vol. 25, ISBN: 0852969163 (cit. on pp. 9–12, 14, 36, 143, 146–149).

[30] A. C. Metaxas and R. J. Meredith, *Industrial microwave heating*, ser. IEE power engineering series. London: Peter Peregrinus, 1993, vol. 4, ISBN: 0906048893 (cit. on pp. 9, 11, 14, 143).

[31] E. T. Thostenson and T.-W. Chou, "Microwave processing: Fundamentals and applications," *Composites Part A: Applied Science and Manufacturing*, vol. 30, no. 9, pp. 1055–1071, 1999 (cit. on pp. 10, 12).

[32] Ian Dunster. (2005). Resonant_Cavity_Magnetron_Diagram.png, [Online]. Available: https://en.wikipedia.org/wiki/File:Resonant_Cavity_Magnetron_Diagram.svg (visited on 08/13/2017) (cit. on p. 13).

[33] G. Link and V. Ramopoulos, "Simple analytical approach for industrial microwave applicator design," *Chemical Engineering and Processing - Process Intensification*, vol. 125, pp. 334–342, 2018 (cit. on p. 15).

[34] M. Wallace, D. Attwood, R. J. Day, and F. Heatley, "Investigation of the microwave curing of the PR500 epoxy resin system," *Journal of Materials Science*, vol. 41, no. 18, pp. 5862–5869, 2006 (cit. on pp. 16, 22, 108).

[35] V. Tanrattanakul and D. Jaroendee, "Comparison between microwave and thermal curing of glass fiber–epoxy composites: Effect of microwave-heating cycle on mechanical properties," *Journal of Applied Polymer Science*, vol. 102, no. 2, pp. 1059–1070, 2006 (cit. on pp. 16, 28, 36).

[36] F. Y. C. Boey and W. L. Lee, "Microwave radiation curing of a thermosetting composite," *Journal of Materials Science Letters*, vol. 9, no. 10, pp. 1172–1173, 1990 (cit. on pp. 16, 22).

[37] C. Nightingale, "Microwave assisted curing of epoxy resins and composites," PhD thesis, Manchester, University of Manchester, 2000 (cit. on pp. 16, 23).

[38] C. Nightingale and R. Day, "Flexural and interlaminar shear strength properties of carbon fibre/epoxy composites cured thermally and with microwave radiation," *Composites Part A: Applied Science and Manufacturing*, vol. 33, no. 7, pp. 1021–1030, 2002 (cit. on pp. 16, 25, 36).

[39] V. Tanrattanakul and K. SaeTiaw, "Comparison of microwave and thermal cure of epoxy-anhydride resins: Mechanical properties and dynamic characteristics," *Journal of Applied Polymer Science*, vol. 97, no. 4, pp. 1442–1461, 2005 (cit. on pp. 16, 24, 36, 108).

[40] F. Y. Boey and T. H. Lee, "Electromagnetic radiation curing of an epoxy/fibre glass reinforced composite," *International Journal of Radiation Applications and Instrumentation. Part C. Radiation Physics and Chemistry*, vol. 38, no. 4, pp. 419–423, 1991 (cit. on pp. 17, 28).

[41] F. Y. Boey and C. Y. Yue, "Interfacial strength of a microwave-cured epoxy-glass composite," *Journal of Materials Science Letters*, vol. 10, no. 22, pp. 1333–1334, 1991 (cit. on pp. 17, 24).

[42] C. Y. Yue and H. C. Looi, "Influence of thermal and microwave processing on the mechanical and interfacial properties of a glass/epoxy composite," *Composites*, vol. 26, no. 11, pp. 767–773, 1995 (cit. on pp. 17, 25).

[43] S. L. Bai, V. Djafari, M. Andréani, and D. François, "A comparative study of the mechanical behaviour of an epoxy resin cured by microwaves with one cured thermally," *European Polymer Journal*, vol. 31, no. 9, pp. 875–884, 1995 (cit. on p. 17).

[44] S. L. Bai and V. Djafari, "Interfacial properties of microwave cured composites," *Composites*, vol. 26, no. 9, pp. 645–651, 1995 (cit. on pp. 17, 24).

[45] F. Boey, B. H. Yap, and L. Chia, "Microwave curing of epoxy-amine system — effect of curing agent on the rate enhancement," *Polymer Testing*, vol. 18, no. 2, pp. 93–109, 1999 (cit. on p. 17).

[46] F. Boey and B. Yap, "Microwave curing of an epoxy–amine system: Effect of curing agent on the glass-transition temperature," *Polymer Testing*, vol. 20, no. 8, pp. 837–845, 2001 (cit. on pp. 17, 22).

[47] R. M. V. G. K. Rao, S. Rao, and B. K. Sridhara, "Studies on Tensile and Interlaminar Shear Strength Properties of Thermally Cured and Microwave Cured Glass–Epoxy Composites," *Journal of Reinforced Plastics and Composites*, vol. 25, no. 7, pp. 783–795, 2006 (cit. on pp. 17, 22, 25, 36).

[48] P. S. Mooteri, B. K. Sridhara, S. Rao, M. R. Prakash, and R. M. V. G. K. Rao, "Studies on Mechanical Behavior of Microwave and Thermally Cured Glass Fiber Reinforced Polymer Composites," *Journal of Reinforced Plastics and Composites*, vol. 25, no. 5, pp. 503–512, 2006 (cit. on pp. 17, 22, 28, 36).

[49] R. Yusoff, "Microwave assisted RTM processing of carbon/epoxy composites," PhD thesis, University of Manchester, Manchester, 2004 (cit. on pp. 18, 36).

[50] D. A. Papargyris, R. J. Day, A. Nesbitt, and D. Bakavos, "Comparison of the mechanical and physical properties of a carbon fibre epoxy composite manufactured by resin transfer moulding using conventional and microwave heating," *Composites Science and Technology*, vol. 68, no. 7-8, pp. 1854–1861, 2008 (cit. on pp. 18, 23, 26, 29, 37).

[51] C. Guan, L. Zhan, G. Liu, X. Yang, G. Dai, C. Jiang, and X. Chen, "Optimization of a high-pressure microwave curing process for T800/X850 carbon fiber-reinforced plastic," *High Performance Polymers*, vol. 32, no. 1, pp. 30–38, 2020 (cit. on pp. 18, 23, 25, 121).

[52] E. T. Thostenson and T.-W. Chou, "Microwave and conventional curing of thick-section thermoset composite laminates: Experiment and simulation," *Polymer Composites*, vol. 22, no. 2, pp. 197–212, 2001 (cit. on pp. 18, 19, 36).

[53] M. Danilov, "Energieeffiziente Mikrowellentemperierung von kohlenstofffaserverstärkten Duroplasten," Dissertation, Technische Universität Carolo-Wilhelmina zu Braunschweig, Köln, 2013 (cit. on pp. 18, 19).

[54] DLR. (2015). Picture - Fricke & Mallah Microwave Oven. Deutsches Zentrum für Luft- und Raumfahrt e. V., Ed., [Online]. Available: https://www.dlr.de/fa/Portaldata/17/Resources/images/leistungsprofil/induction___microwave_heating/Fricke_Mallah_Microwave_Oven.jpg (visited on 05/05/2020) (cit. on pp. 18, 19).

[55] X. Xu, X. Wang, W. Liu, X. Zhang, Z. Li, and S. Du, "Microwave curing of carbon fiber/bismaleimide composite laminates: Material characterization and hot pressing pretreatment," *Materials & Design*, vol. 97, pp. 316–323, 2016 (cit. on pp. 19, 36).

[56] X. Xu, X. Wang, Q. Cai, X. Wang, R. Wei, and S. Du, "Improvement of the Compressive Strength of Carbon Fiber/Epoxy Composites via Microwave Curing," *Journal of Materials Science & Technology*, vol. 32, no. 3, pp. 226–232, 2016 (cit. on pp. 19, 36).

[57] X. Xu, X. Wang, R. Wei, and S. Du, "Effect of microwave curing process on the flexural strength and interlaminar shear strength of carbon fiber/bismaleimide composites," *Composites Science and Technology*, vol. 123, pp. 10–16, 2016 (cit. on pp. 19, 36).

[58] N. Li, Y. Li, X. Hang, and J. Gao, "Analysis and optimization of temperature distribution in carbon fiber reinforced composite materials during microwave curing process," *Journal of Materials Processing Technology*, vol. 214, no. 3, pp. 544–550, 2014 (cit. on pp. 19, 36).

[59] Y. Li, N. Li, and J. Gao, "Tooling design and microwave curing technologies for the manufacturing of fiber-reinforced polymer composites in aerospace applications," *The International Journal of Advanced Manufacturing Technology*, vol. 70, no. 1-4, pp. 591–606, 2014 (cit. on p. 19).

[60] M. Meyer, B. Binder, and M. Graeber, "Mikrowellenautoklav," DE 102005050528 A1, 2007 (cit. on p. 19).

[61] T. Stroehlein, M. Podkorytov, M. Meyer, L. Herbeck, M. Frauenhofer, K. Dilger, and S. Boehm, "Composite Technologies for Future Demands," in *The use of composites in the 21st century to save energy and weight*, M. A. Erath, Ed., SAMPE Europe Conferences, 2007, pp. 481–486, ISBN: 978-3-9522677-5-2 (cit. on p. 20).

[62] L. Herbeck, M. Podkorytov, and T. Stroehlein, "Process Acceleration by Selective and Volumetric Heat Transfer Methods," May 18 - 22, 2008, Long Beach, California, in *SAMPE '08 : material and process innovations: changing our world*, D. Fullwood, Ed., vol. 52, SAMPE, 2008, ISBN: 978-1-934551-03-5 (cit. on p. 20).

[63] M. Wiedman, *CFK – Status der Anwendung und Produktionstechnik im Flugzeugbau: DLR Zentrum für Leichtbauproduktionstechnologie*, Braunschweig, Mar. 26, 2009. [Online]. Available: https://elib.dlr.de/61319/ (cit. on p. 20).

[64] S. Maenz, M. Mühlstädt, K. D. Jandt, and J. Bossert, "Mechanical properties of microwave cured glass fibre epoxy composites prepared by resin transfer moulding," *Journal of Composite Materials*, vol. 49, no. 23, pp. 2839–2847, 2014 (cit. on pp. 20, 21, 29, 36).

[65] N. Li, Y. Li, X. Hao, and J. Gao, "A comparative experiment for the analysis of microwave and thermal process induced strains of carbon fiber/bismaleimide composite materials," *Composites Science and Technology*, vol. 106, pp. 15–19, 2015 (cit. on pp. 20, 21, 36).

[66] M. Kazilas, *Novel Technologies for Composites: Presentation, 3rd Microwave Symposium*, Karlsruhe, Oct. 14, 2015 (cit. on pp. 20, 37).

[67] D. Teufl, *Composite Tooling for Micorwave Processes: Presentation, 3rd Microwave Symposium*, Karlsruhe, Oct. 14, 2015 (cit. on p. 20).

[68] M. Moret. (2015). Final Report Summary - MU-TOOL (Novel tooling for composites curing under microwave heating): Project reference: 286717; Funded under: FP7-SME. European Unition, Ed., [Online]. Available: http://cordis.europa.eu/result/rcn/158268_en.html (visited on 09/07/2015) (cit. on pp. 20, 37, 40, 146).

[69] S. Betz and F. Köster, *Energy and Time Efficient Microwave Curing for CFRP Parts Manufactured by Filament Winding: Presentation, 3rd Microwave Symposium*, Karlsruhe, Oct. 14, 2015 (cit. on pp. 20, 35, 46, 127).

[70] D. Teufl and S. Zaremba, "2.45 GHz Microwave Processing and Its Influence on Glass Fiber Reinforced Plastics," *Materials*, vol. 11, no. 5, p. 838, 2018 (cit. on pp. 20, 105).

[71] F. Gaille, H. Ringwald, and K. Drechsler, "New Composite Manufacturing Process with Microwave Technology," in *Composites - innovative materials for smarter solutions*, M. A. Erath, Ed., SAMPE Europe Conferences, 2009, pp. 403–411, ISBN: 978-3-9522677-9-0 (cit. on pp. 20, 35, 39).

[72] M. Kwak, P. Robinson, A. Bismarck, and R. Wise, "Curing of Composite Materials Using the Recently Developed HEPHAISTOS Microwave," in *ICCM 18 Conference Proceedings*, International Committee on Composite Materials, Ed., ser. International Conference on Composite Materials, ICCM, 2011. [Online]. Available: http://www.iccm-central.org/Proceedings/ICCM18proceedings/data/2.%20Oral%20Presentation/Aug23%28Tuesday%29/T11%20Processing%20and%20Manufacturing%20Technologies/T11-2-IF1073.pdf (cit. on pp. 20, 21, 23, 46).

[73] M. Beaumont and J. Filsinger, "Potential of Microwave Heating for Out-of-Autoclave Compositer Manufacturing of Aerospace Structures," in *SAMPE 2011 Technical Conference Proceedings: State of the Industry: Advanced Materials, Applications, and Processing Technology*, Society for the Advancement of Material and Process Engineering, Ed., ser. CD-ROM, Society for the Advancement of Material and Process Engineering, 2011, ISBN: 978-1-934551-11-0 (cit. on pp. 20, 35).

[74] M. Kwak, P. Robinson, A. Bismarck, and R. Wise, "Microwave curing of carbon–epoxy composites: Penetration depth and material characterisation," *Composites Part A: Applied Science and Manufacturing*, vol. 75, pp. 18–27, 2015 (cit. on pp. 20, 27, 35).

[75] A. Flach, L. Feher, V. Nuss, and T. Seitz, “Mikrowellenresonator, eine aus einem solchen Mikrowellenresonator modular aufgebaute Prozessstrasse, ein Verfahren zum Betreiben und nach diesem Verfahren thermisch prozessierte Gegenstände/Werkstücke mittels Mikrowelle,” EPN 1639865, 2007 (cit. on p. 21).

[76] L. E. Feher, *Energy Efficient Microwave Systems*. Berlin, Heidelberg: Springer Berlin Heidelberg, 2009, ISBN: 978-3-540-92121-9 (cit. on pp. 21, 65).

[77] J. Zhou, Y. Li, N. Li, X. Hao, and C. Liu, “Interfacial shear strength of microwave processed carbon fiber/epoxy composites characterized by an improved fiber-bundle pull-out test,” *Composites Science and Technology*, vol. 133, pp. 173–183, 2016 (cit. on pp. 21, 27, 36, 46).

[78] N. Li, Y. Li, J. Jelonnek, G. Link, and J. Gao, “A new process control method for microwave curing of carbon fibre reinforced composites in aerospace applications,” *Composites Part B: Engineering*, vol. 122, pp. 61–70, 2017 (cit. on pp. 21, 36).

[79] F. Colangelo, P. Russo, F. Cimino, R. Cioffi, I. Farina, F. Fraternali, and L. Feo, “Epoxy/glass fibres composites for civil applications: Comparison between thermal and microwave crosslinking routes,” *Composites Part B: Engineering*, vol. 126, pp. 100–107, 2017 (cit. on p. 23).

[80] R. K. Agrawal and L. T. Drzal, “Effects of Microwave Processing on Fiber-matrix Adhesion in Composites,” *The Journal of Adhesion*, vol. 29, no. 1-4, pp. 63–79, 1989 (cit. on pp. 24, 27).

[81] J. Zhou, C. Shi, B. Mei, R. Yuan, and Z. Fu, “Research on the technology and the mechanical properties of the microwave processing of polymer,” *Journal of Materials Processing Technology*, vol. 137, no. 1-3, pp. 156–158, 2003 (cit. on p. 28).

[82] D. Teufl, S. Zaremba, and K. Drechsler, “Evaluation of tooling concepts for the use in microwave processing of fiber reinforced plastics,” in *Efficient composite solutions to foster economic growth*, SAMPE EUROPE Conference, Ed., SAMPE EUROPE Business Office, 2014, pp. 63–71, ISBN: 978-90-821727-1-3 (cit. on p. 30).

[83] B. Nuhiji, T. Swait, M. P. Bower, J. E. Green, R. J. Day, and R. J. Scaife, “Tooling materials compatible with carbon fibre composites in a microwave environment,” *Composites Part B: Engineering*, vol. 2019, no. 163, pp. 769–778, 2019 (cit. on pp. 36–38).

[84] R. A. Witik, F. Gaille, R. Teuscher, H. Ringwald, V. Michaud, and J.-A. E. Månson, "Economic and environmental assessment of alternative production methods for composite aircraft components," *Journal of Cleaner Production*, vol. 29-30, pp. 91–102, 2012 (cit. on p. 39).

[85] D. Teufl, V. Ramopoulos, S. Zaremba, and K. Drechsler, "Adjustment of 2.45 GHz Microwave Absorbing Heating Laysers for Tooling Applications: Extended Abstract," in *Proceedings PPS 2015*, AIP Publishing LLC, Ed., Sep. 2015 (cit. on p. 40).

[86] Orion Engineered Carbons, *Carbon Black Pigments for Conductive Coatings: Technnical Information 1455*, Orion Engineered Carbons, Ed., Frankfurt am Main, 2013 (cit. on pp. 44, 142).

[87] J. Zhou, Y. Li, L. Cheng, and L. Zhang, "Indirect Microwave Curing Process Design for Manufacturing Thick Multidirectional Carbon Fiber Reinforced Thermoset Composite Materials," *Applied Composite Materials*, vol. 24, no. 6, p. 1265, 2018 (cit. on p. 46).

[88] Y. Li, N. Li, J. Zhou, and Q. Cheng, "Microwave curing of multidirectional carbon fiber reinforced polymer composites," *Composite Structures*, vol. 212, pp. 83–93, 2019 (cit. on pp. 46, 127).

[89] L. Mahlau, "Untersuchung und Anpassung der GFK-Prüfkörperfertigung zur Qualitätssicherung der Mikrowellenaushärtung," bachelor's thesis, Technical University of Munich, München, 2015 (cit. on p. 47).

[90] N. Weiner, "Development of a production process for absorber layers in fiber composite tools," bachelor's thesis, Technical University of Munich, München, 2017 (cit. on p. 50).

[91] L. Ametsbichler, "Homogenisierung von Industrieruß in Epoxidharz zur Herstellung von Mikorwellensuszeptoren," term project, Technical University of Munich, München, Nov. 4, 2016 (cit. on p. 53).

[92] V. Ramopoulos, S. Soldatov, G. Link, T. Kayser, M. Gehringer, and J. Jelonnek, "Microwave system for in-situ dielectric and calorimetric measurements in a wide temperature range using a TE111-mode cavity," in *2015 IEEE MTT-S International Microwave Symposium*, IEEE, 2015, pp. 1–4, ISBN: 978-1-4799-8275-2 (cit. on pp. 56, 58).

[93] "Microwave cavity perturbation technique for high-temperature dielectric measurements," in *IEEE International Wireless Symposium (IWS), 2013: 14 - 18 April 2013, Beijing, China*, Piscataway, NJ: IEEE, 2013, ISBN: 978-1-4673-2141-9 (cit. on p. 56).

[94] V. Ramopoulos, S. Soldatov, G. Link, T. Kayser, and J. Jelonnek, "System for in-situ Dielectric and Calorimetric Measurements During Microwave Curing of Resins," in *2015 German Microwave Conference*, IEEE, 2015, pp. 29–32, ISBN: 978-3-9812668-6-3 (cit. on p. 56).

[95] Michael Oberrauch, "Auswahl und Bewertung eines Prüfverfahrens zur Ermittlung des Aushärteeinflusses auf ein spezifisches Glasfaserlaminat," bachelor's thesis, Technical University of Munich, München, 2016 (cit. on p. 60).

[96] CEN, *DIN EN ISO 14130: Fibre-reniforced plastic composites - Determination of apparent interlaminar shear strength by short-beam method*, Berlin, 1997 (cit. on p. 61).

[97] ——, *DIN EN ISO 14125:Fibre-reinforced plastic composites – Determination of flexural properties*, Berlin, May 2011 (cit. on pp. 62, 63).

[98] A. Buck, "Energieeffizienzbewertung einer industriellen Mikrowellenanlage," bachelor's thesis, Technical University of Munich, München, 2015 (cit. on pp. 65, 85).

[99] Umetrics AB, *MODDE Version 10.1.1.1193 user manual*, 2014 (cit. on p. 71).

[100] Sartorius Stedim Data Analytics AB, *MODDE Pro Version 12.0.1.3948 user manual*, 2017 (cit. on pp. 71, 141).

[101] E. Marand, K. R. Baker, and J. D. Graybeal, "Comparison of reaction mechanisms of epoxy resins undergoing thermal and microwave cure from in situ measurements of microwave dielectric properties and infrared spectroscopy," *Macromolecules*, vol. 25, no. 8, pp. 2243–2252, 1992 (cit. on p. 107).

[102] J. Wei, M. C. Hawley, and M. T. Demeuse, "Kinetics modeling and time-temperature-transformation diagram of microwave and thermal cure of epoxy resins," *Polymer Engineering and Science*, vol. 35, no. 6, pp. 461–470, 1995 (cit. on p. 107).

[103] Y. Sun, "Adaptive and Intelligent Temperature Control of Microwave Heating Systems with Multiple Sources," Dissertation, Karlsruher Institut für Technologie, Karlsruhe, 2016 (cit. on pp. 125, 127).

[104] J. Zhou, Y. Li, N. Li, S. Liu, L. Cheng, S. Sui, and J. Gao, "A multi-pattern compensation method to ensure even temperature in composite materials during microwave curing process," *Composites Part A: Applied Science and Manufacturing*, vol. 107, pp. 10–20, 2018 (cit. on pp. 125, 127).

[105] Di Li, Y. Li, J. Zhou, and Z. Zhao, "A Novel Method to Improve Temperature Uniformity in Polymer Composites Microwave Curing Process through Deep Learning with Historical Data," *Applied Composite Materials*, pp. 1–17, 2019 (cit. on pp. 125, 127).

[106] P. K. D. V. Yarlagadda and T. C. Chai, "An investigation into welding of engineering thermoplastics using focused microwave energy," *Journal of Materials Processing Technology*, vol. 74, no. 1–3, pp. 199–212, 1998 (cit. on pp. 146, 147).

[107] Bob LaPointe. (2001). Electrical Properties of Plastics, [Online]. Available: http://members.tm.net/lapointe/Plastics.htm (visited on 10/22/2018) (cit. on pp. 146–148).

[108] S. Osaki, "Microwave frequency dielectric properties of poly(vinylidene fluoride) films," *Journal of Polymer Science Part B: Polymer Physics*, vol. 33, no. 4, pp. 685–690, 1995 (cit. on p. 148).

[109] L. Chen, Y. Duan, L. Liu, J. Guo, and S. Liu, "Influence of SiO2 fillers on microwave absorption properties of carbonyl iron/carbon black double-layer coatings," *Materials & Design*, vol. 32, no. 2, pp. 570–574, 2011 (cit. on p. 149).

Glossary

4-point bending is the test method according to DIN EN ISO 14125 that is used to determine the flexural properties in either th 0° (A) or 90° (B) direction xix, 7, 59, 62, 103, 105, 112, 116, 121, 122

Cohen's d gives an inidication of the effect strength of a statistically significant difference. A value above 1 is seen as indication of a large effect in this thesis. 103, 104, 108, 112

complex relative permittivity complex representation of the relative permittivity: $\varepsilon_r^* = \varepsilon_r' - j\varepsilon_r''$. See also ε_r' and ε_r'' 10, 140, 141

deleted-studentized-residuals is the raw residual; the difference between observed and predicted values, divided by an estimate of its standard deviation.[100] 74

design of experiments describes the use of statistical methods to minimize the testing necessary to determine the influence of factors and to evaluate the data xix, xxiv, 67, 88, 93

dissipation factor measurement for the loss-rate described by $\tan(\delta) = \frac{\varepsilon_r''}{\varepsilon_r'}$. 11, 89, 93

glass fiber reinforced thermosetting plastic material with thermosetting matrix and glass fiber reinforcement in the context of [9]. "This group also covers materials with a thermoplastic matrix and with either long or continuous fiber reinforcement" xx, 1

grindometer Gage to detect agglomerates in a fluid. One or two sloped grooves, from the surface to a certain depth, are worked into a steel block. The depth of the groove is continously marked. The grindometer is used in three steps: First, a dropplet of the fluid is put in the deep end of the groove. Second, a scraper is used to distribute the fluid inside the groove. The scraper pulls agglomerates with it. As soon as the agglomerates are bigger than the groove's depth, a scratch is visible. Third, after scraping, the groove is investigated and the agglomerate size can be determined by the scratch position. 54

industrial, scientific and medical bands are radio frequencies reserved for public use. The restriction of other non ISM frequencies is done to prevent interferences with critical equipment working at these frequencies. xx, 18

inter-laminar shear strength is the (apparent) shear strength tested according to DIN EN ISO 14130 τ_{ILSS} or a comparable test in either 0° (A) or 90° (B) direction ix, 7, 25, 59, 61, 103, 108, 116, 121, 122

life datasheet are used to control process compliance against set standard procedures. xx, 53

loss factor is used in short for the imaginary part of the complex relative permittivity (ε_r^*) in this thesis 10, 11, 89, 93, 94, 96, 98, 121

master-batch is used as a interstage product during absorber production that has a higher and constant carbon black-content than the final absorber mixture. It thus can be produced in a repeatable way. xx, xxiii, 50–53, 88, 90, 92, 93

MW_120 is the microwave cure cycle that ends after a 45 min dwell time at 122.5 °C 49, 50, 105, 106, 109–111, 114–117

MW_140 is the microwave cure cycle that ends after a 60 min dwell time at 122.5 °C and 30 min dwell time at 142.5 °C 49, 50, 105, 106, 109–111, 114, 115, 117

MW_dyn is the microwave cure cycle that follows a steady temperature rise up to 170 °C and has a 170 °C dwell time of 20 min 49, 50, 105, 106, 110–112, 114, 115, 117

non-crimp-fabric is a fabric that is made of rovings placed parallel to each other that are fixated in some way. The non-crimp-fabric (NCF) can be made up of several layers xx, 43, 140, 148

O_120 is the oven cure cycle that ends after a 60 min dwell time at 120 °C 47, 49, 50, 105, 106, 109, 111–113, 115

O_140 is the oven cure cycle that ends after a 75 min dwell time at 120 °C and 45 min dwell time at 140 °C 49, 50, 105, 106, 109, 111, 113, 115

O_dyn is the oven cure cycle that follows a steady temperature rise up to 170 °C and has a 170 °C dwell time of 35 min 49, 50, 106, 109, 111, 113, 115, 117

oil absorption number is a measurand for the structure or degree of branching of a carbon black[86]. xx, 44

penetration depth is defined as the depth into a material at which the power flux has fallen to e^{-1} of its surface value [29], [30]. xxvii, 10, 11, 30, 31, 33, 34, 40

permittivity is used in short for the real part of the complex relative permittivity (ε_r^*) in this thesis 10, 11, 89, 93, 94, 96, 98, 121

proportional integral derivative is a control loop feedback mechanism that can be configured over three control parameters. It is defined over its proportional (P), integral (I) and derivative (D) part. xx, 65, 120

reference cycle oven cure cycle used to obtain the mechanical and thermal properties of the resin stated in the datasheet having 3 h dwell time at 80 °C, 120 °C, and 140 °C xx, 48, 50, 105, 117

A Appendix

A.1 to Section 2

Tab. A-1 Literature values of dielectric properties for different materials.

Material	f [Hz]	T [°C]	ε_r'	ε_r''	$\tan(\delta)$	D_p [cm]	Year	Source
ABS	2.45E+09		3.24	0.0028	0.00090	1250	1996	Paper [106]
Al2O3	2.45E+09	25	8.9	0.009	0.00101	650	1998	Book [29]
70% Cordierite - 30% Ferrite	2.45E+09	44	6.03	0.42	0.06965	11.4	2015	Project Report [68]
70% Cordierite - 30% Ferrite	2.45E+09	80	6.15	0.59	0.09593	8.2	2015	Project Report [68]
70% Cordierite - 30% Ferrite	2.45E+09	145	6.32	0.98	0.15506	5.0	2015	Project Report [68]
DGEBA	2.45E+09	80	4.95812	1.622	0.32717	2.7	2011	Project Report [19]
DGEBA	2.45E+09	50	3.8251	1.165	0.30455	3.3	2011	Project Report [19]
DGEBA	2.45E+09	120	5.62296	1.101	0.19586	4.2	2011	Project Report [19]
DGEBA	2.45E+09	20	3.9897	0.712	0.17847	5.5	2011	Project Report [19]
DGEBA	2.45E+09	160	5.71827	0.550	0.09618	8.5	2011	Project Report [19]
DGEBA	2.45E+09	200	5.9001	0.419	0.07104	11.0	2011	Project Report [19]
EPDM, 57% silicious chalk	2.45E+09	100	3.1	0.05	0.01613	69	1998	Book [29]
ETFE	1.00E+09	25	2.4	0.0005	0.00021	14780	<2001	Private Homepage [107]
Ethyl alcohol	2.45E+09	25	7	6.5	0.92857	0.9	1998	Book [29]
GH754	2.45E+09		8.9	0.8	0.08989	7.3	2011	Project Report [19]
LDPE	1.00E+09	25	2.2	0.003	0.00136	2360	<2001	Private Homepage [107]

Literature values of dielectric properties for different materials. (Continuation)

Material	f [Hz]	T [°C]	ε_r'	ε_r''	tan (δ)	D_p [cm]	Year	Source
Methyl alcohol	2.45E+09	25	25	15	0.60000	0.7	1998	Book [29]
N-Butyl alcohol	2.45E+09	25	3.6	1.96	0.54444	1.9	1998	Book [29]
N-Propyl alcohol	2.45E+09	25	4.74	2.94	0.62025	1.5	1998	Book [29]
N-Propyl alcohol	2.45E+09	25	30	1	0.03333	11.0	1998	Book [29]
Nylon 66	2.45E+09	25	3.02	0.041	0.01358	83	1998	Book [29]
PC	1.00E+09	25	0.89	0.012	0.01348	380	<2001	Private Homepage [107]
PC	2.45E+09		3.005	0.0004	0.00001	8440	1996	Paper [106]
PC	9.00E+09	15	2.72	0.0034	0.00125	260	1998	Book [29]
PE	2.45E+09	25	2.25	0.0007	0.00031	4170	1998	Book [29]
PE	2.45E+09		2.146	-0.014	-0.00840	200	1996	Paper [106]
PET (high)	1.00E+09	25	2.8	0.005	0.00179	1600	<2001	Private Homepage [107]
PET (low)	1.00E+09	25	2.8	0.003	0.00107	2660	<2001	Private Homepage [107]
PI	1.00E+09	25	3.3	0.004	0.00121	2170	<2001	Private Homepage [107]
PMMA	1.00E+09	25	2.58	0.009	0.00349	850	<2001	Private Homepage [107]
PP	1.00E+09	25	2.2	0.0003	0.00014	23590	<2001	Private Homepage [107]

Literature values of dielectric properties for different materials. (Continuation)

Material	f [Hz]	T [°C]	ε_r'	ε_r''	tan (δ)	D_p [cm]	Year	Source
PS	1.00E+09	25	2.55	0.0005	0.00020	15240	<2001	Private Homepage [107]
PTFE	2.45E+09	25	2.06	0.0005	0.00024	5590	1998	Book [29]
PTFE	2.45E+09	25	2.06	0.00031	0.00015	9020	1998	Book [29]
PVC	1.00E+09	25	2.8	0.019	0.00679	420	<2001	Private Homepage [107]
PVC	2.45E+09	96	2.7	0.058	0.02148	55	1998	Book [29]
PVC	2.45E+09	76	2.7	0.036	0.01333	89	1998	Book [29]
PVC	2.45E+09	47	2.8	0.021	0.00750	155	1998	Book [29]
PVC	2.45E+09	20	2.85	0.016	0.00561	210	1998	Book [29]
PVDF	4.00E+09	25	3	0.15	0.05000	14.0	1995	Paper [108]
RTM6	2.45E+09	120	5.1	0.987	0.19353	4.5	2011	Project Report [19]
RTM6	2.45E+09	80	4.56	0.92	0.20175	4.5	2011	Project Report [19]
RTM6	2.45E+09	100	4.89	0.926	0.18937	4.7	2011	Project Report [19]
RTM6	2.45E+09	160	5.4	0.836	0.15481	5.4	2011	Project Report [19]
RTM6	2.45E+09	40	3.91	0.54	0.13811	7.1	2011	Project Report [19]
RTM6	2.45E+09	200	5.47	0.612	0.11188	7.5	2011	Project Report [19]
RTM6	2.45E+09	20	3.33	0.26	0.07808	14.0	2011	Project Report [19]
Rubber ,natural (pale crepe)	2.45E+09	25	2.2	0.006	0.00273	480	1998	Book [29]

Literature values of dielectric properties for different materials. (Continuation)

Material	f [Hz]	T [°C]	ε_r'	ε_r''	$\tan(\delta)$	D_p [cm]	Year	Source
Rubber, neoprene compound, 0.4% carbon black plus inert fillers	2.45E+09	24	4	0.14	0.03500	28	1998	Book [29]
Silicon Carbide	2.45E+09	20	30	11	0.36667	1.0	1998	Book [29]
SiO2	2.45E+09	25	3.35	0.0001	0.00003	35640	2010	Paper [109]
Water destilled	2.45E+09	25	77	13	0.16883	1.3	1998	Book [29]
Water destilled	2.45E+09	85	56	3	0.05357	4.9	1998	Book [29]

A.2 to Section 3.3

Tab. A-2 Architecture of ±45° non-crimp-fabric (NCF) X-E-PB-627g/m^2-1270mm according to datasheet by Saertex, see A.5.

	Build-Up	Areal weight (g/m^2)	Tolerance (±%)	Material
Top	**Powder**	15	20	Momentive Epikote Resin 05390
	45°	300	5	E-Glass 300 tex
	90°	3	5	E-Glass 68 tex
	0°	3	5	E-Glass 68 tex
Bottom	**−45°**	300	5	E-Glass 300 tex
	Stitching	6	±1 g/m²	PES 76 dtex

Tab. A-3 Architecture of 0° NCF U-E-PB-606g/m^2-1200 mm according to datasheet by Saertex, see A.5.

	Build-Up	Areal Weight (g/m^2)	Tolerance ±%	Material
Top	**0°**	520	5	E-Glass 1,200 tex
	90°	54	5	E-Glass 68 tex
Bottom	**Powder**	15	20	Momentive Epikote Resin 05390
	Stitching	17	±3 g/m²	PES 76 dtex

A.3 to Section 4.2

A.3.1 Homogeneity-Study Experimental Design and Results

Tab. A-4 Overview of all trials made and evaluated for the homogeneity-study.

Run			Factors					Responses			Further Values			
Name	**Order**	**Used**	**Load**	**Stir**	**Sin**	**MCoun**	**MChan**	**Mean**	**cov**	**rel**	**Frame**	**SD**	**Max**	**Min**
N1	4	Incl	No	Off	0	1	0	49	0.0673	0.463	316	3.3	64.8	42.1
N2	10	Incl	No	Off	120	5	0	48.9	0.0327	0.282	315	1.6	57.2	43.4
N3	18	Excl	Yes	Off	120	1	0	48.3	0.0642	0.545	317	3.1	68	41.7
N4	1	Excl	Yes	Off	0	5	0							
N5	20	Incl	Yes	Off	60	3	0	50.6	0.0415	0.298	318	2.1	60.4	45.3
N6	5	Excl	No	On	120	1	0	49.2	0.0467	0.380	314	2.3	61.7	43
N7	19	Incl	No	On	0	5	0	45	0.0178	0.178	312	0.8	48.6	40.6
N8	22	Incl	Yes	On	0	1	0	47.6	0.0294	0.269	320	1.4	54.7	41.9
N9	15	Incl	Yes	On	120	5	0	46.2	0.0152	0.173	312	0.7	50.3	42.3
N10	11	Incl	No	Off	120	3	10	49.5	0.0283	0.228	312	1.4	55	43.7
N11	3	Incl	Yes	Off	0	1	10	43.4	0.0207	0.168	309	0.9	47.7	40.4
N12	8	Excl	No	On	60	1	10	48.2	0.0187	0.189	312	0.9	51.9	42.8
N13	23	Excl	No	Off	120	1	30	49	0.0286	0.284	317	1.4	57.5	43.6
N14	16	Incl	No	Off	0	5	30	45.4	0.0198	0.152	321	0.9	48.6	41.7
N15	9	Incl	Yes	Off	0	1	30	47.1	0.0255	0.236	319	1.2	53.9	42.8
N16	24	Incl	Yes	Off	120	5	30	43	0.0186	0.147	316	0.8	45.7	39.4
N17	14	Incl	No	On	0	1	30	49.4	0.0202	0.190	325	1	53.1	43.7
N18	7	Incl	No	On	120	5	30	46.6	0.0172	0.200	314	0.8	51.4	42.1
N19	21	Excl	Yes	On	120	1	30	46.7	0.0171	0.173	311	0.8	50.2	42.1
N20	12	Incl	Yes	On	0	5	30	41.2	0.0121	0.124	311	0.5	43.2	38.1

Overview of all trials made and evaluated for the homogeneity-study. (Continuation)

	Run		Factors					Responses			Further Values			
Name	**Order**	**Used**	**Load**	**Stir**	**Sin**	**MCoun**	**MChan**	**Mean**	**cov**	**rel**	**Frame**	**SD**	**Max**	**Min**
N21	13	Incl	Yes	On	60	3	10	44.5	0.0135	0.162	313	0.6	47.5	40.3
N22	2	Excl	Yes	On	60	3	10	40.1	0.0150	0.157	301	0.6	43.8	37.5
N23	17	Incl	Yes	On	60	3	10	45.8	0.0153	0.155	308	0.7	48.9	41.8
N24	6	Incl	No	Off	120	5	30	45.9	0.0174	0.198	302	0.8	50.5	41.4
N25	25	Incl	Yes	Off	0	5	0	43.2	0.0231	0.167	313	1	47.2	40
N26	26	Incl	Yes	Off	60	3	10	46	0.0152	0.154	316	0.7	48.7	41.6

A.3.2 Thermo Camera Images used for Evaluation

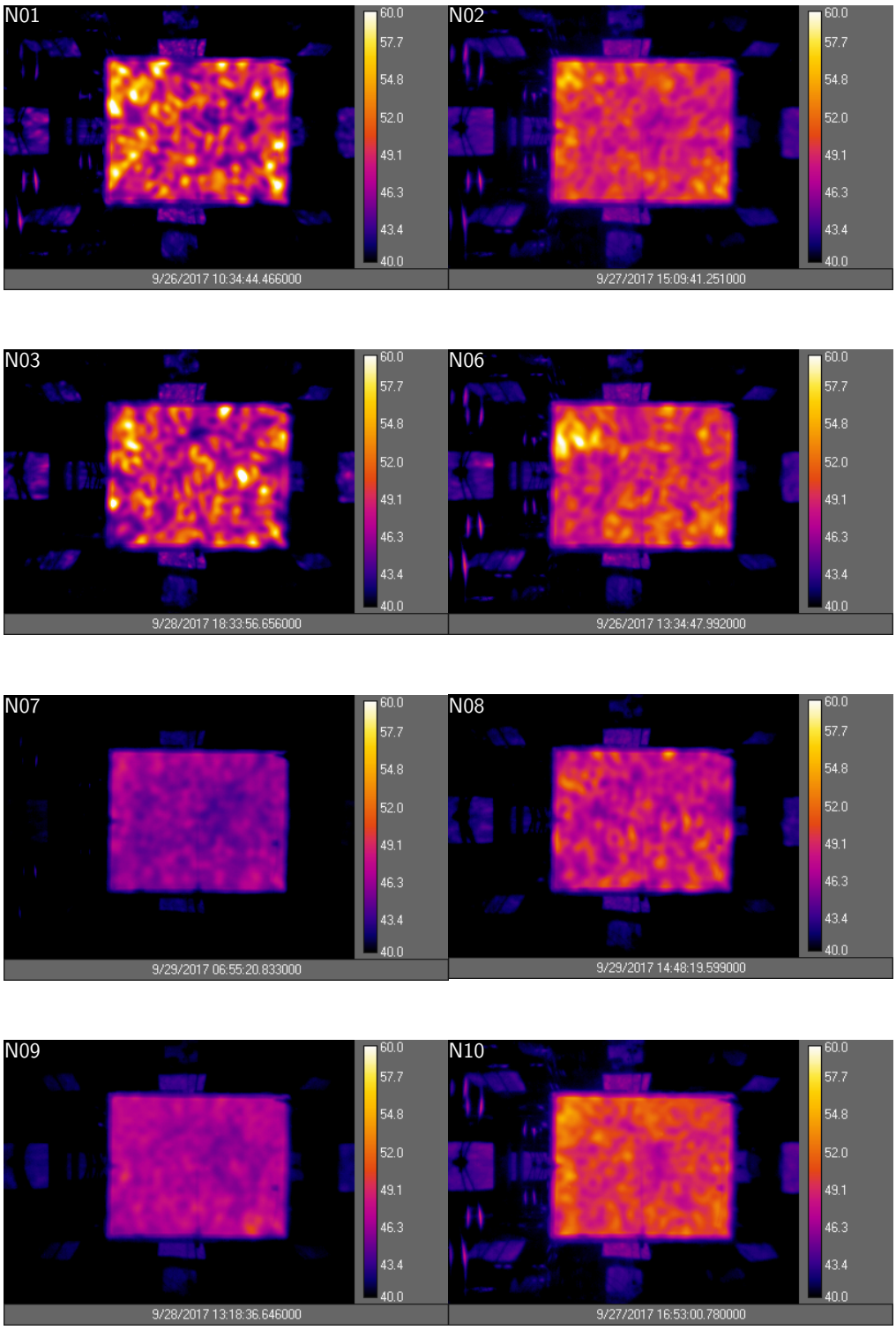

Fig. A-1 Thermo camera images evaluated in homogeneity study set 1/3.

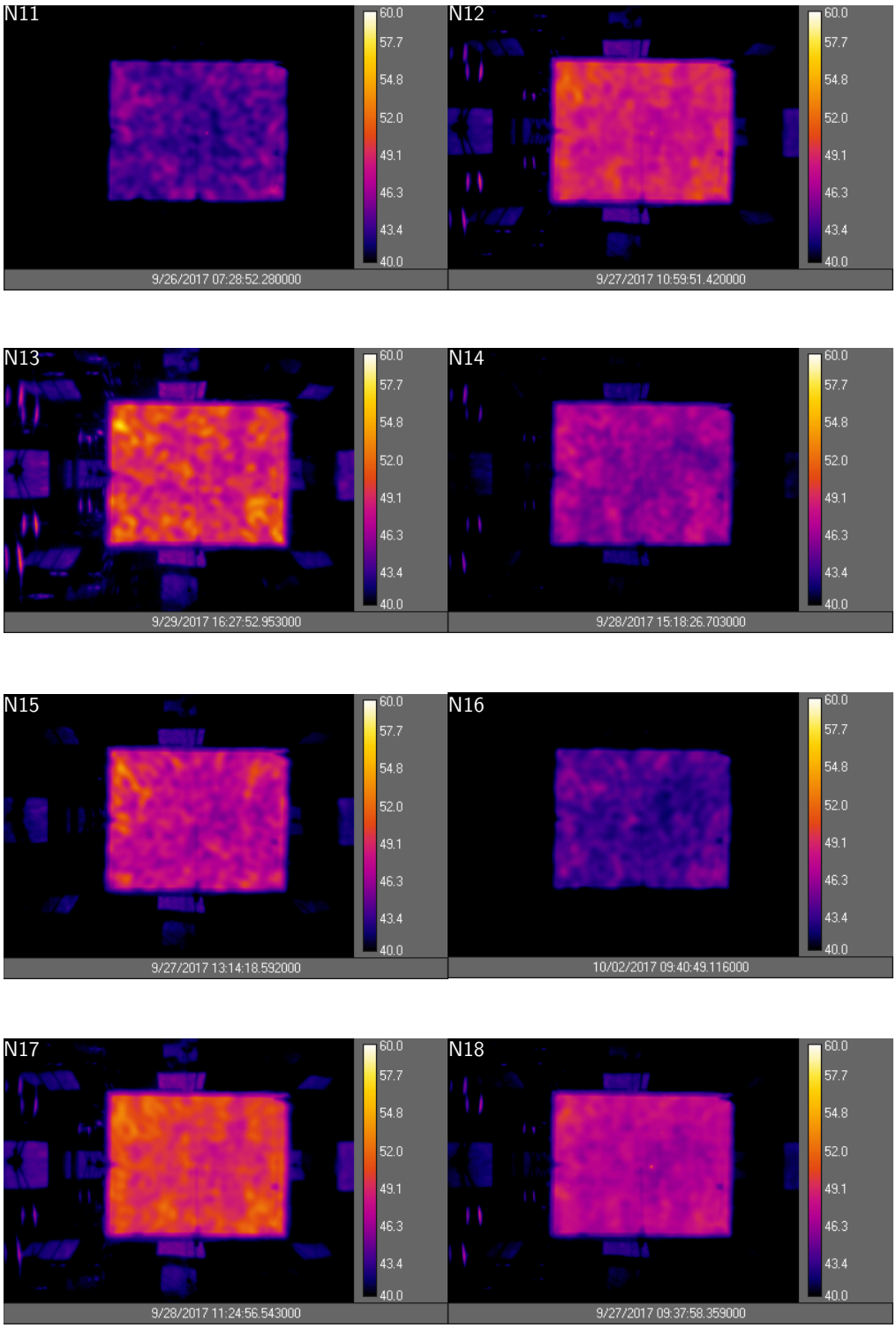

Fig. A-2 Thermo camera images evaluated in homogeneity study set 2/3.

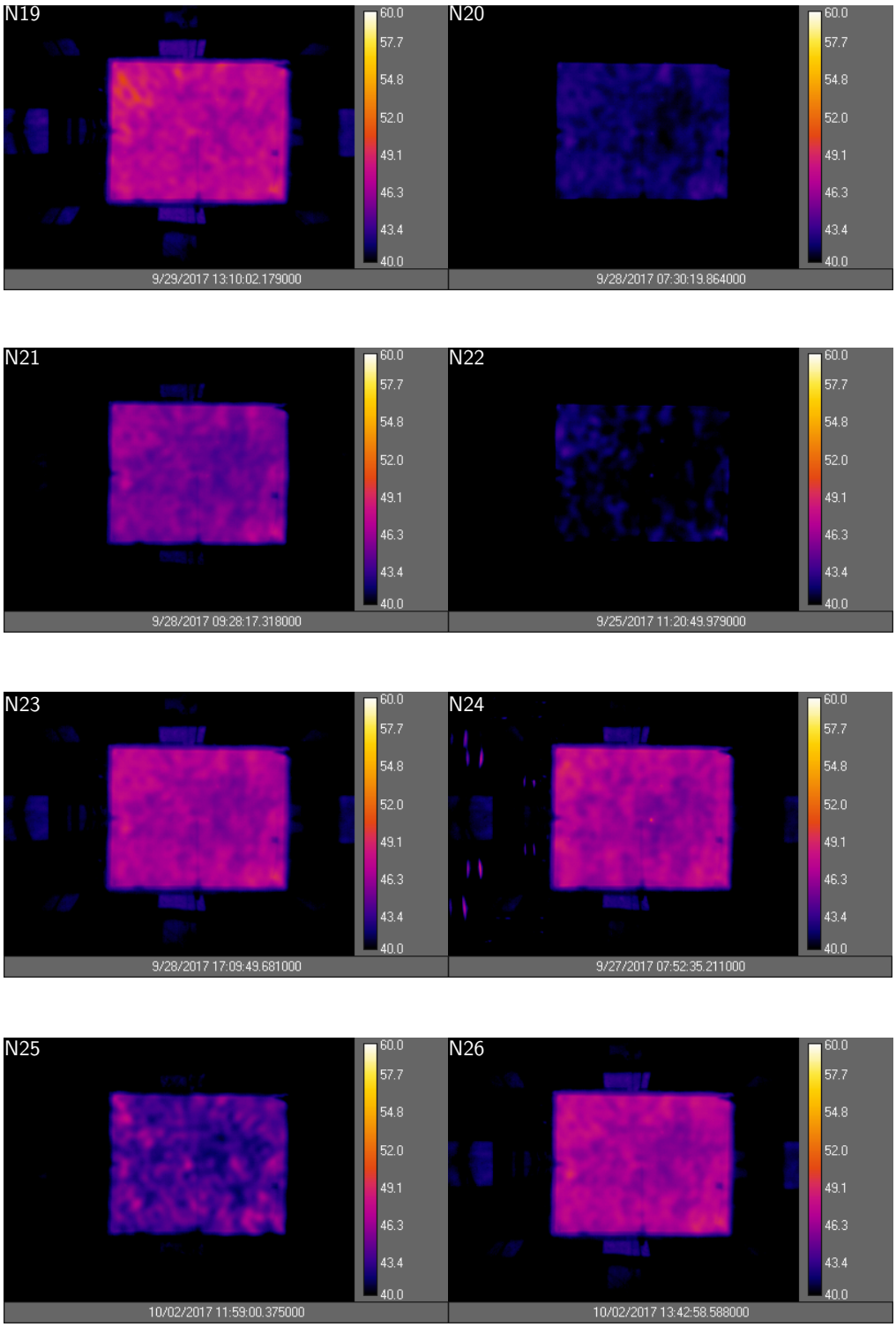

Fig. A-3 Thermo camera images evaluated in homogeneity study set 3/3.

A.3.3 Graphs of Homogeneity Study

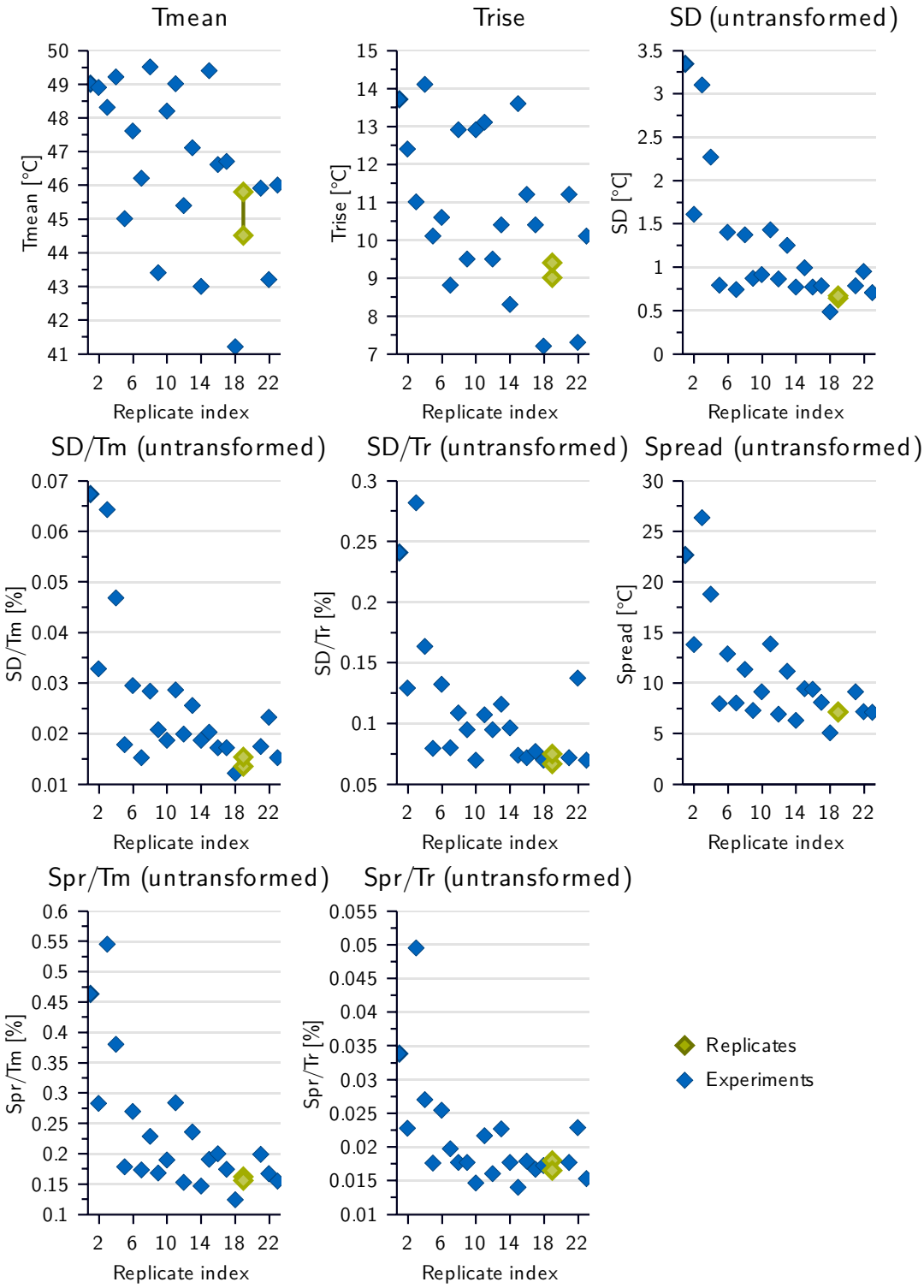

Fig. A-4 Replicate plots of all factors of the homogeneity study.

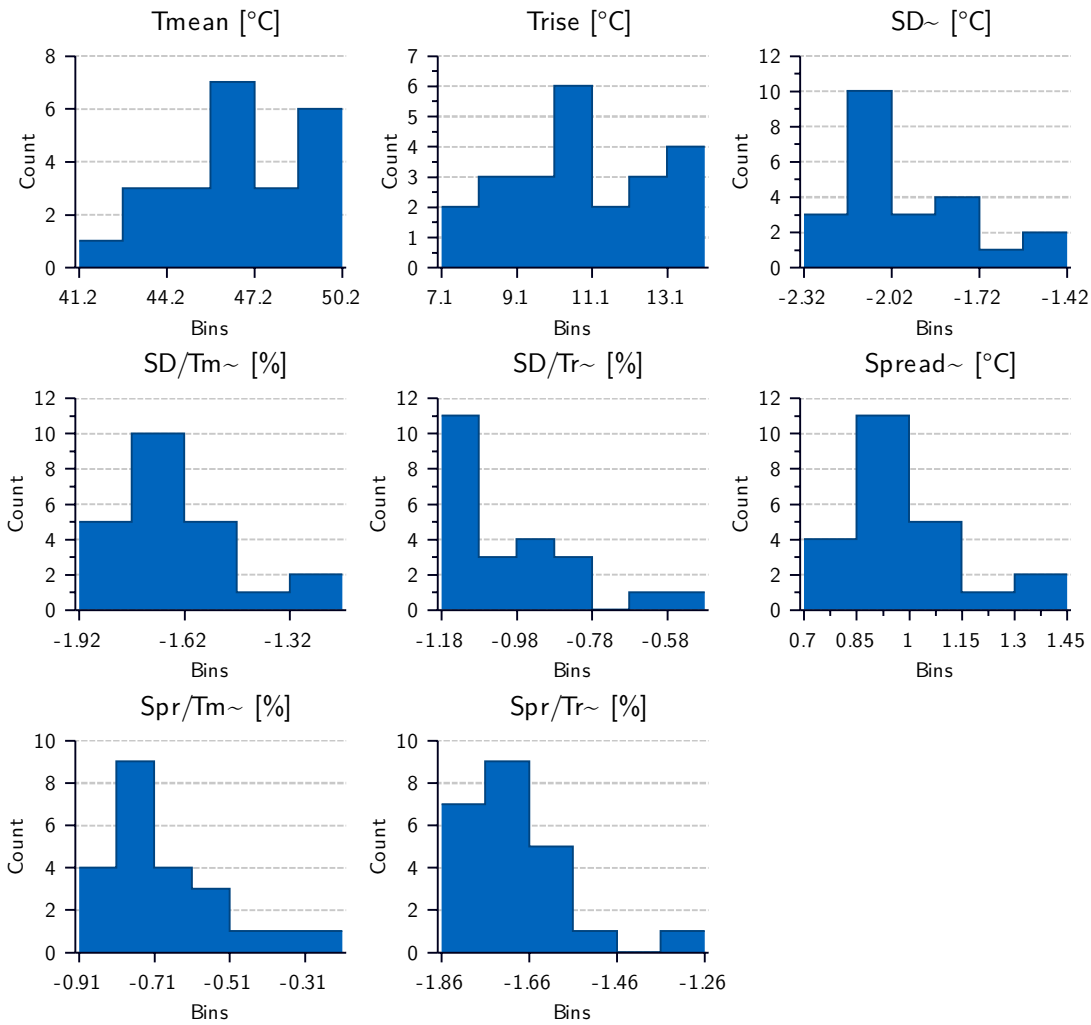

Fig. A-5 Histograms of all factors of the homogeneity study.

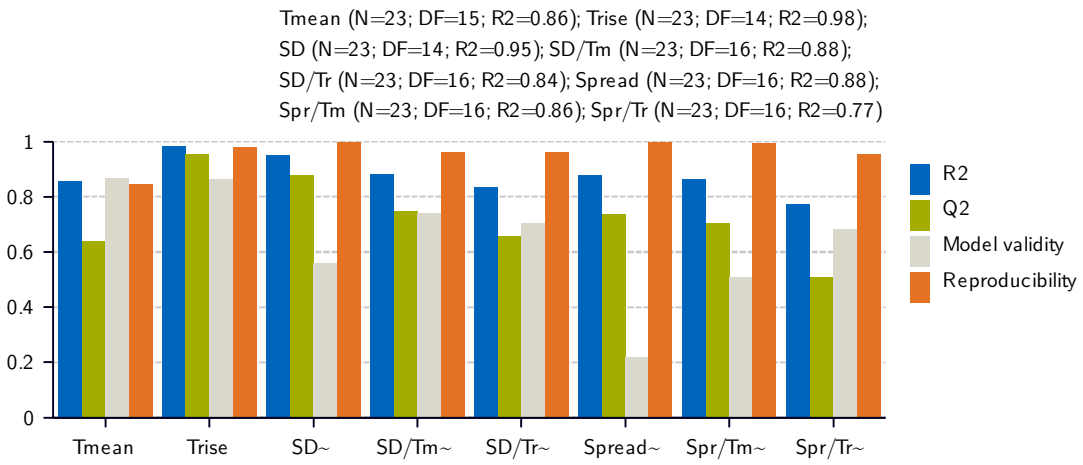

Fig. A-6 Model qualities of homogeneity study.

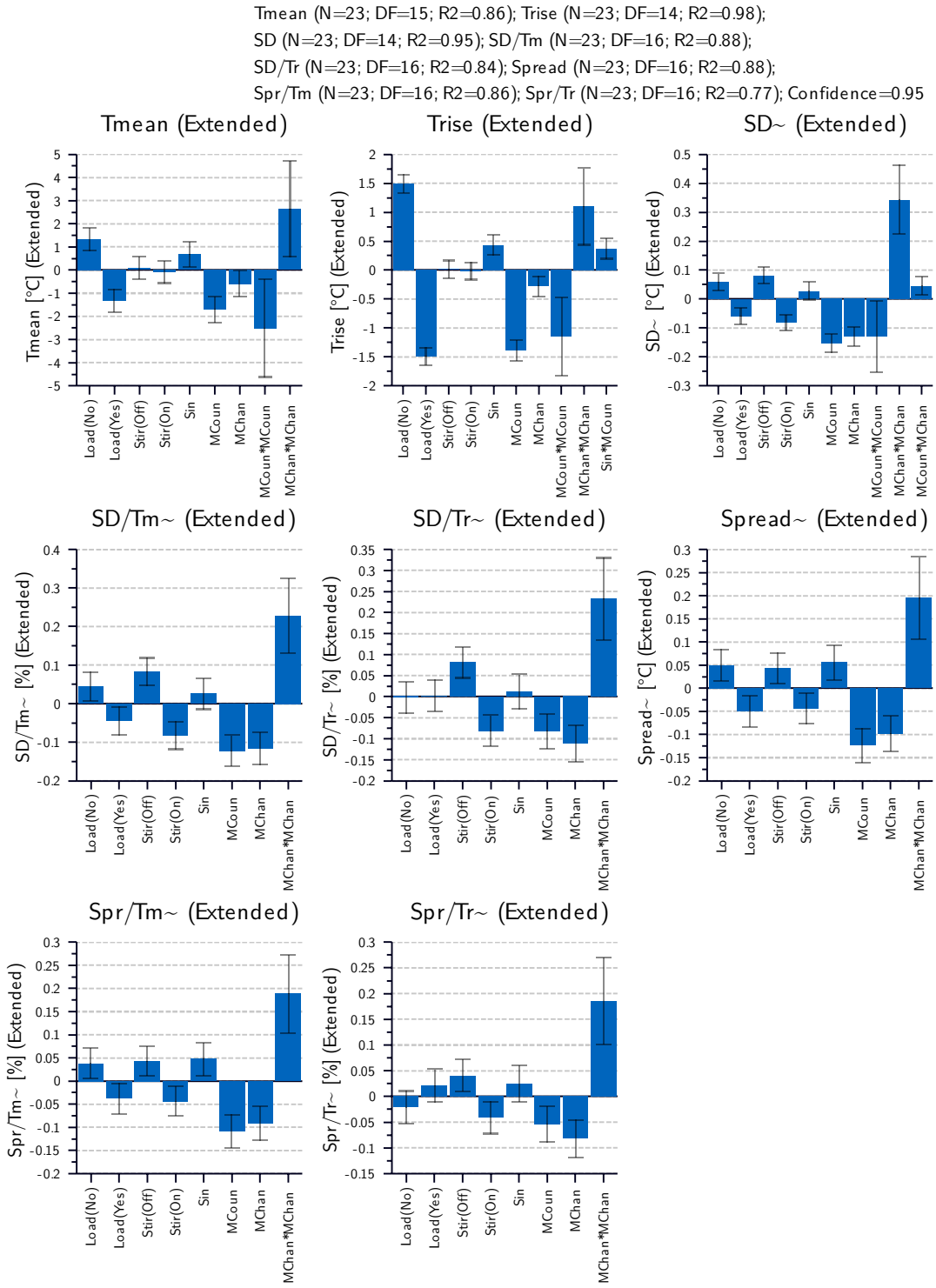

Fig. A-7 Coefficient plots of all factors of the homogeneity study.

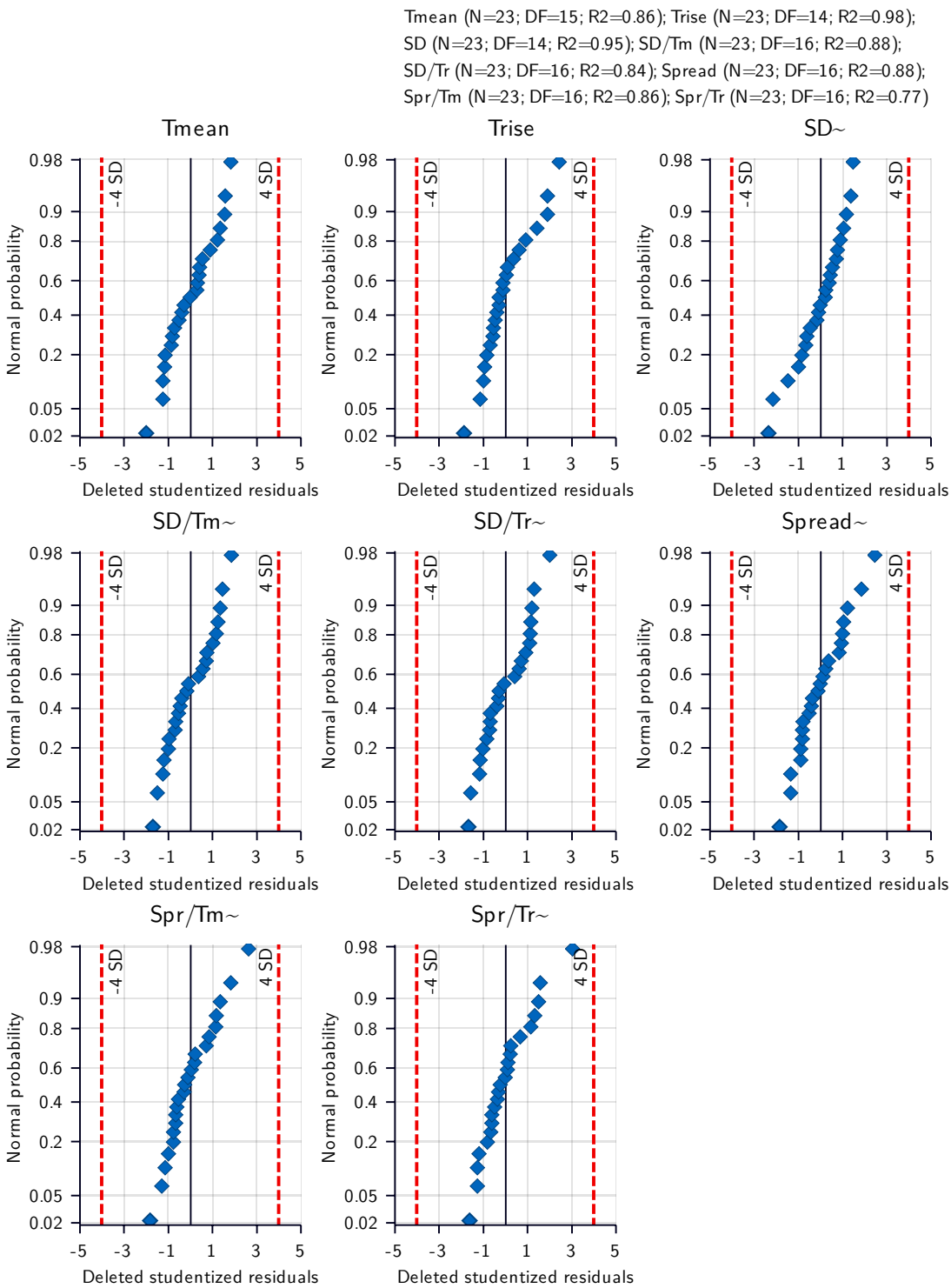

Fig. A-8 Normal probability plots of homogeneity study without detected outlier and programming error N5.

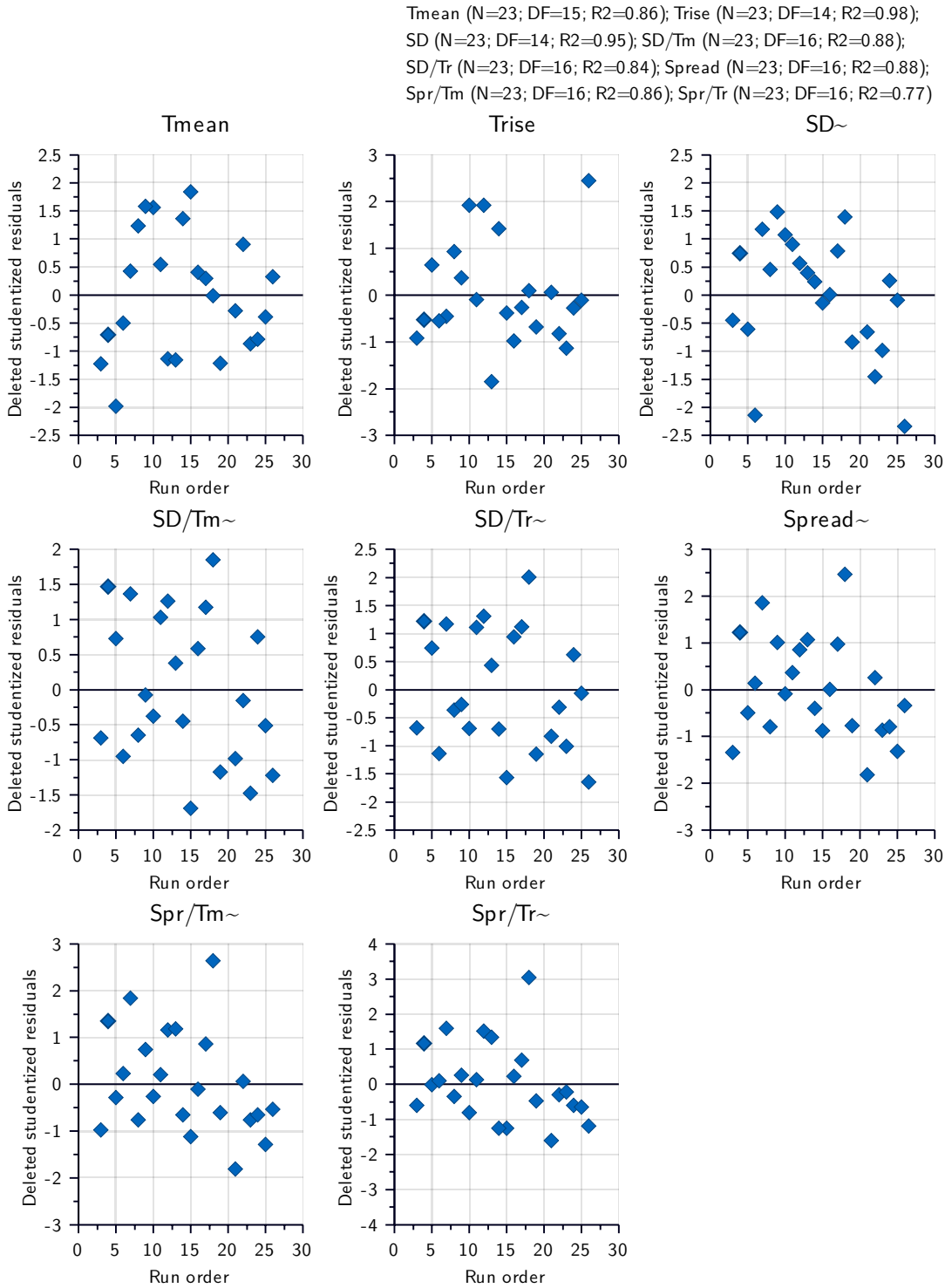

Fig. A-9 Residuals over run order for homogeneity study.

A.4 to Section 5.2

Tab. A-5 Overview of all configurations manufactured and measured during the absorber study.

Run Name	Run Order	Factors LB [%]	XE2B [%]	SiC [%]	Measurements, Derivates, Statistics ε_r'	ε_r''	$\tan(\delta)$	D_p [mm]	cov ε_r' [%]	cov ε_r'' [%]
CR141-2-1-0.5	3	0.499	0.000	0.000	3.29	0.177	0.054	199.9	0.23	0.56
CR141-2-1-2	13	1.996	0.000	0.000	4.26	0.680	0.160	59.3	0.27	1.14
CR141-10-1/1200-0.5/1.5	17	0.499	0.000	1.499	3.51	0.247	0.070	148.0	0.22	0.74
CR141-10-1/1200-2/1.5(b)	12	1.999	0.000	1.498	4.50	0.740	0.164	56.0	0.35	1.38
CR141-2-0-0.5	1	0.000	0.499	0.000	4.50	1.239	0.275	33.7	1.17	3.8
CR141-10-0/1200-0.5/1.5	11	0.000	0.499	1.497	4.80	1.348	0.281	32.0	0.97	2.24
CR141-10-1/1200-1.25/0.75(a)	9	1.248	0.000	0.751	3.95	0.509	0.129	76.1	0.32	0.87
CR141-10-1/1200-1.25/0.75(b)	16	1.244	0.000	0.749	3.77	0.395	0.105	95.8	0.64	1.48
CR141-10-1/1200-1.25/0.75(c)	4	1.249	0.000	0.751	3.83	0.418	0.109	91.3	0.54	1.53
CR141-10-0/1200-0.5/8	2	0.000	0.499	7.990	6.40	1.948	0.304	25.6	1.04	2.09
CR141-10-1/1200-0.5/8	15	0.499	0.000	7.988	4.84	0.622	0.129	68.9	0.62	1.9
CR141-10-0/1200-1.25/0.75	10	0.000	1.248	0.751	7.22	3.263	0.452	16.4	2.27	3.17
CR141-2-0-1.25	14	0.000	1.248	0.000	7.36	4.047	0.550	13.5	1.16	4.26
CR141-2-1-1.25	5	1.269	0.000	0.000	3.69	0.380	0.103	98.7	0.16	1.27
CR141-10-0/1200-1.25/1.5	6	0.000	1.251	1.502	7.66	3.915	0.511	14.2	0.85	3.44
CR141-10-1/1200-1.25/1.5	18	1.248	0.000	1.501	3.98	0.451	0.113	86.2	0.49	1.18
CR141-1/0-0.625/0.625	8	0.625	0.625	0.000	5.40	1.988	0.368	23.1	0.45	1.73
CR141-10-1/1200-0,5/1,5(b)	7	0.500	0.000	1.498	3.51	0.239	0.068	152.8	0.36	1.33

A.5 Datasheets

Tooling & Composites

Produktdatenblatt
Version 01 / 2011

Biresin® CR141
Compositeharz-System für Heisshärtung

Anwendungsgebiete
- insbesondere zur Verarbeitung im Pultrusions- und Filament Winding Verfahren
- speziell für Anwendungen, die eine niedrige Reaktivität und eine lange Topzeit benötigen

Produktvorteile
- durch niedrige Mischviskosität bei erhöhter Verarbeitungstemperatur schnelle Infiltration der trockenen Fasern
- Anpassung der Topfzeit über die Beschleunigerkomponente

Beschreibung
- Basis 3K-EP-System
- Harz **Biresin® CR141**, Epoxidharz, transluzent
- Härter **Biresin® CH141**, Carbonsäure Anhydrid, transparent
- Beschleuniger **Biresin® CA141**, Amin, bernsteinfarben

Physikalische Daten		Harz	Härter	Beschleuniger
Einzelkomponenten		**Biresin® CR141**	**Biresin® CH141**	**Biresin® CA141**
Viskosität, 25°C	mPas	8.250	< 10	200
Dichte, 25°C	g/ml	1,16	1,20	0,98
Mischungsverhältnis	in Gewichtsteilen	100	90	2
			Mischung	
Topfzeit, 100 g / RT, ca. Werte	h		> 24	
Mischviskosität, 25°C, ca. Werte	mPas		600	

Mechanische Kennwerte der Reinharzprobe			
ca.-Werte nach 3 h / 80°C + 3 h / 120°C + 3 h / 140°C (Quelle: Sika intern)			
Biresin® CR141 Harz	mit **Biresin® CH141** Härter und **Biresin® CA141** Beschleuniger		
Dichte	ISO 1183	g/cm³	1,20
Shore-Härte	ISO 868	-	D 87
Biege-E-Modul	ISO 178	MPa	3.100
Zug-E-Modul	ISO 527	MPa	3.200
Biegefestigkeit	ISO 178	MPa	145
Druckfestigkeit	ISO 604	MPa	122
Zugfestigkeit	ISO 527	MPa	78
Zugdehnung	ISO 527	%	3,3
Schlagzähigkeit	ISO 179	kJ/m²	18

Verarbeitung
- Vor der Entformung ist eine entsprechende Temperung erforderlich.
- Zur sofortigen Reinigung von Pinseln und Arbeitsgeräten eignet sich Sika Reinigungsmittel 5.

Thermische Kennwerte der Reinharzprobe			
Biresin® CR141 Harz	mit **Biresin® CH141** Härter und **Biresin® CA141** Beschleuniger		
Wärmeformbeständigkeit	ISO 75B	°C	137*
	ISO 75C	°C	122*
Glasübergangstemperatur	ISO 11357	°C	139*

* Werte nach Temperung: 3 h / 80°C + 3 h / 120°C + 3 h / 140°C

Verpackung
Einzelgebinde	**Biresin® CR141** Harz	1000 kg; 220 kg; 10 kg netto
	Biresin® CH141 Härter	1100 kg; 220 kg; 9 kg netto
	Biresin® CA141 Beschleuniger	10 kg; 0,2 kg netto

Lagerung
- In temperierten Räumen (18 - 25°C) und ungeöffneten Originalgebinden beträgt die Lagerfähigkeit von Biresin® CR141 Harz mindestens 24 Monate und von Biresin® CH141 Härter und CA141 Beschleuniger mindestens 12 Monate.
- Durch ungünstige Lagerbedingungen kristallisiertes Harz ist durch vorsichtiges Erwärmen auf max. 80°C wieder zu verflüssigen.
- Angebrochene Gebinde sind stets sofort wieder dicht zu verschließen und baldmöglichst zu verarbeiten.

Gefahrenhinweise
Für den Umgang mit unseren Produkten sind die wesentlichen physikalischen, sicherheitstechnischen, toxikologischen und ökologischen Daten den stoffspezifischen Sicherheitsdatenblättern zu entnehmen. Die einschlägigen Vorschriften, z. B. die Gefahrstoffverordnung, sind zu beachten.
In nicht ausgehärtetem Zustand sind unsere Erzeugnisse in der Regel wassergefährdend und dürfen deshalb nicht in die Kanalisation, in Gewässer und in das Erdreich gelangen.
Auf Wunsch stellen wir Ihnen unsere „Hinweise zum Arbeitsschutz beim Umgang mit Produkten der Sika Deutschland GmbH“ zur Verfügung.

Entsorgung
Nicht ausgehärtete Produkte sind in der Regel besonders überwachungsbedürftige Abfälle und müssen ordnungsgemäß entsorgt werden. Ausgehärtetes Material kann nach Absprache mit der jeweils zuständigen Behörde oder Deponie als Haus- / Gewerbeabfall entsorgt werden.
Auskunftspflichtig für die ordnungsgemäße Entsorgung sind die örtlichen Behörden, wie z.B. Landratsamt, Umweltschutzamt oder Gewerbeaufsichtsamt.

Datenbasis
Alle technischen Daten, Maße und Angaben in diesem Datenblatt beruhen auf Labortests. Tatsächlich gemessene Daten können in der Praxis aufgrund von Umständen außerhalb unseres Einflussbereiches abweichen.

Rechtshinweise
Die vorstehenden Angaben, insbesondere die Vorschläge für Verarbeitung und Verwendung unserer Produkte, beruhen auf unseren Kenntnissen und Erfahrungen im Normalfall, vorausgesetzt die Produkte wurden sachgerecht gelagert und angewandt. Wegen der unterschiedlichen Materialien, Untergründen und abweichenden Arbeitsbedingungen kann eine Gewährleistung eines Arbeitsergebnisses oder eine Haftung, aus welchem Rechtsverhältnis auch immer, weder aus diesen Hinweisen, noch aus einer mündlichen Beratung begründet werden, es sei denn, dass uns insoweit Vorsatz oder grobe Fahrlässigkeit zur Last fällt. Hierbei hat der Anwender nachzuweisen, dass er schriftlich alle Kenntnisse, die zur sachgemäßen und erfolgversprechenden Beurteilung durch Sika erforderlich sind, Sika rechtzeitig und vollständig übermittelt hat. Der Anwender hat die Produkte auf ihre Eignung für den vorgesehenen Anwendungszweck zu prüfen. Änderungen der Produktspezifikationen bleiben vorbehalten.
Schutzrechte Dritter sind zu beachten. Im übrigen gelten unsere jeweiligen Verkaufs- und Lieferbedingungen. Es gilt das jeweils neueste Technische Merkblatt, das von uns angefordert werden sollte.

Weitere Informationen:
Sika Deutschland GmbH
Niederlassung Bad Urach
Stuttgarter Str. 139
D - 72574 Bad Urach
Deutschland
Tel: +49 (0) 7125 940 492
Fax: +49 (0) 7125 940 401
Email: tooling@de.sika.com
Internet: www.sika.de

SAERTEX
Reinforcing Your Ideas!
SAERTEX GmbH & Co. KG
Brochterbecker Damm 52
48369 Saerbeck / Germany
tel phone +49-25 74-9 02 0
fax +49-25 74-9 02 209
e-Mail: info@saertex.com

DATENBLATT

(nach EN 13473-1)

SAP-MATERIAL-NR.
30002524

TEXTILE STRUKTUR
7002338

ARTIKEL-BEZEICHNUNG
X-E-PB-627g/m²-1270mm

Z ▲

KONSTRUKTION	FLÄCHENGEWICHT [g/m²]	TOLERANZ [+/-%]	MATERIAL
Oberlage			
Pulver	15	20	Momentive Epikote Resin 05390
45 °	300	5	E-Glas 300 tex
90 °	3	5	E-Glas 68 tex
0 °	3	5	E-Glas 68 tex
-45 °	300	5	E-Glas 300 tex
Unterlage			

X/Y

NÄHFADEN:	6 g/m²	+/- 1 g/m²	PES 76 dtex

Nähbindung:	Franse	Nähfeinheit :	5,0
Breite::	1.270 mm		
Flächengewicht:	627 g/m²	Gesamttoleranz:	5,5 %

SAERTEX
Reinforcing Your Ideas!
SAERTEX GmbH & Co. KG
Brochterbecker Damm 52
48369 Saerbeck / Germany
tel phone +49-25 74-9 02 0
fax +49-25 74-9 02 209
e-Mail: info@saertex.com

DATENBLATT ENTWURF

(nach EN 13473-1)

SAP-MATERIAL-NR.
20004532

TEXTILE STRUKTUR
7004408

ARTIKEL-BEZEICHNUNG
U-E-PB-606g/m²-1200mm

Z ▲

KONSTRUKTION	FLÄCHENGEWICHT [g/m²]	TOLERANZ [+/-%]	MATERIAL
Oberlage			
0 °	520	5	E-Glas 1.200 tex
90 °	54	5	E-Glas 68 tex
Pulver	15	20	Momentive Epikote Resin 05390
Unterlage			

X/Y

NÄHFADEN:	17 g/m²	+/- 3 g/m²	PES 110 dtex

Nähbindung:	Trikot	Nähfeinheit :	10,0
Breite::	1.200 mm		
Flächengewicht:	606 g/m²	Gesamttoleranz:	5,7 %

SCHOTT NEXTREMA®

Glass-ceramics engineered and designed for extreme conditions

NEXTREMA® is a unique family of glass-ceramics. This material combines the glossy appearance of glass with exceptional thermal, chemical, optical and mechanical properties like an attractive bending strength of 100 – 160 MPa for materials with a thickness of around 4 mm. With a thermal resistance of 950 °C or for specific applications even higher, combined with a thermal shock resistance of 700 – 820 °C, it ensures a reliable material performance even under extreme temperature conditions. Our six unique glass-ceramic types combined with the wide range of sizes and thicknesses varying from 2 mm to 6 mm (> 6 mm on request) will open up new possibilities in product design and performance. The unique transmission spectra provide new ideas for combining innovative infrared heating functionalities with attractive lighting effects. The versatility of this material will surely impress you.

Key properties

- Very low coefficient of linear thermal expansion
- Excellent temperature and thermal shock resistance
- High transmission in infrared range and unique visible light transmission profiles
- Excellent chemical resistance
- High mechanical strength

The six glass-ceramic types

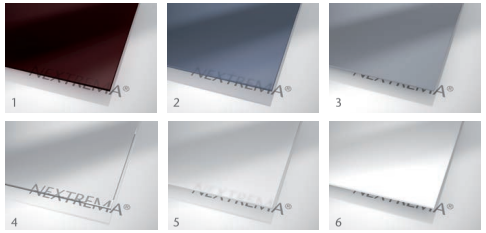

1 | NEXTREMA® tinted
2 | NEXTREMA® translucent bluegrey
3 | NEXTREMA® opaque grey

4 | NEXTREMA® transparent
5 | NEXTREMA® translucent white
6 | NEXTREMA® opaque white

Transmission [%]

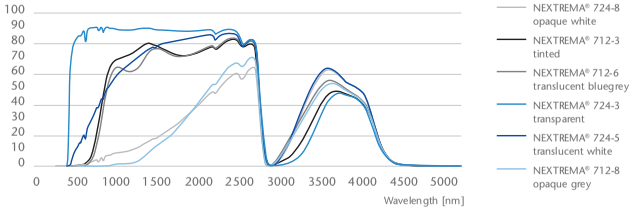

This graph is based on data from individual measurements. Deviations may result from manufacturing process. Internal transmissions graph of different ceramization status with sample thickness of approximately 4 mm.

SCHOTT
glass made of ideas

SCHOTT NEXTREMA®

Glass-ceramics engineered and designed for extreme conditions

Standards forms of delivery

	Standard length	Standard width
Thickness	Min. - Max.	Min. - Max.
2 mm	50 – 1555 mm	50 – 860 mm
3 mm	50 – 1930 mm	50 – 1075 mm
4 mm	50 – 1930 mm	50 – 1075 mm
5 mm	50 – 1930 mm	50 – 1075 mm
6 mm	50 – 1930 mm	50 – 1060 mm
≥ 8 mm	50 – on request	50 – 960 mm

Overview of dimensions: Cut to size panels

Bent panels

Formats of bent panels on request.

Surface characteristics

Porosity (ISO 9385): 0 %
Roughness: Material 724-3 (t = 4 mm)
$R_a \leq 0.20$ µm
Rms ≤ 0.25 µ

Chemical characteristics

The chemical resistance of NEXTREMA® is more extensive than that of most other comparable materials.

Acid resistance (DIN 12116) S 1 – 3
Alkaline resistance (ISO 695) A 1 – 2
Hydrolytic class (DIN ISO 719) HGB 1

All materials fullfill the terms of RoHS without any concerns.

Mechanical characteristics (at room temperature)

Density: ρ approx. 2.5 – 2.6 g/cm³
Modulus of elasticity (ASTM C-1259): E approx. 84 – 95 x 10³ Mpa
Poisson's ratio (ASTM C-1259): µ approx. 0.25 – 0.26
Knoop hardness (ISO 9385): $HK_{0.1/20}$ approx. 570 – 680
Bending strength (DIN EN 1288, Part 5, R45): σ_{bB} approx. 100 – 160 Mpa

All information is subject to change without prior notice.
For detailed material properties please see material type specific datasheets.

Thermal characteristics

CTE in different temperature ranges	
$\alpha_{(-50\,°C;\,100\,°C)}$	-0.8 – 0.6 x 10^{-6} K^{-1}
$\alpha_{(0\,°C;\,50\,°C)}$	-0.8 – 0.6 x 10^{-6} K^{-1}
$\alpha_{(20\,°C;\,300\,°C)}$	-0.4 – 0.9 x 10^{-6} K^{-1}
$\alpha_{(300\,°C;\,700\,°C)}$	0.1 – 1.6 x 10^{-6} K^{-1}

Thermal conductivity (DIN 51936, ASTM E 1461-01) $\lambda_{(90\,°C)}$ 1.5 – 1.7 W / (m x K)

Specific heat capacity $C_{p\,(20-100\,°C)}$ 0.80 – 0.85 J / (g x K)

MTG 400 – 800 K
Resistance of the material to temperature differences between a defined hot zone and cold edge of room temperature, without cracking due to thermal stress.

TSR 700 – 820 °C (1,292 - 1,508 °F)
Resistance of the material to thermal shock when the hot material is splashed with cold water at room temperature, without cracking due to thermal stress.

Homogeneous heating of the material	
TTLC / Short term load (1h)	[°C] 880 – 950
TTLC / Continuous load (5000 h)	[°C] 700 – 850

Inhomogeneous heating of the material	
TTLC / Short term load (1h)	[°C] 450 – 750
TTLC / Continuous load (5000 h)	[°C] 400 – 560

Electrical characteristics

Specific electrical volume resistance (DIN 52326)		
$\log \rho_{(250\,°C)}$	Ω · cm	6.6 – 7.2
$\log \rho_{(350\,°C)}$	Ω · cm	5.2 – 5.7
$*t_{K100}$	°C	170 – 205

*Temperature for a specific electric volume resistivity of 10^8 Ω·cm

Home Tech
SCHOTT AG
Hattenbergstrsse 10
55122 Mainz
Germany
Phone: +49 (0)6131/66-25431
Fax: +49 (0)3641/28889162
info.nextrema@schott.com

www.schott.com/nextrema

SCHOTT
glass made of ideas

B0244 ENGLISH-BOW 01/2017 all/mo Printed in Germany

AIRTECH INTERNATIONAL INC.
5700 Skylab Road
Huntington Beach
CA 92647 USA
Phone : +1 714-899-8100
Fax : +1 714-899-8179
E-mail : airtech@airtechintl.com
Website : www.airtechonline.com

Data Sheet

TOOLFUSION® 3

High temperature infusion resin with low initial cure temperature

TECHNICAL DATA

Material type	Epoxy
Color	Black : Clear (A : B)
Mix ratio by weight	100 : 85 (A : B)
Pot life	300 minutes (100 g at 72 °F or 22 °C)
Viscosity (initial at 72 °F or 22 °C)	450 cps (initial at 72 °F or 22 °C)
Density	1.15 g/cm^3
Glass transition temperature	425 °F (218 °C)
Hardness	89 Barcol
Shrinkage	0.9%
Shelf life	12 months from date of shipment when stored in original packaging at 72°F (22°C)

SIZES

Packaging Part A	Packaging Part B	Weight Part A	Weight Part B
5 gallons	5 gallons	45 Lbs (20.4 Kg)	40 Lbs (18.1 Kg)

CURING DATA

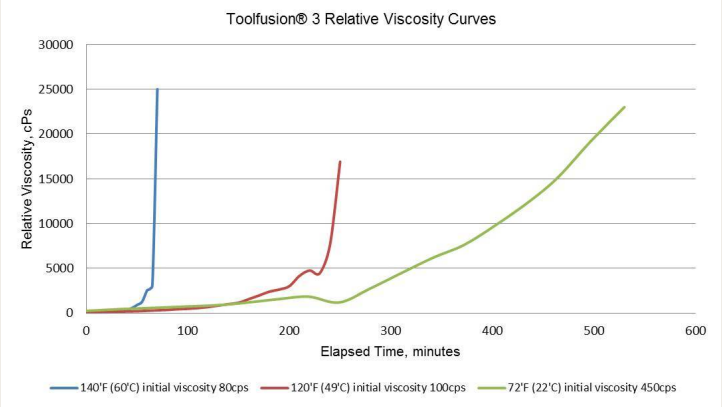

Last updated : 2016-01-25

Catalog position : Resin infusion products

AIRTECH INTERNATIONAL INC.
5700 Skylab Road
Huntington Beach
CA 92647 USA
Phone : +1 714-899-8100
Fax : +1 714-899-8179
E-mail : airtech@airtechintl.com
Website : www.airtechonline.com

Data Sheet

TOOLFUSION® 3

High temperature infusion resin with low initial cure temperature

DESCRIPTION

Toolfusion® 3 is a two part low viscosity epoxy infusion resin formulated to produce pre-preg quality, composite molds. Toolfusion® 3 has a low initial cure temperature of 120 °F (49 °C) and can be post cured to achieve a high glass transition temperature of 425 °F (218 °C). Void contents of less than 1% are achievable. Toolfusion® 3 will work in various RTM and VARTM processes including single and double bag arrangements to produce autoclave quality laminates.

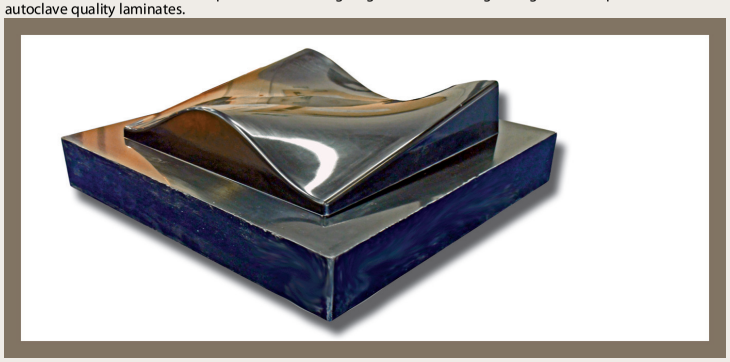

BENEFITS

> Resin infusion process delivers very high quality laminates with low manufacturing costs, no refrigeration costs, no autoclave running costs.
> Low initial cure temperature for low thermal expansion effect during curing and ability to use low cost master model materials.
> Nano technology delivers outstanding toughness & high Tg. (425 °F or 218 °C) for long tool life and reduced life cycle cost.
> Low viscosity allows infusion of thicker and more complex laminates with fewer resin feed lines.
> In comparison to metallic tools, Toolfusion® 3 composite tools are lighter weight for easier manual handing.
> In comparison to metallic tooling, Toolfusion® 3 composite tools have faster heat up and cool down rates for reduced production costs.
> Toolfusion® 3 composite tooling laminates have vacuum integrity for vacuum bag processing of parts in oven and autoclave.

Last updated : 2016-01-25

Catalog position : Resin infusion products

As the conditions or methods of use, including storage, are beyond our control, Airtech International, Inc. does not assume responsibility for the performance of this material for any particular use. The material is sold "as is". Airtech International, Inc. disclaims, and buyer waives, any and all implied warranties, including without limitation the implied warranties of merchantability and of fitness for particular use. The information contained herein represents typical properties and should not be used for specification purposes. Any translation is provided for your convenience only. The official language is English and the official law is California, USA.

AIRTECH INTERNATIONAL INC.
5700 Skylab Road
Huntington Beach
CA 92647 USA
Phone : +1 714-899-8100
Fax : +1 714-899-8179
E-mail : airtech@airtechintl.com
Website : www.airtechonline.com

Data Sheet

TOOLFUSION® 3

High temperature infusion resin with low initial cure temperature

Initial cure:
> Cure laminate on master model with full vacuum applied.
> Raise temperature to 120 °F (49 °C) and hold for 12 hours.
> Remove vacuum bagging materials and attach back-up structure if required.
> Carefully remove the laminate continue with post cure.

Post cure schedule:
> Ramp to 150 °F (65 °C) and hold for 60 minutes.
> Ramp to 200 °F (93 °C) and hold for 60 minutes.
> Ramp to 250 °F (121 °C) and hold for 60 minutes.
> Ramp to 300 °F (149 °C) and hold for 60 minutes.
> Ramp to 350 °F (177 °C) and hold for 60 minutes.
> Ramp to 400 °F (204 °C) and hold for 120 minutes.

Note: Part A and Part B are sold separately.

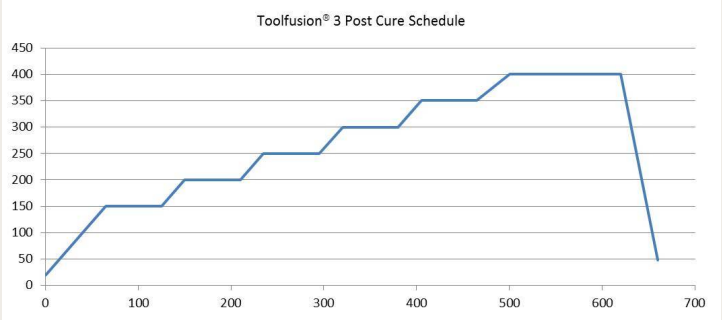

Last updated : 2016-01-25

Catalog position : Resin infusion products

Promat Technisches Datenblatt

PROMAGLAF®-HTI steife Platten

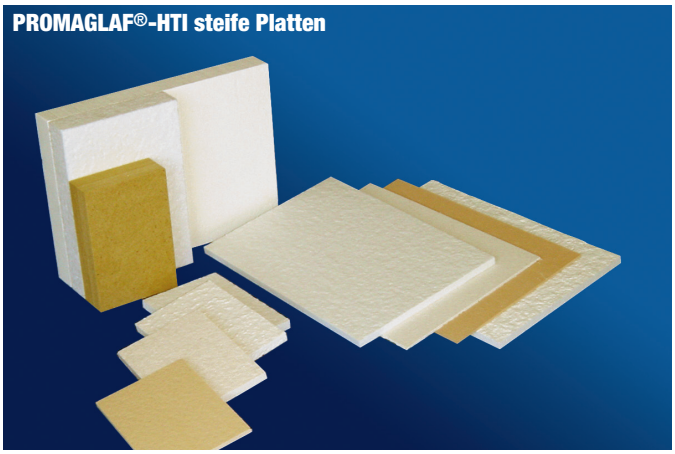

Technische Daten

		PROMAGLAF®-HTI steife Platten		
Typ		-850	-1100	-1250
Farbe		weiß/bräunlich	weiß	weiß
Klassifizierungstemperatur		850 °C	1100 °C	1250 °C
Schwindung		< 4% (800 °C)	<4 % (1100 °C)	<4 % (1250 °C)
Rohdichte		250 - 350 kg/m³	250 - 300 kg/m³	250 - 300 kg/m³
Spezifische Wärmekapazität		0,85 kJ/kg K	1,04 kJ/kg K	1,04 kJ/kg K
Wärmeleitfähigkeit	**200 °C**	0,09 W/m K	0,09 W/m K	0,08 W/m K
	400 °C	0,12 W/m K	0,10 W/m K	0,10 W/m K
	600 °C	0,15 W/m K	0,12 W/m K	0,12 W/m K
	800 °C	0,23 W/m K	0,15 W/m K	0,16 W/m K
	1000 °C	-	-	0,21 W/m K
Chemische Analyse	**Al_2O_3**	15 %	<1 %	-
	SiO_2	45 %	65 %	75 %
	CaO	33 %	30 %	-
	MgO	6 %	4,5 %	18-27 %
	GV	<6 %	<9 %	<9 %
Lieferformen				
Länge x Breite		1000 mm x 610 mm	1000 mm x 610 mm	1000 mm x 610 mm
Dicke		20 - 100 mm	5 - 100 mm	5 - 100 mm

Materialbeschreibung
PROMAGLAF®-HTI ist eine Hochtemperaturwolle auf Basis von Erdalkalisilikat. Die Platten bestehen aus AES-Wolle und werden in unterschiedlichen Dicken und Rohdichten produziert. Das Material ist biolöslich und entspricht den geltenden deutschen und europäischen Vorschriften (67/548/EWG und TRGS 905).

Anwendungsgebiete
PROMAGLAF®-HTI steife Platten werden für die Wärmedämmung von Hochtemperaturanlagen als Keramikfaserersatz verwendet, wenn der Nachweis ausreichender Haltbarkeit erbracht wurde.

Beispiele sind:
- Auskleidungen für Industrieöfen
- Haushaltsgeräteindustrie
- Nichteisenmetallurgie, insbesondere Aluminium

Verarbeitung
PROMAGLAF®-HTI lässt sich mit handelsüblichen Werkzeugen schneiden und bearbeiten. Geeignet sind Messer mit Wellschliff, Bandsägen und Stanzmaschinen.

Bei der Bearbeitung und Montage entsteht Staub. Der Staub kann gesundheitsschädlich sein. Kontakt mit Augen und Haut vermeiden. Staub nicht einatmen, Staub ist abzusaugen. Die Staubgrenzwerte sind zu beachten. Sicherheitsdatenblatt anfordern.

Promat GmbH · Postfach 10 15 64 · 40835 Ratingen · Tel. 02102/493-0 · Fax 02102/493-115 · verkauf3@promat.de · www.promat.de

ENGINEERED CARBONS

PRINTEX® XE 2 B

Produktinformation PI 130

Physikalisch-chemische Eigenschaften			
Jodadsorption	mg/g	1125	ASTM D1510
OAN	ml/100 g	420	ASTM D2414
Feuchtigkeit beim Verpacken	%	≤ 1,0	ASTM D1509
Feingehalt (Silo, Big Bag)	%	≤ 7	ASTM D1508
Siebrückstand, 45 µm	ppm	≤ 250	ASTM D1514
Schüttdichte	g/dm³	130	ASTM D1513

Registrierstatus		
Registriernummer CAS No 1333-68-4		
Australien	AICS	gelistet
China	IECS	gelistet
Europa	EINECS REACH	215-609-9 registriert
Japan	ENCS	5-3328
Kanada	DSL	gelistet
Korea	KECI	KE-04682
Neuseeland	NZIoC	HSNO gelistet
Philippinen	PICCS	gelistet
USA	TSCA	gelistet

1. Allgemeine Beschreibung
Carbon Black zur Anwendung in elektrisch leitfähigen Gummimischungen.

2. Chemische Beschreibung
Kohlenstoff, industriell hergestellter Carbon Black.

3. Anwendung
PRINTEX® XE 2 B ist ein Carbon Black mit einer Oberfläche, die weit über der von üblichen verstärkenden Carbon Blacks liegt. Er verleiht Gummimischungen höchste elektrische Leitfähigkeit. Daher wird er hauptsächlich in elektrisch leitfähigen Gummiwaren eingesetzt. Bereits kleine Mengen führen zu niedrigen Oberflächen- und Durchgangswiderständen von Vulkanisaten. Abhängig von der gewünschten elektrischen Leitfähigkeit lässt sich PRINTEX® XE 2 B mit anderen Verstärkerrußen verschneiden.
Anwendungsgebiete sind elektrisch leitfähige, antistatisch eingestellte technische Gummiartikel.

4. Lagerstabilität
Die Lagerstabilität beträgt 12 Monate.
Carbon Black sollte in kühlen und trockenen Räumen gelagert werden. Weitere Einzelheiten entnehmen Sie bitte unserem Sicherheitsdatenblatt.

5. Lieferformen
5 kg Sack

6. Produktsicherheit
Informationen bezüglich der Sicherheit deses Produktes finden Sie in dem Sicherheitsdatenblatt, das Sie mit der ersten Lieferung oder bei Erscheinen einer überarbeiteten Version erhalten. Wir empfehlen, die Sicherheitsdatenblätter sorgfältig zu lesen, bevor das Material verwendet wird.

7. Zusätzliche Informationen
Zusätzliche Information über den Einsatz von Carbon Black können bei der Anwendungstechnik Tire & MRG oder bei der Abteilung Produktsicherheit angefordert werden. Die Kontaktdaten dieser Abteilungen finden Sie unten.

ENGINEERED CARBONS

Orion Engineered Carbons GmbH
Anwendungstechnik Reifen & MRG
Harry-Kloepfer-Straße 1
50997 Köln
Germany

Telefon +49 2233 964-684
Fax +49 2233 964-622
rubberblacks@orioncarbons.com

Orion Engineered Carbons GmbH
Produktsicherheit
Rodenbacher Chaussee 4
63457 Hanau-Wolfgang
Germany

Telefon +49 6181 59-4454
Fax +49 6181 59-4205
rubberblacks@orioncarbons.com

www.orioncarbons.com

OEC-PI 30-02/2012

ENGINEERED CARBONS

Customer Specification

Marketing Department

Dr. Konrad Rockstein
+49 69 365054-187
Michaela Tellmann
+49 2233 964-631

1108
Orion Engineered Carbons GmbH
Harry-Kloepfer-Strasse
50997
Koeln Germany

Date Printed	27.05.2014
Specification	Orion Engineered Carbons GmbH
Date	01-SEP-14
Revision	02
Customer material	
Material Code	110000927
Material Description	20 KG POLY BAG 800 KG PRINTEX® L BEADS

Characteristic	Unit	Reference	Min	Target	Max
Tint Strength, IRB=100%	%	ASTM D3265	97,0	104,0	111,0
Oil Absorption Number	cc/100	ASTM D2414	110,0	117,0	124,0
Sieve residue 45 µm, DIN (ppm)	ppm	ISO 787_18			25
Toluene Extract	%	ATTP 11			0,100

PIEPLOW & BRANDT GmbH

PRODUCT INFORMATION **SILICON CARBIDE BW plus (black)**

Product Description

Type:	**SILICON CARBIDE**
Colour:	**Black**
Hardness:	2300 – 3000 ($Knoop_{100}$)
Specific gravity:	3.2 g / ccm
Crystal structure:	αSiC hexagonal and rhombohedral
Shape of grains:	block-like, sharp-edged

Chemical Structure

SiC:	98.60%
SiO_2:	0.25%
Si:	0.15%
Fe_2O_3:	0.05%
Free C:	0.15%

Applications

SILICON CARBIDE BW plus is particularly used for lapping of ceramics, for polishing in the glass and optical industry as well as in granite processing.

Types and Grains available

SILICON CARBIDE is available in 2 different grades: black and green.
Our SILICON CARBIDE is produced in accordance with F.E.P.A. standards (Féderation Européenne des Fabricants de Produits Abrasifs). Strict quality control of each batch produced certifies the conformity with those standards. The following grains are available:

Mikro FEPA 42-2:2006	50% Value	Tolerance	94 % Value	3 % Value
F 230	53.0	± 3.0	34.0	82
F 240	44.5	± 2.0	28	70
F 280	36.5	± 1.5	22	59
F 320	29.2	± 1.5	16.5	49
F 360	22.8	± 1.5	12	40
F 400	17.3	± 1.5	8	32
F 500	12.8	± 1.0	5	25
F 600	9.3	± 1.0	3	19
F 800	6.5	± 1.0	2	14
F 1000	4.5	± 0.8	1	10
F 1200	3.0	± 0.5	1	7

Date: 06/2010

MÜHLMEIER
MAHLTECHNIK

MÜHLMEIER GMBH & CO. KG
GOTTLITZWEG 2
95671 BÄRNAU - GERMANY

WWW.MUEHLMEIER.DE

PHONE +49 9635 9202-31
FAX +49 9635 9202-73
MAHLTEC@MUEHLMEIER.DE

Produktinformation

R -C Z P

Zirkonoxid (Cerium-stab.) ZrO_2 79 %

Eigenschaften und Anwendung:

- Homogene Mikrostruktur
- Hohe Dichte und Härte entsprechend der Viskosität des Mahl-und Dispergiergutes
- Minimiert die Verunreinigung aufgrund hoher Abriebfestigkeit
- Lange Haltbarkeit durch hohe mechanische Festigkeit und hohe Bruchfestigkeit
- Die homogene und glatte Oberfläche ist optimal zum Dispergieren und Mahlen
- Ungiftig, nicht radioaktiv, chemisch resistent und temperaturbeständig

Durchmesser:

0,8 mm (0,70-0,90)	1,0 mm (0,90-1,10)	2,2 mm (2,20-2,40)
	1,5 mm (1,40-1,60)	

Technische Eigenschaften

Form	rund
Dichte (spez. Gewicht)	**>6,2 g/cm³**
Härte nach Vickers	>1250 HV
Wärmeausdehnungskoeffizient	$10x10^{-6}$/°C (20-400°C)
Oberfläche	glatt, homogen
Elastizitätsmodul	---
Schüttdichte	**>3,9 kg/dm³**
Reinheit	---

Chemische Zusammensetzung

ZrO_2	79,0 ± 0,50 %
CeO_2	21,0 ± 0,30 %
Al_2O_3	0,6 ± 0,05 %

Verpackung:

- in Kunststoffkanistern mit je 25 kg

Lagerung:

in trockenen Räumen

Alle Informationen erfolgen nach bestem Wissen und Gewissen, jedoch ohne Gewähr.

110814 D-r-czp 16.03.2016

B Publications

Journal papers

[P1] D. Teufl and S. Zaremba, ”2.45 GHz Microwave Processing and Its Influence on Glass Fiber Reinforced Plastics”, *Materials*, vol. 11, no. 5, pp. 838, 2018.

Conferences

[C1] D. Teufl, S. Zaremba, and K. Drechsler, ”Evaluation of tooling concepts for the use in microwave processing of fiber reinforced plastics”, in *Proceedings of SETEC 14, 9th SAMPE Europe Technical Conference & Table Top Exhibition*, 2014, pp. 63–71.

[C2] D. Teufl, ”Composite Tooling for Micorwave Processes”, in *3rd Microwave Symposium by Vötsch Industrietechnik in Karlsruhe*, 2015.

[C3] D. Teufl, S. Zaremba, and K. Drechsler, ”Influence of microwave processing on the ilss-properties of glass fiber reinforced plastics”, in *15th LIGHTer International Conference*, 2015.

[C4] D. Teufl, V. Ramopoulos, S. Zaremba, and K. Drechsler ”Adjustment of 2.45 GHz Microwave Absorbing Heating Laysers for Tooling Applications”, in *Proceedings of Polymer Processing Society Conference*, 2015.

[C5] D. Teufl and S. Zaremba ”Processing of (Glass) Fiber Reinforced Plastics wit 2.45 GHz Microwaves”, in *Proceedings of the 18th European Conference on Composite Materials*, 2018.

C Supervised Student Theses

During my employment at *Institute for Carbon Composites –Lehrstuhl füer Carbon Composites* – I supervised the following student theses:

[S1] F. Hofbauer, "Konstruktion und Inbetriebnahme eines Einbausystems zum Recyceln von CFK-Bauteilen mittels Mikrowellentechnik", *Bachelor's thesis*, 2015.

[S2] P. Schwab, "Einbringung und Homogenisierung von Partikeln in Kunststoffen zur Erhöhung der Mikrowellenabsorptionsfähigkeit", *Bachelor's thesis*, 2015.

[S3] L. Mahlau, "Untersuchung und Anpassung der GFK Prüfkörperfertigung als Referenz zur Qualitätssicherung der Mikrowellenaushärtung", *Bachelor's thesis*, 2015.

[S4] A. Buck, "Energieeffizienzbewertung einer industriellen Mikrowellenanlage", *Bachelor's thesis*, 2015.

[S5] P. Hoffmann, "Auslösen eines gipsbasierten Kernsystems mittels Mikrowellen", *Bachelor's thesis*, 2015.

[S6] M. Oberrauch, "Auswahl und Bewertung eines Prüfverfahrens zur Ermittlung des Aushärteeinflusses auf ein spezifisches Glasfaserlaminat", *Bachelor's thesis*, 2015.

[S7] N. Weiner, "Development of a production process for absorber layers in fiber composite tools", *Bachelor's thesis*, 2015.

[S8] F. Weber, "Verbesserung der elektrischen Leitfähigkeit von kohlenstofffaserverstärkten Kunststoffen mit Hilfe von Kohlenstoffnanoröhren", *Term project*, 2012.

[S9] A. Röhrl, "Konstruktion einer mikrowellenkompatiblen Werkzeughalterung", *Term project*, 2012.

[S10] A. Dietrich, “Optimierung der Mikrowellenhärtung von GFK-Laminaten ”, *Term project*, 2015.

[S11] M. Eßwein, “Einbringen von Mikrowellenabsorbern in Faserverbundwerkzeuge ”, *Term project*, 2016.

[S12] L. Ametsbichler, “Homogenisierung von Industrieruß in Epoxidharz zur Herstellung von Mikrowellensuszeptoren”, *Term project*, 2016.

Parts of the following theses contributed to the underlying doctoral thesis: [S3], [S4], [S6], [S7], [S10], [S12]